R-00-23

Geophysical and geological investigations of the Boda area

Stefan Wänstedt
GEOSIGMA AB

April 2000

Svensk Kärnbränslehantering AB
Swedish Nuclear Fuel
and Waste Management Co
Box 5864
SE-102 40 Stockholm Sweden
Tel 08-459 84 00
+46 8 459 84 00
Fax 08-661 57 19
+46 8 661 57 19

ISSN 1402-3091
SKB Rapport R-00-23

Geophysical and geological investigations of the Boda area

Stefan Wänstedt
GEOSIGMA AB

April 2000

Keywords: Boda, caves, remote analysis, GPR, slingram, VLF, gravimeter

Abstract

The studies conducted in the Boda area exhibit the presence of a severely fractured rock mass with occasional caves. The Boda area appears to be intersected by a few significant zones, obvious from a study of the topography but do appear in some of the geophysical investigations as well. The structures in the area have quite efficiently isolated the rock plint where the caves are located. It is not possible from these investigations, however, to draw far-reaching conclusions about the age and genesis of the zones or about their continuation towards depth.

The geological investigation shows, apart from the caves, no unusual features. The rock types in the investigated area correspond with rock types found elsewhere in the region.

The area is highly unsuitable for geophysical surface investigations. Part of the area consists of scattered and quite large blocks that constitute obstacles when making measurements in the area. Since there is little or no soil between the blocks some measurements (e.g. resistivity) are not possible to carry out. Furthermore, the scattered blocks cause unwanted reflections and other difficulties that deteriorate the quality of the geophysical data.

The radar measurements with two different frequencies show an interesting result of importance not only to this investigation. The lower frequency appears to penetrate through the rocky overburden and is able to detect the soil-rock interface. The higher frequency is severely disturbed by the overburden but caves show much more clearly in this data.

The fractured rock around Boda appears to be a shallow feature, since the radar measurements show a quite significant feature throughout most of the profiles, which appears to be the upper boundary of the bedrock. There are, however, some occasional strong reflectors below the interface between fractured and competent rock.

Sammanfattning

Utförda undersökningar i Bodaområdet visar på ett kraftigt sprucket berg med enstaka grottor. Bodaområdet verkar genomlöpas av några få signifikanta zoner vilket är uppenbart vid en studie av topografin, men som även framkommer i några av de geofysiska undersökningarna. Strukturerna i området har på ett effektivt sätt isolerat bergplinten vari grottorna återfinns. Det är inte möjligt att utifrån dessa mätningar dra för långtgående slutsatser om åldern och bildningssättet hos zonerna eller om deras fortsättning mot djupet.

Den geologiska undersökningen visar, frånsett grottorna, inte på några ovanliga företeelser. Bergarterna i undersökningsområdet motsvarar de som återfinns utanför området.

Området är synnerligen olämpligt för markgeofysiska undersökningar. Delar av området består av utspridda, ganska stora block vilka utgör hinder vid utförandet av mätningar i området. Den sparsamma förekomsten av jord mellan blocken förhindrar utförandet av vissa mätningar (t.ex. resistivitet). De utspridda blocken bidrar dessutom till oönskade reflexer och andra svårigheter vilka försämrar kvaliteten hos geofysiska mätdata.

Radarmätningarna med två olika frekvenser uppvisar bland annat ett, inte bara för detta projekt, viktigt resultat. Den lägre frekvensen verkar penetrera de blockiga lagren och visa gränsytan mellan jordlager och berg. Den högre frekvensen är kraftigt störd av lagren medan grottorna framträder betydligt bättre i dessa data.

Det sprickiga berget omkring Boda verkar vara ett ytligt fenomen, i det att radarmätningarna visar på en tydlig struktur i de flesta profiler, vilken tolkas vara det hela bergets överyta. Det finns emellertid några utspridda starka reflektorer under kontaktytan mellan sprucket och helt berg.

Contents

List of Figures

List of Tables

1 Introduction

At Boda, a system of superficial caves in the crystalline bedrock has been discovered and mapped. This is a geological phenomenon only rarely observed and there is some discussion on the origin of the caves. An investigation regarding the cause of the caves commenced late 1997.

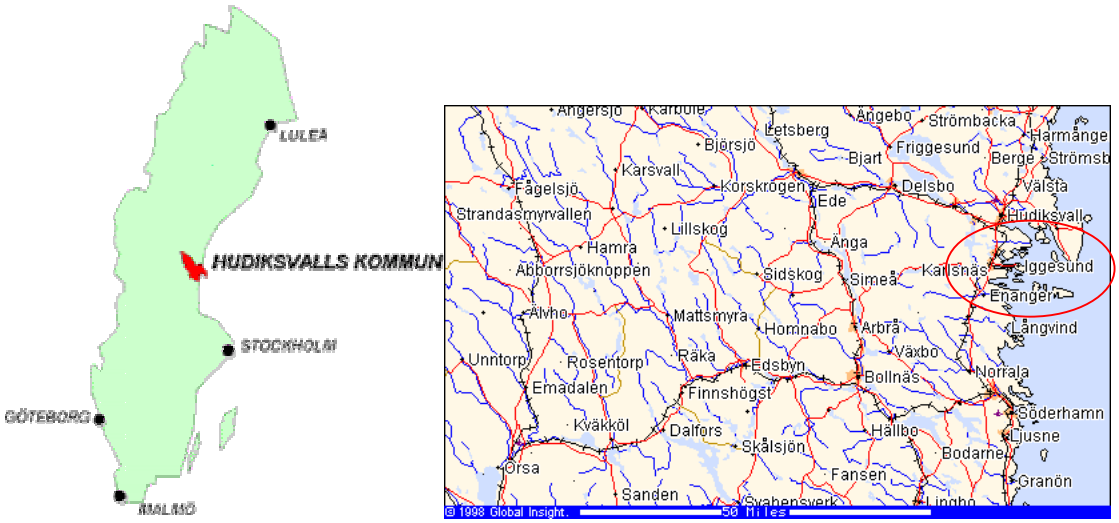

Figure 1-1 Location of Hudiksvall municipality (left) and Iggesund (right, within ellipse).

This report presents the geophysical and geological investigations performed by GEOSIGMA AB and others in the Boda area, close to Iggesund in Hudiksvall's municipality, at the eastern coast of Sweden, figure 1-1. The investigations comprise remote analysis based on aerial photos as well as relief maps, geological field investigations and geophysical investigations.

Figure 1-2 is a close-up of the area showing the topography, the coordinates of the area surrounding the cave, the investigated area and, finally, a rectangle approximately outlining the cave area. The investigated area covers 400 x 400 m. The actual cave area is somewhat smaller, about 150 x 150 m.

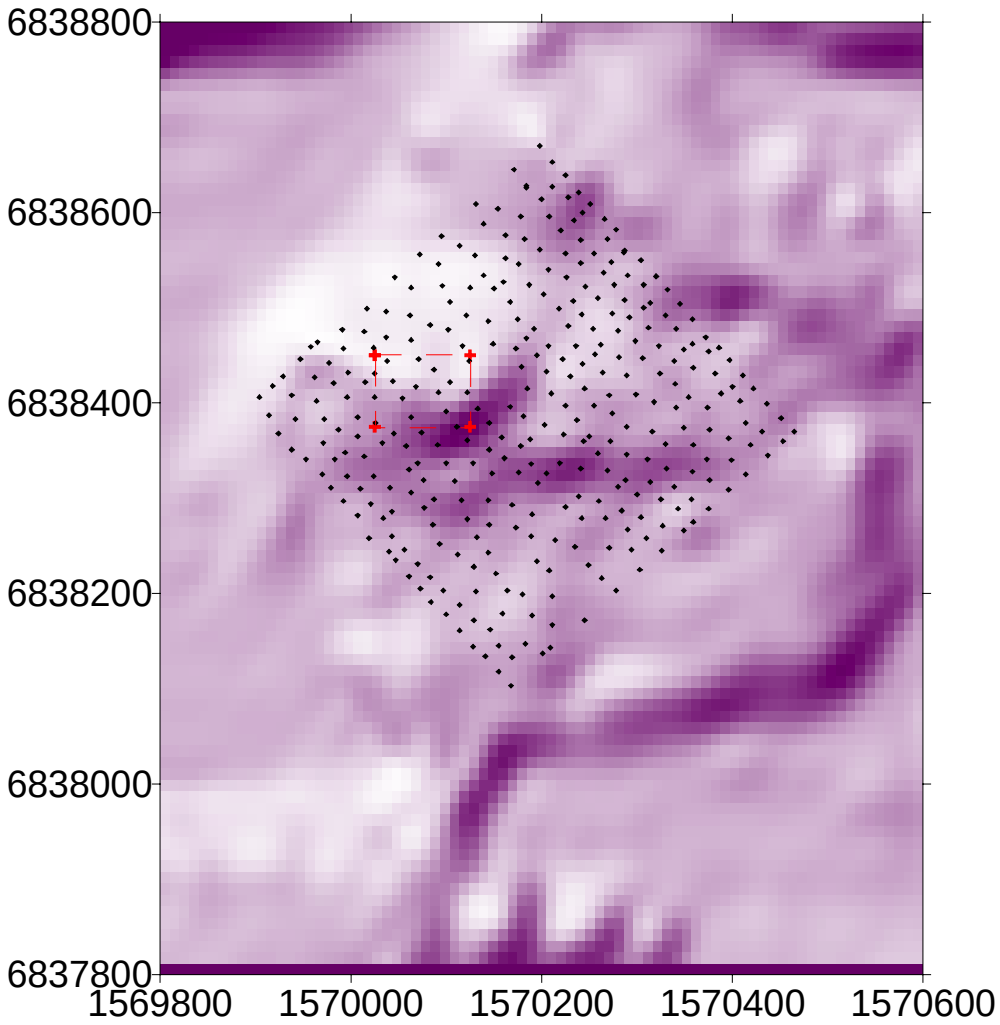

Figure 1-2 Relief map based on the digital elevation database of the area. Dots on map refer to grid points described in section 3. The dashed rectangle outlines the cave area.

1.1 Objective

The objective of the geological investigations and geophysical surveys presented in this report is to produce information that can help in outlining and determining the processes behind the geological phenomena observed at the Boda site.

An important objective of the geological investigation is to find potential lithological and structural differences between the bedrock in the cave area and its surroundings

The main idea with the geophysical investigations is to try to delineate structures within the cave area that extend towards depth. In case of subsequent drilling, the information gained from the surface investigations can be used to choose optimal locations for the placement of boreholes as well as to correlate geology between boreholes.

2 Remote analysis

Remote analysis usually provides important input to site investigations whether it concerns construction on the surface or below. Due to the potential gain, a remote analysis of the structural patterns was performed, although not really part of this project. The objective of the investigations was primarily to place and orient the stake system in order to utilise the geophysical investigations as good as possible. However, the results also give an idea of the regional structural setting, which may help explain the results of the subsequent geological field investigations and geophysical measurements.

2.1 Definition

Remote analysis usually means any investigation/interpretation performed from a birds-eye perspective without physical contact with the studied objects or areas. The main source of information is electromagnetic waves, with wavelengths either within or out of the visible spectrum. Every wavelength of electromagnetic radiation has characteristic properties not only at the source but also in the way the radiation interacts with the earth, through e.g. reflection and absorption. The electromagnetic wave will interact with earth and the reflected energy carries information on the objects from which they were reflected. Examples of carriers of instruments are aeroplanes, helicopters and satellites. Both methods used in this project, which concern structural geological analysis, rely on remote analysis.

Lineaments are structures on the surface of the earth that in one way or another resemble or mimic the structural pattern of the underlying rock mass. The original definition of a lineament (Hobbs, 1903, 1912) concerned topographical patterns in the terrain. However, in well-exposed areas, structures such as fractures and fracture zones may be studied and recorded on outcrops by studying aerial photos. The boundary between lineament interpretation and direct fracture mapping is not well defined. The two types of investigations should be recorded in different ways. This is not the case in the present investigation but, in general, fracture patterns in outcrops are displayed as detailed visualizations of short structures. The longer structures are topographical lineaments. In the Boda area there is also a type of feature not portrayed in topography, fracture patterns or exposed outcrops. This feature appears as a band of a more fine-grained and darker soil type. This feature, discussed in more detail below, is interpreted to be related to the rock mass patterns since it connects to a larger fracture mirror where the structure intersects a smaller rock ridge.

2.2 Material

Remote analysis was performed on two different scales, a regional scale and a detailed scale. LMV's relief map of central Hälsingland (scale 1:250000) provided the base data for the regional scale investigation. This map depicts LMV's digital elevation database

on a 50 by 50 m grid. Detailed remote analysis relied on aerial greyscale photos (scale 1: 30 000, 79 937 01 01-03 SV 157 1 19000 79-05-06, scale 1:30 000). The interpretation of the relief map was performed ocularly while a WILD Aviopret APT1 was used to interpret the aerial photos.

2.3 Interpretation Procedure

2.3.1 Manual interpretation

The relief map or photo is covered with a plastic and interpreted structures are drawn with a 0.3 mm point pencil on the plastic. Only the part of a structure that is visible on the map or photo is actually drawn. Consequently, although a structure can occur at different locations over a distance, the different sections are not connected. All detected structures are recorded irrespective of their respective lengths. The origin of structures with no elevation difference on opposite sides is set as the midpoint of the structure. Where such an elevation difference occurs, the origin of the structure is set to the downside or where the structure is believed to submerge into the ground.

The interpretation is subsequently digitized and systematized. Some corrections of the location of the structures are required in the process since the scale varies within an aerial photo.

2.3.2 Uncertainty

Relief map:

The accuracy in the origin of interpreted structures is about 50 m sideways and in length (as reproduced on the map) approximately 10 to 150 m. The length-measure of a structure, that is the trace drawn on the map, represents the minimum length of the structure.

Interpretation of aerial photos:

The uncertainty in location of interpreted structures depends on the variability in the scale of the photos and the error when transferring the interpretations from the plastic film to the maps. The error is estimated to about 20 to 30 m. Errors in orientation of very short (<25 m) structures is believed to be less than 10 degrees, while for longer structures the error is nil.

Sources of error:

The largest source of error to the interpretation is structures created by man or animals. In forestland, the interpretation is affected by the presence of plantations, boundaries, trenches, electrical facilities and roads. Tracks of different types may disturb the interpretation. Tracks and boundaries often follow natural “boundaries”, such as ravines or river plains. Hence, such features cannot always be interpreted as artifacts

and therefore disregarded. Occasionally the features correlate well. In areas with developed land, such as farmland, structures can be distinguished from variations in the soil humidity.

2.4 Short description of the Boda caves

The Boda caves are located in a relatively flat, coastal, low-elevation area that coincides with the sub-Cambrian peneplain (Rudberg, 1954; Lidmar-Bergström, 1986), which is the flattened rock surface on which relatively thick strata of Cambrian to Devonian sediments began to be deposited about 600 Ma ago. The total thickness of the sedimentary layers was probably some kilometers (Larsson and Tullborg, 1993). Most of these sediments have probably been eroded, at least on land. Cambro-Silurian sediments can be found east of the site in the Baltic Sea. Approximately 10 to 15 km inland from the coast there is a pronounced increase in elevation along a line striking north south (N-S). An elevated plateau characterizes the land beyond this line. Due to erosion, the plateau is now mountainous/hilly terrain, that is, an area with distinct valleys that delimits hills with a relatively constant maximum elevation. The N-S trending barrier between lowland and the plateau is of tectonical origin, probably a fault. Although the age of the fault is a bit uncertain, it was presumably active during Tertiary. The ice movement direction in the area is towards southeast.

2.5 Interpretation of the LMV relief map

The Dellen Lakes are located about 25 km WNW of the Boda cave area, where they cover the central parts of a major topographical depression caused by a meteor impact dated to around 90 million years ago (Pesonen, 1996). The crater is 15 to 19 km wide, which is about the same as the distance to the caves. At the time of the impact, a major part of the sediments was not eroded. The effect of the Dellen impact on the surrounding rock mass is unknown.

Two regional fault lines, oriented WNW-ESE, intersect the Dellen Lakes, cf. Figures 2-1 and 2-2. These structures, with a length of about 50 km, extend towards the coast and control the pattern of the Bay of Hudiksvall. A similar fault line that intersects the Southern Dellen passes about 5 km north of the caves. These structures affect the topography of the Dellen Lakes. A hill, some hundreds of meters north of the caves, is oriented in the direction of the regional fault.

Just south (about 400 m) of the Boda caves an ENE-WSW striking structure can be traced from west at Orsjön to Hornslandet to the east, a distance of around 55 km. Shorter structures (traceable 10 km or less) appear parallel to the above described features. Furthermore, several structures oriented E-W and NNW-SSE occur.

2.6 Interpretation of aerial photos

The major part of the area surrounding the caves is covered with soft deposits, occasionally with large blocks. The blocks usually have sharp edges and rectangular or perpendicular sides. Some sets of blocks originate from a large single block that has fallen apart in place. This suggests that the blocks are of local origin and that new blocks have been formed after transport (by ice). The bedrock is locally exposed along ridges and elevated hills delineated by fractures.

Hills consist of moraine with blocks, fractured blocks to solid rock. Areas with outcrops are usually ridges oriented WNW-ESE. The fracture pattern in outcrops is usually regular. Some of the hills with blocky moraine are more elevated than the ridges consisting of solid exposed rock.

The hill with the Boda caves, cf. Figure 2-2, shows a conforming fracturing in the eastern part. This regular pattern becomes increasingly distorted towards west due to the widening of fracture apertures and concurrent rotation of the blocks. In spite of this, fractures can be traced across the area. The more diffuse parts of the area have a marked variation in block sizes. Towards south, an accentuated NE-SW striking boundary delineates the area with caves, which corresponds to the northern boundary of a depression intersecting the ridge. A less pronounced depression cuts through the western part of the cave area, striking NS (actually just east of north). In the western parts, also an east-westerly depression appears to be discontinued against the NS striking depression. The cave area comprises two perpendicular fracture directions that delineate the blocks. They are NNE and WNW.

The interpretation of the aerial photos also reveals fractures striking NNE-SSW, apart form the fracture directions seen in the relief map. Orientations of structures that coincide in the two sets of interpretations are WNW-SSE.

The area has been influenced by human activities, such as logging and conveyance of vehicles. Consequently, the top layers have been affected significantly. In forested areas, the vegetation is too dense for studies of the ground from aerial photos.

There are no visible disturbances or deformations of soil layers in the cave area.

North of the Byfjärden bay near Iggesund, the railway intersects a sharp structure in the moraine soil cover striking NNE-SSW. This structure, which appears as a dark band in the moraine, extends towards an area with outcrops where it connects with a fracture surface. The structure needs to be studied in the field to determine if the material has been deposited in conjunction with the deformation of the soil layers. No displacements of the ground surface can be detected. This structure is relatively young and may have formed from deformation of the underlying rock mass. If so, the pressure wave formed from an earthquake pressed finer material (soil) up to the surface. This phenomenon is referred to as liquefaction.

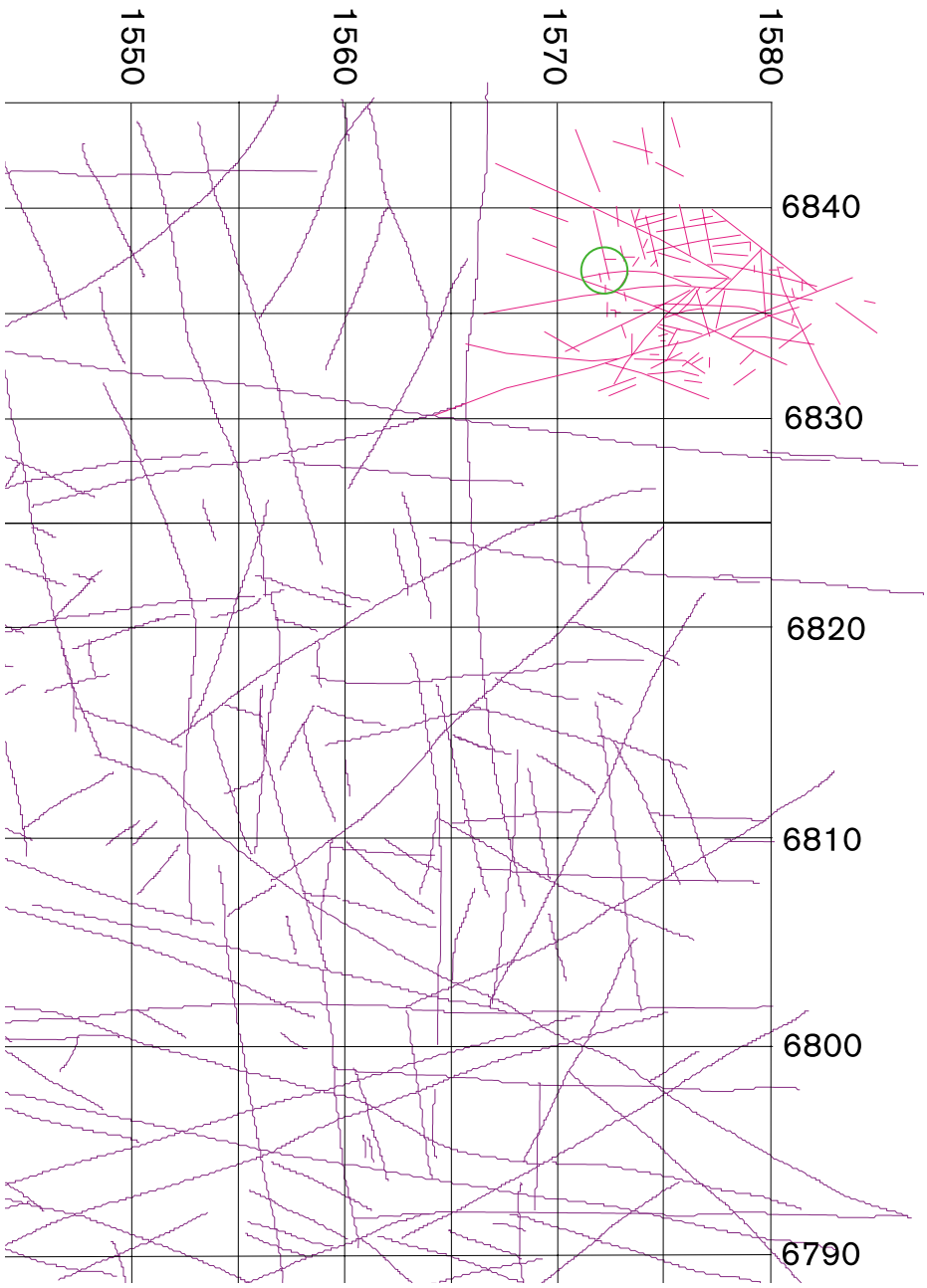

Figure 2-1 Regional lineament map interpreted from a relief map of central Hälsingland, Sweden. The Boda area shows in the northeastern part with a lighter color. Caves are within 1570050 to 1570125 (E-W) and 6838375 to 683425 (N-S), see circle. Note that the area north of 6830 and east of 1565 is interpreted with more detail due to the vicinity to the caves.

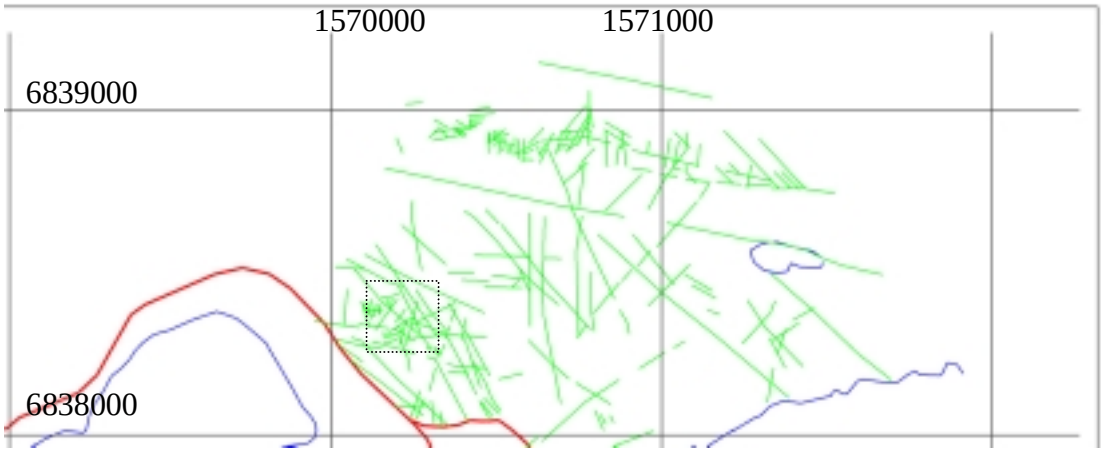

Figure 2-2 Detailed lineament map interpreted from aerial photos of the Boda cave area. Cave area outlined by dotted square.

3 Gridding

From the results of the remote analysis, an area of 400 by 400 m was selected for detailed investigations. The square was rotated to enable as good an investigation as possible of the major structural features found in the remote analysis.

The locations of the points in the grid at the Boda site were determined using the global positioning system (GPS). The grid has been used for all the geophysical investigations performed at the site. In general, GPS provides coordinates with fairly high accuracy (within 1 m) in the horizontal plane. The main reasons for using a GPS-receiver for this project are that the topography is difficult and that vegetation in the area cannot be harmed, as this is a nature reserve. Due to the dense vegetation and variable topography, normal coordinate determination with a theodolite would be very tedious.

3.1 Short description of GPS

The Global Positioning System (GPS) is a worldwide radio-navigation system formed from a constellation of 24 satellites and their ground stations. GPS uses these "man-made stars" as reference points to calculate positions accurate to a matter of meters. With advanced forms of GPS it is possible to make measurements to better than a centimeter. In a sense, it is like giving every square meter on the planet a unique address. GPS receivers have been miniaturized to just a few integrated circuits and so are becoming very economical and that makes the technology accessible to virtually everyone.

The GPS receiver has an internal clock that has to be synchronized with the clocks in the satellites. Furthermore the GPS receiver downloads an almanac from the satellites with information on e.g. orbit (position of satellite) and clock corrections. Timing is essential and recorded times have to be very accurate for the system to work. Very simplified, the receiver works as follows. The satellite sends a message giving an identification number and a time. This message is transmitted with the speed of light to the GPS receiver. The receiver compares the time (given by the satellite) with its internal clock and calculates the transfer time. Since time and velocity are known, the distance to the receiver can be determined. If the receiver is in contact with three or more satellites, it is possible to calculate the horizontal position. If the distances to four or more satellites are known, the elevation at the GPS-receiver can be calculated. The accuracy increases with more satellites.

The satellites used for the positioning were financed by the US military. Consequently, the military authorities want to keep some of the advantages compared to commercial units. Therefore, the signals contain some noise that severely deteriorates the accuracy of positioning. By using a differential system, with a stationary GPS at a known position, it is possible to filter out the noise and to improve the accuracy.

Differential measurements (DGPS) imply that the receiver uses differential corrections from a reference receiver placed at a known location. Alternatively, the corrections may

be received from fixed reference stations. Comparing the reference receiver's absolute recorded position to the known position results in corrections that significantly improve the accuracy (to <1-5 m depending on equipment and terrain). Usually the corrections are transmitted by means of radio in the form of so called RTCM messages enabling corrections in real time.

For the work at Boda we used a differential GPS receiver developed by TRIMBLE Pathfinder ProXL/XR. Corrections to the GPS signals were received from a net of reference stations provided by the Swedish national administration of shipping and navigation. The net consists of seven reference stations that, together with neighboring countries, provide correctional data for the Baltic Sea area. Although, the stations are primarily there for naval users others can use it. This system for correction worked well for this work, since the caves are located fairly near the coast. Farther into the country, a system such as EPOS maintained by Teracom (on the FM band) is better.

3.2 Operation procedure

Prior to the fieldwork, the starting and ending coordinates of each line were picked from a map and entered into the field computer. During fieldwork, the approximate ($\pm$ 1-3 m) location of each point was located using the GPS. At each point several (more than 20) GPS readings were taken, the average of the recordings enabling a more accurate determination of the coordinates for that point.

Initially the starting and ending points were meant to be sufficient to conduct fieldwork in this area. However, due to the difficult terrain and vegetation a grid of wooden splinters, dense enough to ensure ocular contact between points, was established. As results, about 15 coordinate pairs were recorded along each of the 20 lines.

3.3 Results

Combining GPS data and the digital elevation map of the area has produced coordinate files for each profile, Figure 3-1. The files include X, Y and Z coordinates where the Z coordinates are calculated from the digital elevation database (50 by 50 m grid). The main reason for using information from the digital elevation database rather than GPS elevations is due to an assumed poor GPS resolution in height in this area. Elevations are more difficult to establish than the horizontal position, and since vegetation in parts of the area was very dense, elevations where not possible to determine accurately. If a DGPS system manages an accuracy of 1 to 10 m RMS on the horizontal plane the error in height is 5 times as large or up to 50 m (Diggelen, 1998; Starpal, 1998).

The erroneous behavior is obvious in Figure 3-2, which shows a comparison of GPS elevations and data from the digital elevation database. In one of the profiles, the correlation between the two measures of altitude is very good. The other picture, in which some discrepancy appears, is unfortunately more common. All references to elevation in the report hereafter refer to the digital elevation database, except for the elevations used for processing the gravimeter measurements.

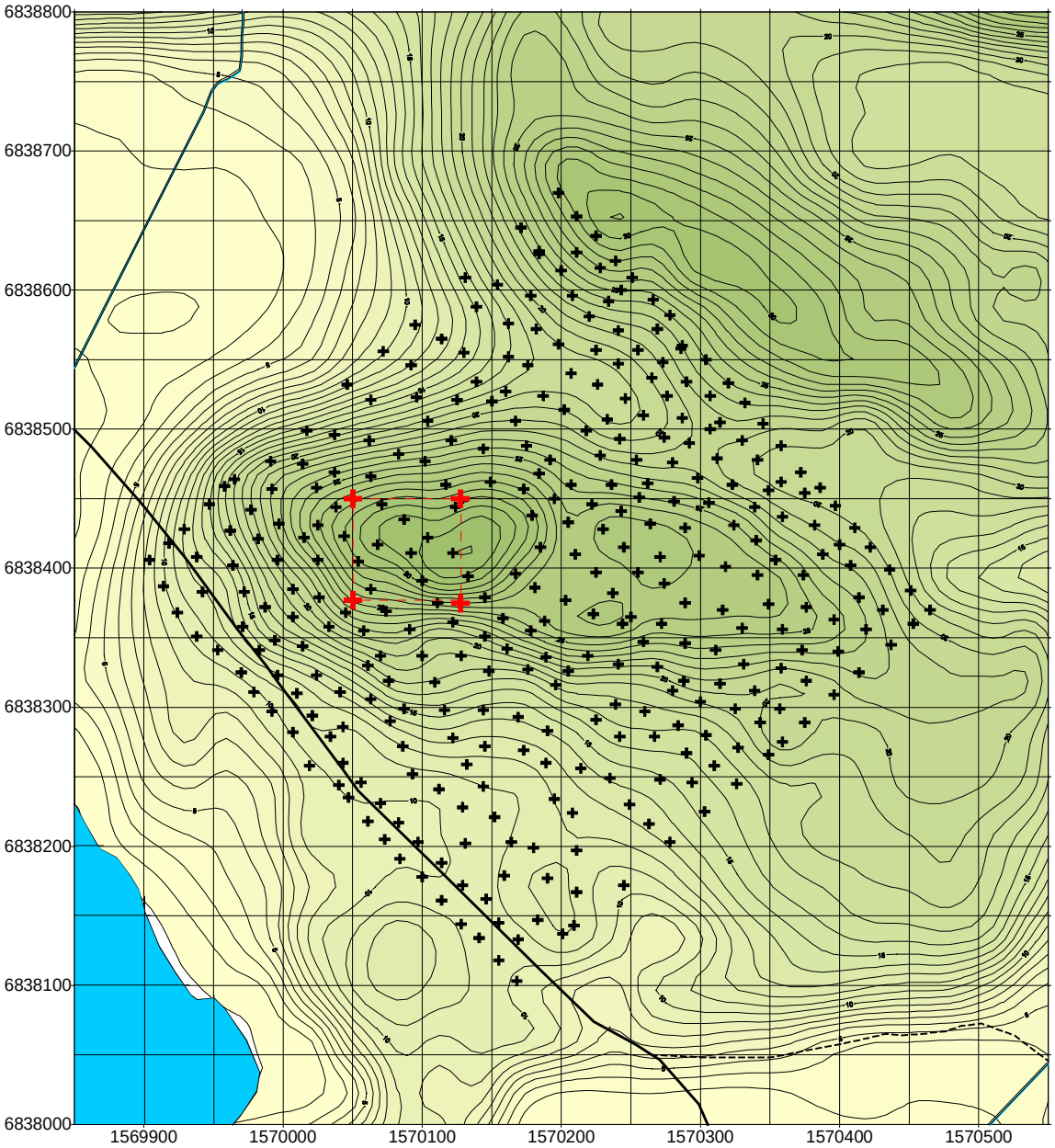

Figure 3-1 Map of area with locations of grid points recorded with GPS. Pluses represent GPS positions. The two linear features are roads where positioning was done with GPS. The dashed square outlines the cave area.

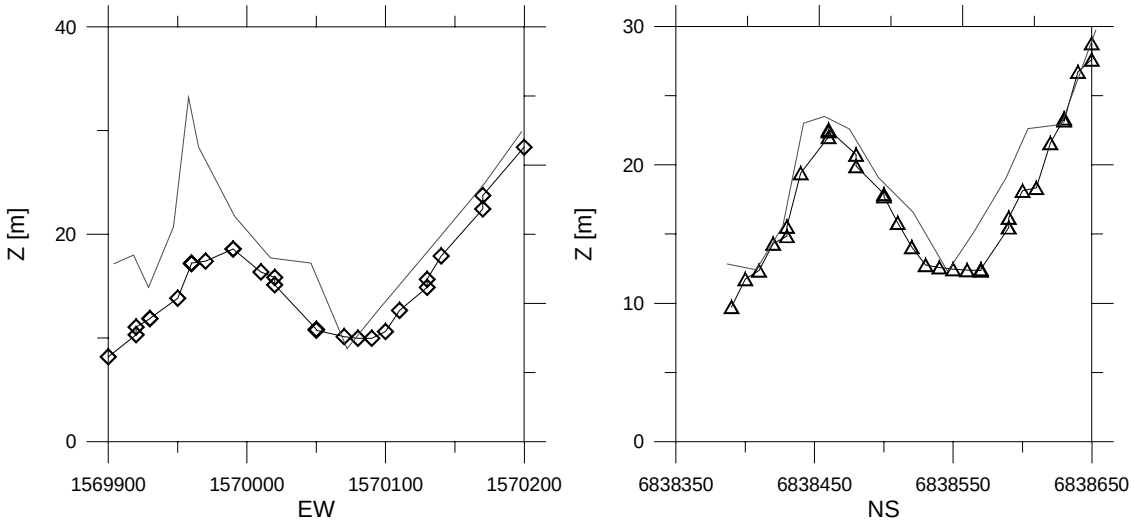

Figure 3-2 Comparison of elevation profile from digital database to GPS from two adjacent profiles showing variation in GPS elevations. Lines with symbols are from digital elevation database.

4 Geologic mapping of the bedrock

This investigation of the bedrock conditions covers an area of about two square kilometers[1]. An important objective of this work was to find potential lithological and structural differences between the bedrock in the cave area and its surroundings. Since rock outcrops are quire scarce in the area, except for around the caves, the outcrops were studied carefully. At each rock surface all current parameters such as rock type, texture, structure etc. were observed (rock surface observations) and recorded. A number of susceptibility measurements were also carried out, primarily for correlation between rock types and the aeromagnetic map. Furthermore, some of the larger cave passages were surveyed, with the aid of a local amateur speleologist, Alf Sidén, to investigate possible discrepancies in the geology underground. The boundary of the cave area on the geologic map (Figure 4-1) is not entirely accurate, since some parts of the field grid are missing. In addition to rock surface observation, a few very large blocks were investigated.

The earth-covered parts in the area were also explored and a detailed survey was carried out in the cave area. The documentation consists of four representative rock samples and 13 slides (of characteristic rock types and essential photographs). To be able to put the bedrock in the Boda caves area in its proper regional context, the immediate surroundings were surveyed and appropriate rock surfaces were visited. The bedrock was extrapolated from the regional bedrock map (SGU Ai 64) in the external parts of the investigated area, were the rock exposure is poor. The results of the investigation are presented in Figure 4-1, which shows the geological map produced for this project, and described in the subsequent sections.

4.1 Material

Topographical maps on the scale of 1:5000 and 1:2500 were supplied by GEOSIGMA AB. Air photo interpreted rock surfaces were transferred to the economical map (LMV, gula kartan 1:20 000). The bedrock map 15H Hudiksvall NV, on the scale of 1:50 000, with the associated aeromagnetic map (SGU Ai 64) was used as a basis for the regional geological interpretation. The VLF-map (SGU unpublished) served to interpret brittle deformation zones in the area.

4.2 Regional geological setting

The bedrock in the southeastern part of Norrland belongs to the Svecokarelian orogeny. This bedrock complex is 1.8 to 2 Ga old and forms a large part of the crystalline basement in eastern Sweden. The Ljusdal Batholith, a granitoid intrusion that extends from the coast of the Baltic Sea to the southern part of the county of Jämtland,

[1] Mapped by Hans Delin, SGU

dominates the bedrock. Its composition varies from granitic to tonalitic, and the characteristic rock type in the intrusion is a gneissic granodiorite with K-feldspar augen, called Ljusdalsgranite. The age of the intrusion has been determined to 1.85 Ga by a number of radiometric datings. The other major bedrock unit in the area consists of transformed (veined and migmatised) sedimentary rocks, generally of argillitic origin, intruded by the above-mentioned granitoides. The bedrock in this region has been subjected to ductile deformation resulting in schistosity and mylonitisation. Heating of the bedrock, together with a pronounced pressure effect due to deformation, has exposed the original rocks in the area of metamorphism up to amphibolite facies. Especially the sedimentary rocks were affected by this and became partially melted (migmatisation). An odd feature in the bedrock is the Dellen Lakes about 20 km northwest of Hudiksvall. The Dellen Lakes resulted from a meteorite impact, forming one of Sweden's greatest meteoric craters, in which the older bedrock (mostly granitoides) was crushed and partially melted into impact rocks. They are the youngest rock formations in the region and have been dated to 100 million years.

4.3 The bedrock at Boda

The bedrock in the investigated area is dominated by an intrusion of Svecokarelian granitoides. In the northwestern part of the area a continuous section of meta-argillite occurs, which also appear as fragments (xenolithes) in granodiorite in an eastwest passage south of lake Drevstjärnen. The rocks are generally strongly metamorphosed and subjected to ductile deformation. The youngest rocks in the area, pegmatite and aplite appear as scattered, cross cutting veins. Figure 4-1 shows the result of the mapping in this project.

4.3.1 Granodiorite

The granodiorite, commonly with augen texture, covers approximately 80% of the mapped area. The gneissic granodiorite is partly veined, red gray to light gray in color, medium-grained and rich in biotite and magnetite. The augen, consisting of light red microcline, vary in appearance and amount within the area. In the eastwestern part of the area, south of lake Drevstjärnen, the rock surfaces become granitic due to an increased concentration and size of augen (increasing the amount of K-feldspar). In this area, a lot of garnets and some cordierite occur in the rock, due to assimilation of aluminum-rich meta-argillite. Further south, approximately in the middle of the area, a narrow passage of augen-free granodiorite appears. The southern part of the mapping area seems to consist of a homogenous granodiorite with small microcline augen. No garnets were observed in this area.

4.3.2 Granite

Granite is found in the northern part of the area. It is gneissic and somewhat veined, red to grayish red in color, medium-grained, and garnet-rich. It generally occurs as augen-granite, but parts without augen exist. Minor amounts of a lightgrey and fine-grained granite appear in the granodiorite passage immediately south of lake Drevstjärnen.

GEOLOGIC MAP OF THE AREA SURROUNDING THE BODA CAVES.

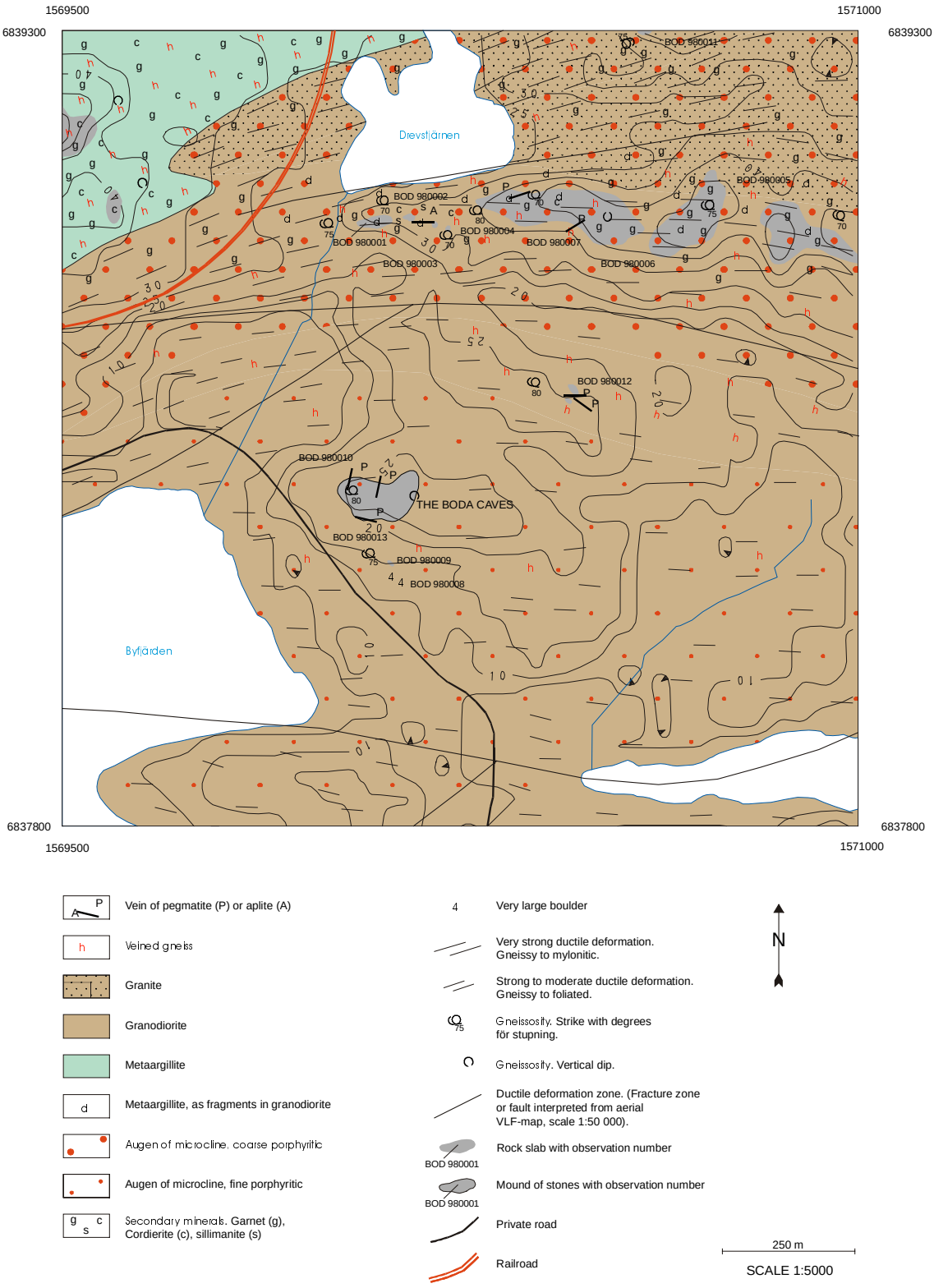

Figure 4-1 Geological map of the area. The cave area shows as an irregular gray shape in the map.

4.3.3 Meta-argillite

Meta-argillite is a metamorphosed, clay-rich sedimentary rock. It occurs in the northwest part of the investigation area, outside the Boda cave area, and as fragments in the north part of the granitoid intrusion. The meta-argillite is generally gneissic and veined, its color gray and grain size fine. It contains garnets in large amounts, a great deal of cordierite, and in some parts even sillimanite. It is also rich in magnetite, which is reflected in high susceptibility ratings. In some locations long drawn out skarn lenses occur, originally formed by carbonate-rich layers in the clay-rich sediments. Occasional fragments of meta-argillite are folded and relatively well preserved, i.e. less metamorphosed.

4.3.4 Veins

In the exposed parts of the investigation area veins of pegmatite are rather common, figure 4-2. A few veins of granite/aplite were also observed. The thickness of the veins varies from 1 cm to 2-3 dm, and the color is red. Most veins dip steeply. The strike, on the other hand, is highly variable.

Figure 4-2 Example of a pegmatite vein.

4.3.5 Ductile deformation

The bedrock in the investigated area has undergone intensive east-west trending ductile deformation, except for veins of pegmatite etc., all formed after the deformation. In the northern part of the area, where a more intensive deformation seems to have taken place, the structure of the rock varies between strongly gneissic and mylonitic. Towards the south, deformation is less pronounced. At the caves, the structure of the granodiorite is gneissic to foliate. The east-west trending structure is regional and can be clearly seen on the aeromagnetic map. The performed structural measurements indicate an approximately east-westerly orientation with a steeply dipping plunge towards south.

4.3.6 Brittle deformation

The most prominent structural evidence of brittle deformation is a couple of faults or fracture zones enclosing the inner part of the Boda cave area. These faults are not exposed, but interpreted from positive VLF-anomalies. Sub-horizontal fracture planes connect some of the large, steeply plunging fractures. The fracture system divides the bedrock into rectangular blocks, a phenomenon quite obvious in the cave area. The rock in the blocks contains few fractures.

4.3.7 Metamorphism

In connection with the above-mentioned ductile deformation, the area was metamorphosed, with the exception of the younger hypabyssal rocks. The occurrence of highly metamorphic minerals such as garnet, cordierite and sillimanite indicates a metamorphic grade of upper amphibolite facies. The bedrock is more or less cut through by narrow, concordant sills of granitic or pegmatitic composition. This implies a temperature of metamorphism close to partial fusion, i.e. anatexis. The sills are more frequent in the northern part of the area and become sparser towards south.

4.3.8 The caves in the area

The exposed parts of the Boda area reveal a central part containing large block slabs, surrounded by an accumulation of somewhat smaller blocks, Figure 4-3 and 4-4. The accumulation of blocks is more pronounced at the southern slope. A survey of the caves proved the more slab-like parts to be somewhat displaced from their original position.

The central area is positioned approximately in its original location, and the larger rock blocks have probably been dislodged at most of a few meters. This conclusion is based on the orientation of the bedrock schistosity in the blocks, that corresponds to structural measurements on surrounding rock surfaces and the regional structure rendered from the aeromagnetic map. One large block with a long travel distance, i.e. well rounded, was observed, Figure 4-5. The entire central area and more than 90% of the surrounding block material consist of a gneissic, light gray, and somewhat porphyritic granodiorite. Minor veins of pegmatite are generally observed, as well as in the caves. The veins are oriented approximately N20°E and N80°W with a generally steeply dipping plunge.

Figure 4-3 Overview of blocks in the central part of the cave area.

Figure 4-4 Overview from the top of the cave area towards west (left). The large entrance to the caves.

Figure 4-5 A well-rounded block.

4.4 Results

Although the investigated area comprises relatively few rock surfaces, the detailed mapping of them displays a lithologically and structurally homogenous bedrock in and around the Boda caves area. The rock is representative of the bedrock in the south of Norrland. The caves are situated in a plinthlike area of accumulated blocks, i.e. local bedrock with relatively small vertical and lateral displacements. The bedrock in the caves consists of gneissic granodiorite with K-feldspar augen. Scattered veins of pegmatite intersect the granodiorite, which is very homogenous. Besides the block-like, large scale, fracture system, the bedrock is relatively free from fractures. The giant blocks southeast of the cave area consist of granodiorite identical with the rock within the caves. In conclusion, there is no indication of any lithological, petrological, or structural anomalies in the bedrock at the Boda caves compared to the surrounding bedrock.

More comprehensive information about the bedrock in the region can be found on the bedrock maps 15H Hudiksvall (SGU Ai64-66), 14H Söderhamn (SGU Ai 27-28) and 16G Ljusdal (SGU Ai 33-36). Detailed petrological information is found in the description accompanying the bedrock map in the county of Gävleborg (SGU Ba 22). The most modern regional survey is found on the map ‘Sveriges berggrund’, in the Swedish National Atlas, volume Berg och Jord.

5 Slingram

The electromagnetic tools are used to measure the bulk conductivity (the inverse of resistivity) of subsurface material beneath the instrument's transmitter and receiver coils This geophysical technique is based on the physical principles of inducing and detecting electrical current flow within geologic strata. Equipment for electromagnetic measurements consists of a source for alternating current, a transmitter, a receiver and an instrument for indicating or recording the resulting signals. A common type of electromagnetic system normally used in site investigations consists of coplanar transmitter and receiver coils with fixed separation. This system is often referred to as a slingram. The slingram, with a horizontal coplanar configuration, operates in the frequency domain, where the current flowing in the transmitter coil is sinusoidal with time, running at a fixed frequency.

In a slingram system, the transmitter and receiver consist of portable coils. Recording of data is performed with a fixed distance between the coils of 20 to 100 m. Both coils are moved along a profile. An alternating current through the transmitter results in a primary EM field. The secondary field is presented in percent of the primary field. The current induced in the receiving coil is divided into a real and an imaginary component. The frequency of the alternating current through the receiver coil is usually in the range 2 to 18 kHz. In areas where the electric conductivity is high (such as clay), a lower frequency might have to be chosen, since a high conductivity reduces the depth penetration.

The depth to which a conductor can be detected depends on several factors. Frequency and electric properties in the ground are important. Other features that affect the detectability are the geometrical properties of the conductor or body to be investigated, the strike of the body and the distance between transmitter and receiver. Typically, increasing the coil separation increases the depth of exploration. A rule of thumb is that steep conductors can be detected at a depth equal to ¾ of the coil distance. Rules of thumb for qualitative interpretation of EM anomalies are summarized in table 5-1.

Table 5-1 Rules of thumb for qualitative interpretation of EM anomalies.

Real	Imaginary	Conductivity of feature
Large	Small	High
Middle	Middle	Average
Small	Large	Poor

5.1 Field setup

The system used here, the SGAB Slingram system, produces an output in units of secondary field as a percentage of the primary field. The transmitting frequency of this system is 18 kHz. The equipment allows measurement of both the "in-phase" (or "real") component and "out-of-phase" (or "quadrature") components of the induced magnetic field. Depth of penetration is roughly considered one-half the coil separation, which would be about 30 m with the separation of 60 m used here. Measurements were recorded every 20 m along each line in the measurement grid.

5.2 Results

Results are presented as contours of real and imaginary components respectively. The variation in the slingram values is small, especially the imaginary values. It is noticeable that the slingram does not seem to be affected by the powerline that runs along the road.

Plots of each profile are available in Appendix 2. The most pronounced anomaly corresponds to the location of the maximum elevation.

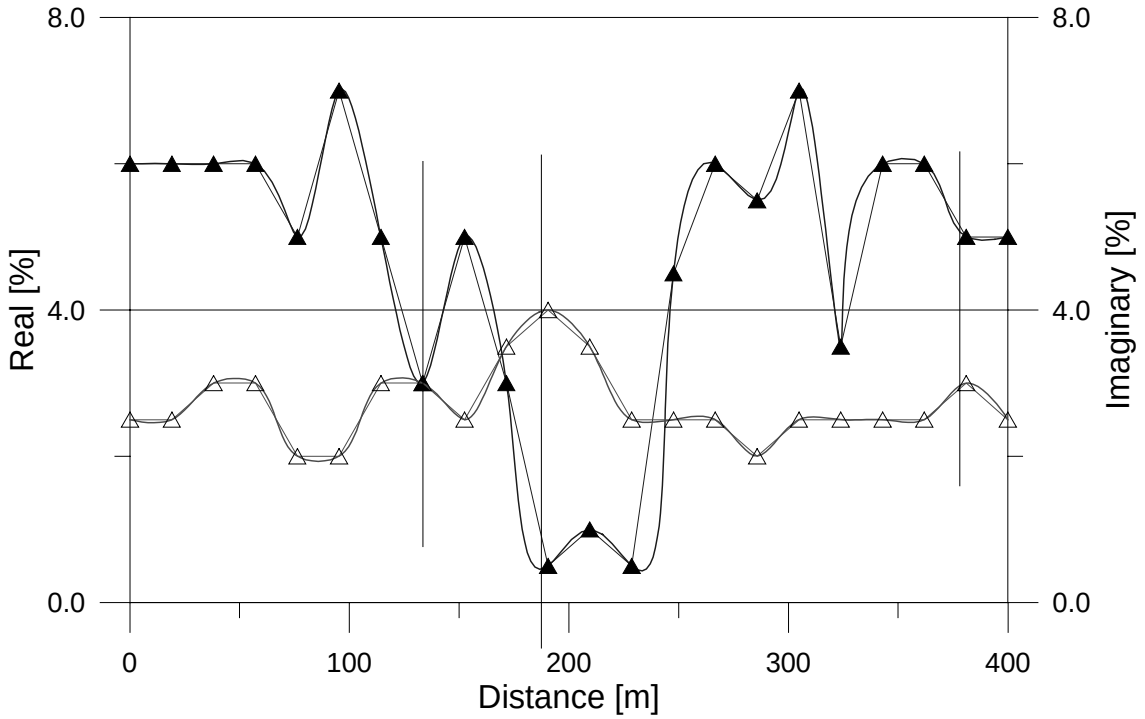

Figure 5-1 Example of slingram profile (profile no. 9). Filled triangles represent real component.

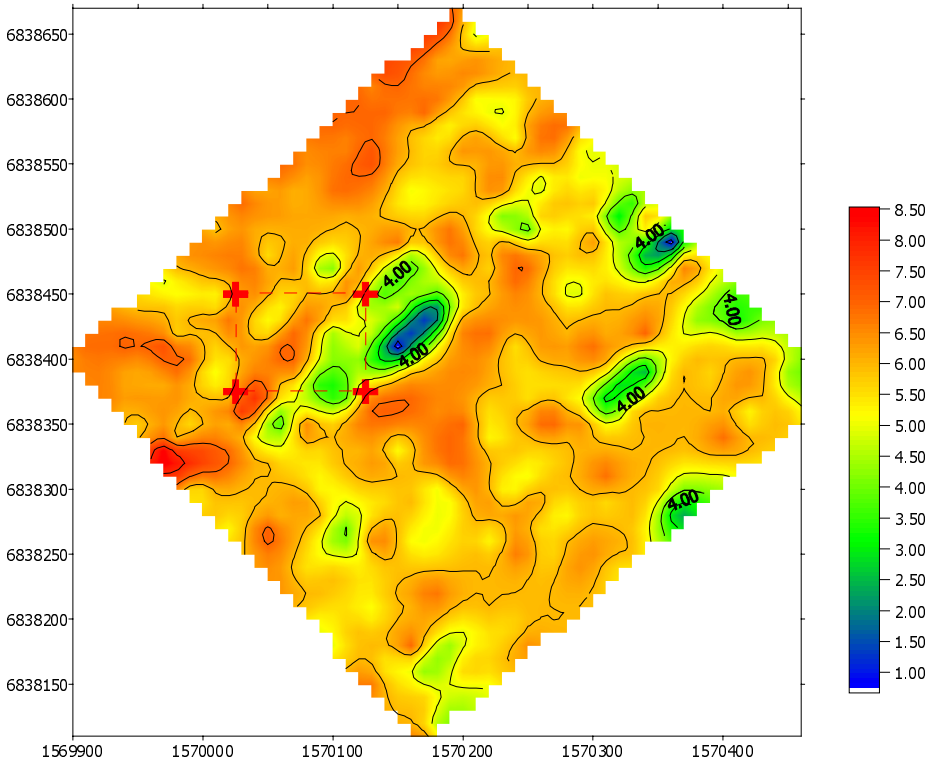

Figure 5-2 Real component of slingram measurement in the Boda area. Dashed square show approximate location of cave area.

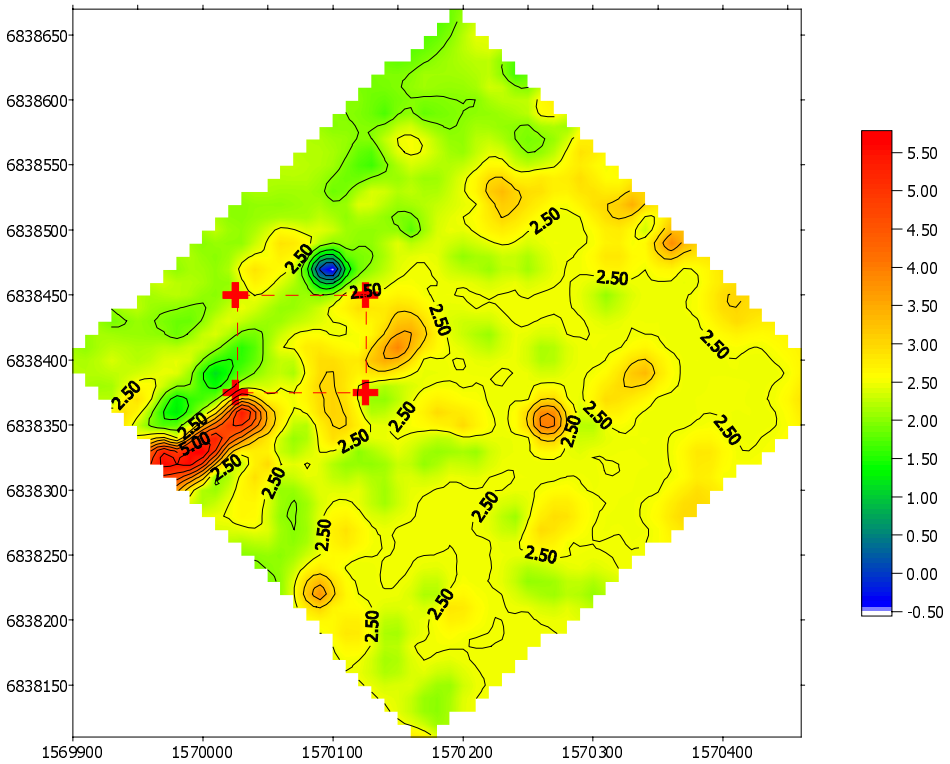

Figure 5-3 Imaginary component of slingram measurement in the Boda area. Dashed square show approximate location of cave area.

6 Ground penetrating radar

The ground penetrating radar (GPR) method provides subsurface information ranging in depth from several tens of meters to only a fraction of a meter. A basic understanding of the function of the GPR instrument, together with knowledge of the geology and mineralogy of the site, can help determine if a GPR survey will be successful. When possible, the GPR technique should be integrated with other geophysical and geologic data to provide the most comprehensive site assessment.

The GPR method uses a transmitter that emits pulses of high-frequency electromagnetic waves into the subsurface. The transmitter is either moved slowly across the ground surface or moved at fixed station intervals. The penetrating electromagnetic waves are scattered at changes in the complex dielectric permittivity, which is a property of the subsurface material dependent primarily upon the bulk density, clay content and water content of the subsurface. The electromagnetic energy is reflected back to the surface-receiving antenna and is recorded as a function of time.

The plot produced by most GPR systems is analogous to a seismic reflection profile; that is, the data are presented with the horizontal axis as distance units along the GPR traverse and the vertical axis as time units (nanoseconds) or depth. During the interpretation, the time axis is converted into distance. Very high resolution (as great as $\pm$ 0.1 m) is possible using GPR. It is necessary to calibrate the recorded features with accurate velocity determinations, actual depth measurements from boreholes or from the results of other geophysical investigations for accurate depth determinations.

Under optimal conditions, GPR data can resolve changes in soil horizons, bedrock fractures, voids and other geological features.

6.1 Field setup

Two sets of data were recorded using different frequencies, 50 MHz and 100 MHz respectively. Data were primarily positioned along a grid (400 by 400 m) with profiles at 20 m distances striking about NNW across the area. The 50 MHz antennas were used to record data along the log lines.

6.2 Processing sequence

A few geometrical corrections are needed before data can be adequately interpreted. Such corrections are here included in the discussion of the processing required. First the data were "connected" to the coordinate system and grid oriented through GPS equipment (raw data contains a length measure only). A third dimension, namely elevation, was added from the digital elevation database described in a previous section. Vertical depths to reflections depend on the velocity used during the interpretation.

These data were converted into depth increments using a constant velocity. This is not entirely correct since the velocity in rock is higher than that in soil. However, the errors in depth are not expected to be very large. These corrections were somewhat tedious and significantly more time-consuming compared to the actual data processing.

When the interpretation software reads raw data, the variation in DC-current is removed simultaneously. Further enhancement of the signals is difficult in most cases and therefore not used very often in this project. The first step of processing involves finding the zero time or the arrival of the airwave pulse. Due to difficult measurement conditions and possible malfunctioning equipment it was necessary to correct for time differences. Once rudimentarily filtered, the depth axis is converted from time to depth.

6.3 Results

Two sets of profiles were recorded in the area. A set of longer profiles recorded with a lower transmitter frequency and a set of shorter, more densely placed, recorded with a higher transmitter frequency. The idea is that the lower frequency signals will penetrate to a larger depth to help in determining the depth of the fractures that appear in conjunction with the caves. The higher frequency would then enable reasonably detailed studies of the cave system.

Examples of data and interpretations can be seen in the figures in the following section while plots of all the radar data are presented in Appendix 3. Note that the plots are not to scale, but vary slightly around 1:1500. Furthermore, there is some confusion in the length annotations since length on the radargrams are given in true coordinates while lengths on the interpretations are given in meters from the start of the profile. Comparisons are still quite easy since the two types of plots have the same length.

6.3.1 Long profiles

The quality of measurements with the 50 MHz antennas varies over the area. During the project, several difficulties occurred, mainly due to the topography and the weather. Nevertheless, the measurements show a sharp boundary that has been interpreted as the boundary between the rock rubble on top and the underlying solid rock mass. In other words, the measurements imply that the caves are merely a superficial phenomenon. Although, this reflection is usually distinct there are short sections where no horizontal reflection can be seen, Figure 6-1.

There are certainly reflections at depths below the “boundary”, Figure 6-2. These reflections are spurious and cannot be traced across longer distance or more than one profile. The quality difficulties mentioned above possibly distort such features, since the deep reflections are significantly weaker than those from the boundary.

There are linear non-horizontal reflections suggesting fractures or other features in the ground. The angles of some of these reflections with the horizontal imply that features on the surface may have caused some reflections.

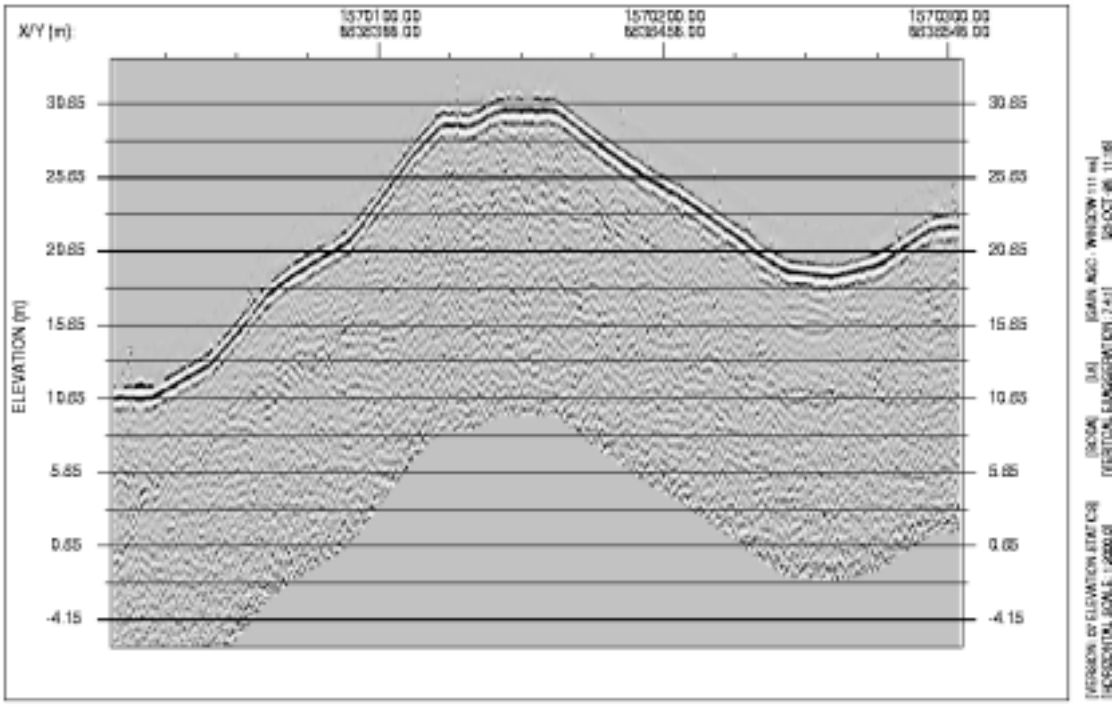

Figure 6-1 Example of radar survey.

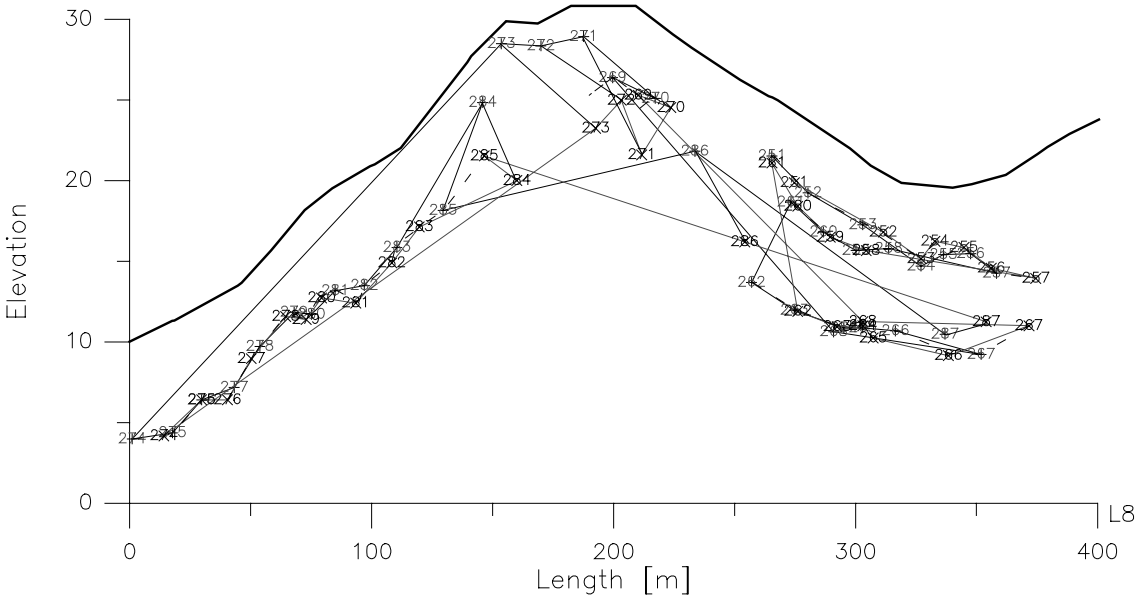

Figure 6-2 Interpretation of radar survey in Figure 6-1. Dashed line corresponds to the interpreted crushed-solid interface. The major part of this interface is probably soil-rock. Straight lines are usually caused by fractures in the rock mass or at block boundaries.

Caves usually appear as hyperbolas on the radar maps, Figure 6-1. Due to the blocky material here, all hyperbolas are, however, not due to caves. Therefore, the map in Figure 6-3 shows locations of all hyperbolas rather than location of caves. The caves show up more distinctly in the measurements with the higher frequency.

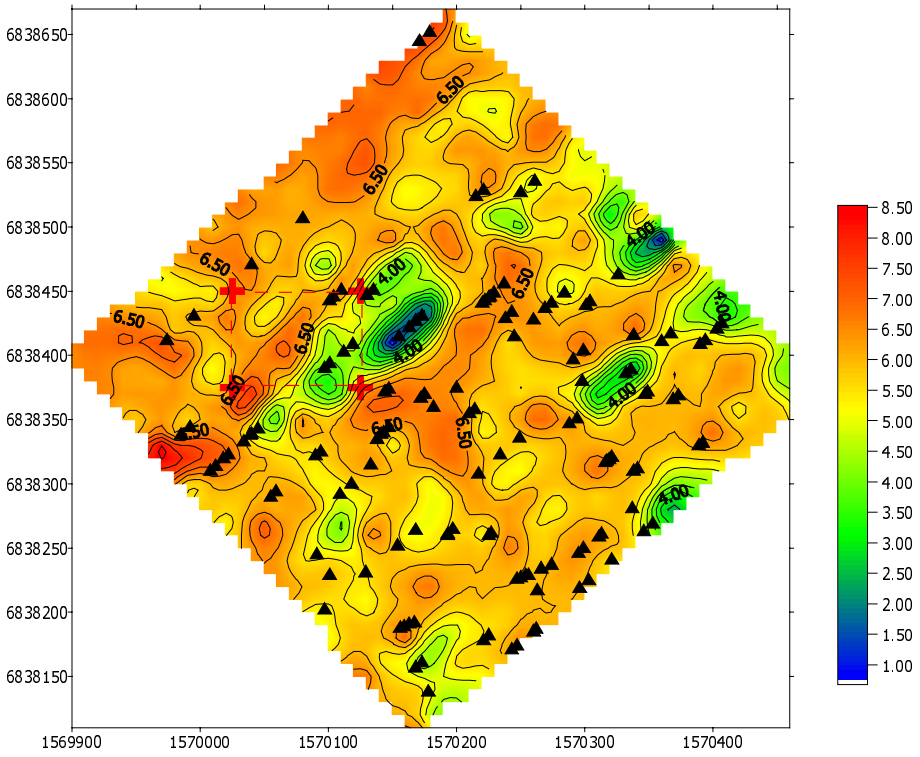

Figure 6-3 Locations of hyperbolas (triangles) plotted together with real component from slingram measurements.

The location of possible caves, Figure 6-3, is plotted together with the real component of the slingram. In some areas, the locations of hyperbolas coincide with anomalies in the real component. In such areas, there are probably cavities. In the center of the area a significant low appears to coincide with several hyperbolas.

If the interpreted boundary is interpolated between the profiles, it is possible to draw a map of the elevation of the rock mass surface, Figure 6-4. Difficulties occur in areas where it is not possible to pick a boundary, for example in the parts most subjected to fracturing, such as in the figure above. The plot of the interpreted rock surface closely resembles the map of elevations from the digital elevation database.

Appendix 3 comprises plots of all profiles.

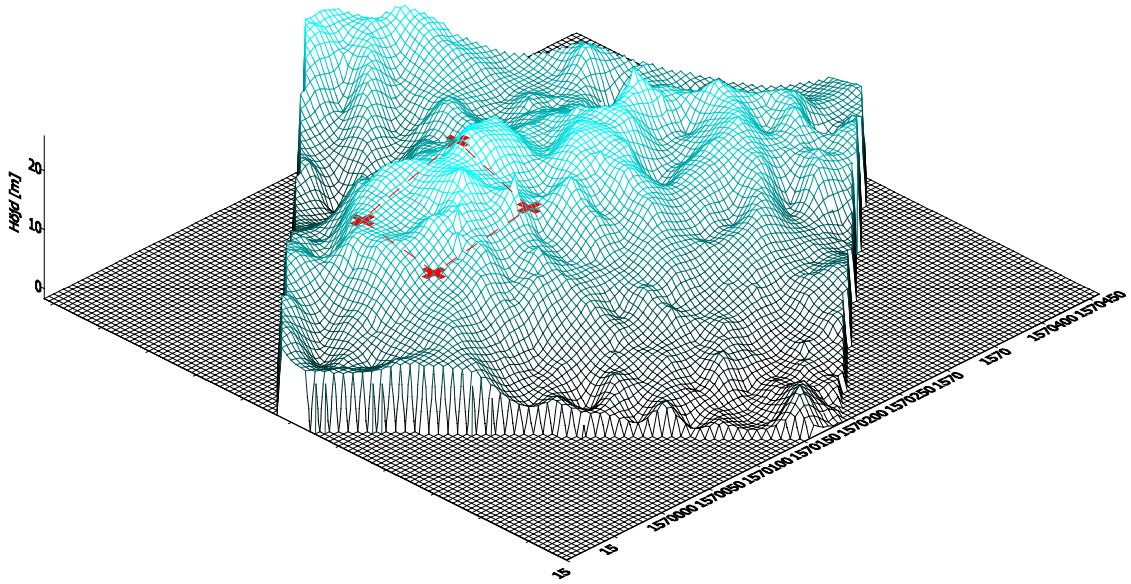

Figure 6-4 3D-plot of interpreted rock surface. Dashed square show approximate location of cave area.

6.3.2 Short profiles

The profiles recorded with the higher frequencies show a slightly different picture. Most importantly, the quite marked layer interpreted as the interface between compact rock and overburden does not appear as clearly. Furthermore, there are more reflections, too many to follow any pattern. This naturally results in difficulties during the interpretation. Caves appear clearly with reflections from the roof as well as from the floor of the opening. In some caves there appears to be layers of water, which results in very strong reflections. Figure 6-5 illustrates an example of a short profile, with the corresponding interpretation in Figure 6-6. Finally, in Figure 6-7 the locations of possible caves are plotted.

The short profile does not help in explaining the origin of the caves. They do, however, give snapshots of the location of caves in the area.

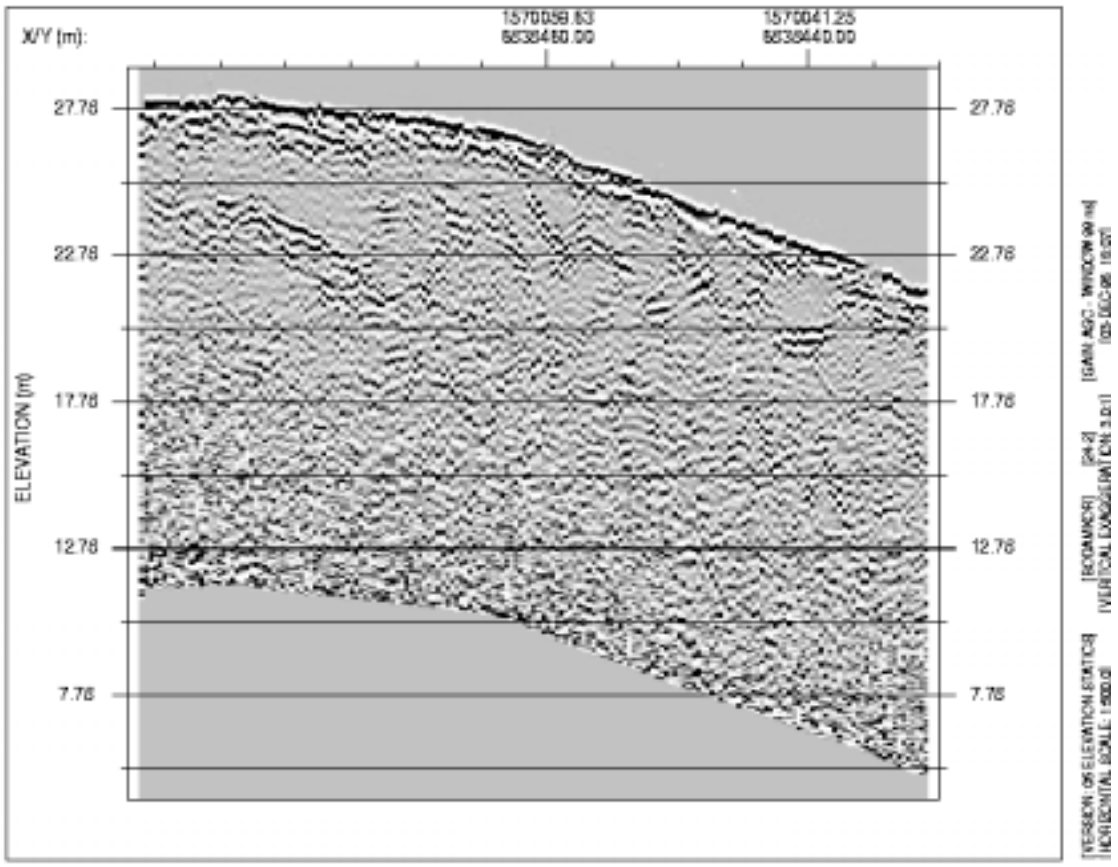

Figure 6-5 Short profile recorded across cave area

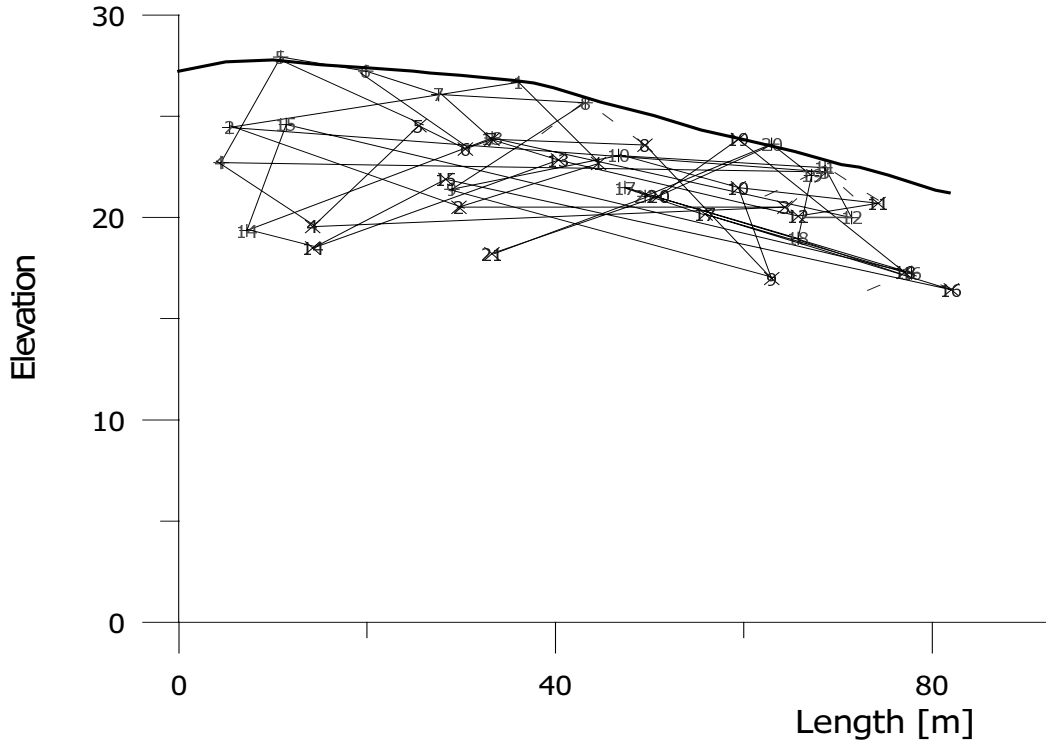

Figure 6-6 Example of interpretation.

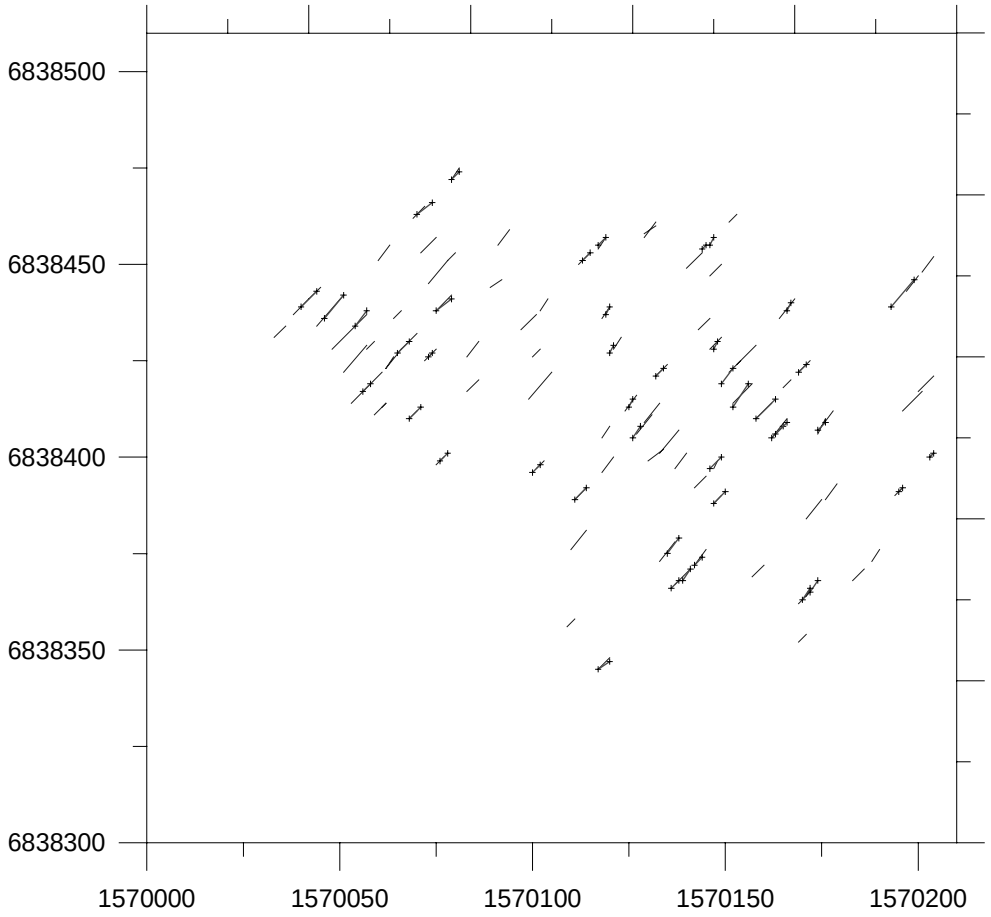

Figure 6-7 Location of possible caves.

Appendix 4 contains plots of all profiles and interpretations.

7 Very Low Frequency measurements

The very-low frequency (VLF) electromagnetic method detects electrical conductors by utilizing radio signals in the 15 to 30 kHz range used for military communications. The VLF method is very effective for locating zones of high electrical conductivity, such as mineralized or water-filled fractures or faults within the bedrock. Another advantage of VLF is that data collection is fast, inexpensive and requires a field crew of only one person. Several VLF transmitting stations operated by the military are located worldwide.

The VLF instrument compares the magnetic field of the primary (transmitted) signal to that of the secondary signal (induced current flow within the subsurface electrical conductor). In the absence of subsurface conductors, the transmitted signal is horizontal and linearly polarized. When a conductor is crossed, the magnetic field becomes elliptically polarized and the major axis of the ellipse tilts with respect to the horizontal axis. The anomaly associated with a conductor exhibits a crossover. As with other frequency domain electromagnetic systems, both the in-phase ("real" or "tilt-angle") and the out-of-phase ("imaginary", "ellipticity", or "quadrature") components are measured.

The VLF method is affected by all electrical conductors, including those that are man-made (power-lines, wire fences, pipes, etc.). The bearing or direction from the VLF transmitting station to the intended target must be located nearly parallel to the strike (or long axis) of the conductor, or intended target for it to be detected. Unfortunately there are only a limited number of transmitting stations available with enough primary field strength to be usable, thus limiting the direction that traverses can be collected. Therefore, the geometry of the target, the survey traverses and the bearing to the VLF transmitting station(s) must be resolved in the survey plan.

7.1 Results

Data were recorded[2] along the same grid as the slingram measurements, which is along 21 lines striking about NW-SE across the cave area. A suitable transmitter is active in Norway, and signals from there were used throughout the survey.

At first data appear to show nothing mainly due to a significant anomaly at the southeastern end of the area caused by a power-line. Removing this anomaly enhances the picture and unveils patterns in the data that suggest a few but significant lineaments that intersect the cave area.

Data do, however, include some other potential errors. The most important being the differences in levels caused by recorded direction and an apparent gradient or trend in the real component. In the plots below, the data are sorted into two groups based on the direction in which data were recorded. Due to potential errors, the data and interpretations therefore should be treated with some care. Significant features that

[2] Recorded by Tröften

appear in both sets of data are probably of geological nature. Some details, however, may, be due to artifacts or a result of the processing.

The relation between imaginary and real components was treated in a previous chapter. Normally VLF data are interpreted according to such theory. Here no interpretation of single profiles is performed. Instead, the VLF surveys are presented in a number of plots showing real and imaginary components of the two different groups of data. The idea is that significant geological features will affect several lines resulting in linear features on a contour map of the data.

Trends in the real component were removed. The effects of the power-line were removed simply by truncating the first 100 m of the data lines. Figure 7-1 shows an example of a VLF profile with trends removed but power-line present. Note that all anomalies are weak compared to the one in the first 100 m of each profile.

Figures 7-2 and 7-3 illustrate the imaginary component of the data. Two marked anomaly trends appear in the plots. The first is an almost N-S trending feature that intersects the x-axis near 107100. The second feature strikes NW-SE (or possibly WNW-ESE). There are other possible features but not as obvious. Figures 7-4 and 7-5 show maps of the real component including lineaments conditioned by the topography.

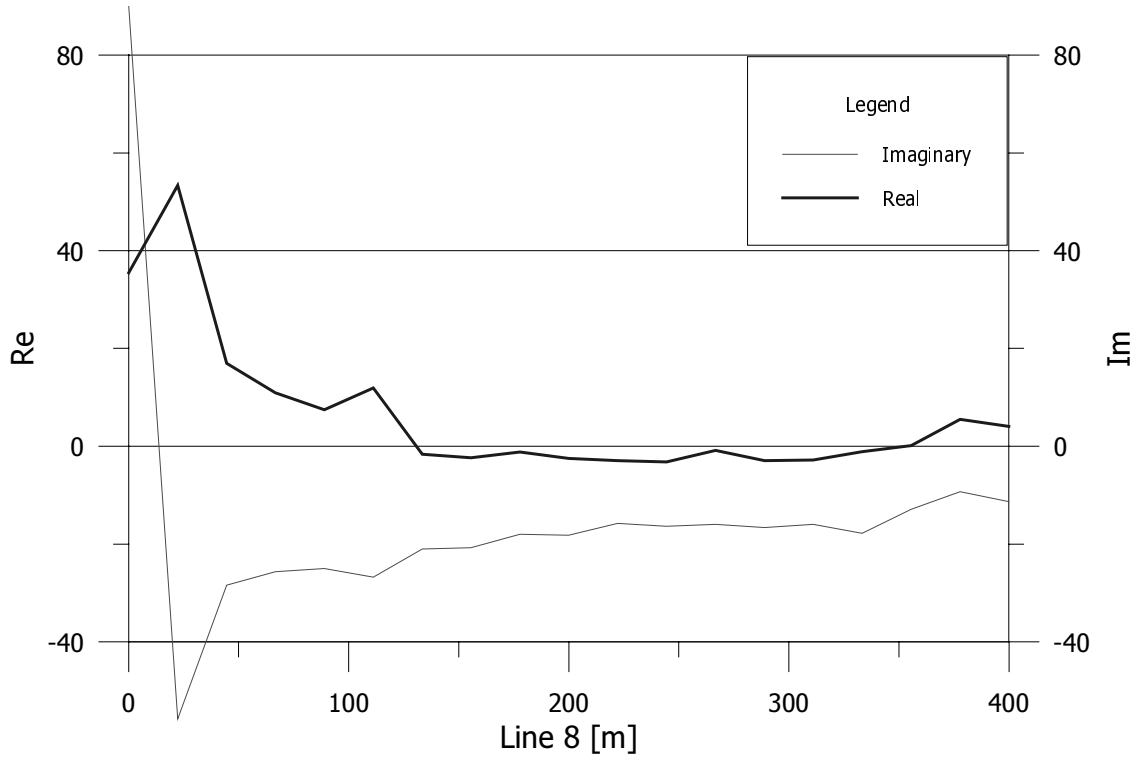

Figure 7-1 Example of single line recorded with VLF. Note the extreme values created by the adjacent power-line at the left end of the plot.

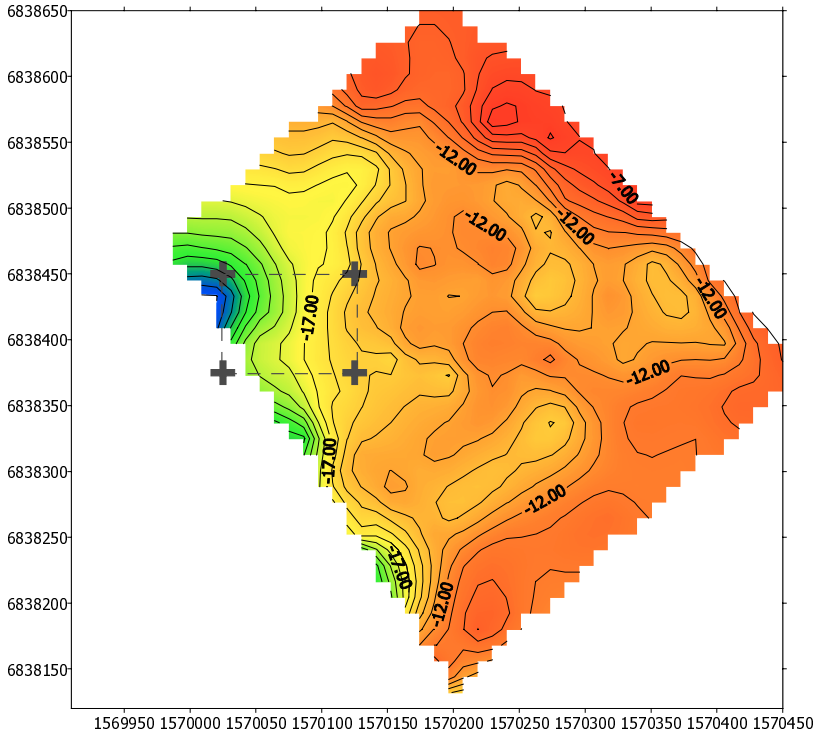

Figure 7-2 Contoured map of imaginary component of VLF surveys recorded east. The effect of the power-line has been truncated.

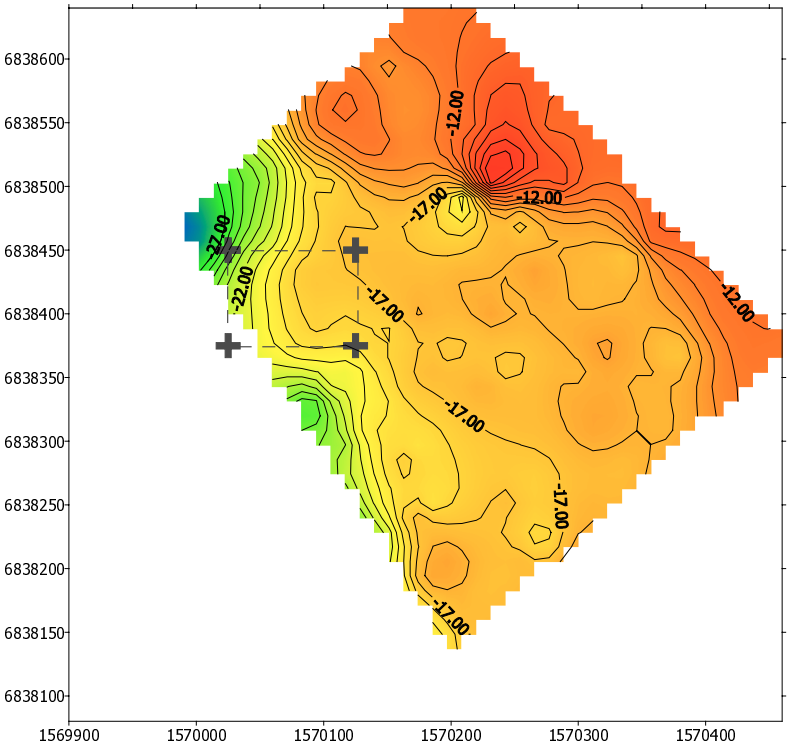

Figure 7-3 Contoured map of imaginary component of VLF surveys recorded west. The effect of the power-line has been truncated.

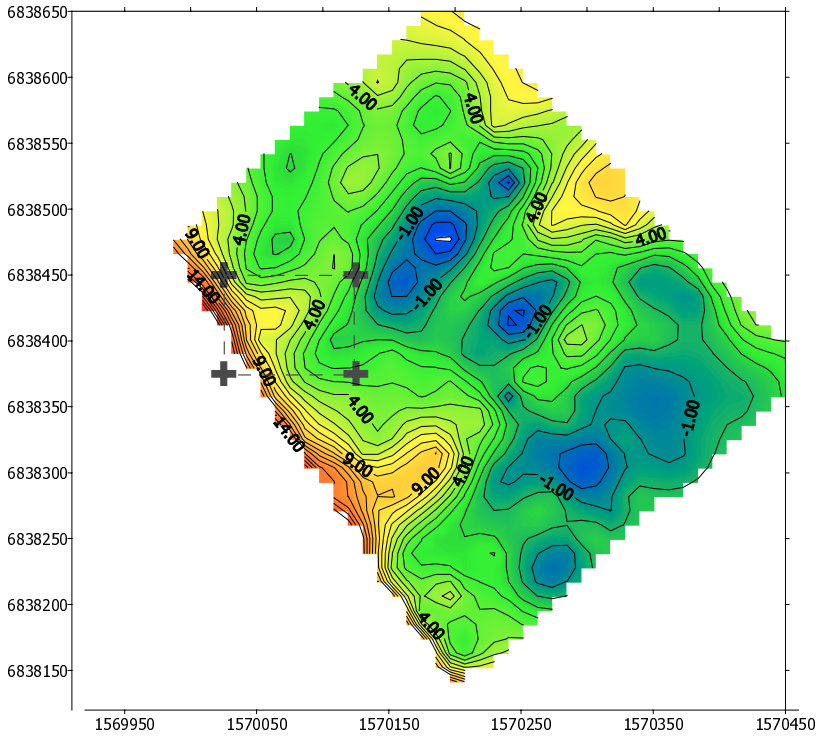

Figure 7-4 Contoured map of real component of VLF surveys recorded east. The effect of the power-line has been truncated.

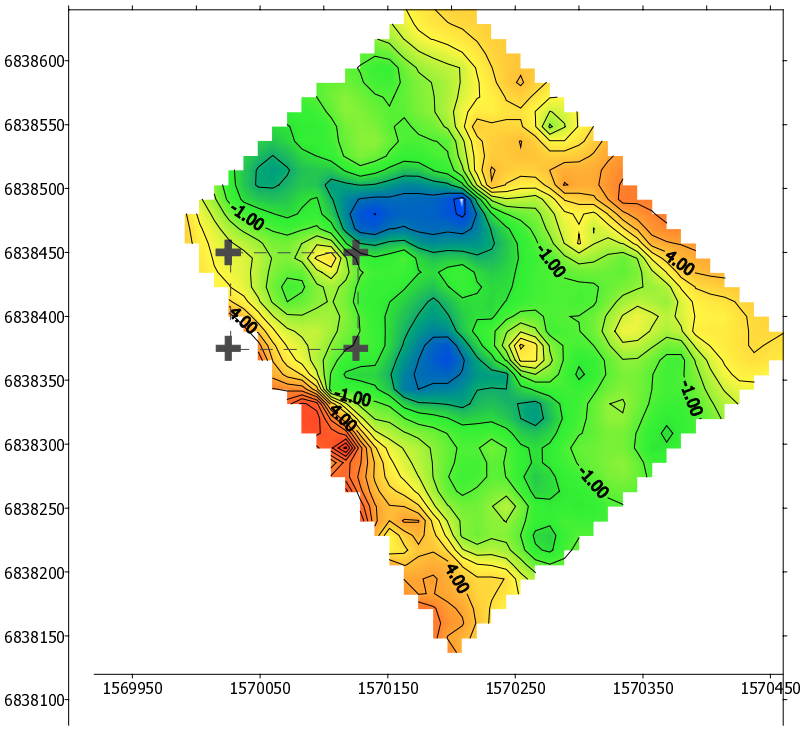

Figure 7-5 Contoured map of real component of VLF surveys recorded west. The effect of the power-line has been truncated.

8 Gravimeter

The gravity method involves measuring the acceleration due to the gravitational field of the earth. The measurements are normally made on the surface of the earth. A gravity meter or gravimeter is used to measure variations in the earth's true gravitational field at a given location. These variations in gravity depend upon lateral changes in the density of the subsurface near the measuring point. Because density variations are very small and uniform, the instruments used are very sensitive. The acceleration due to the gravity of the earth is approximately 9.8 m/s^2 (the unit of measurement commonly used in gravity surveys). The gravity method is useful in delineating buried valleys, bedrock topography, geologic structures and voids.

A disadvantage of the gravity method is that each station has to be precisely surveyed for elevation and latitude control. This could be costly and time consuming, especially in surveys covering large areas. The accuracy of vertical and horizontal positioning is directly related to the resolution capabilities of the gravity method.

8.1 Field procedure

The objective of the gravity survey was to investigate possible anomalies around the caves in the Boda area. This application requires as high accuracy as possible during the measurements. A potentially large error is inaccurate elevation data. The requirements on accurate elevation data were fulfilled using conventional trigonometric measurements. The fixed stake line L0 served as input orientation while an approximate starting elevation was picked from the topographic map.

Measurements were performed with a Worden gravimeter. The reference point was located in the western part of the area. No reference has been made to SGU's or LMV' gravity grid. Measurements were performed every 30 to 80 m in the outer areas, while a point distance of 2 to 25 m was used in the central parts. The surrounding terrain governed the exact location of each point. To obtain the required high accuracy, measurements were usually performed on large rock blocks. Furthermore, to enable surveying there could not be any obstacles deteriorating visibility. Instrumental problems lead to that the northern and eastern part had to be excluded (see below).

8.2 Sources of error

The "real" accuracy of the gravimeter readings is estimated to between 0.2 and 1 m/s^2. The lower number corresponds to points located upon large rock blocks while the higher relates to points located on softer ground. The accuracy of the elevation measurements is better than 1 cm. Some error is accumulated with each new station but as a whole, the error in elevation is estimated not to affect the accuracy of the gravity survey, e.g. result in a maximum error less than 0.1 $m/s^{2.}$

Measurements on the reference point were performed repeatedly to compensate for instrument drift etc. A linear instrument drift is assumed between these recordings. Furthermore, four temporary reference points were established in the area. The error in the reference level depends on whether the assumption regarding linear drift is correct. A reasonable estimate of this error is between 0.2 and 1 m/s^2. The larger number is related to the time interval between reference measurements. This error, however, is corrected for through averaging between adjacent points.

The total error is estimated to 0.3 to 1.5 m/s^2. In the central part of the area, the measurement conditions are good and consequently the errors small, especially concerning differences between adjacent points.

8.3 Corrections and data processing

Measurements have been corrected for instrument drift. Furthermore, data reduction involved calculating the "free-air" and "Bouguer" corrections as well as latitude correction. A density of 2670 kg/m^3 was used for the Bouguer correction. No further terrain correction was performed.

The results were interpolated with kriging to a 4 by 4 m grid. Two different versions are presented where the data variance in the first case was set to zero and in the other to 0.1 (= 0.316 m/s^2). The interpolated values in the prior case connect to the measured values while they in the latter case deviate with an amount related to the given variance.

8.4 Comments on results

The results of the measurements are presented as contoured maps. The top map in Figure 8-1 illustrates the results with a variance of zero, while the lower map corresponds to a variance of 0.1 $(m/s^2)^2$. The latter shows smooth contours with statistically significant gravity anomalies. No major differences between the two maps can be observed. Figure 8-2 shows the gravity map on top of the elevation contours in the area.

Since the objective of the measurements was to locate density contrasts (the caves), the negative anomalies are the most interesting ones. It is quite clear that the anomalies correlate closely with the topography in the area. There is probably a contribution from the fact that the density assumed for the Bouguer correction is lower than 2670 kg/m^3, since there are numerous open fractures. The sharp gradients on the anomalies suggest that shallow structures or features cause the anomalies. There is no negative anomaly over the cave near the entrance (see arrow Figure 8-1).

The gravimeter malfunctioned during the last day in the field prior to completion of the entire area. The northern and eastern outer parts are therefore not covered with gravity data. Since there is no negative anomaly related to the cave, except for the lower density caused by fractures near the surface, there is probably no need to spend more time on

gravity field measurements. Numerical modeling could possibly reduce some error caused by the irregular terrain.

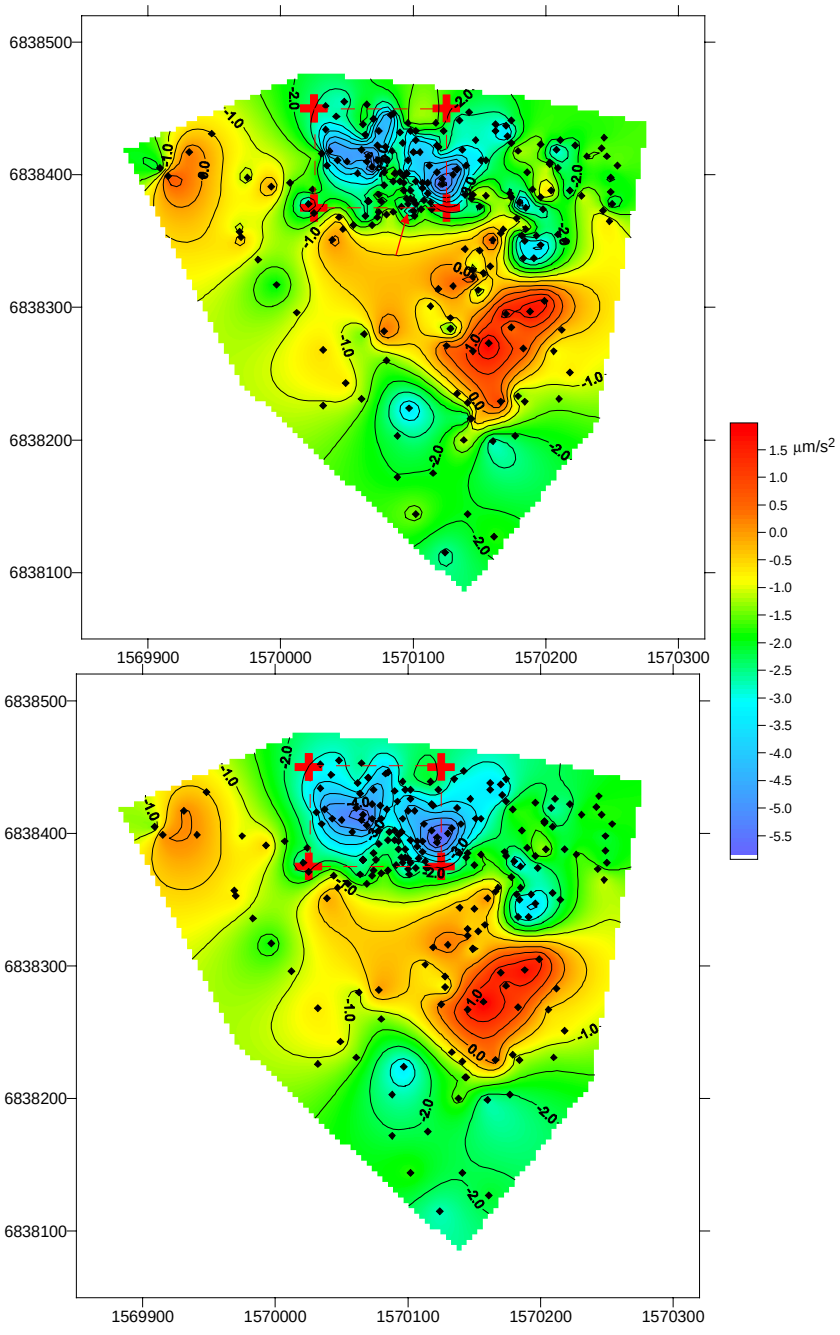

Figure 8-1 Kriged gravity contours with and without variance.

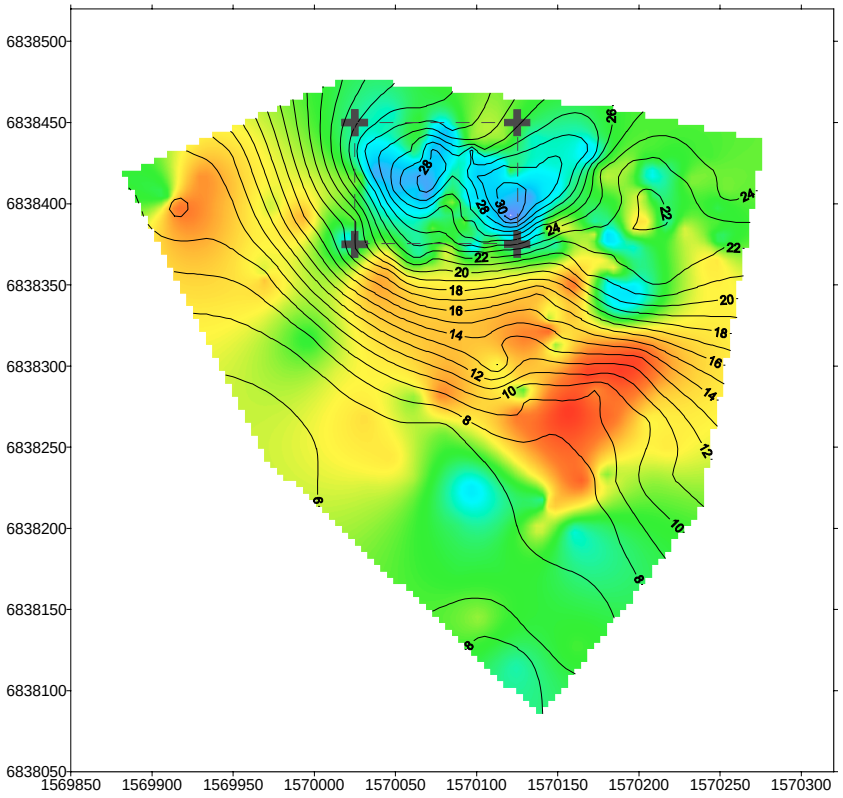

Figure 8-2 Gravity data plotted with elevation contours.

9 Discussion of results

The studies conducted in the Boda area exhibit a severely fractured rock mass with occasional caves. The area appears to be intersected by a few significant zones, obvious from a study of the topography but do appear in some of the geophysical investigations as well. The structures in the area have quite efficiently isolated the rock plint where the caves are located, see Figure 9-1. It is not possible from these investigations, however, to draw far-reaching conclusions about the age and genesis of the zones or about their continuation towards depth.

The geological investigation shows, apart from the caves, no unusual features. The rock types coincide with the rocks found in the region.

The area is highly unsuitable for geophysical investigations. Part of the area consists of scattered and quite large blocks that create giant hurdles for anyone wanting to move around in the area. Since there is little or no soil between the blocks some measurements are not possible to carry out. Furthermore, the scattered blocks cause unwanted reflections and other difficulties that deteriorate the quality of the geophysical data. Nevertheless, data were collected and the results of the investigations are discussed below.

A comparison of some of the different investigations is plotted in figure 9-1. The measurement anomalies are clearly correlated to the topography (lower right) with a significant anomaly corresponding to the maximum elevation. This is not very surprising since larger structures, that may give rise to geophysical anomalies, help shape the topography.

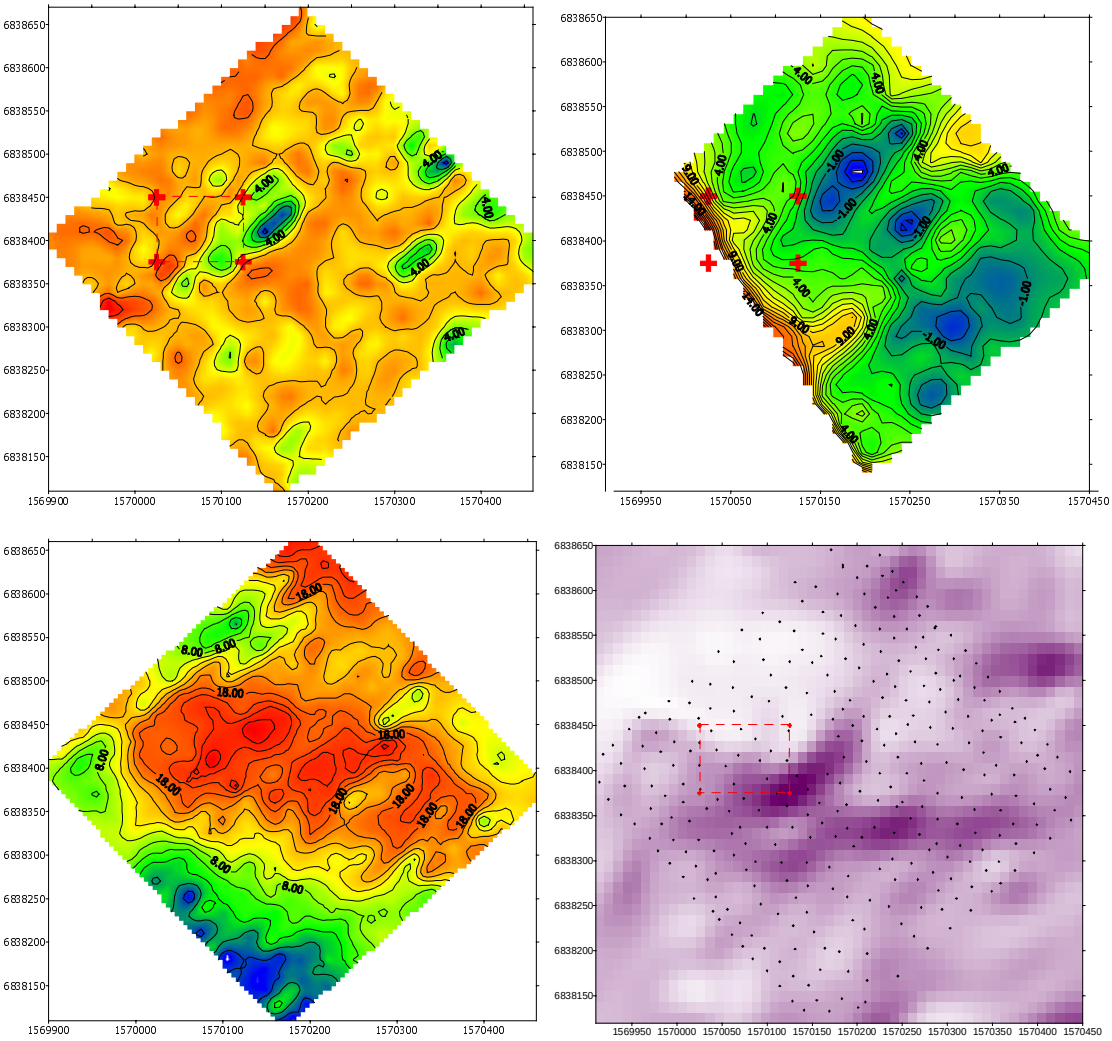

Figure 9-1 A comparison of the various investigations performed at the Boda area. Top left is slingram real component. Top right is real component VLF. Left bottom is interpreted rock surface from radar data. Lower right is topography from digital elevation database.

The radar measurements with the two different frequencies show an interesting result of importance not only to this investigation. The lower frequency appears to penetrate through the rocky overburden and is able to visualize the soil-rock interface. The higher frequency is severely disturbed by the overburden but caves show much more clearly in this data. In this sense the different data sets complement each other although they give little information concerning the possible origin of the caves.

The fractured rock around Boda appears to be a surface feature, since the radar measurements show a quite significant feature throughout most of the profiles, which appears to be the upper boundary of solid rock. There are, however, some occasional strong reflectors below the interface between fractured and competent rock.

The gravity measurements further support the results of the radar survey, since the relatively sharp gradients in the area suggest that the causes are located near the surface.

In conclusion, the investigation described in the report reveal no significantly unusual characteristics of the rock mass except for the significant fracturing. The features possible to investigate with the geophysical methods appear to be located near the surface.

References

Hobbs, W. H., 1903: Lineaments of the Atlantic Border Region. Geological Society of America Bulletin 15, pp. 483-506.

Hobbs, W. H., 1912: Earth features and their meaning. Macmillan Co., New York, p. 506.

Larsson, S.-Å. and Tullborg, E.-L., 1993: Tectonic regimes in the Baltic Shield during the last 1200 Ma - A review. SKB Technical Report 94-05, Swedish Nuclear Fuel and Waste Management Co., Stockholm.

Lidmar-Bergström, K., 1986: Sveriges Relief. Lantmäteriverket, Gävle.

Pesonen, L. J., 1996: The impact cratering record of Fennoscandia. In: H. Rickman and M.J. Valtonen (eds.). Worlds in interaction: Small bodies and Planets of the Solar System. Kluwer Academic Publ., Dordrecht, 377-393. Also appeared in Earth, Moon, and Planets, Vol.72, Nos. 1-3, 377-393.

Rudberg, S., 1954: Västerbottens berggrundsmorfologi, ett försök till rekonstruktion av preglaciala erosionsgenerationer i Sverige. Geographica 25, skrifter från Uppsala universites geografiska institution, Uppsala, p. 457.

SGU Ai 27. 14H Söderhamn NV/NO. 1995. S Sukotjo & S Aaro. Sveriges Geologiska Undersökning, berggrundskartor (för prospektering).

SGU Ai 28. 14H Söderhamn SV/SO. 1995. S Sukotjo & S Aaro. Sveriges Geologiska Undersökning, berggrundskartor (för prospektering).

SGU Ai 33. 16G Ljusdal NV. 1989. H Delin, H Henkel & B Wållberg. Sveriges Geologiska Undersökning, berggrundskartor (för prospektering).

SGU Ai 34. 16G Ljusdal NO. 1989. H Delin, H Henkel & B Wållberg. Sveriges Geologiska Undersökning, berggrundskartor (för prospektering).

SGU Ai 35. 16G Ljusdal SV. 1989. H Delin, H Henkel & B Wållberg. Sveriges Geologiska Undersökning, berggrundskartor (för prospektering).

SGU Ai 36. 16G Ljusdal SO. 1989. H Delin, H Henkel & B Wållberg. Sveriges Geologiska Undersökning, berggrundskartor (för prospektering).

SGU Ai 64. 15H Hudiksvall NV. 1995. S Sukotjo. Sveriges Geologiska Undersökning, berggrundskartor (för prospektering).

SGU Ai 65. 15H Hudiksvall NO. 1995. S Sukotjo. Sveriges Geologiska Undersökning, berggrundskartor (för prospektering).

SGU Ai 66. 15H Hudiksvall SV/SO. 1995. S Sukotjo. Sveriges Geologiska Undersökning, berggrundskartor (för prospektering).

SGU Ba 22. Berggrundskarta över Gävleborgs län. P H Lundegårdh & T Lundqvist. Karta i två blad. Skala 1:200 000. 1966.

Starpal (1998) How to choose a GPS system that suits your needs. http://www.starpal.com/GPS_DGPS.html

Van Diggelen, F. (1998) GPS Accuracy: Lies, Damn Lies, and Statistics. http://www.gpsworld.com/columns/9805innov.html

Appendix 1: Observations of outcrops

The below section discusses a number of geological observations from the Boda area. Each observation is labelled and corresponding labels can be found on the geological map. Numbers in the parenthesis refer to coordinates on the geological map.

Observation no. **BOD980001** (6838935; 1570075) GRANODIORITE, gneissic, redgrey, augen texture, Figure A1-1.

Figure A1-1 Outcrop of augenbearing granodiorite at Observation no. BOD980001. Right picture shows detail.

The rock in intruded by numerous microcline augen, both long and rounded (≤ 10 cm), and a rather dark, biotite-rich matrix. Some drawn-out fragments of meta-argillite containing skarn lenses exist. There are plentiful of garnets, generally in the form of aggregates (≤ 5 cm), and cordierite. Concordant sills of granite/aplite occur occasionally. The granodiorite is strongly deformed, and in part mylonitic.

Schistosity:	N85°E / 75°S
	E-W / 70°S
Susceptibility:	200, 400, 600, 800, and 2000 (10^{-5} SI-units)

Observation no. **BOD980002** (6838945; 1570150) on the geological map.

A GRANODIORITE, gneissic, redgrey, augen texture.

B. META-ARGILLITE, veined gneiss, gray, fine-grained.

C. GRANITE, foliated, light gray, medium-grained.

The main rock (A) is identical with the rock in the previous observation. In the granodiorite, there is a drawn-out fragment of meta-argillite (B) containing garnet and cordierite in great amounts, and some sillimanite in thin layers. Both rocks are strongly deformed and in part mylonitic. A younger concordant sill of aplite-granite (C), with a

thickness of about 2 dm, cuts through the former rocks. The rock surface is transected by a large fracture.

Schistosity:	A. N85°W / 80°N
	B. N85°W / 80°N
Fracture:	N80°W / vertical
Susceptibility:	A. 300, 600, 800, and 2000 (10^{-5} SI-units)
	B. 1000, 2000, and 3000 (10^{-5} SI-units)
	C. 10 (10^{-5} SI-units)

Observation no. **BOD980003** (6838930; 1570205). GRANITE, gneissic, light gray to redgrey, medium-grained.

The rock, with its granitic composition and lack of microcline-augen and garnet, differ from previous observations. It is also somewhat less deformed. Occasionally narrow veins of red granite occur. A large fracture was observed.

Schistosity:	E-W / 70°S
Fracture:	N75°E / vertical
Susceptibility:	5, 20, 40, 80 (10^{-5} SI-units)

Observation no. **BOD980004** (6838920; 1570225). GRANODIORITE/GRANITE, gneissic, redgrey to gray, medium-grained.

A continuation of the previous locality. The rock is somewhat grayer, and the composition is between granodiorite and granite. A small section of the garnet-bearing augengneiss (BOD980001) is visible at the southern border of the rock surface.

Schistosity:	E-W / 80°S
Susceptibility:	100, 200, 400, and 700 (10^{-5} SI-units)

Observation no**. BOD980005** (6839000; 1570735).

A GRANITE, gneissic, greyred, augen texture.

B. GRANITE, gneissic, redgrey, medium-grained.

Rock (A) is characterized by a lot of large, red microcline augen, implying a granitic composition (compare with the granodiorite in BOD980001-2). Fragments of meta-argillite are found in the granite. The matrix of the granite contains garnets. Rock (B) lacks augen and garnets, and is relatively fine-grained. Both rocks are considered protomylonitic, due to strong ductile deformation and slight veining of red granite. The rock surface is fairly free from fractures with large smooth surfaces, completely without steeply plunging fractures.

Schistosity:	N75°E / 75°S
Susceptibility:	A. 400, 800, 1500, and 3000 (10^{-5} SI-units)
	B. 200, 400, and 2000 (10^{-5} SI-units)

Observation no. **BOD980006** (6838920; 1570535). GRANODIORITE, gneissic, redgrey, augen texture, Figure A1-2.

Numerous augen of microcline and small garnets. Strong ductile deformation. Sparse veins of red granite.

Schistosity: E-W / vertical
Susceptibility: 400, 600, and 1000 (10^{-5} SI-units)

Figure A1-2 Perpendicular fracture system illustrating the formation of blocks at observation no. BOD980006.

Observation no. **BOD980007** (6838955; 1570400), Figures A1-3 and A1-4.

A. GRANODIORITE, gneissic, redgrey, augen texture.

B. META-ARGILLITE, veined gneiss, gray, fine-grained.

Rock A is stuffed with red, microcline augen. It is sparsely veined with relatively thick veins of red granite/aplite. A few minor streaks of equigranular granite is observed, and garnet generally occurs. Rock B occurs as numerous, large, either angular or strongly drawn-out, fragments in rock A. The meta-argillite, partly well preserved, contains some skarn lenses, and plenty of garnets and cordierite. The area is gneissic and almost mylonitic in some parts. A few veins of coarse pegmatite cut the schistosity at a low angle.

Figure A1-3 Perpendicular fracture system shows the formation of blocks at observation no. BOD980007.

Figure A1-4 Outcrop with augenbearing granite/granodiorite at observation no. BOD980007.

Schistosity: A. N85°E / 70°S
B. E-W / 70°S
Susceptibility: A. 200, 600, and 1000 (10^{-5} SI-units)
B. 400, 800, 1000, and 4000 (10^{-5} SI-units)

Observation no. **BOD980008 (a large block)** (6838250; 1570130). GRANODIORITE, gneissic, redgrey, augen texture.

The rock surface consists of one very large block and three large blocks. They all consist of a homogenous augengneiss with small microcline augen (smaller than previous observations further north). Some concordant sills and a narrow folded vein of pegmatite were observed.

Susceptibility: 400, 600, 800 and 1000 (10^{-5} SI-units)

Observation no**. BOD980009** (6838295; 1570120). GRANODIORITE, gneissic, redgrey, augen texture.

The granodiorite contains rather small augen of microcline and a few narrow veins of red pegmatite. No garnets or other mineral indicators were observed.

Schistosity: N85°E / 75°S
Susceptibility: 600, 1000 and 1500 (10^{-5} SI-units)
Miscellaneous: Bearing in mind the size of the blocks at the previous observation, some uncertainty about the rock surface being a block or not exist, but the orientation of schistosity agree with the general orientation in the area.

Observation no. **BOD980010 (blocks)** (6838435; 1570025). GRANODIORITE, gneissic, redgrey, augen texture, Figure A1-5.

The rock surface is situated within the cave area and gives a first impression of solid rock. An underground survey proved this part somewhat lifted/moved. However, the strike and dip of the rock is in accordance with other measurements in the area. The granodiorite is exceedingly homogenous with large (1-2 cm) augen of microcline, most of which are lens shaped. A cm-thick vein of pegmatite was observed.

Schistosity: N85°E / 80°S
Susceptibility: 400 and 600 (10^{-5} SI-units)

Observation no. **BOD980011** (6839290; 1570600). GRANITE, gneissic, greyred, medium-grained.

The rock surface is situated at the northern border of the investigation area. The homogenous granite is strongly gneissic, partly red in color, and contains garnets in abundance. The magnetic susceptibility of the granite is low compared with the dominating granodiorite rock in the Boda area.

Schistosity: N60°E / 75°N
Susceptibility: 10, 20 and 200 (10^{-5} SI-units)

Figure A1-5 Outcrop with porfyric granodiorite in the cave area, observation no. BOD980010.

Observation no. **BOD980012** (6838625; 1570460). GRANODIORITE, gneissic, redgrey, medium-grained.

A very homogenous rock with a limited number of pegmatite veins. A few augen of microcline are scattered here and there. A large, concordant sill of coarse pegmatite intersects the rock surface, and a narrow (2 cm) pegmatite vein runs perpendicular to the former.

Schistosity:	N70°W / 65°S
Contact:	N80°W / not meas. (pegmatite vein)
	N55°W / not meas. (pegmatite vein)
Susceptibility:	1000, 1500, and 2000 (10^{-5} SI-units)

Observation no. **BOD980013 (blocks)** (6838385; 1570065). Figure A1-6. GRANODIORITE, gneissic, redgrey, augen texture.

The rock surface is situated at the main entrance of the Boda caves. The granodiorite contains numerous small (≤ 1 cm) augen of microcline, and a couple of large augen as well. A coarse vein of red pegmatite cuts through the rock. Besides the general schistosity, a narrow concordant ductile shear zone was observed. The measured orientations must be considered approximate because of block emplacement. However, the strike and plunge do not diverge particularly much from the general orientation of the bedrock in the area.

Schistosity: N80°E / varying plunge
Contact: N75°W / varying plunge (pegmatite vein)
Susceptibility: 400, 600, 800, and 1000 (10^{-5} SI-units)

Figure A1-6 Outcrop with porfyric granodiorite in the cave area, observation no. BOD980013.

Appendix 2: VLF and Slingram, Profile 1.

VLF (top), Slingram (middle), GPR anomalies (bottom)
VLF measurements have been truncated in vicinity of powerline.

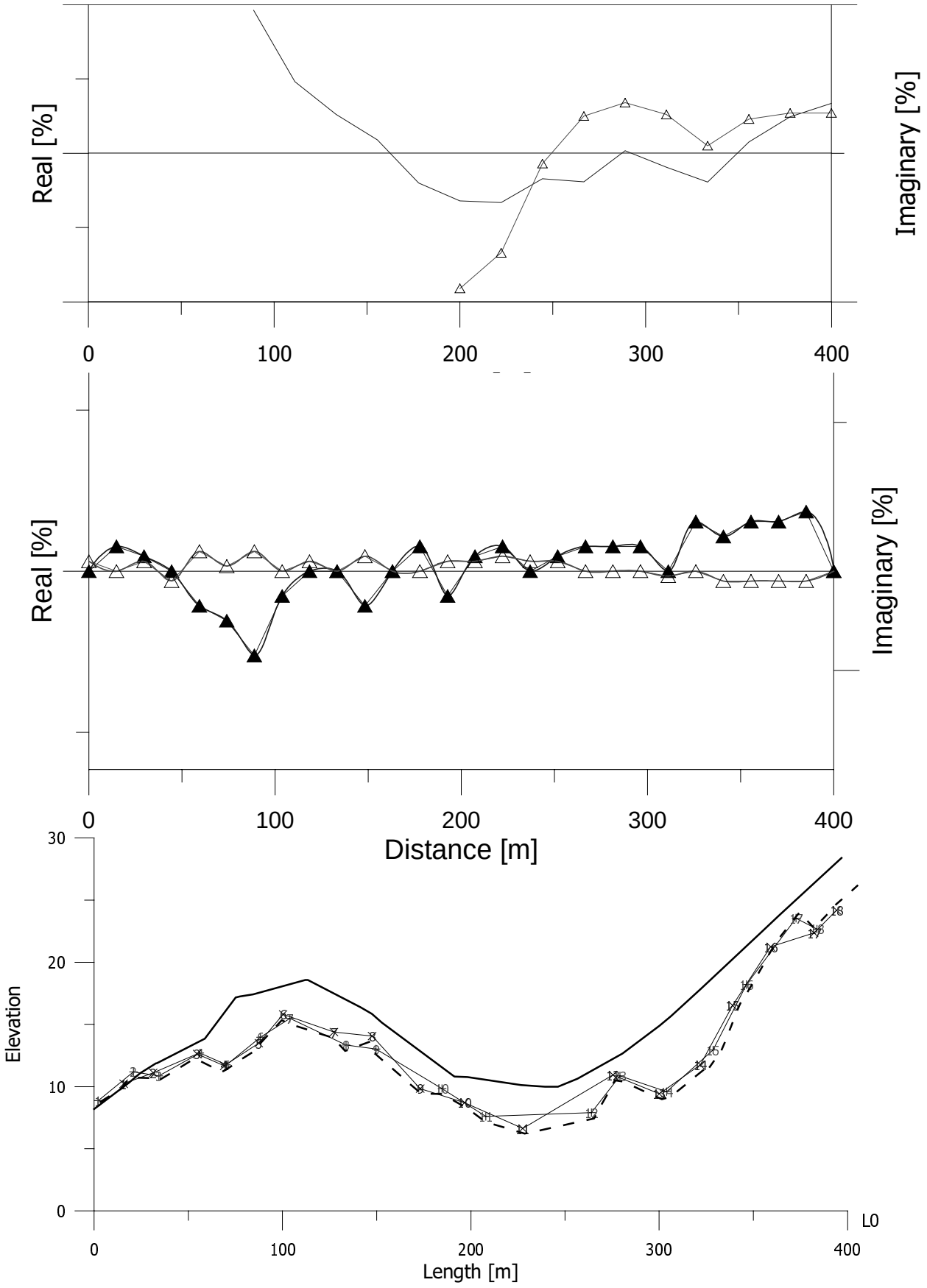

Profile 2.

VLF (top), Slingram (middle), GPR anomalies (bottom)
VLF measurements have been truncated in vicinity of powerline.

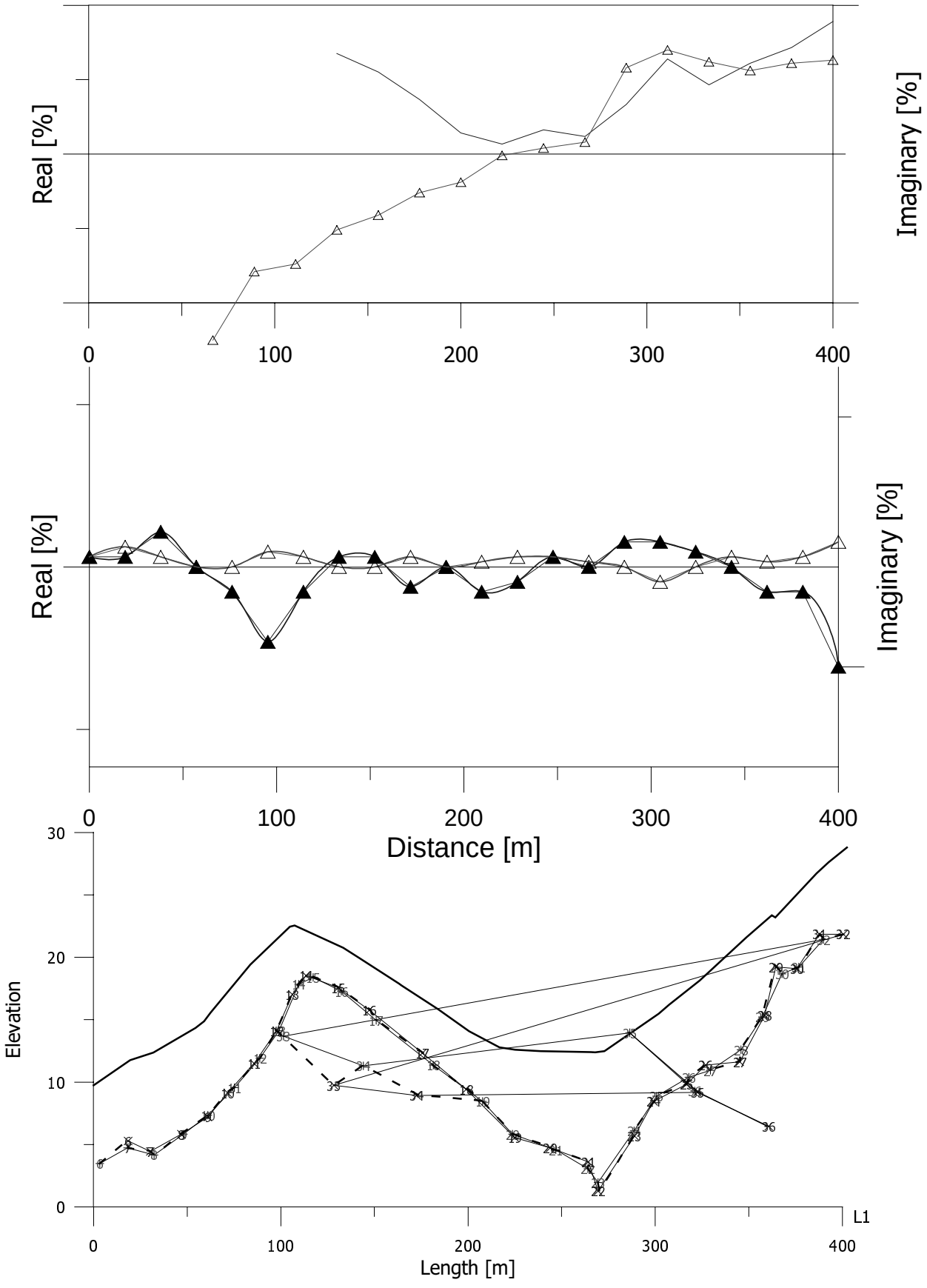

Profile 3.

VLF (top), Slingram (middle), GPR anomalies (bottom)
VLF measurements have been truncated in vicinity of powerline.

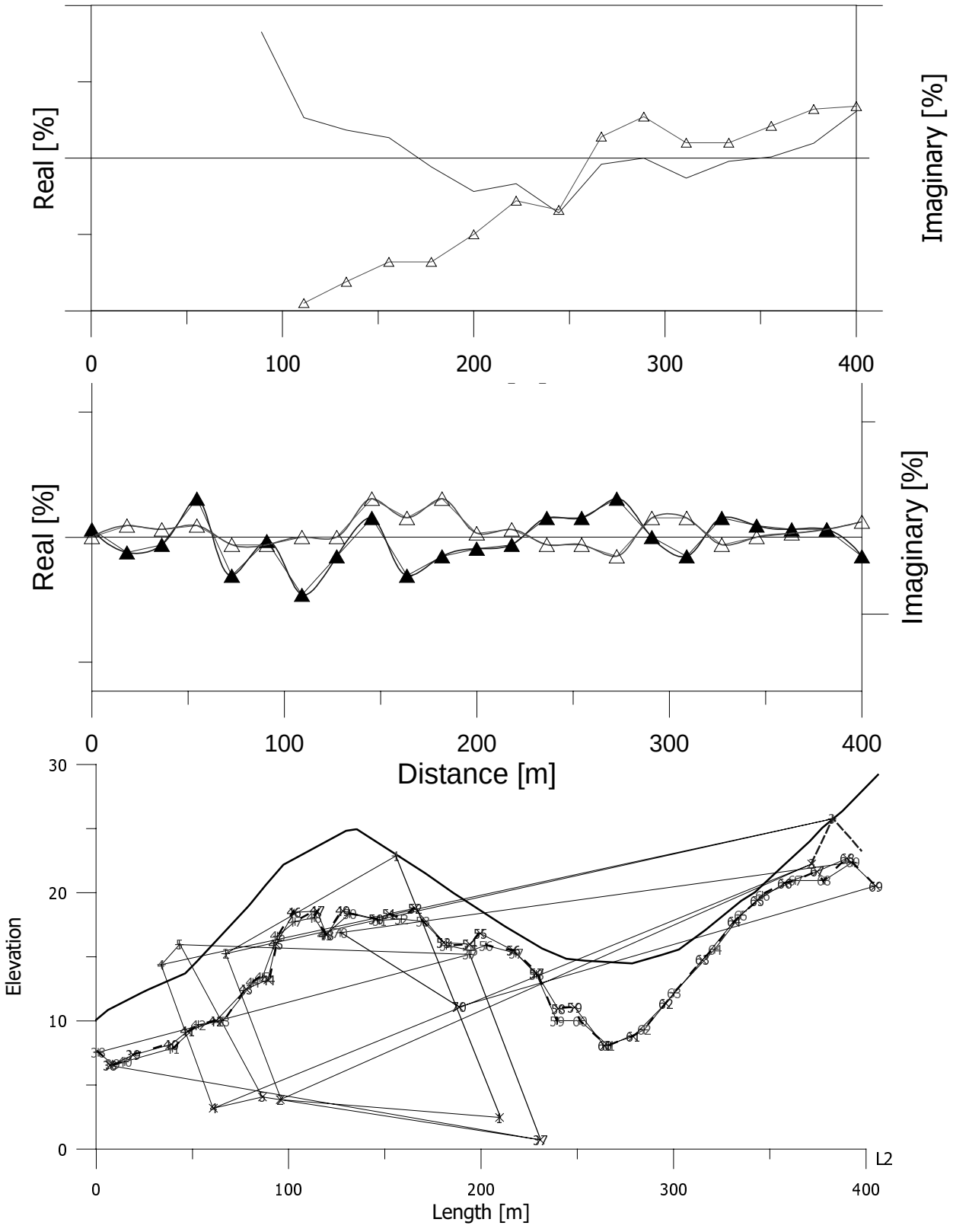

Profile 4.

VLF (top), Slingram (middle), GPR anomalies (bottom)
VLF measurements have been truncated in vicinity of powerline.

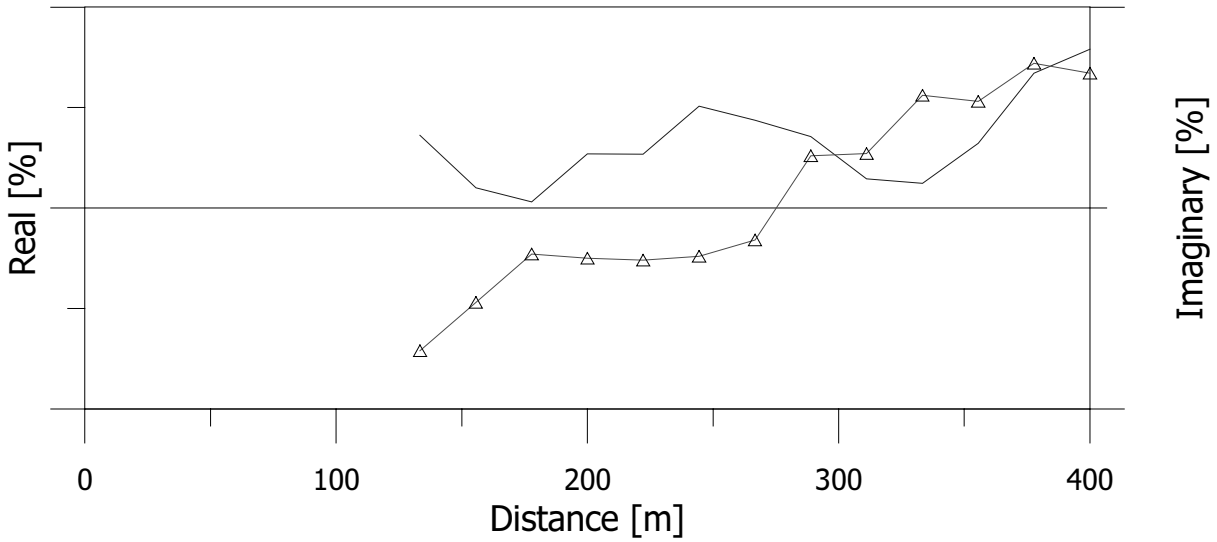

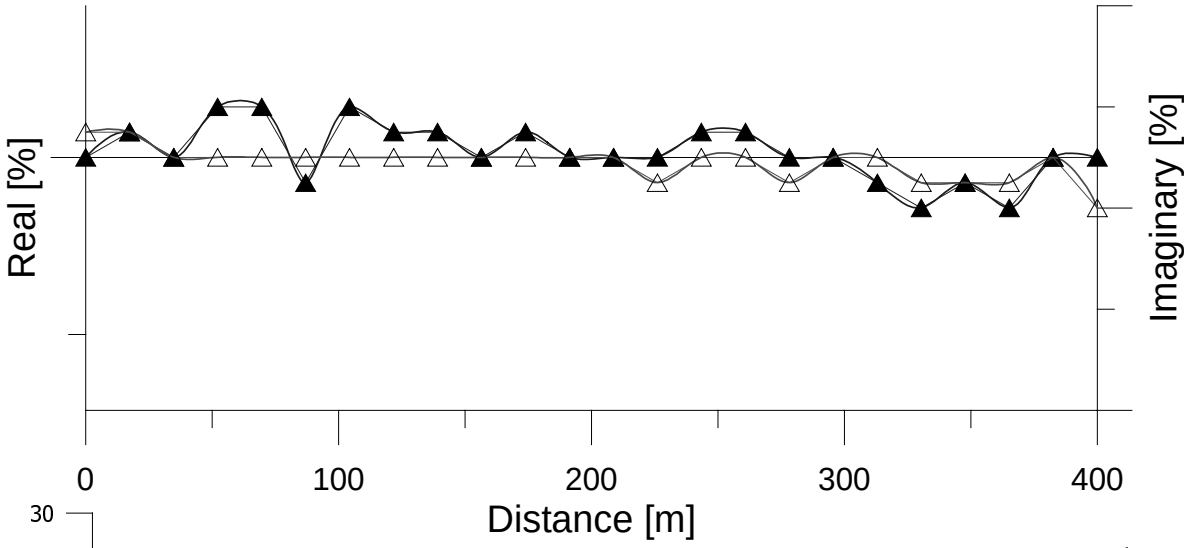

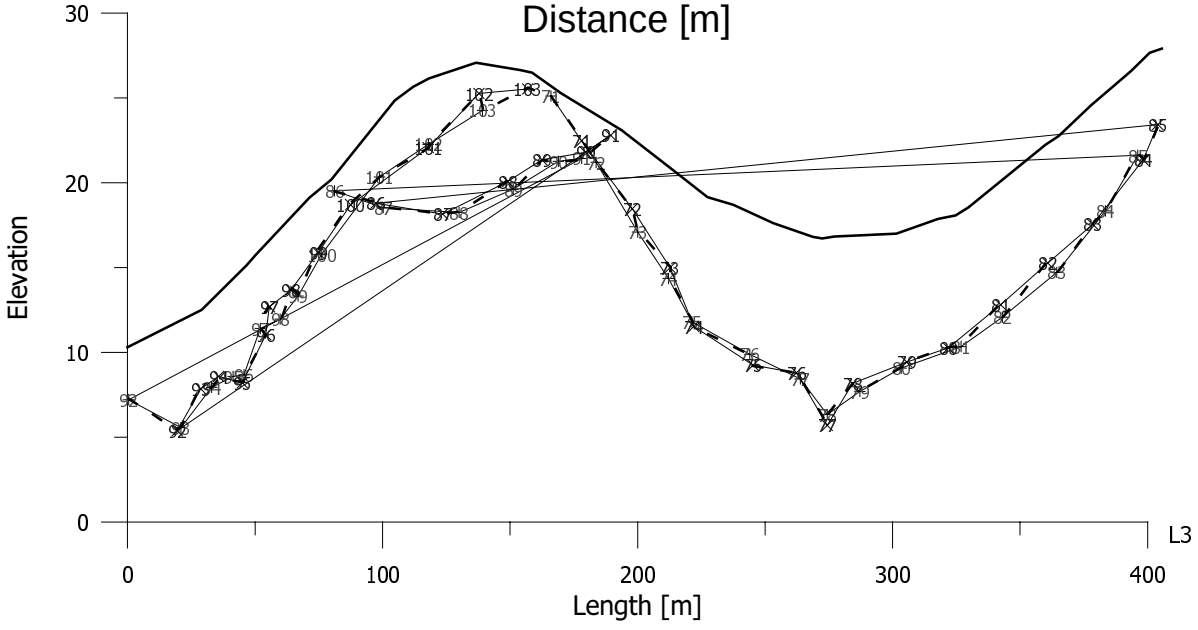

Profile 5.

VLF (top), Slingram (middle), GPR anomalies (bottom)
VLF measurements have been truncated in vicinity of powerline.

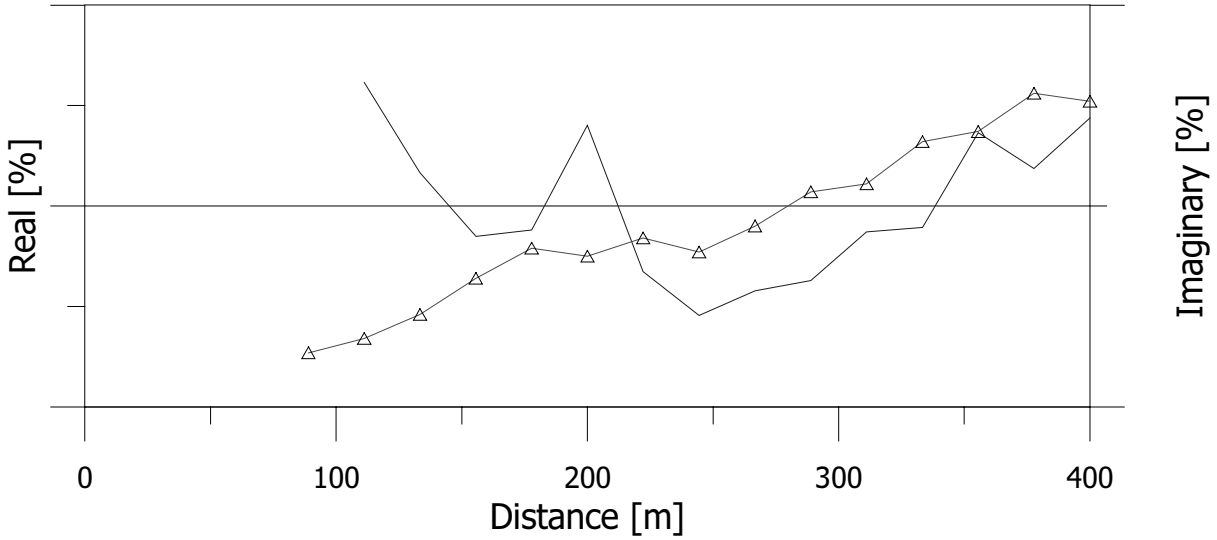

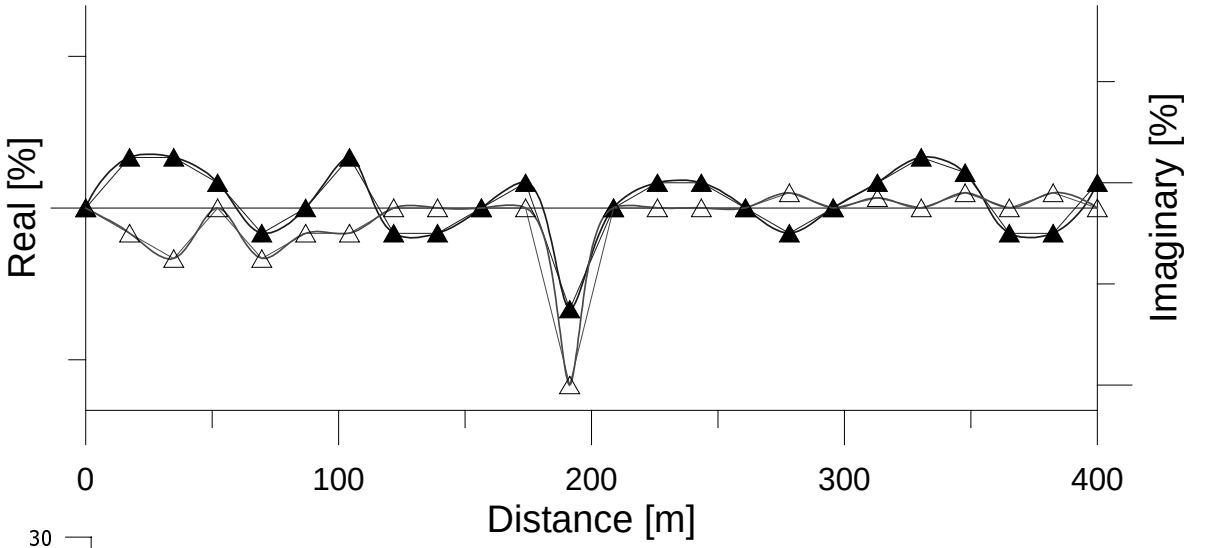

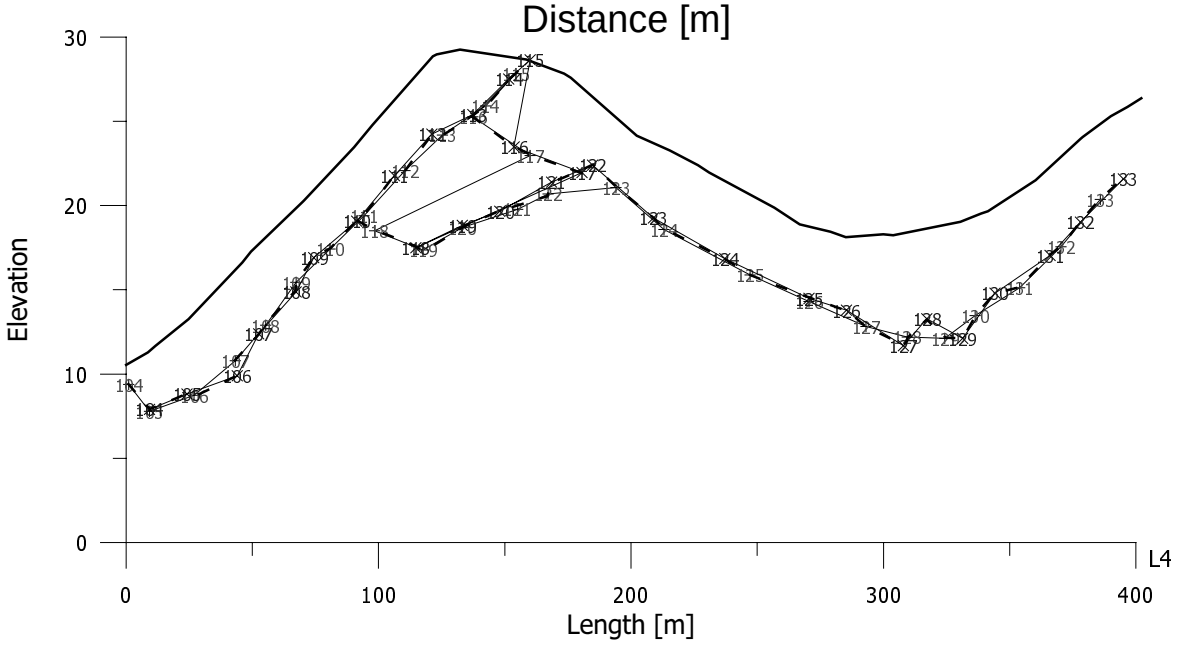

Profile 6.

VLF (top), Slingram (middle), GPR anomalies (bottom)
VLF measurements have been truncated in vicinity of powerline.

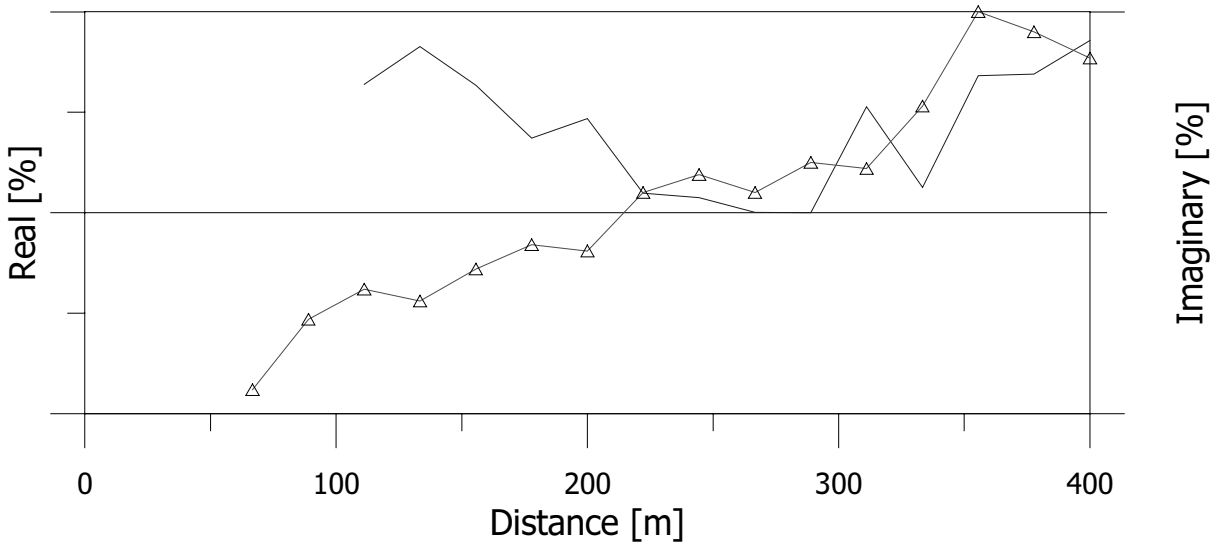

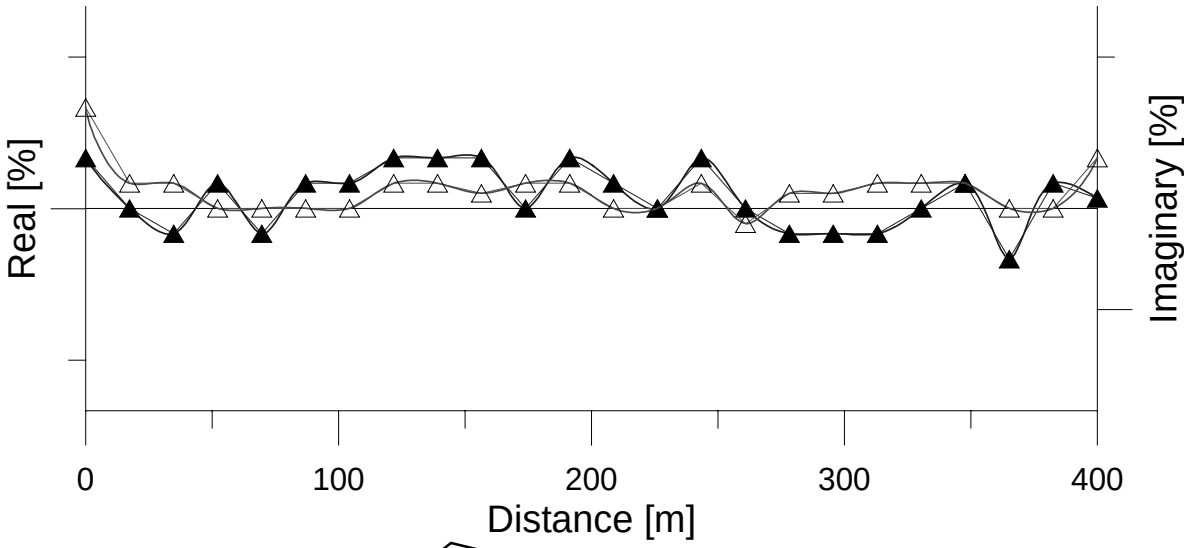

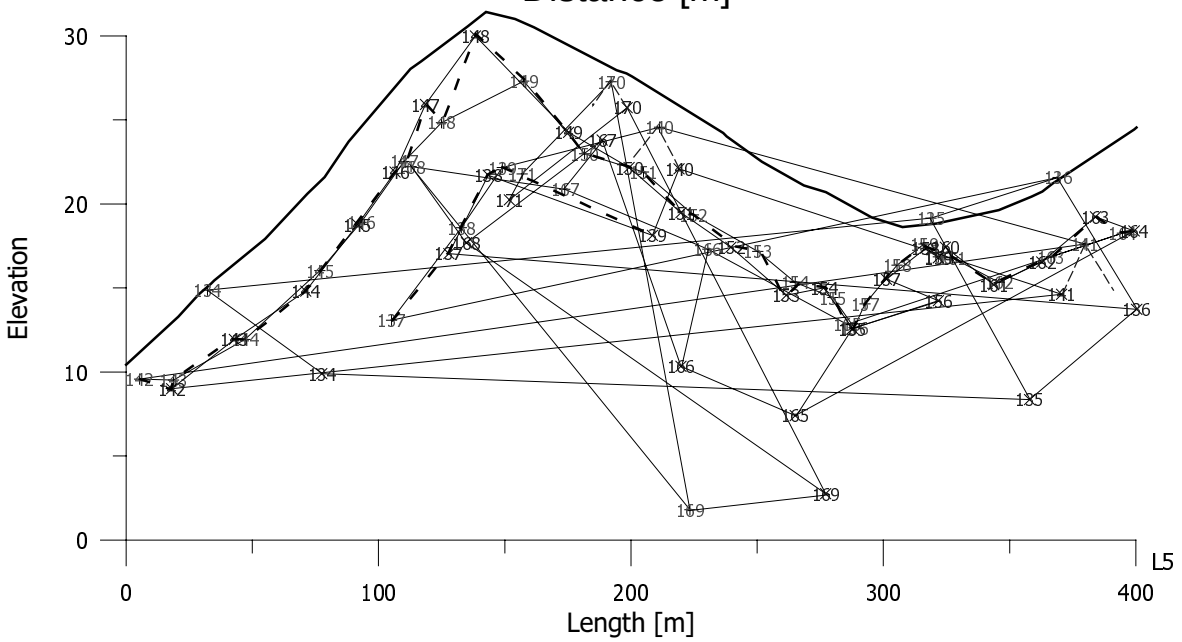

Profile 7.

VLF (top), Slingram (middle), GPR anomalies (bottom)
VLF measurements have been truncated in vicinity of powerline.

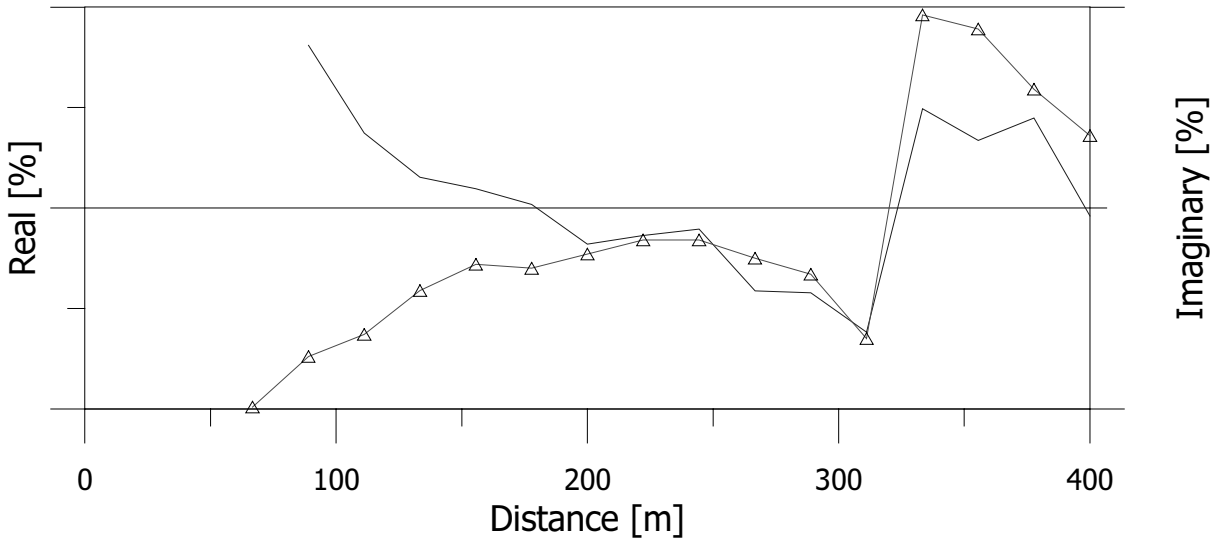

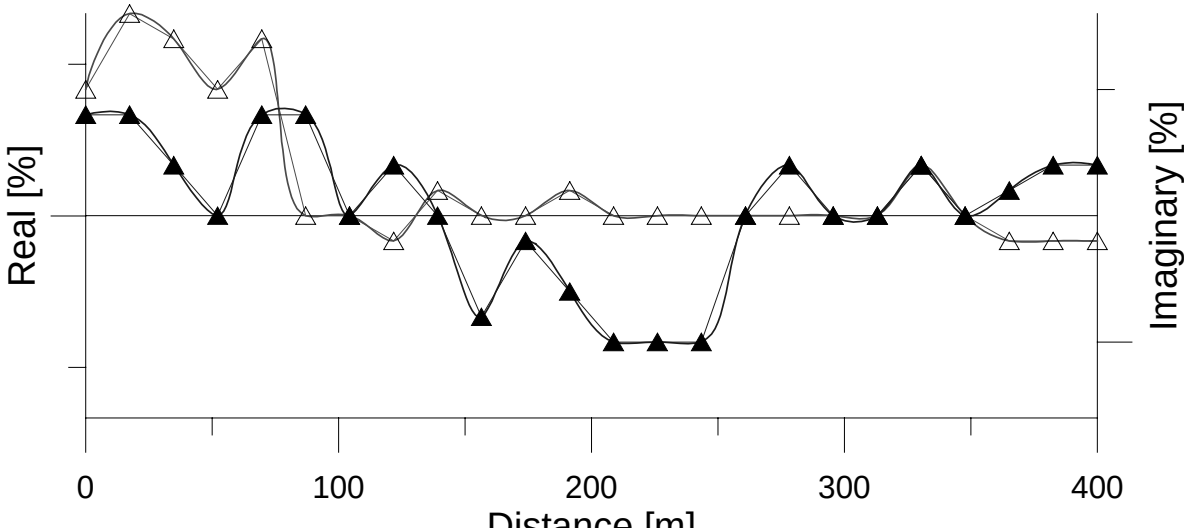

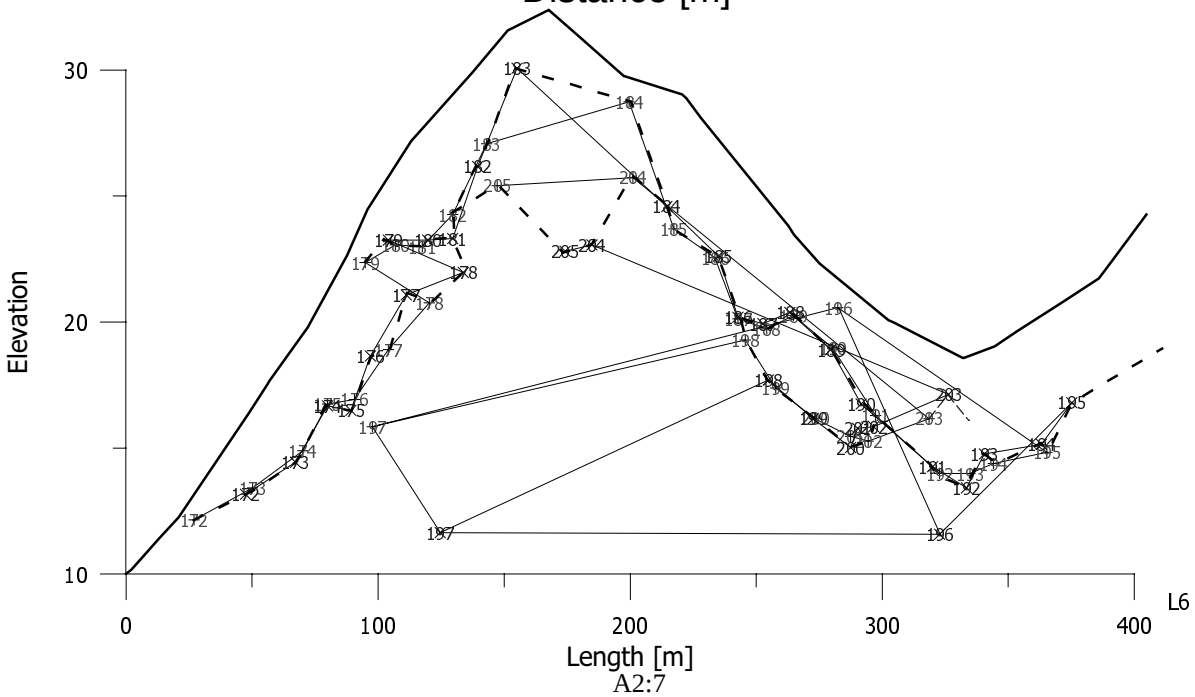

Profile 8.

VLF (top), Slingram (middle), GPR anomalies (bottom)
VLF measurements have been truncated in vicinity of powerline.

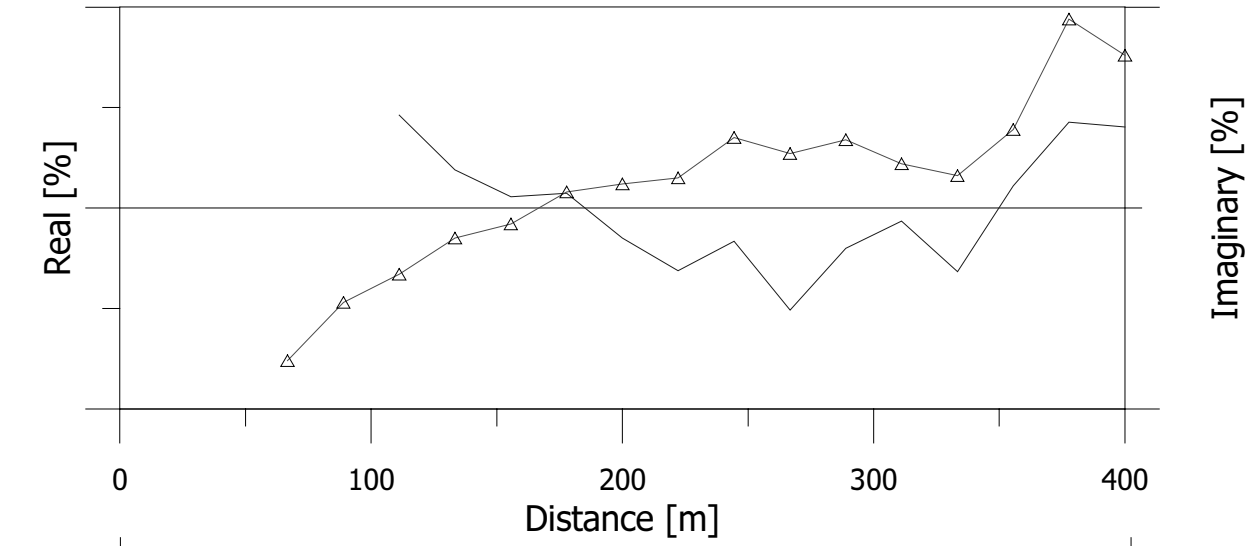

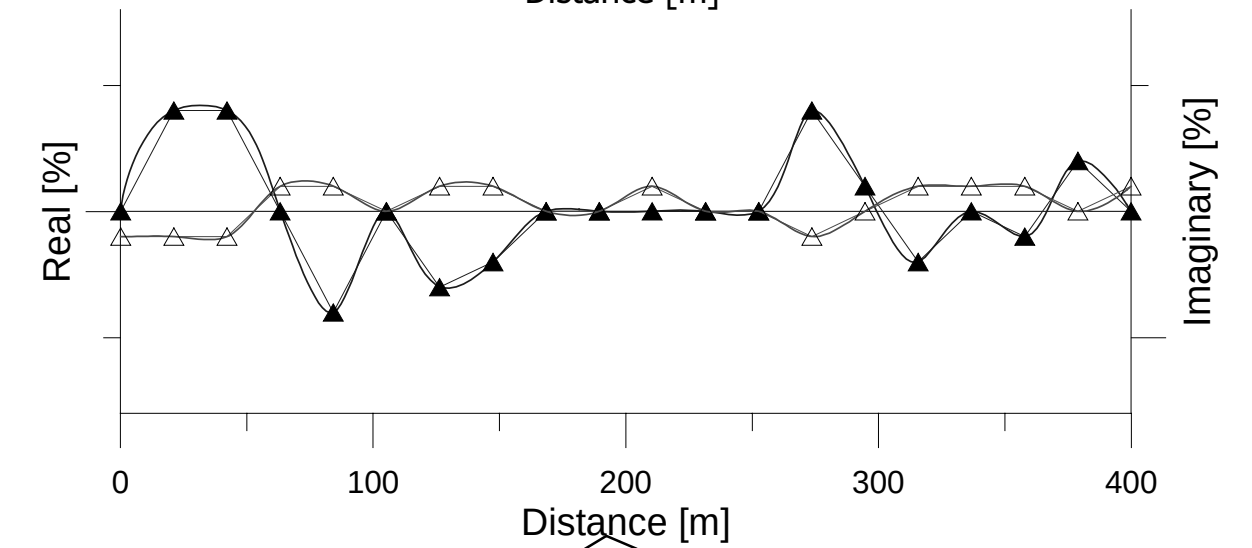

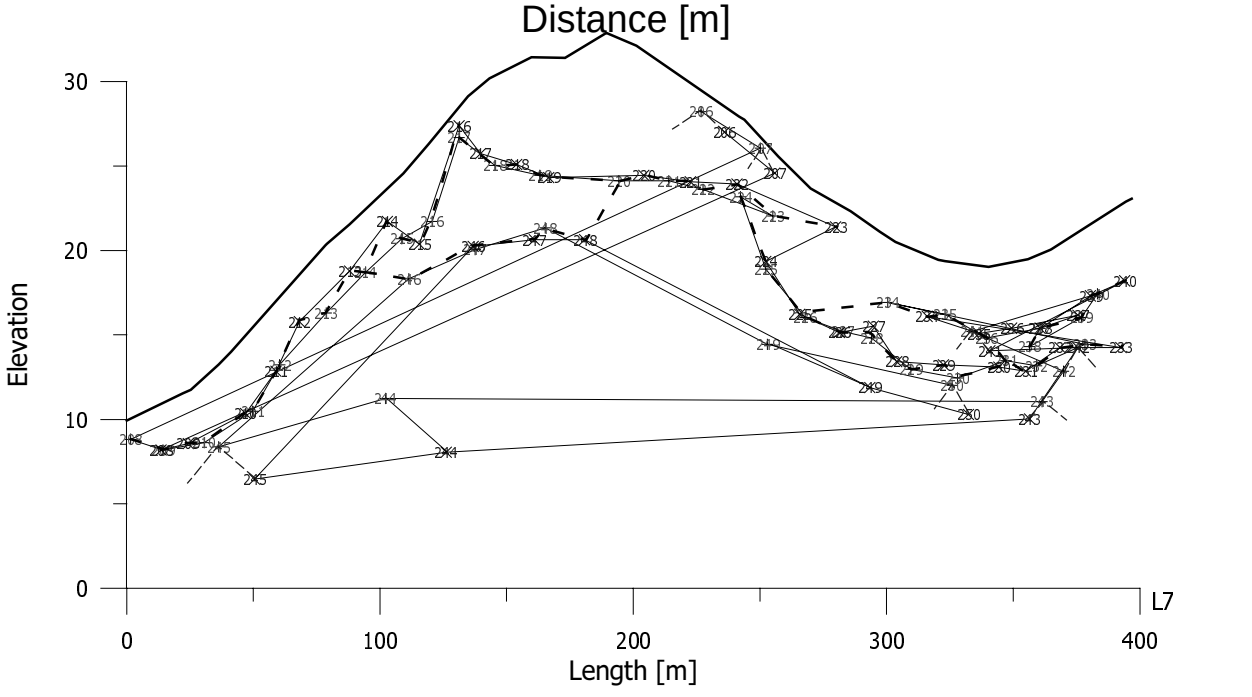

Profile 9.

VLF (top), Slingram (middle), GPR anomalies (bottom)
VLF measurements have been truncated in vicinity of powerline.

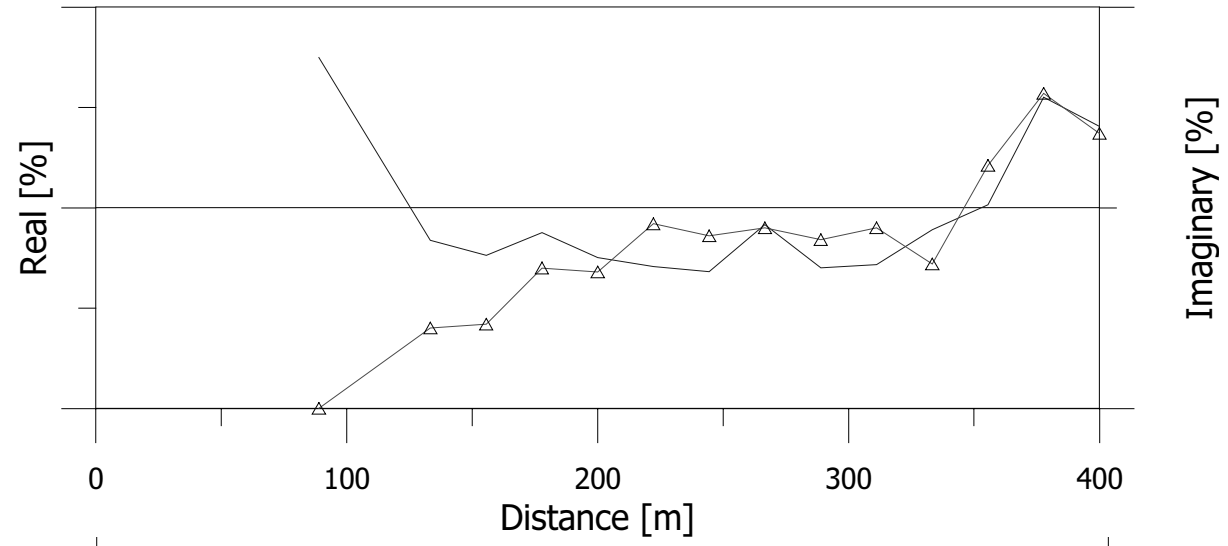

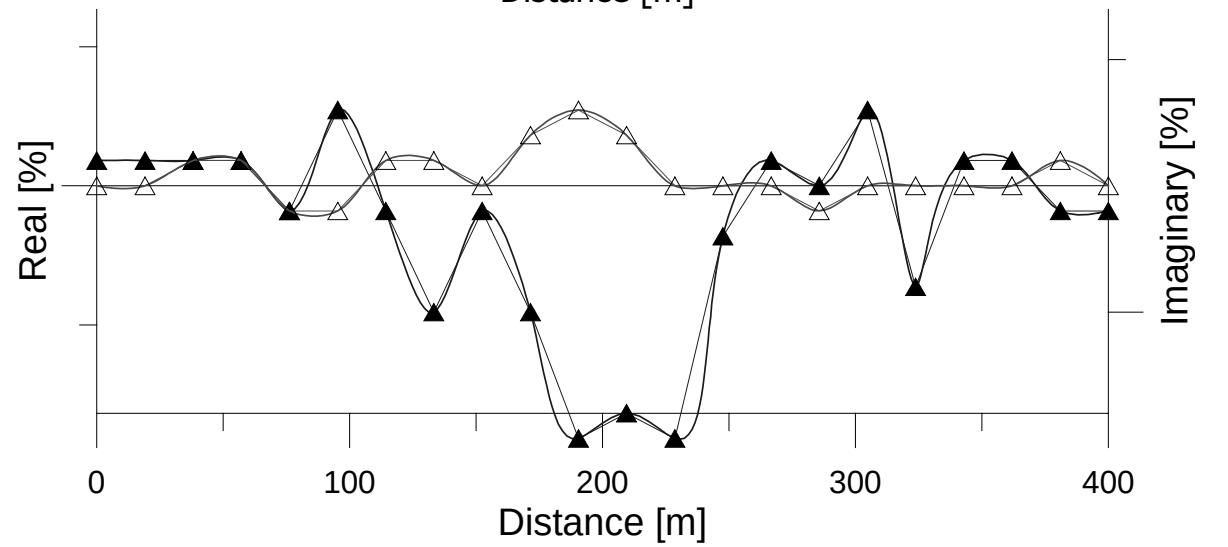

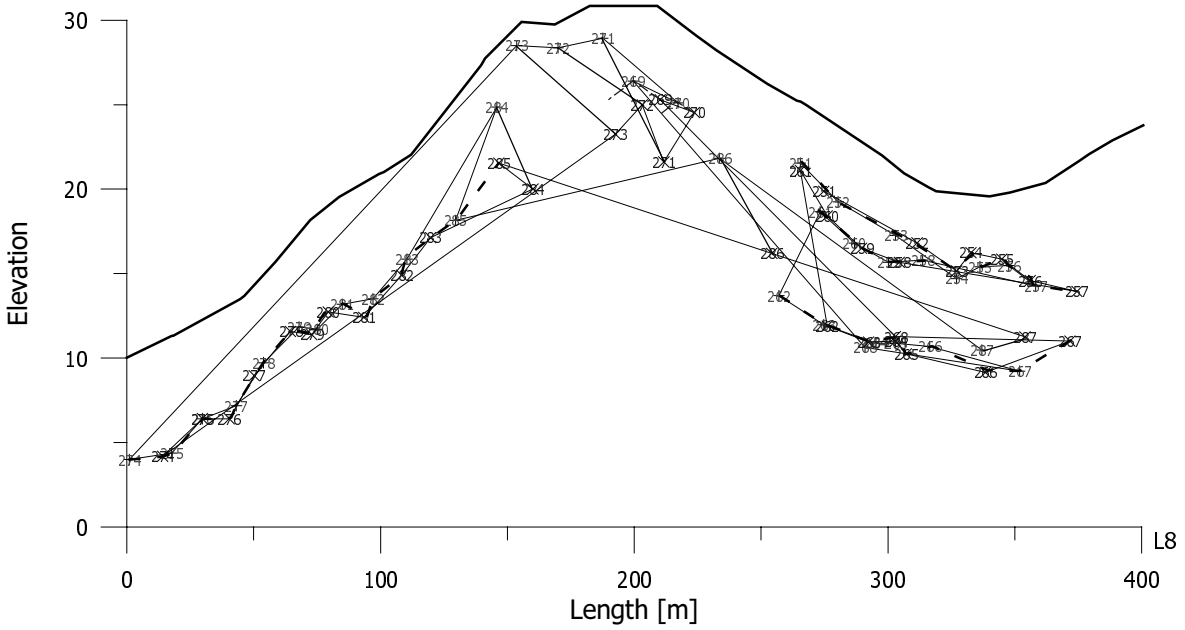

Profile 10.

VLF (top), Slingram (middle), GPR anomalies (bottom)
VLF measurements have been truncated in vicinity of powerline.

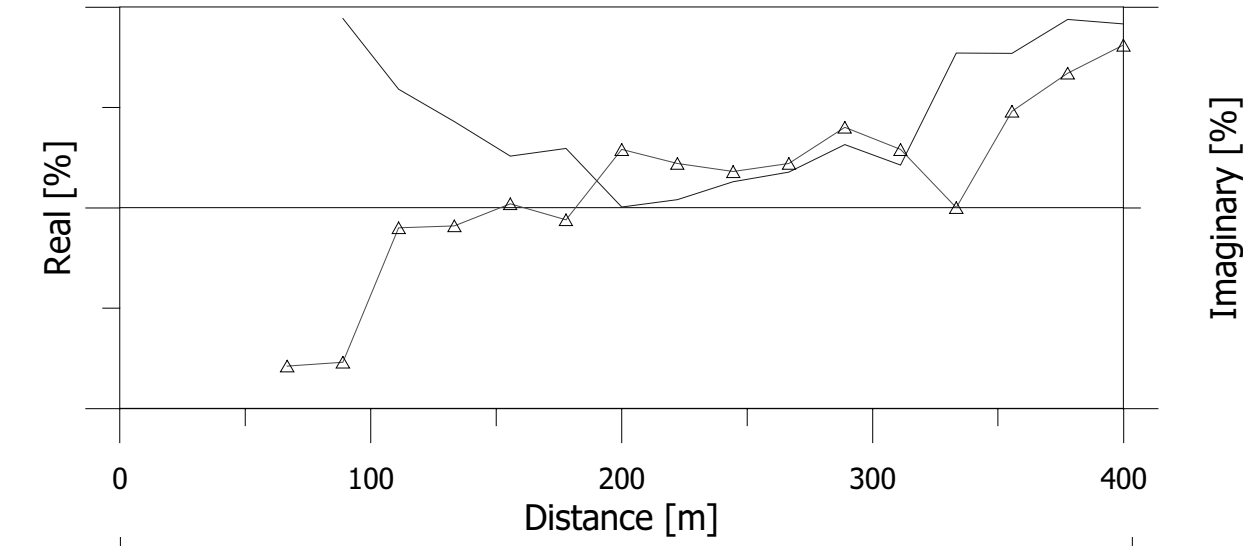

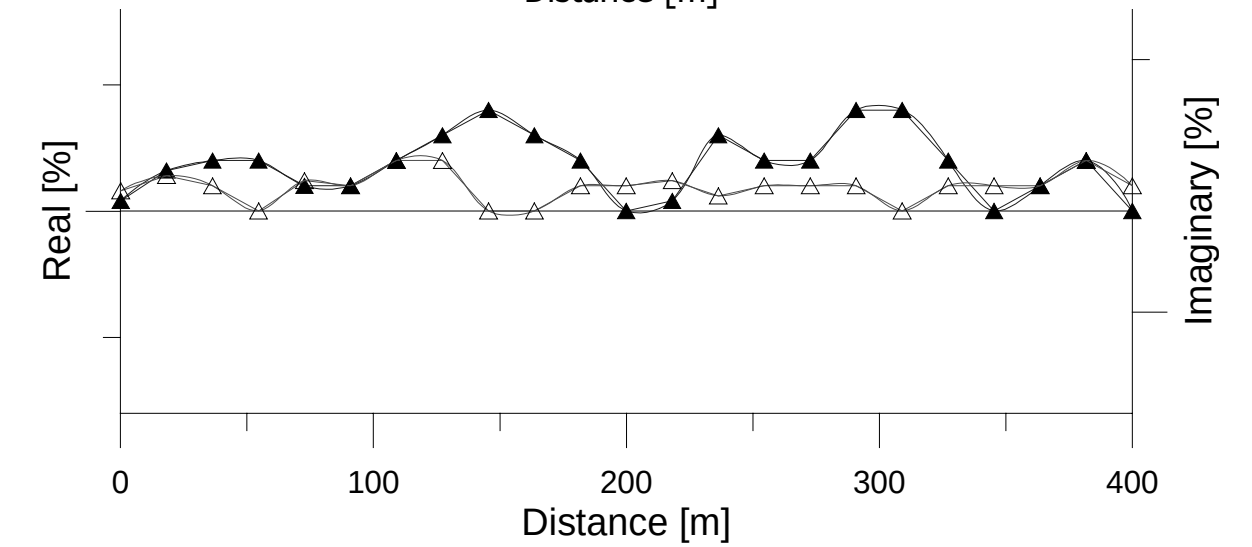

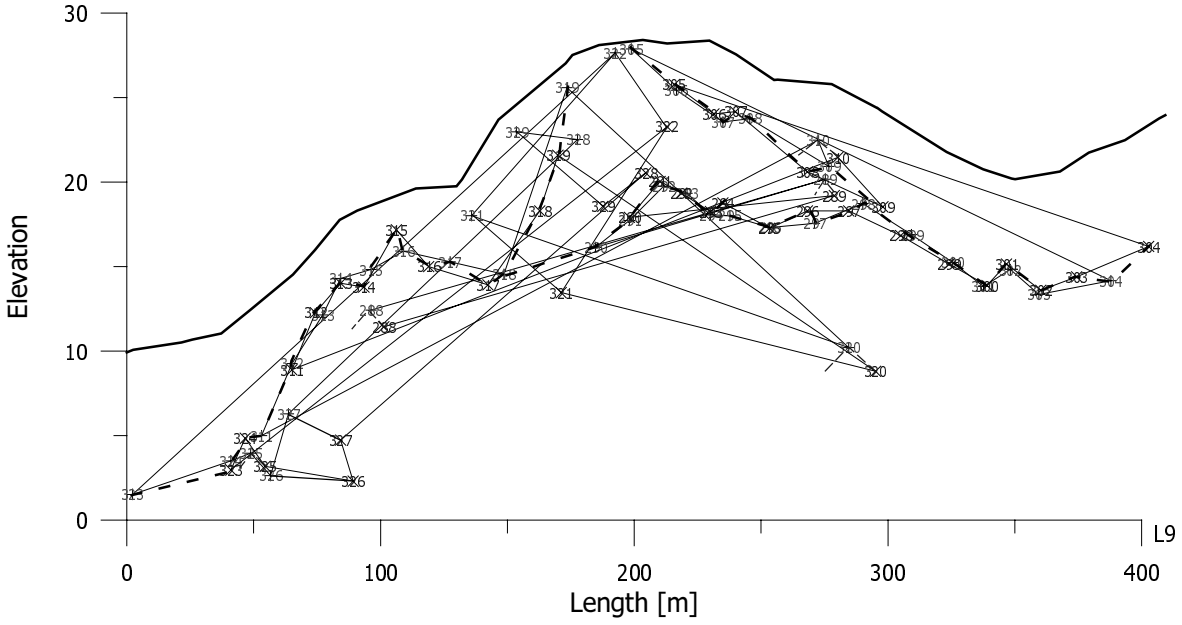

Profile 11.

VLF (top), Slingram (middle), GPR anomalies (bottom)
VLF measurements have been truncated in vicinity of powerline.

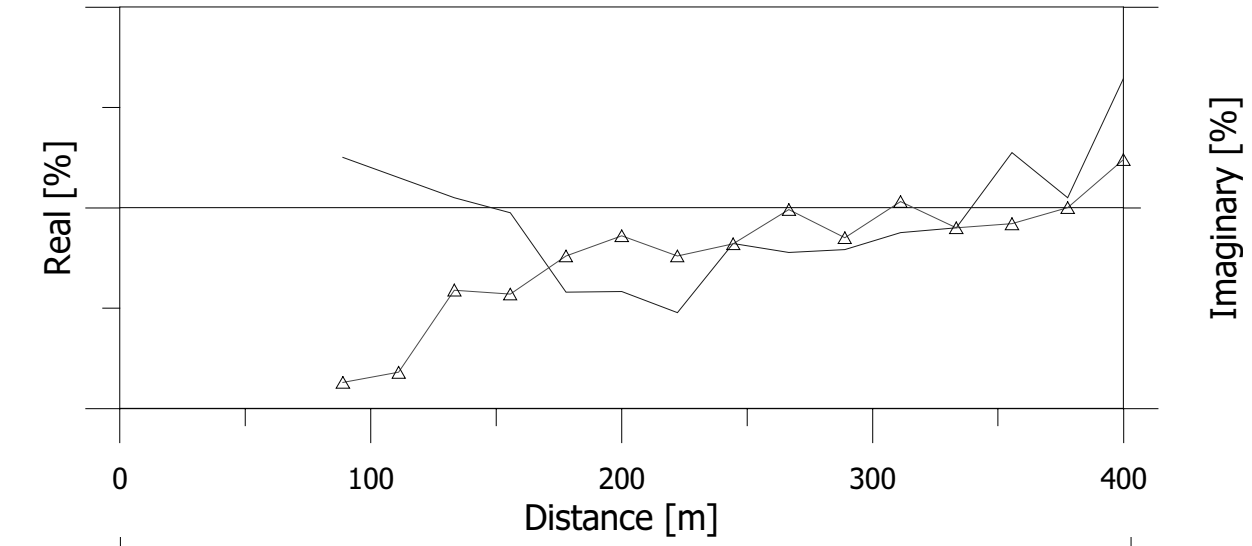

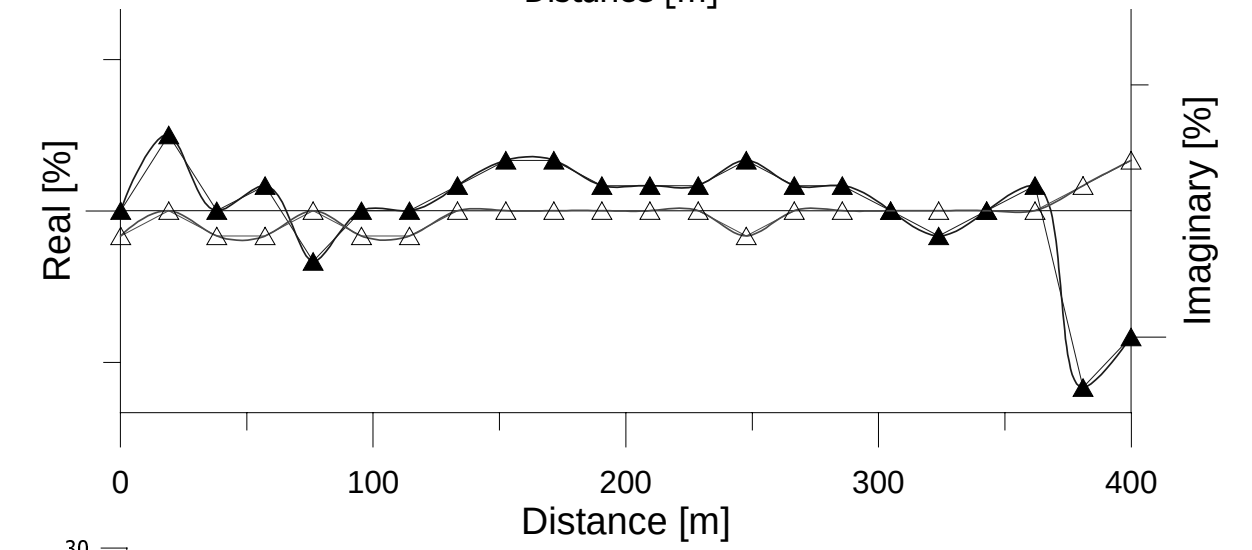

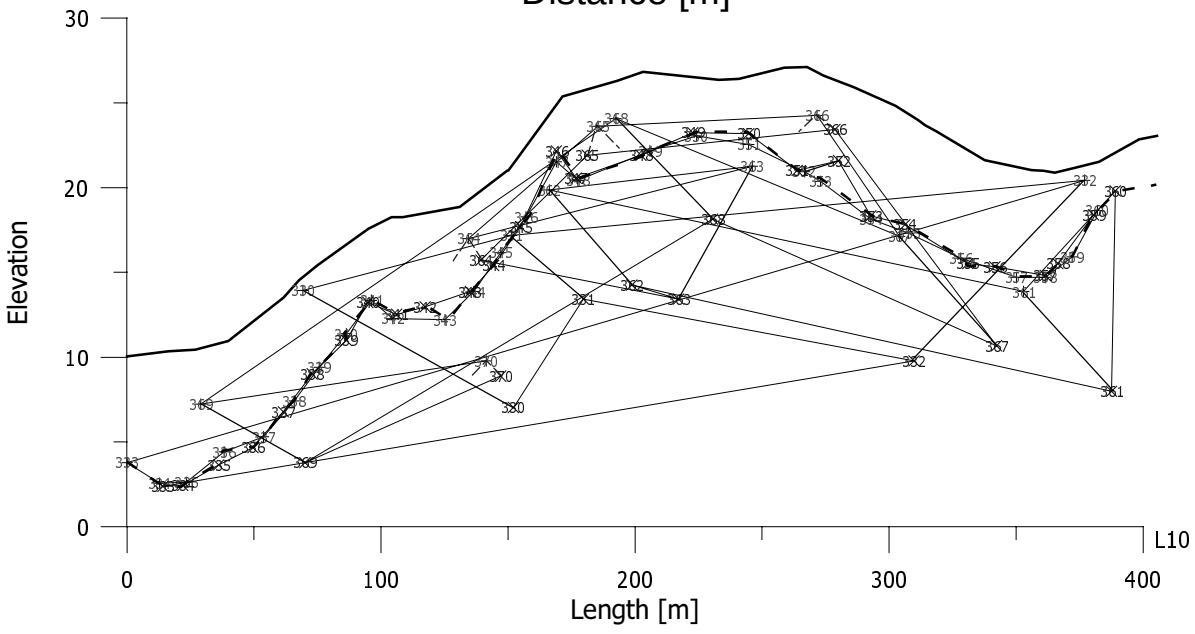

Profile 12.

VLF (top), Slingram (middle), GPR anomalies (bottom)
VLF measurements have been truncated in vicinity of powerline.

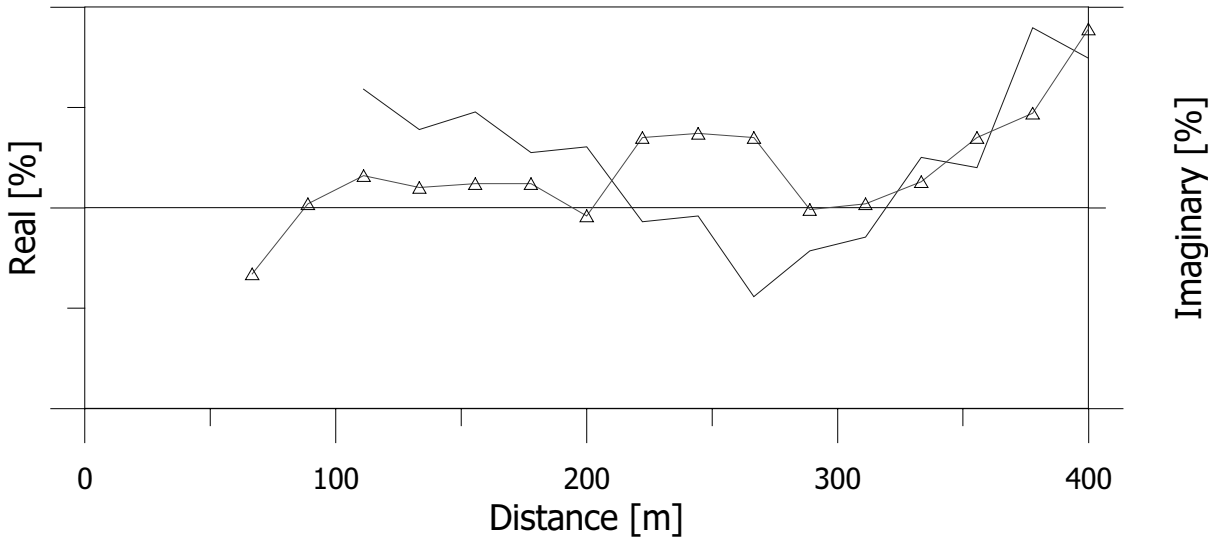

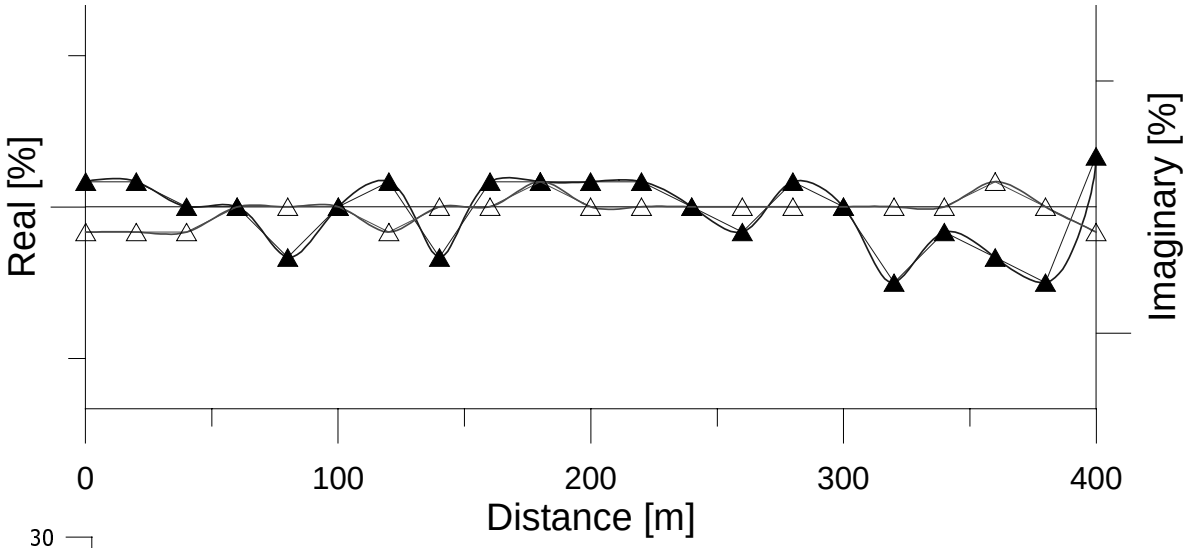

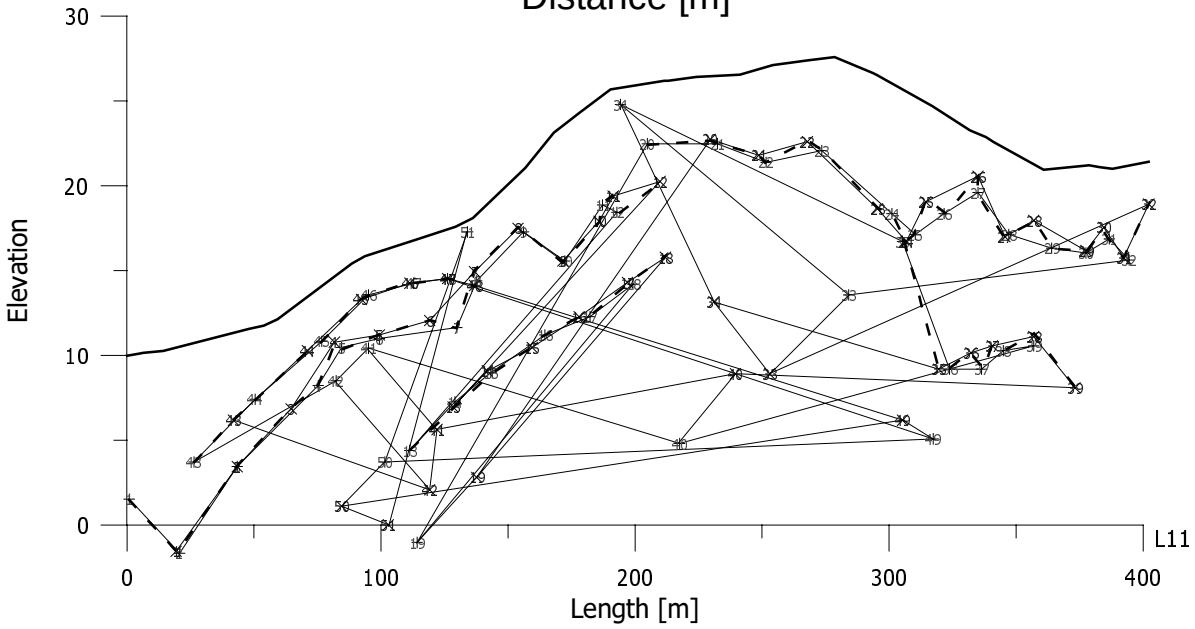

Profile 13.

VLF (top), Slingram (middle), GPR anomalies (bottom)
VLF measurements have been truncated in vicinity of powerline.

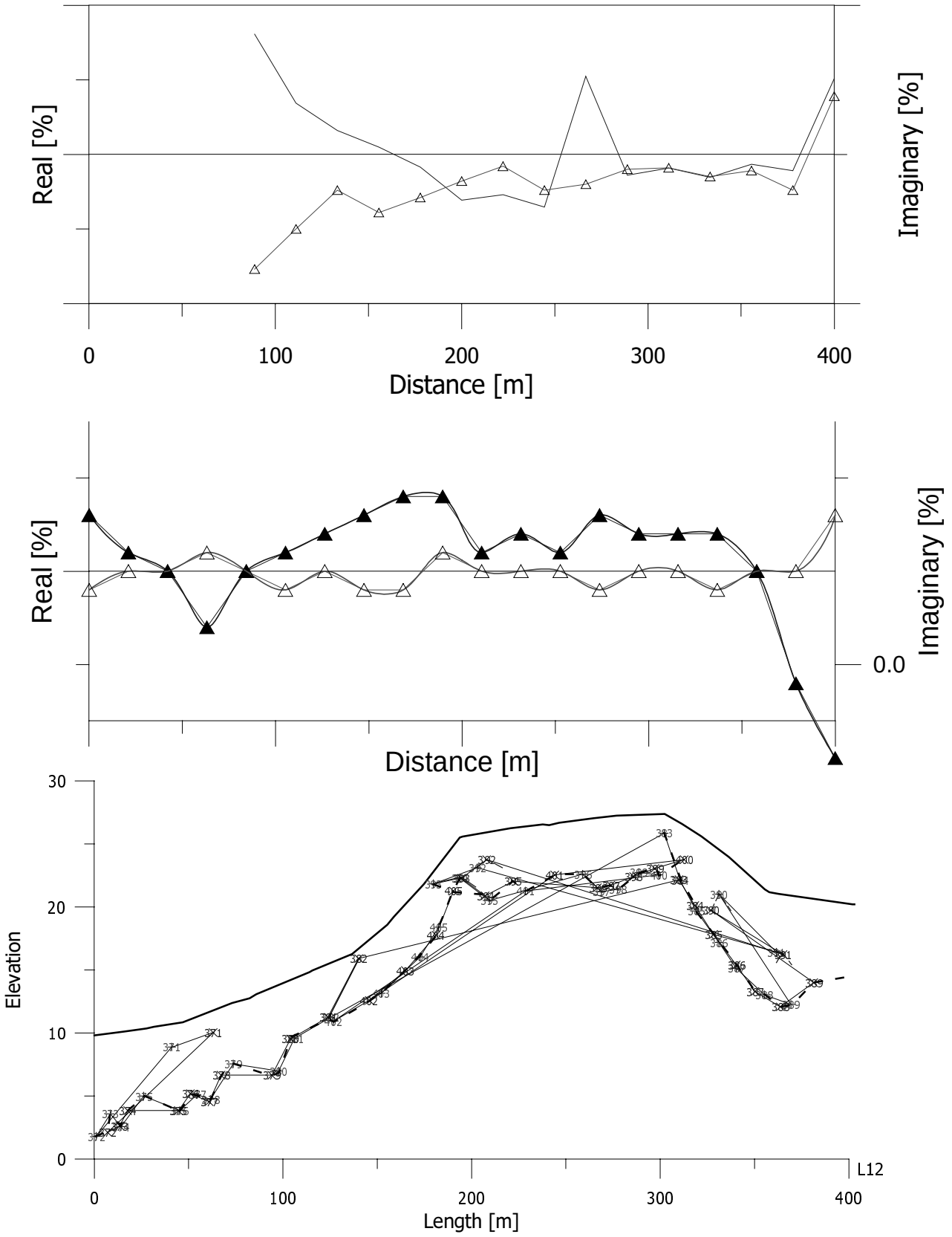

Profile 14.

VLF (top), Slingram (middle), GPR anomalies (bottom)
VLF measurements have been truncated in vicinity of powerline.

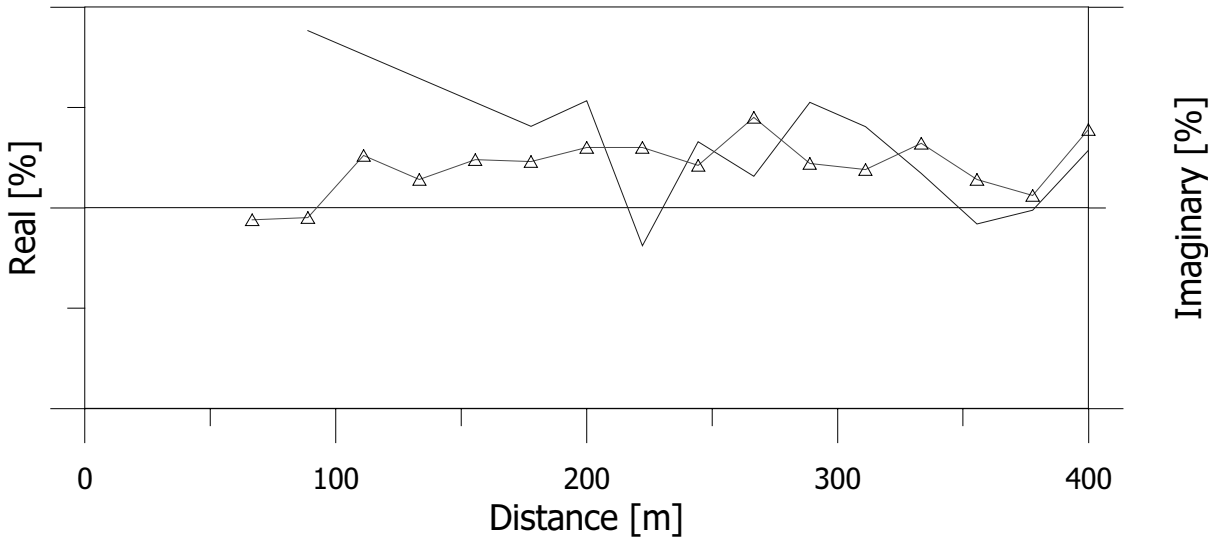

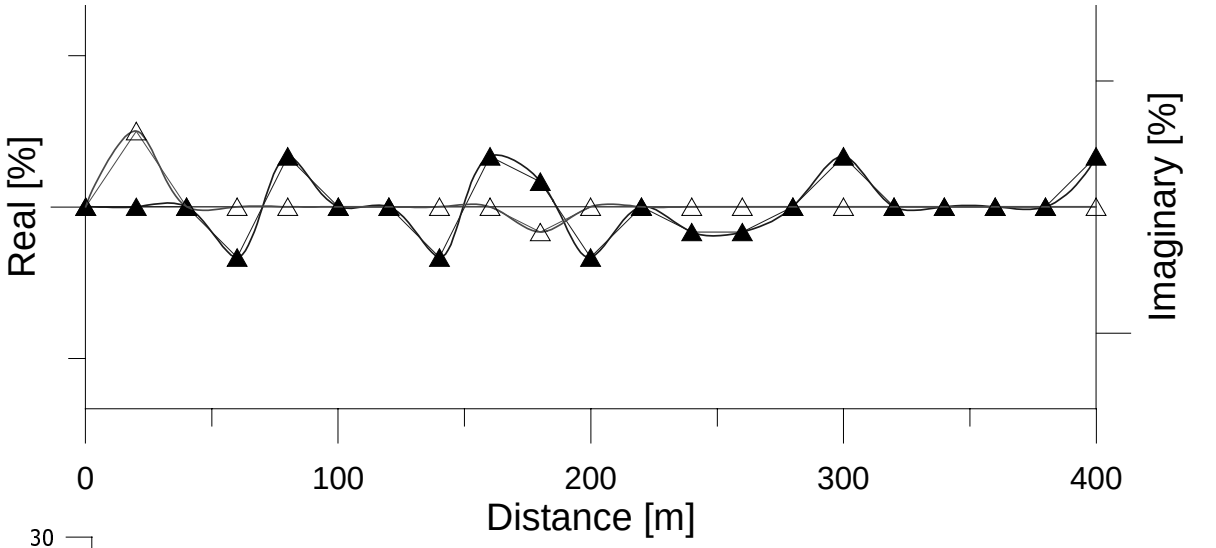

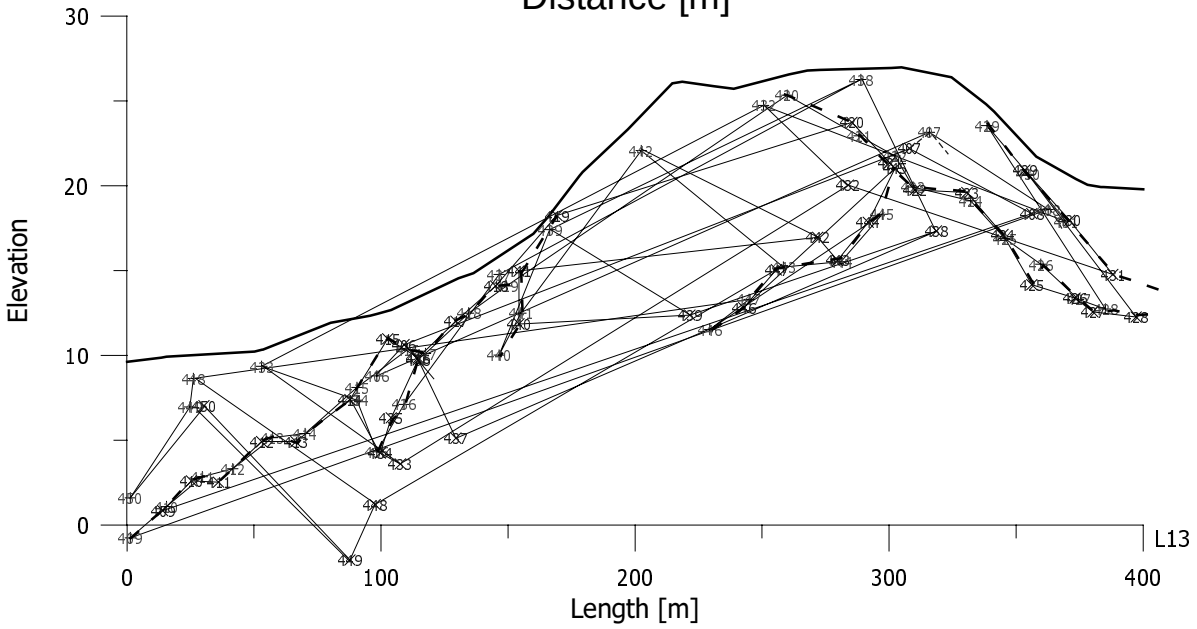

Profile 15.

VLF (top), Slingram (middle), GPR anomalies (bottom)
VLF measurements have been truncated in vicinity of powerline.

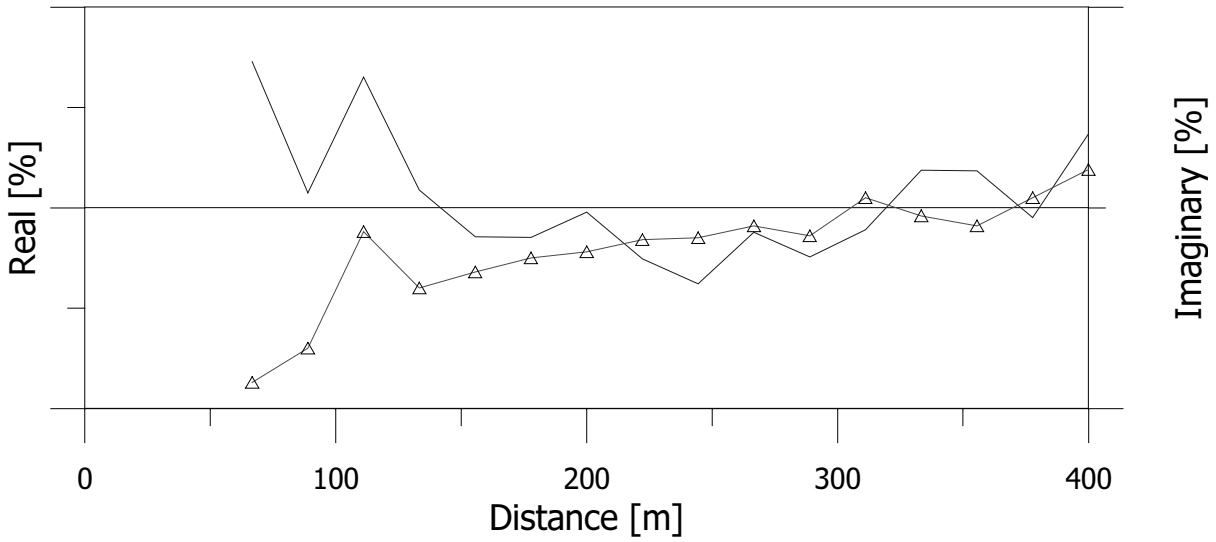

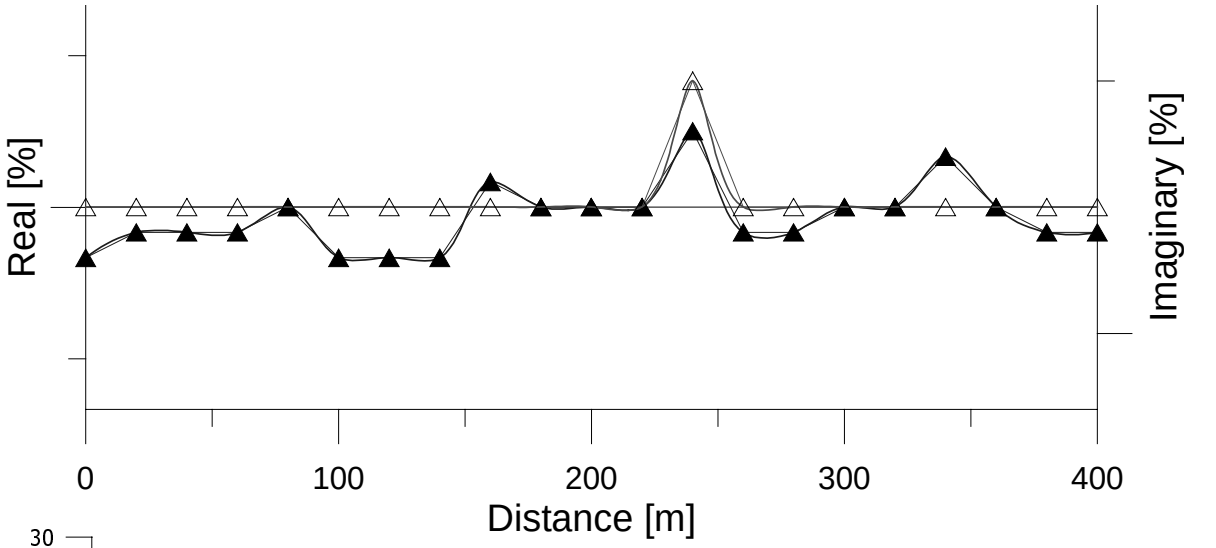

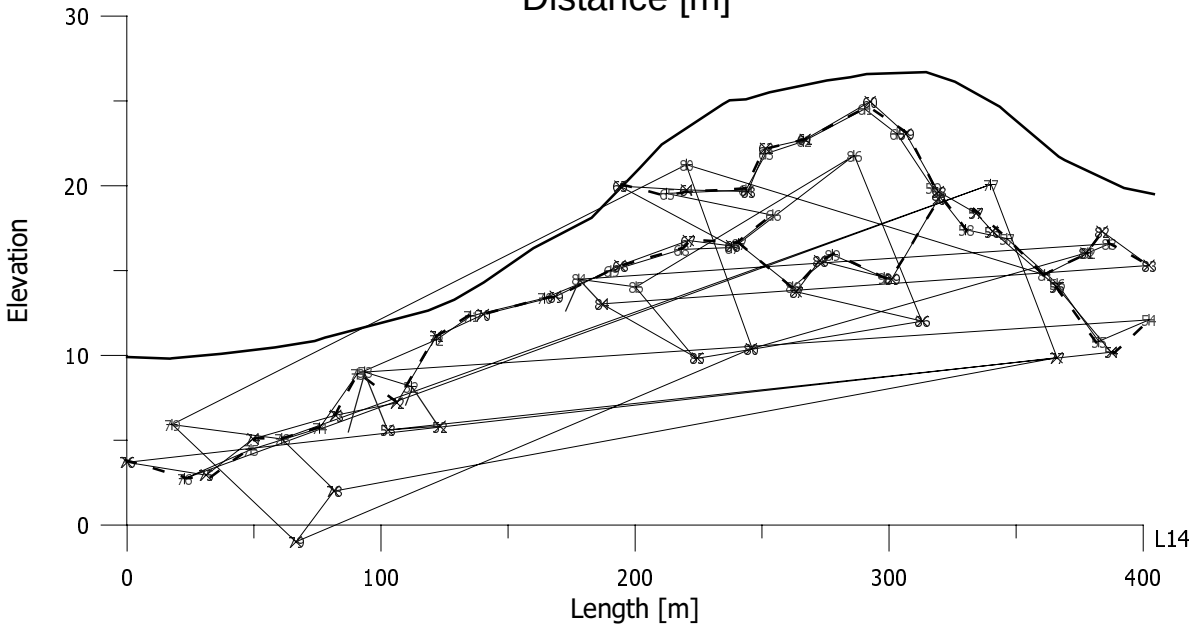

Profile 16.

VLF (top), Slingram (middle), GPR anomalies (bottom)
VLF measurements have been truncated in vicinity of powerline.

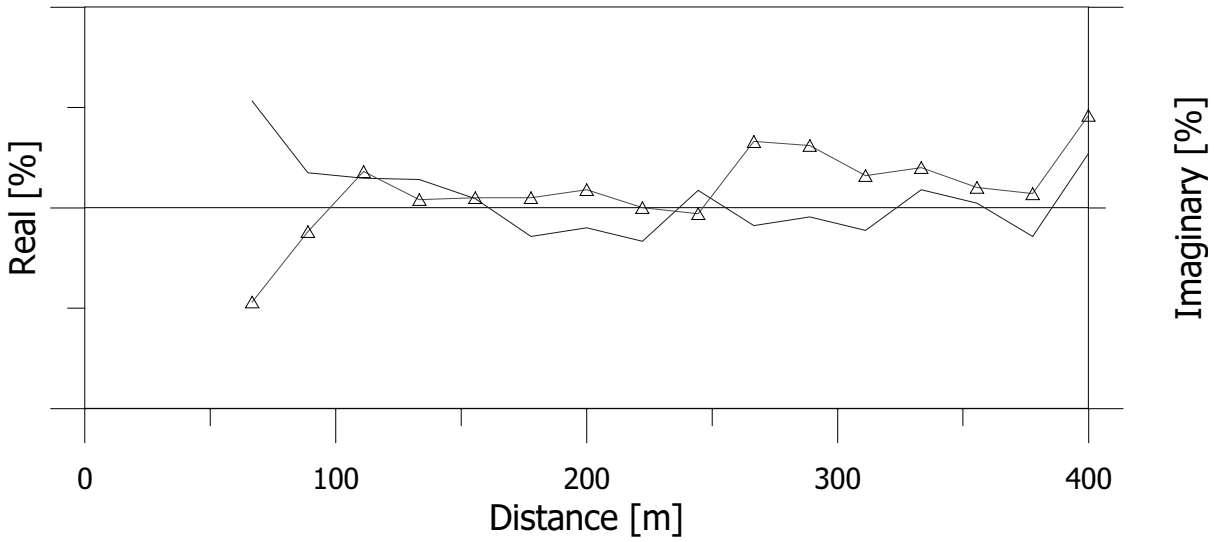

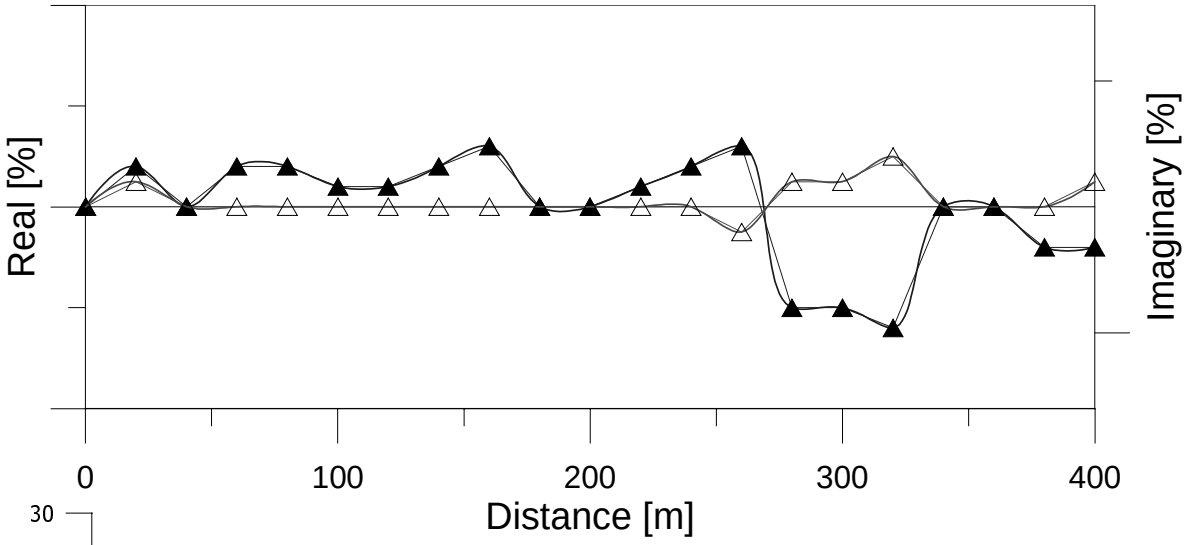

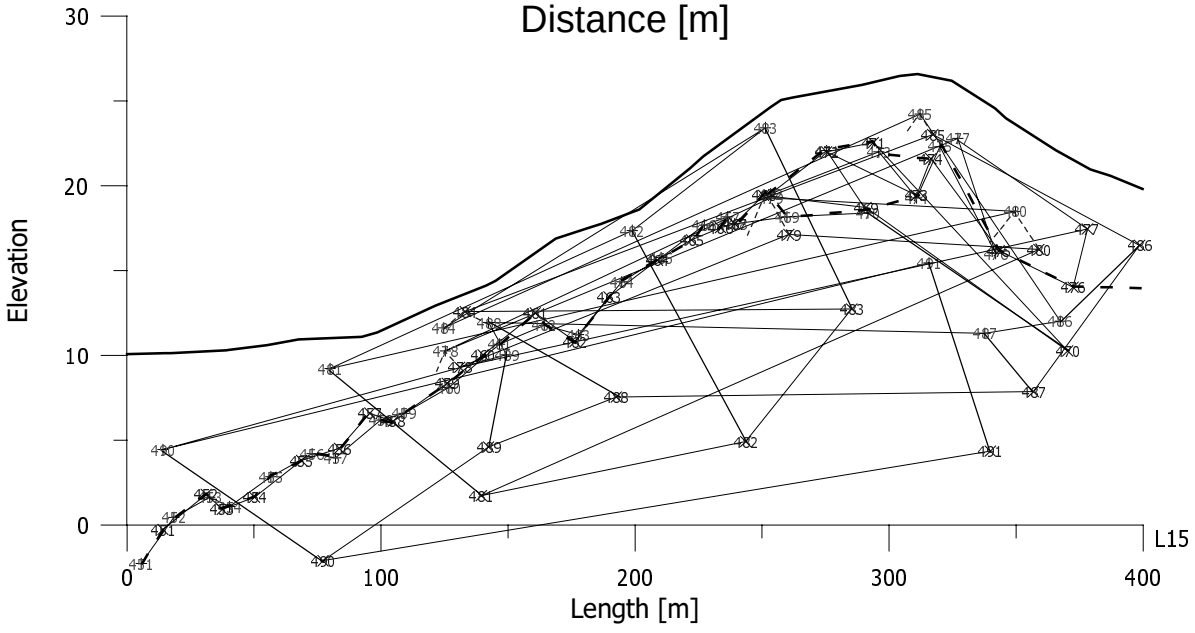

Profile 17.

VLF (top), Slingram (middle), GPR anomalies (bottom)
VLF measurements have been truncated in vicinity of powerline.

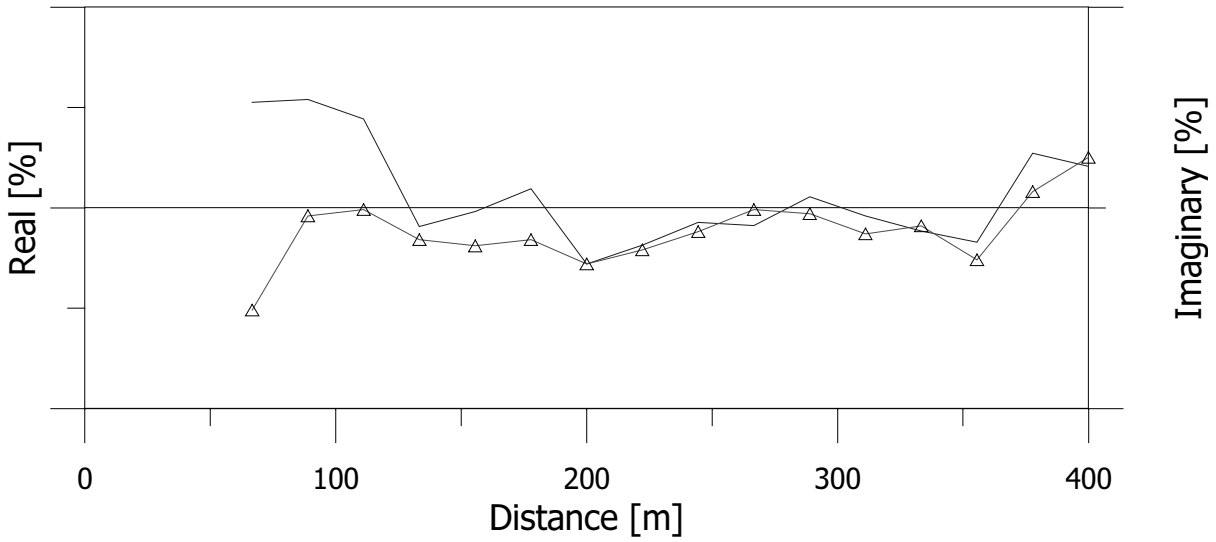

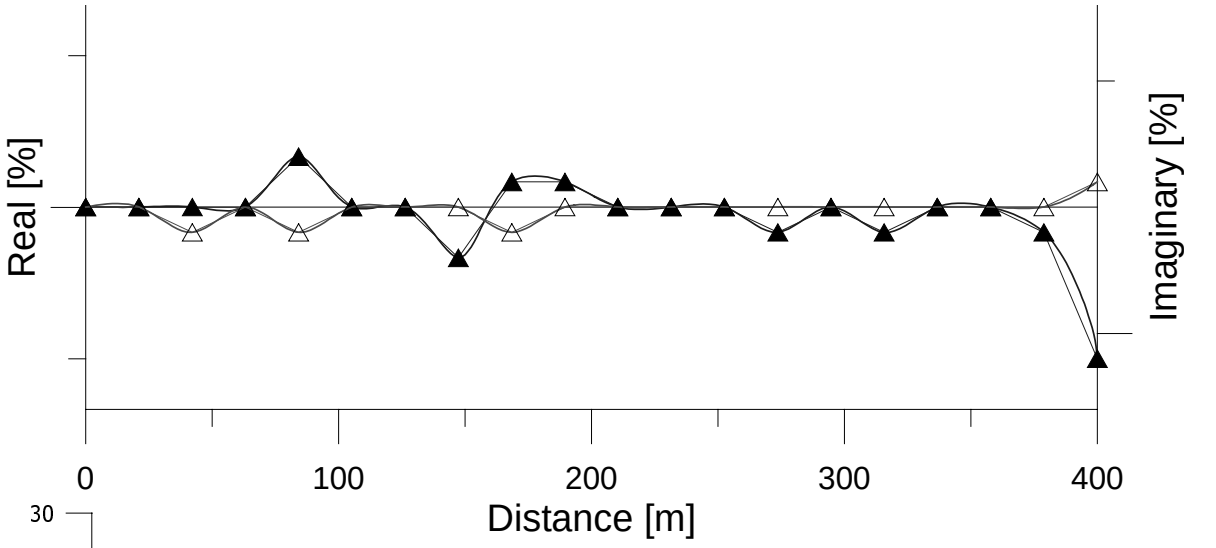

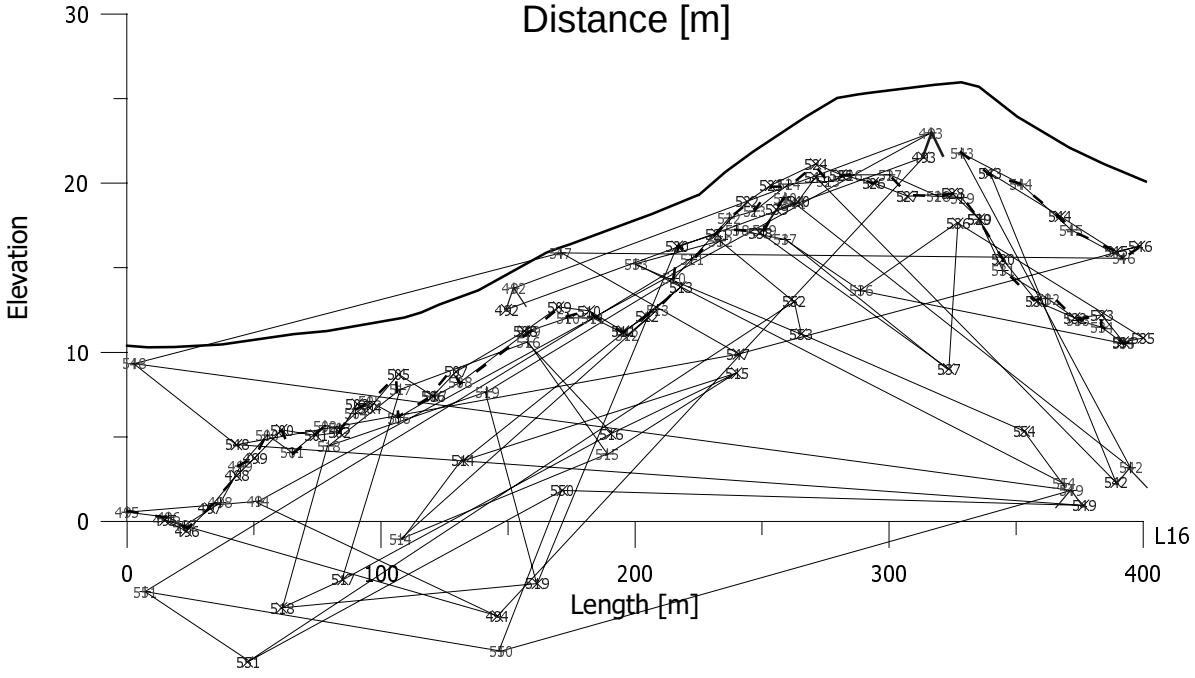

Profile 18.

VLF (top), Slingram (middle), GPR anomalies (bottom)
VLF measurements have been truncated in vicinity of powerline.

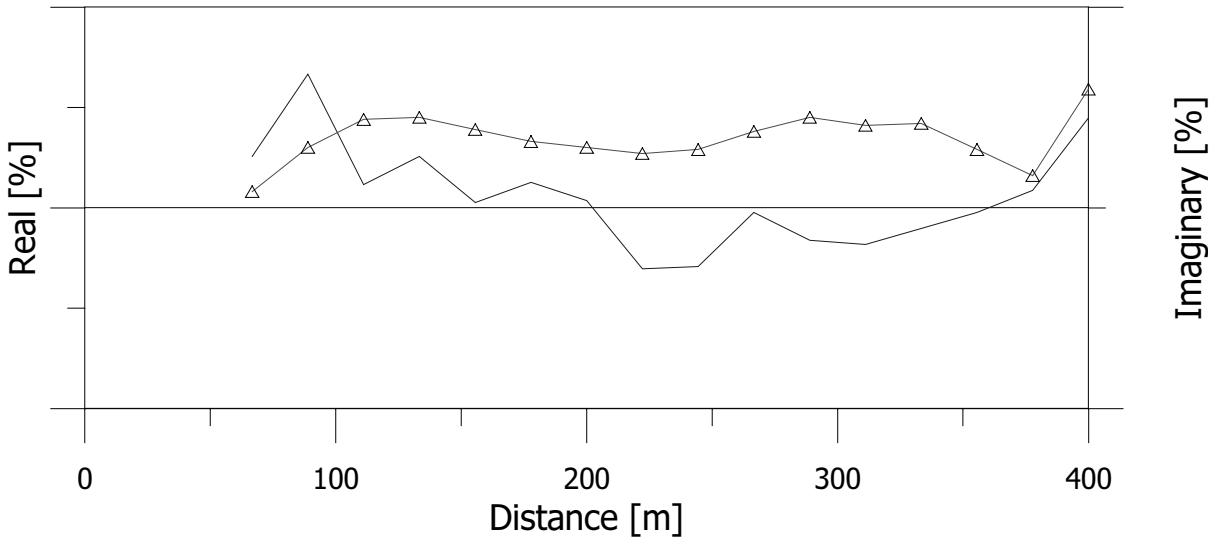

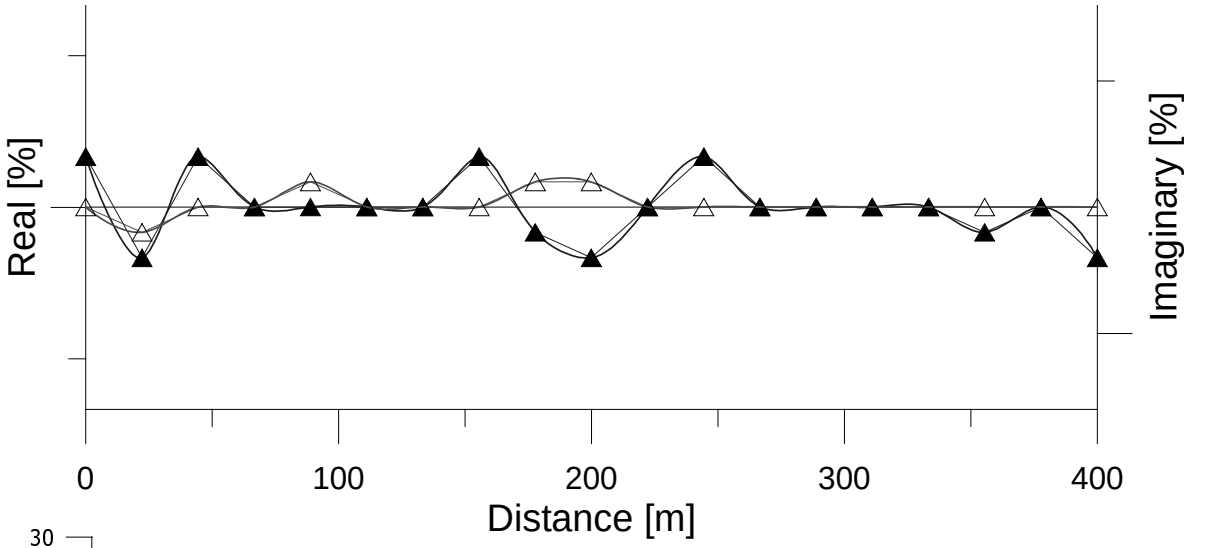

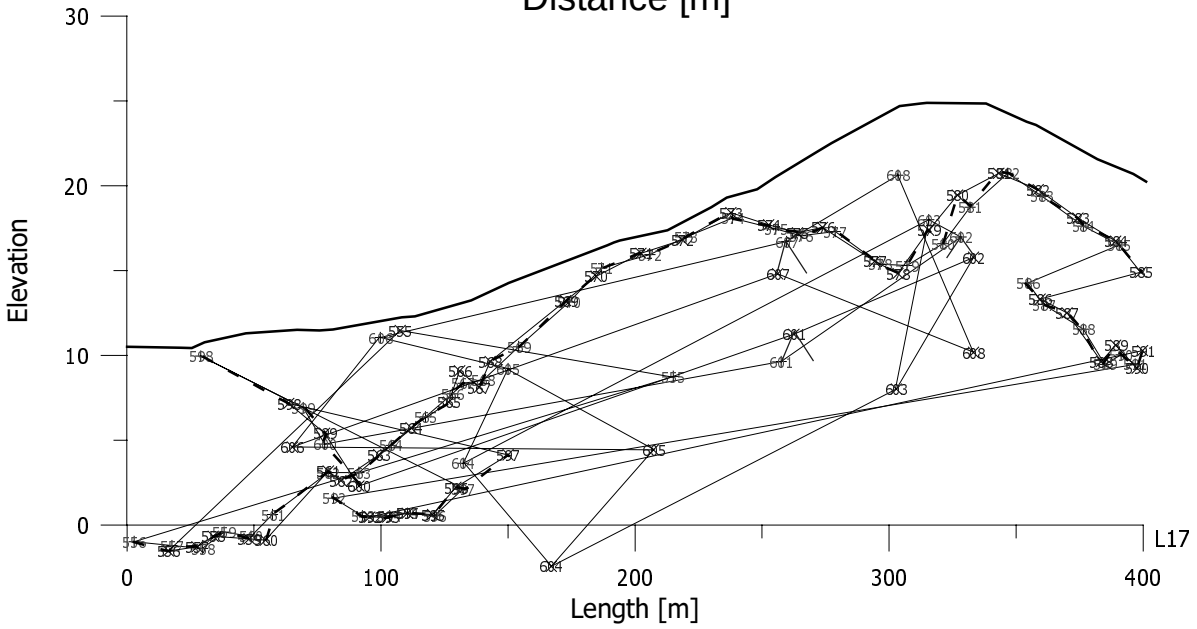

Profile 19.

VLF (top), Slingram (middle), GPR anomalies (bottom)
VLF measurements have been truncated in vicinity of powerline.

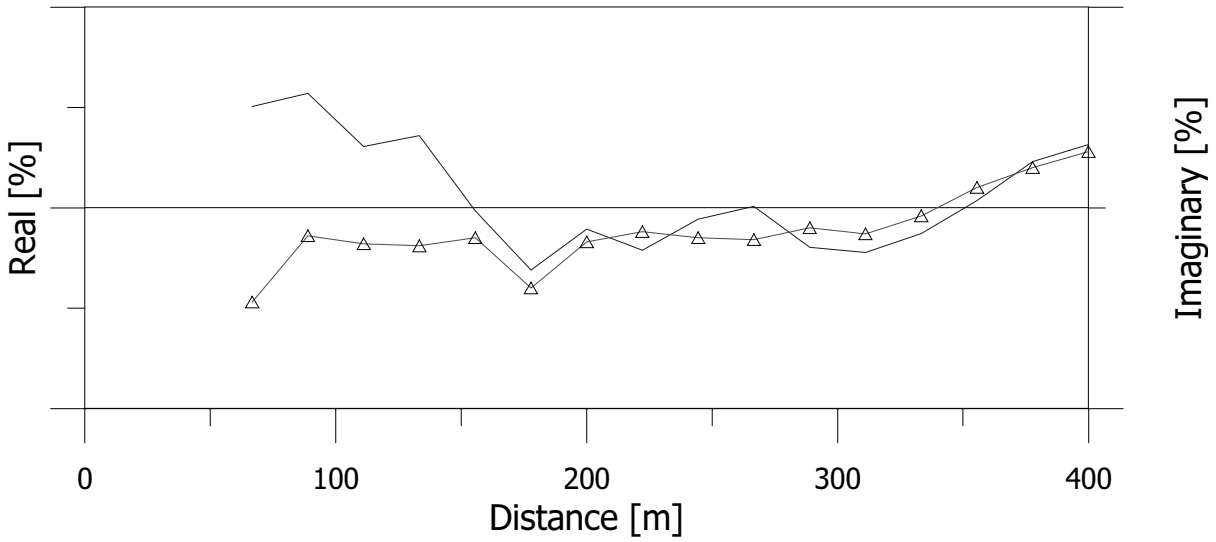

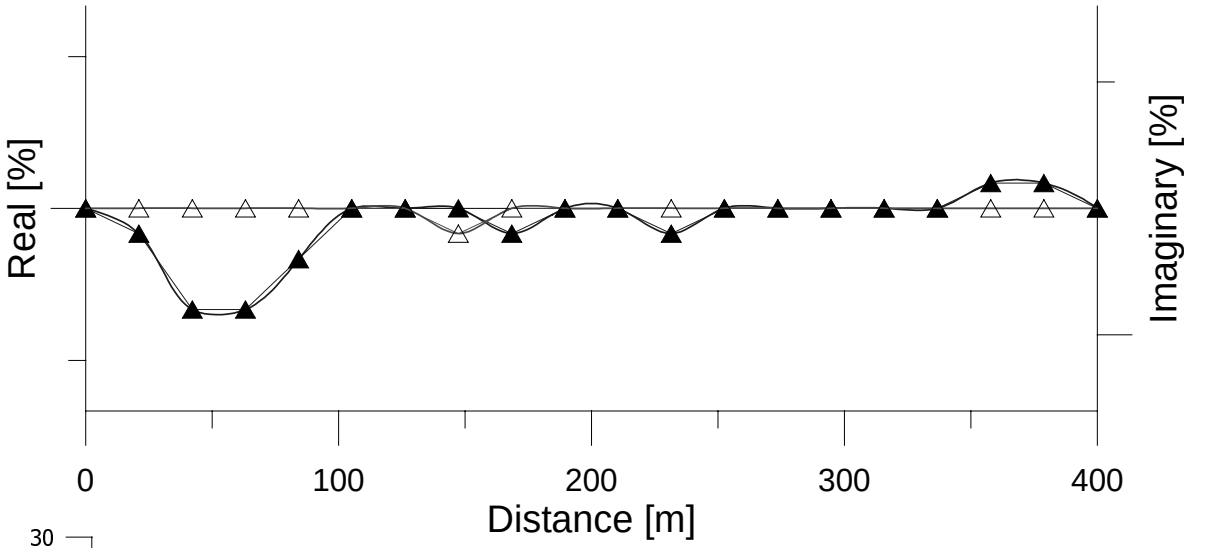

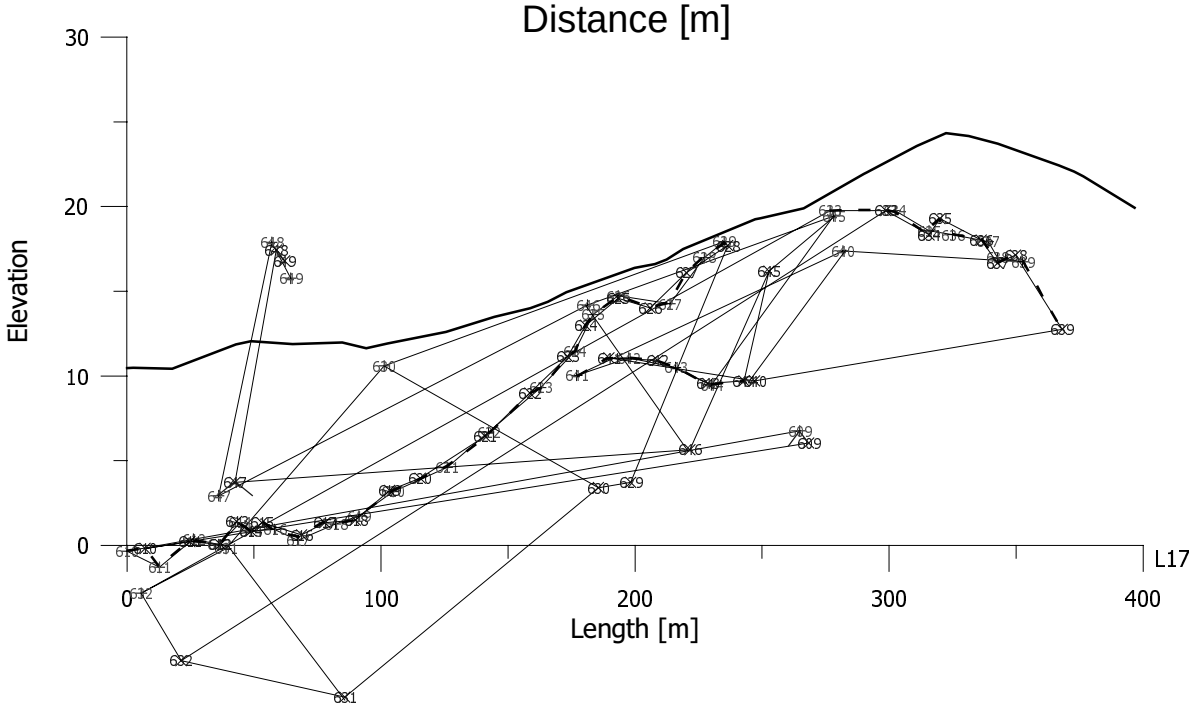

Profile 20.

VLF (top), Slingram (middle), GPR anomalies (bottom)
VLF measurements have been truncated in vicinity of powerline.

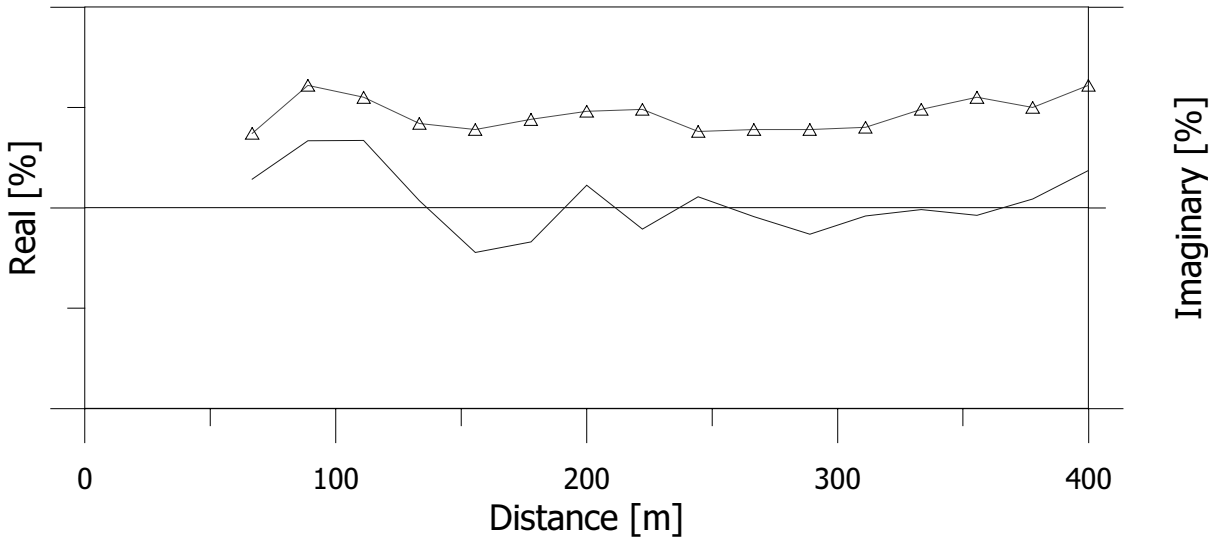

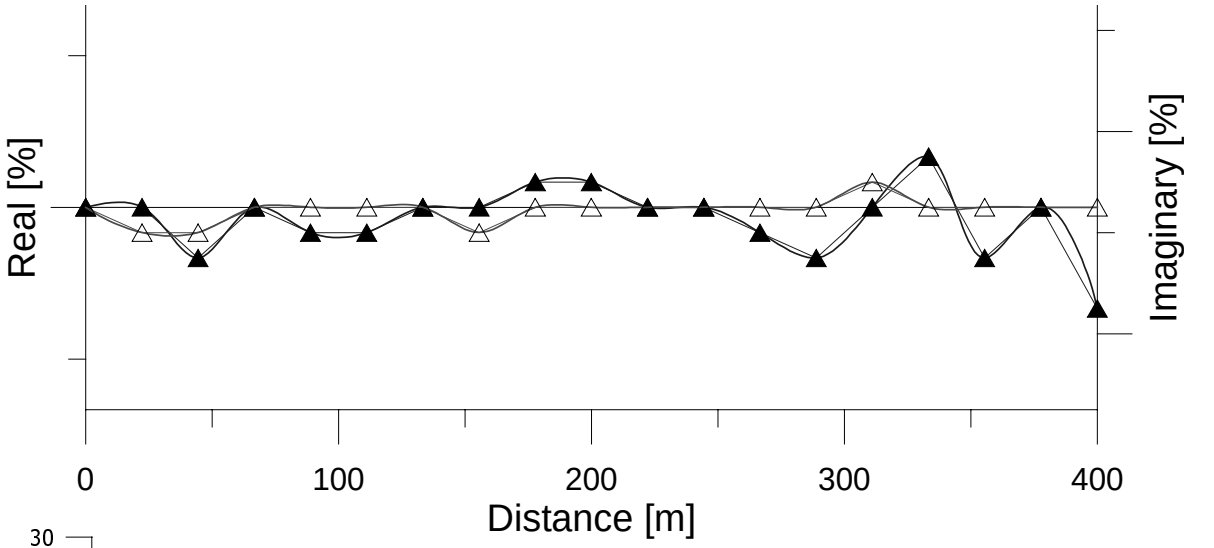

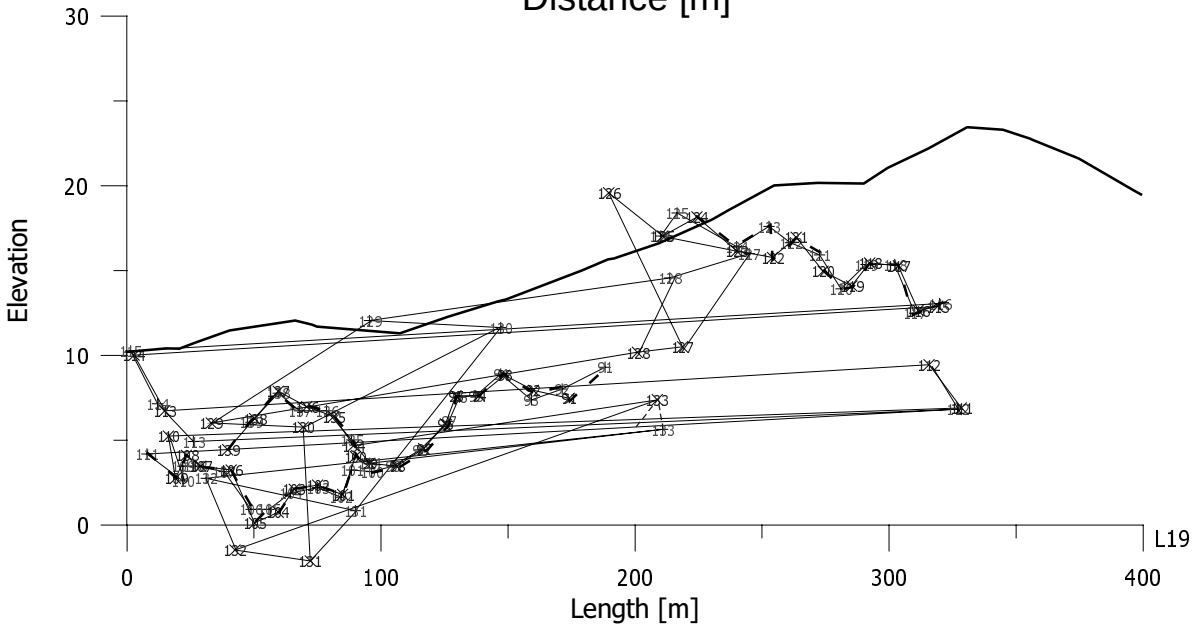

Profile 21.

VLF (top), Slingram (middle), GPR anomalies (bottom)
VLF measurements have been truncated in vicinity of powerline.

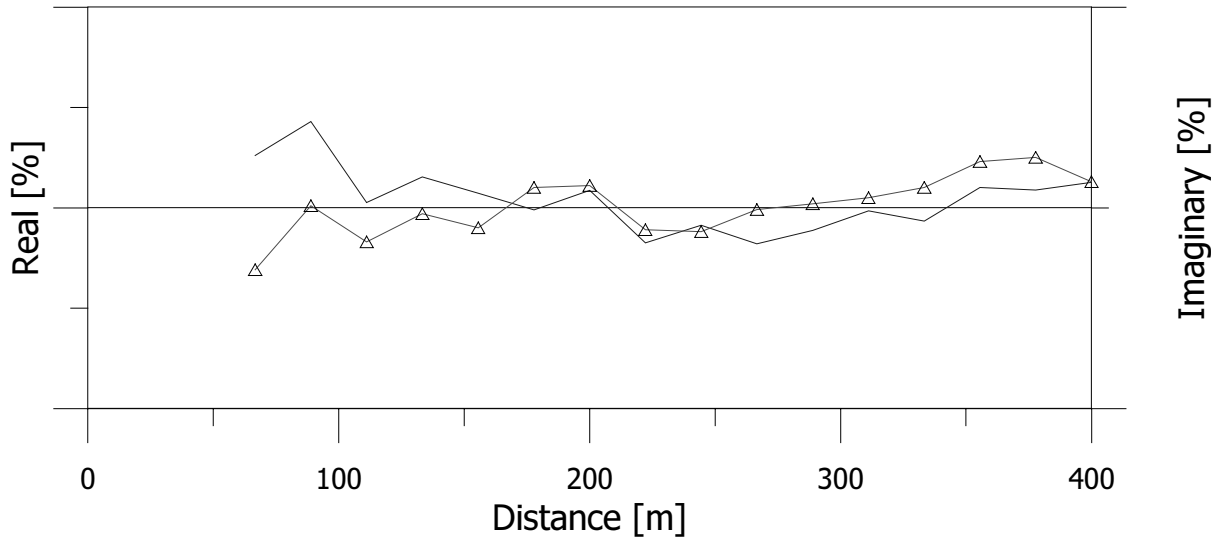

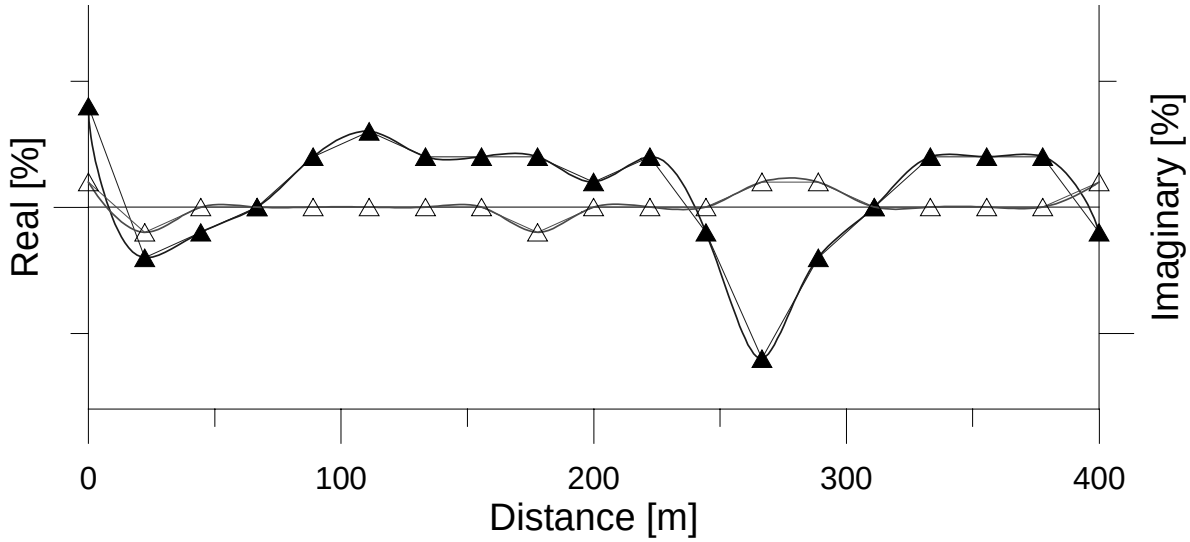

(contd. on page A2:22)

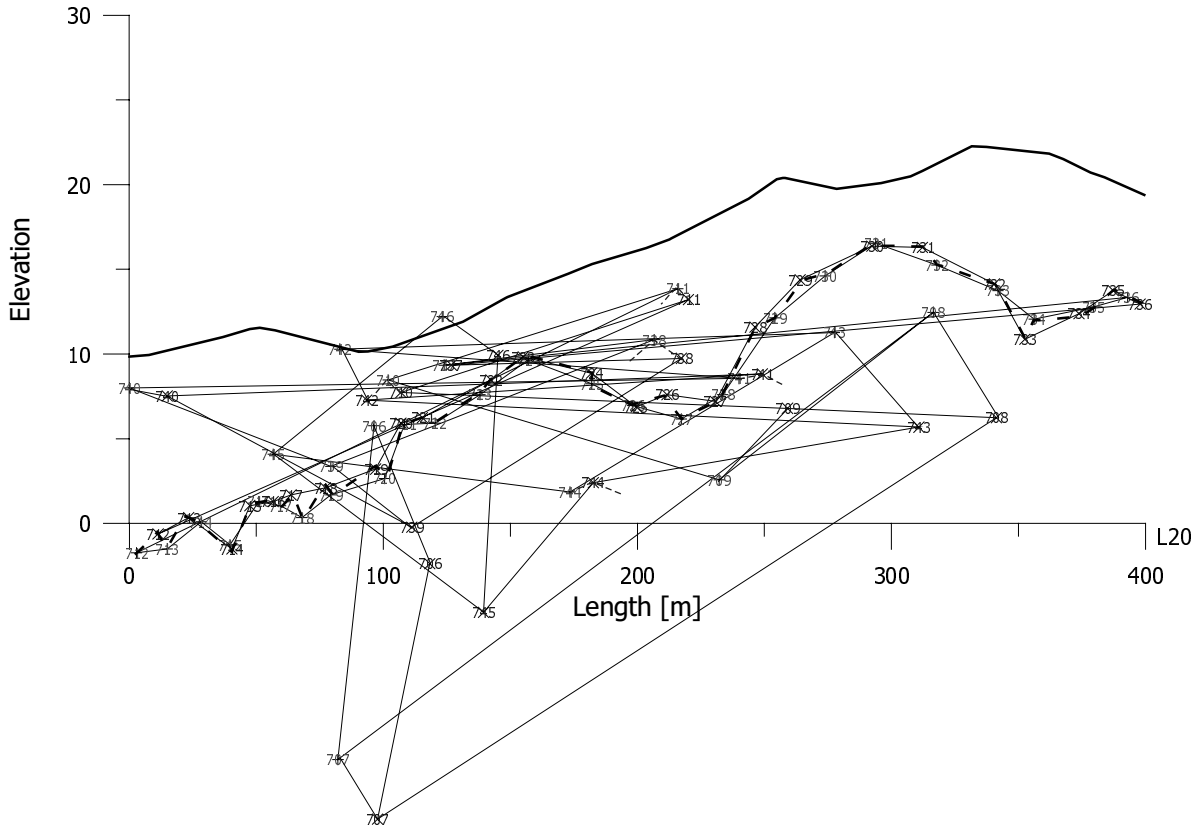
30
20
10
0
Elevation
0
100
200
300
400
Length [m]
L20

Appendix 3: Long GPR Profiles

This section comprises plots of the GPR profiles and picked reflectors. Both sets of data are corrected for elevation, however, only the GPR profiles are given in true coordinates. The interpretations are only measured in distance.

GPR Profile 0

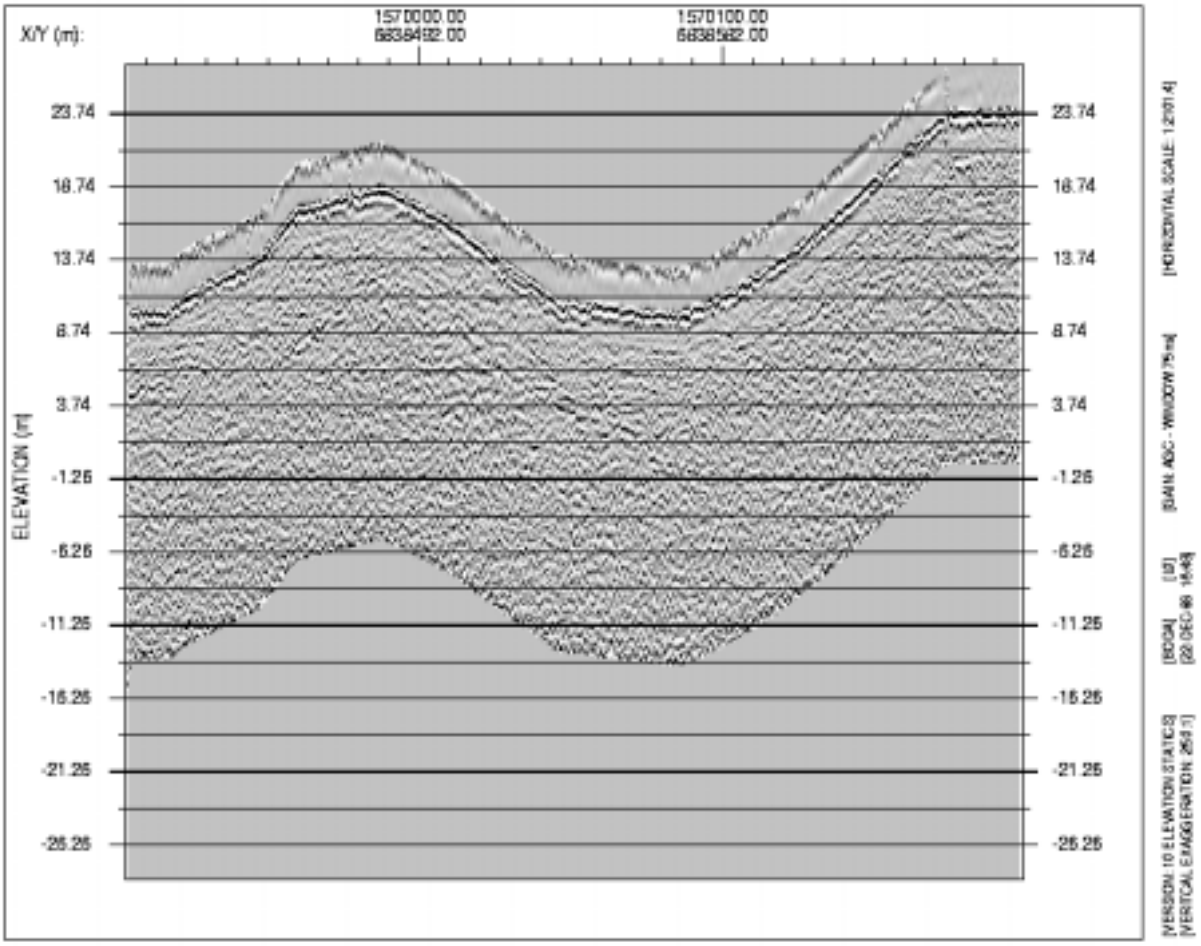

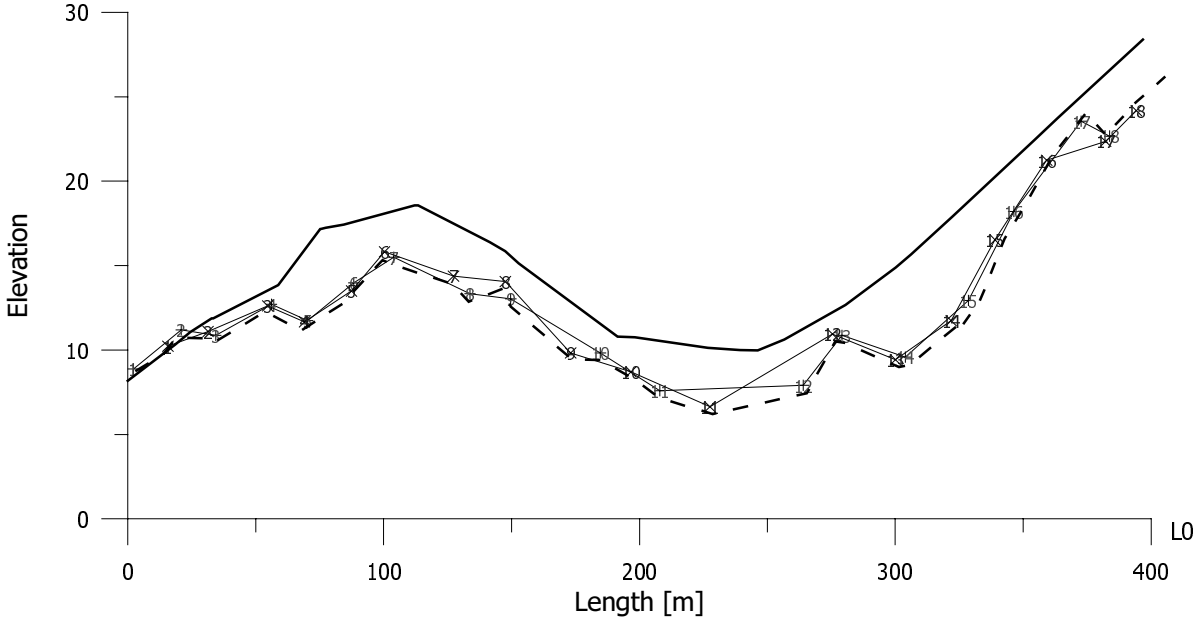

GPR Profile 1

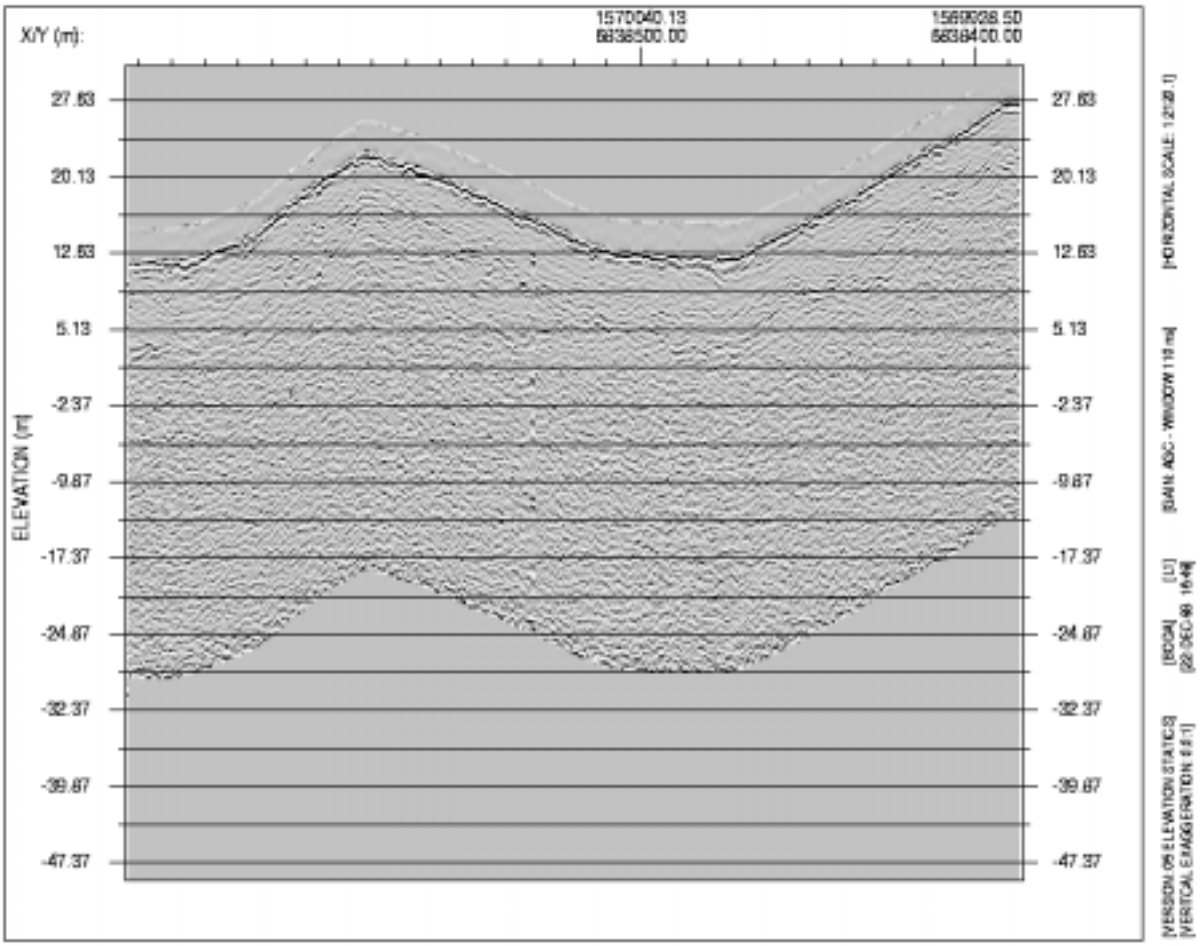

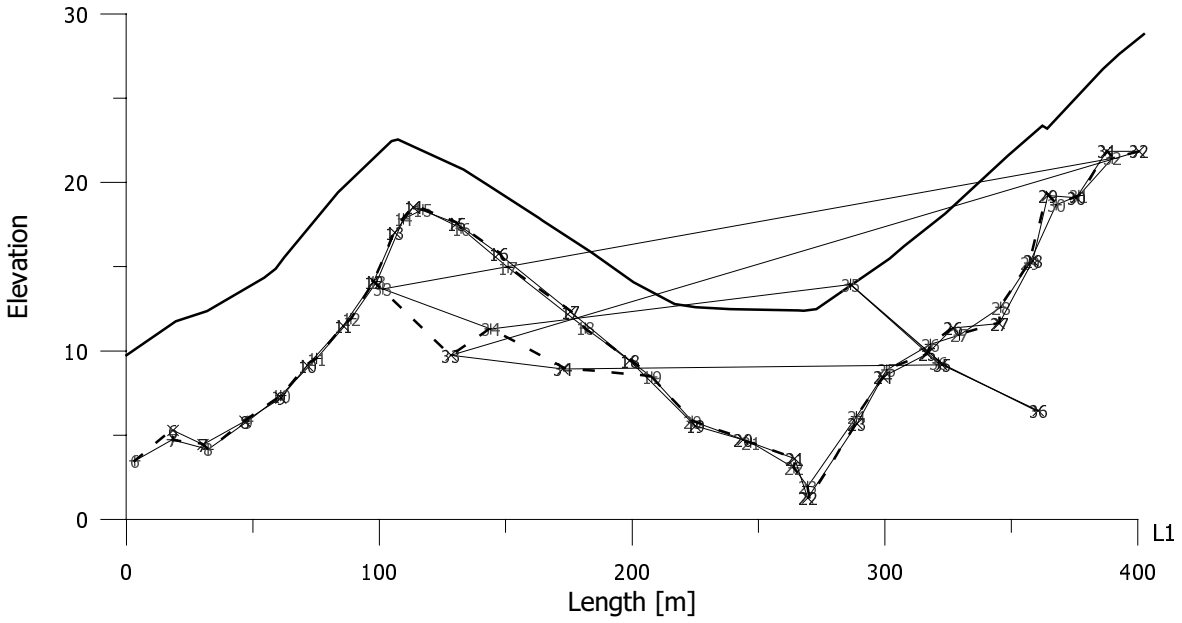

GPR profile 2.

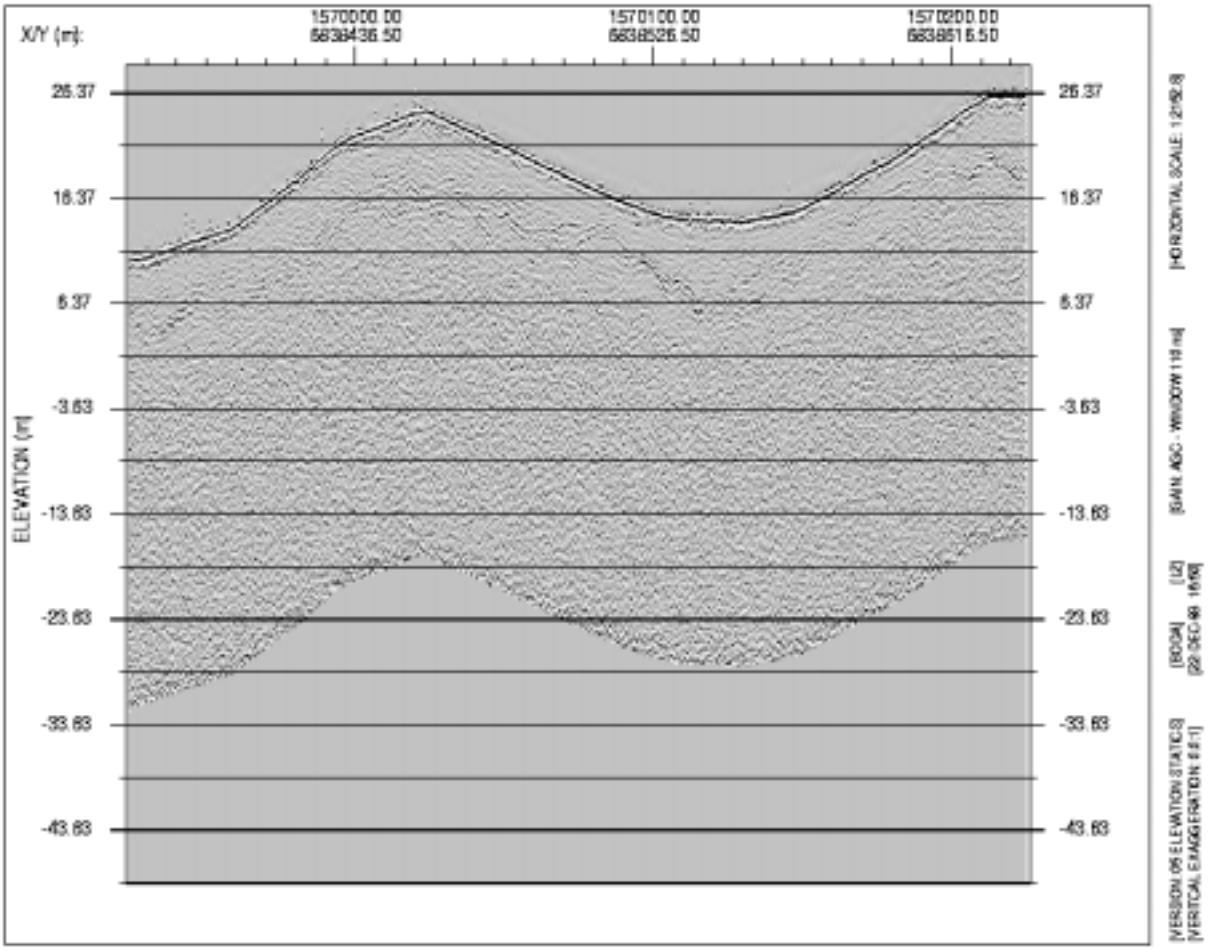

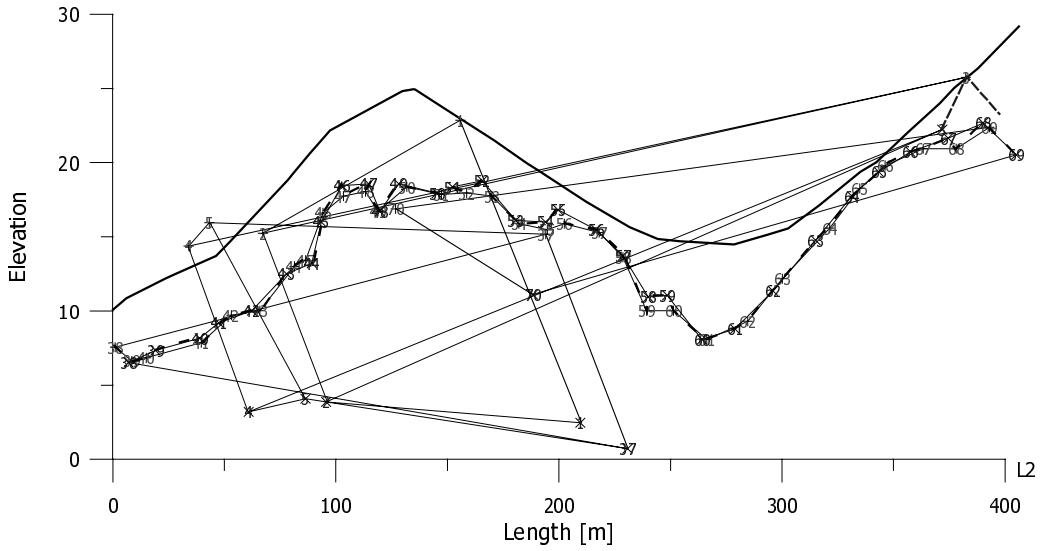

GPR profile 3.

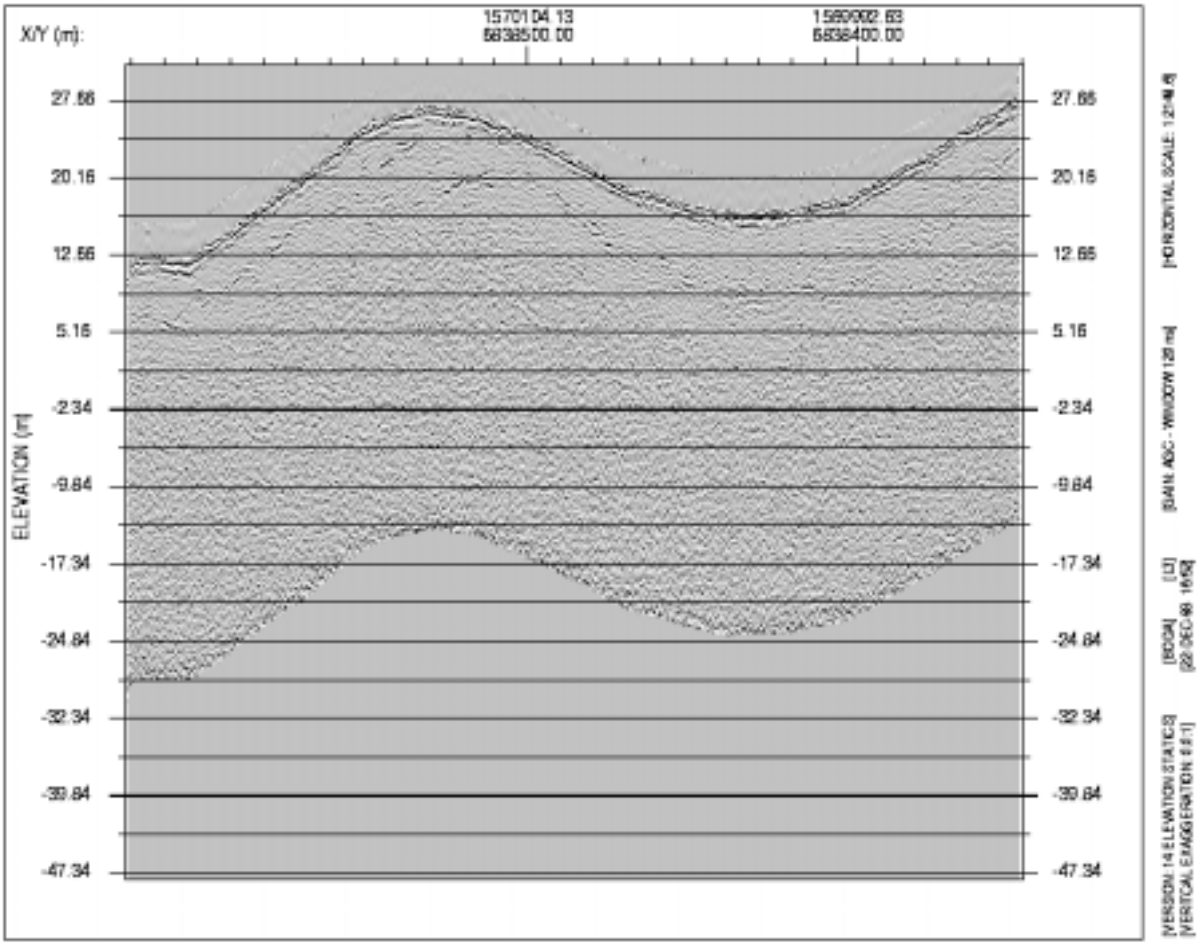

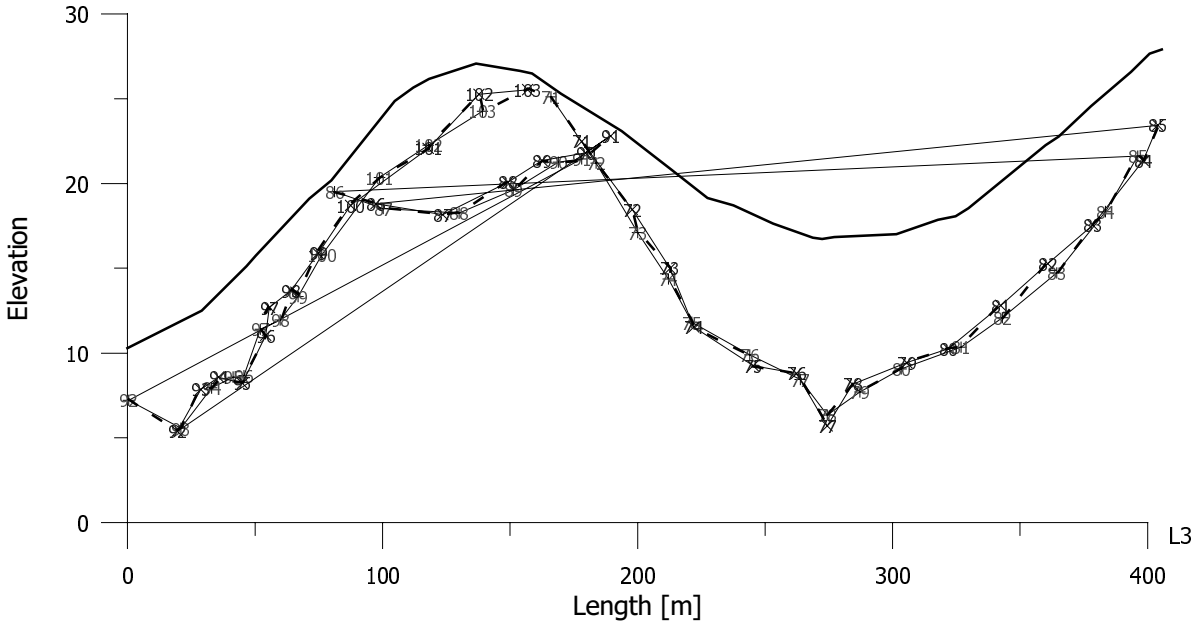

GPR profile 4.

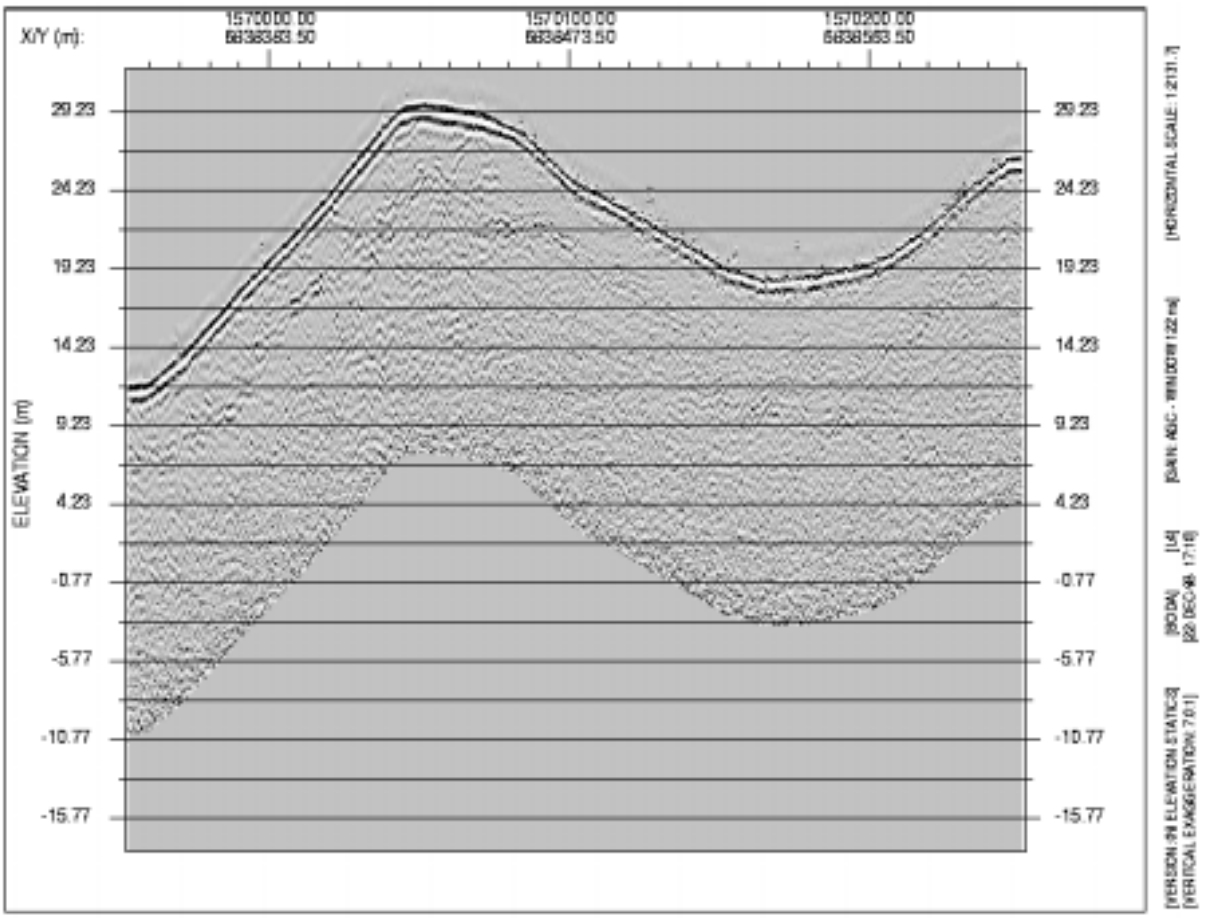

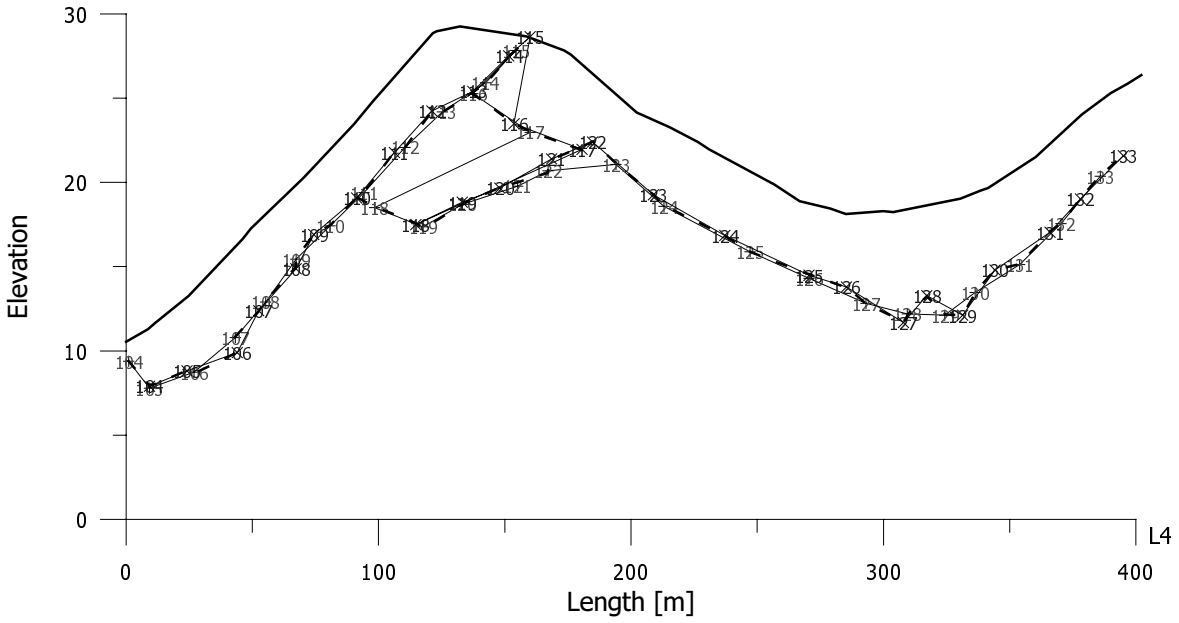

GPR profile 5.

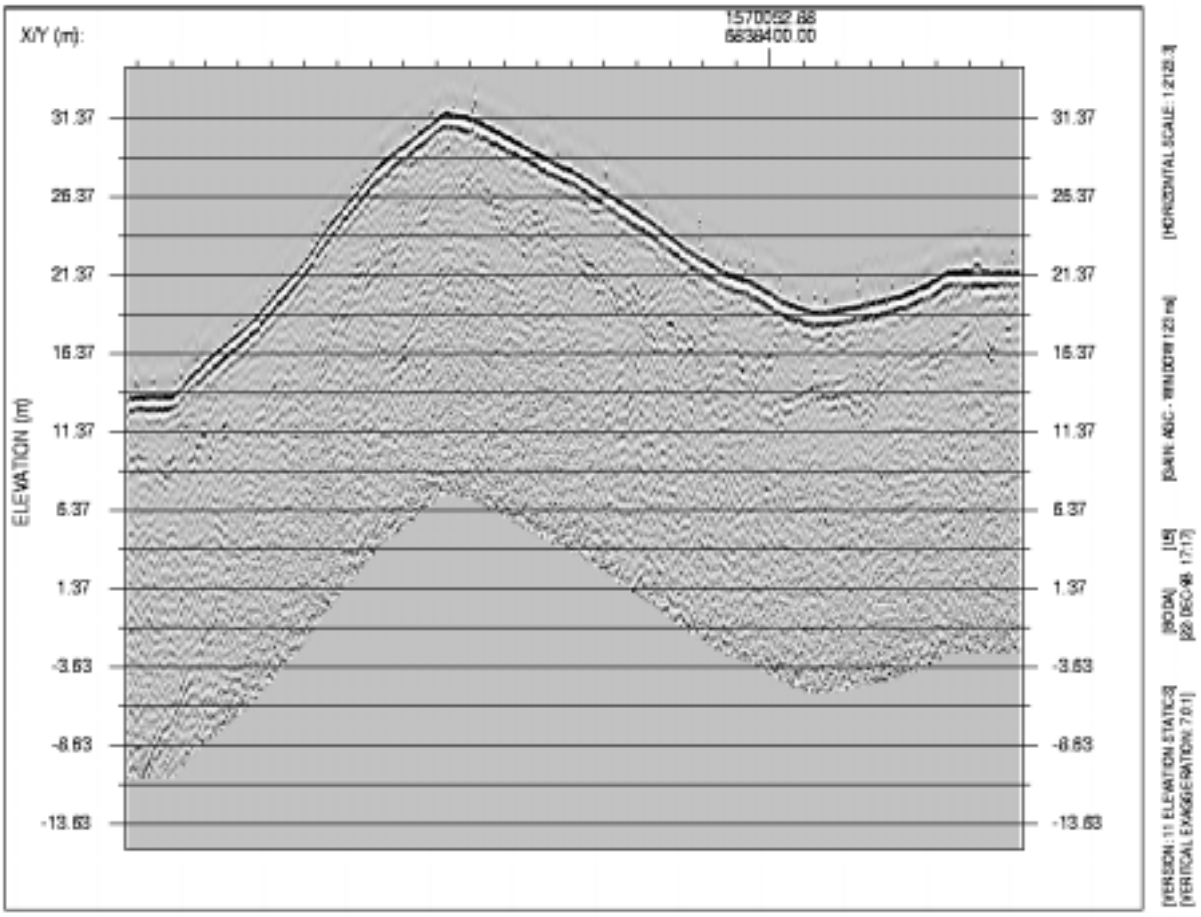

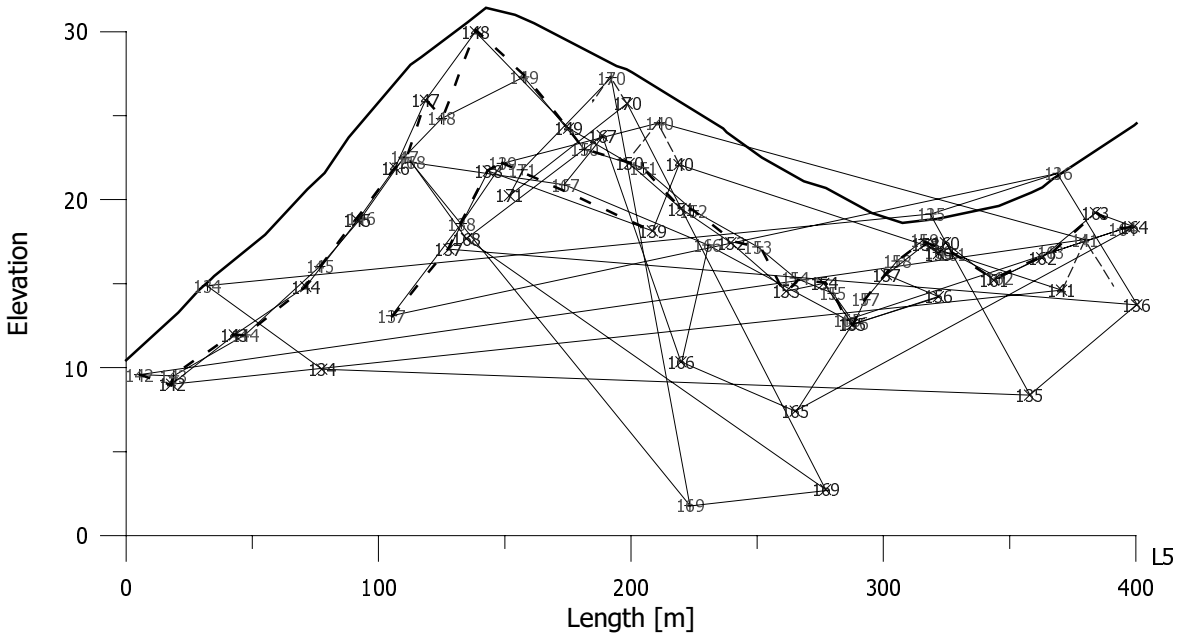

GPR profile 6

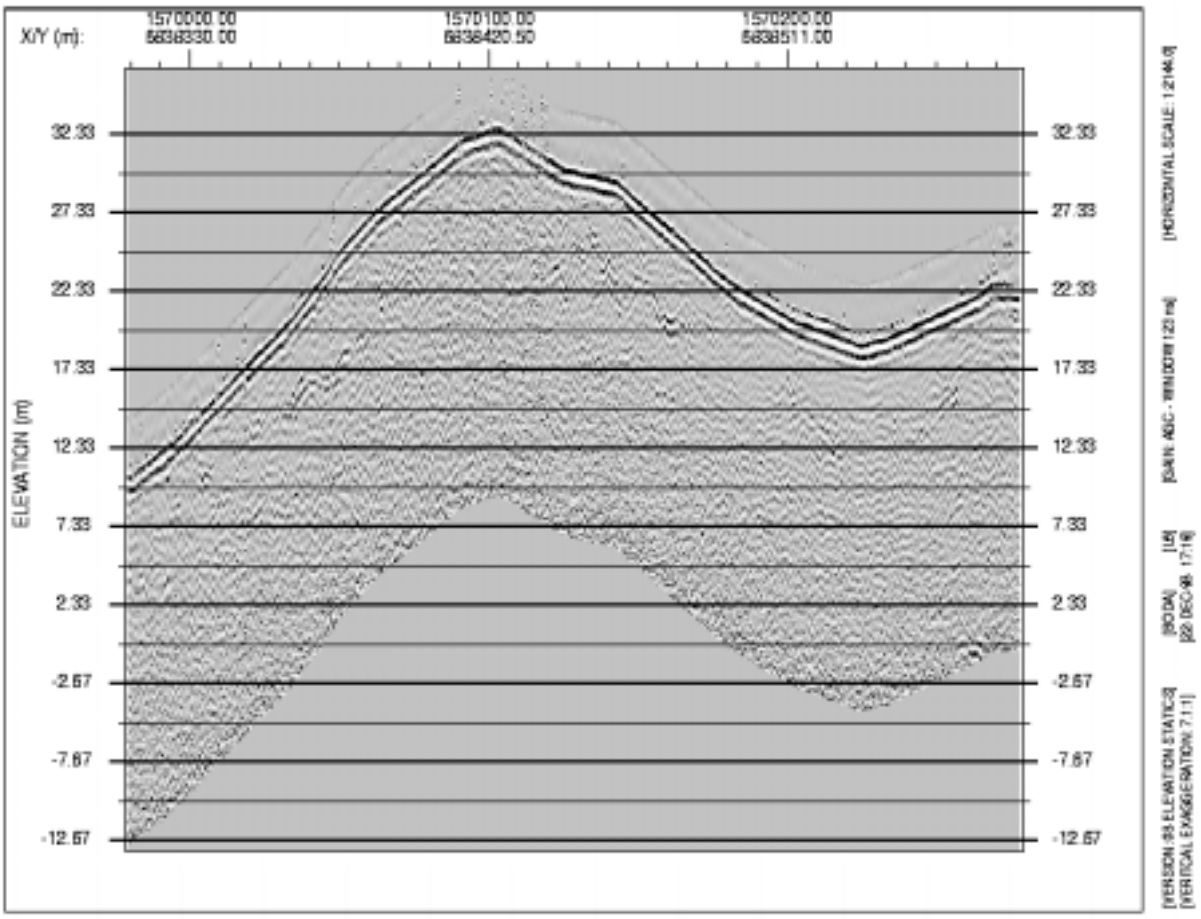

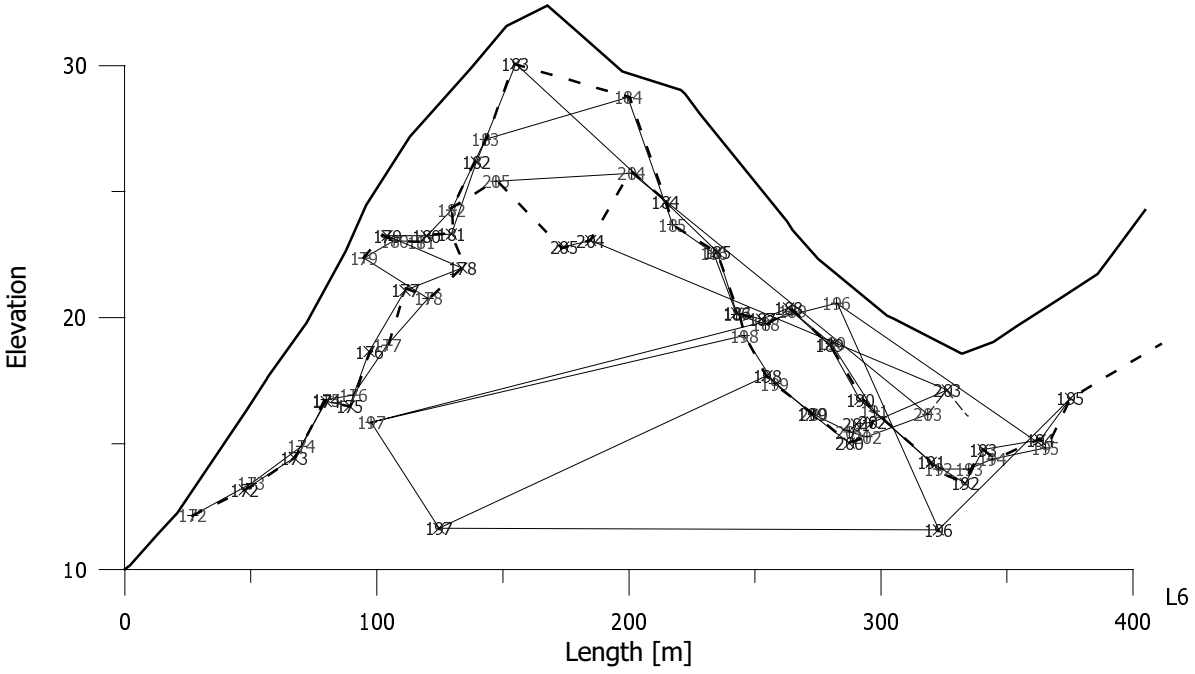

GPR profile 7

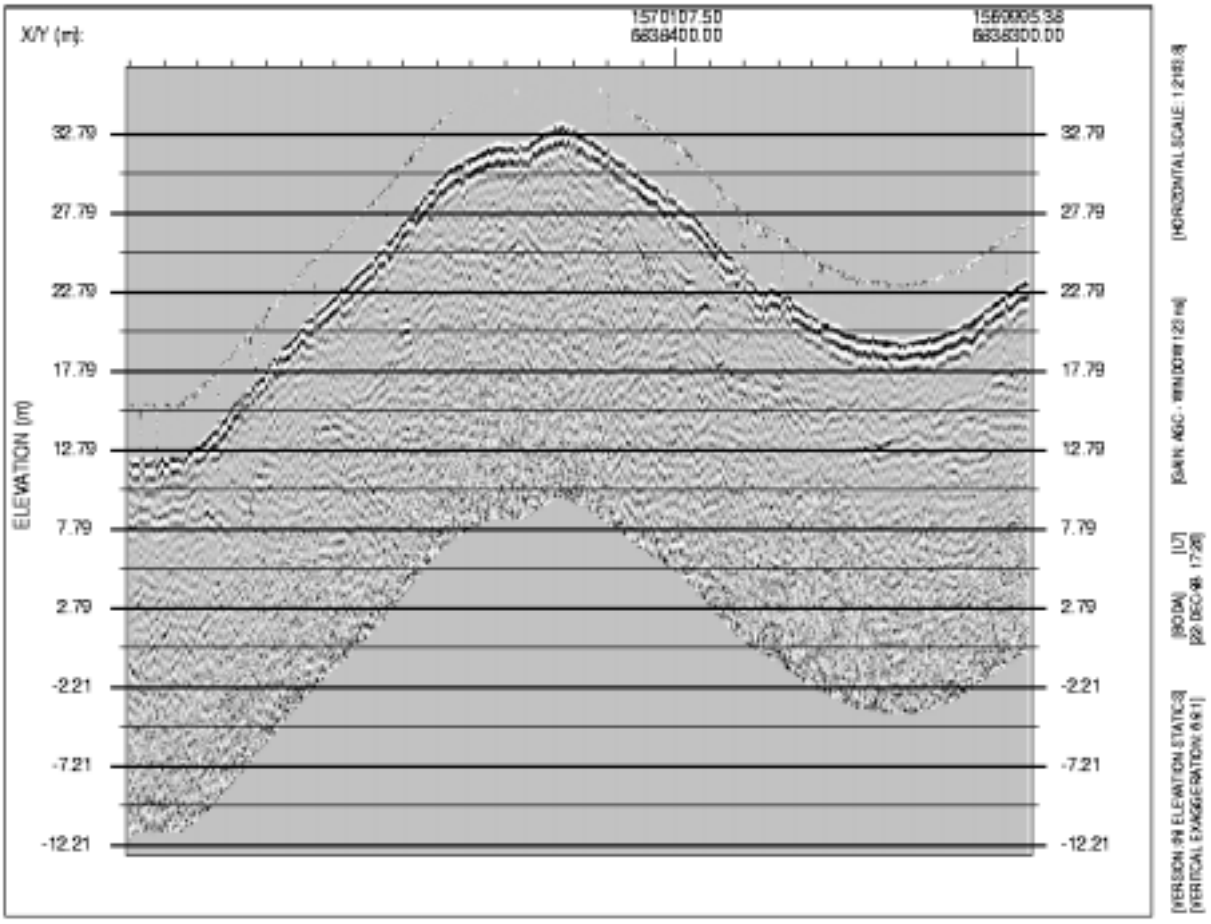

.

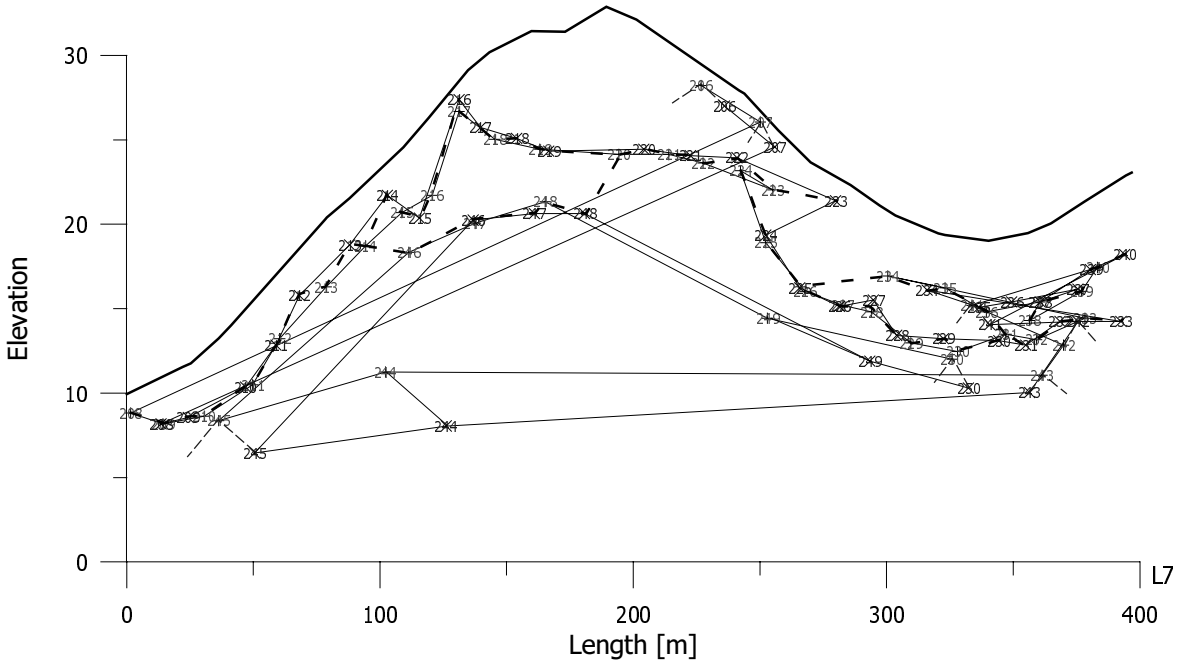

GPR profile 8.

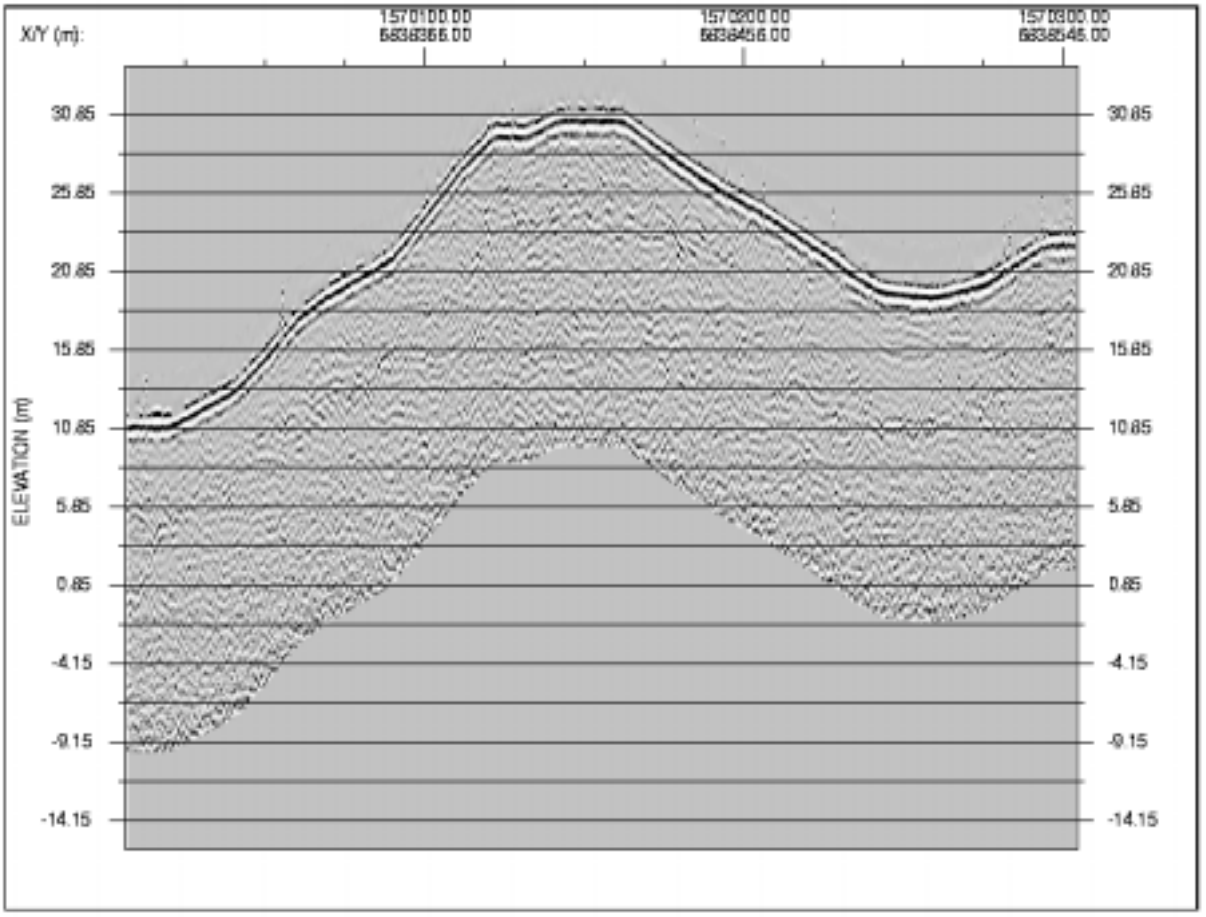

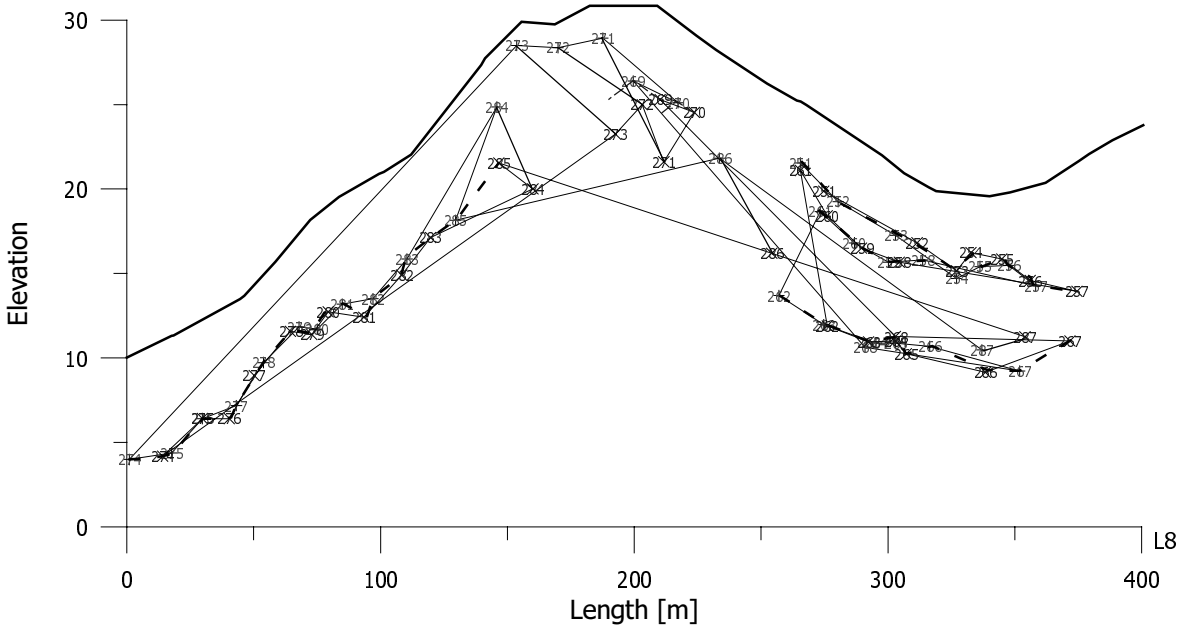

GPR profile 9

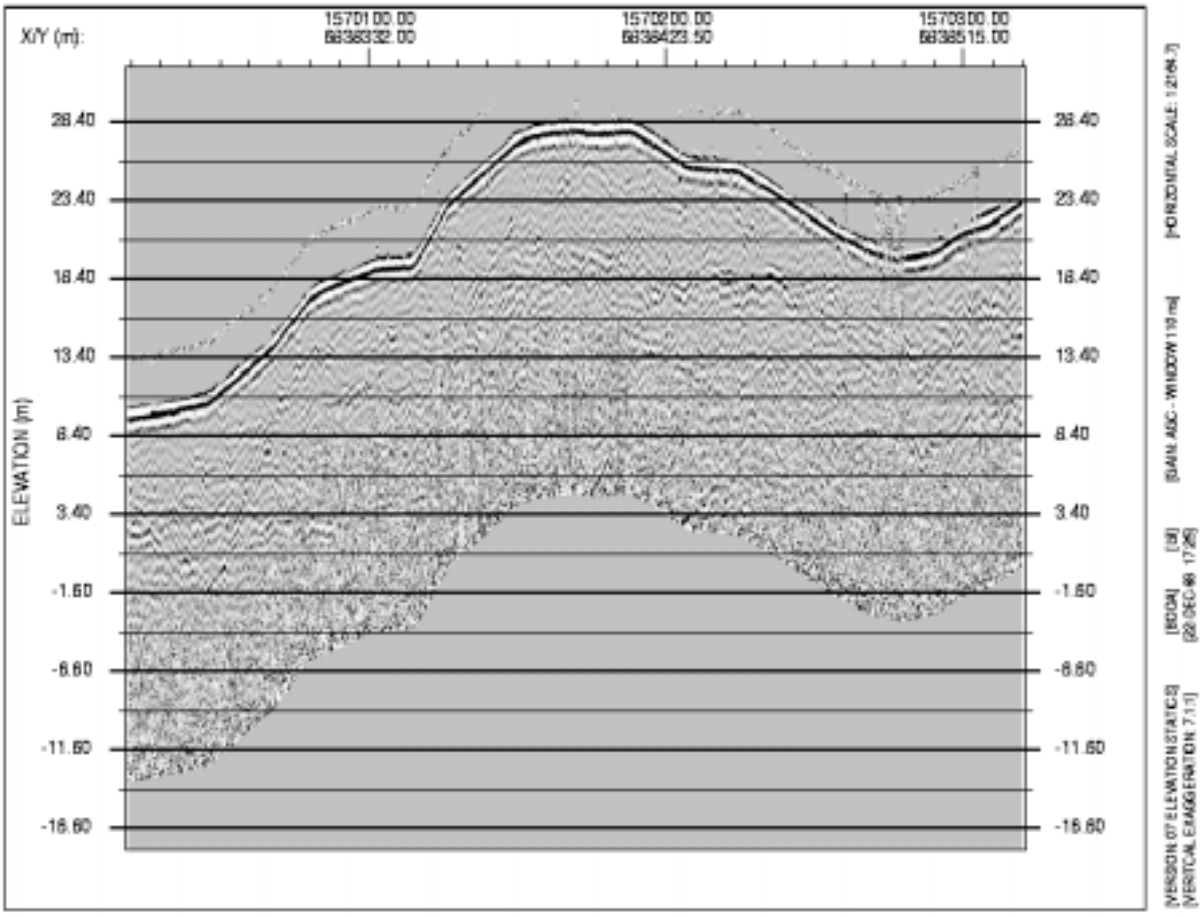

.

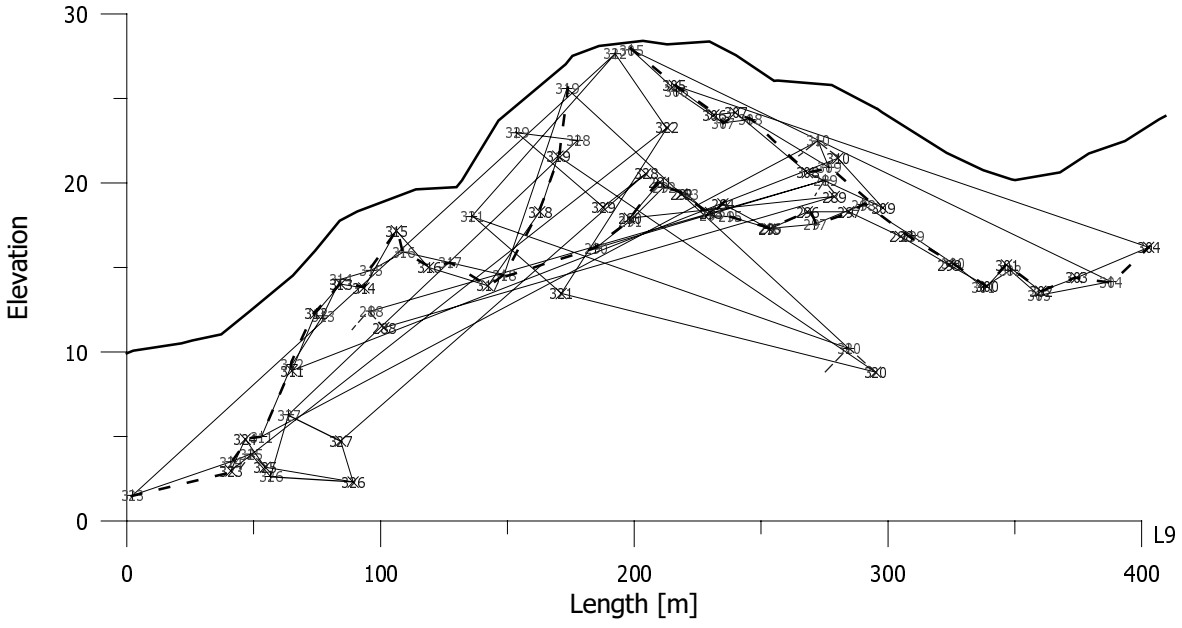

GPR Profile 10

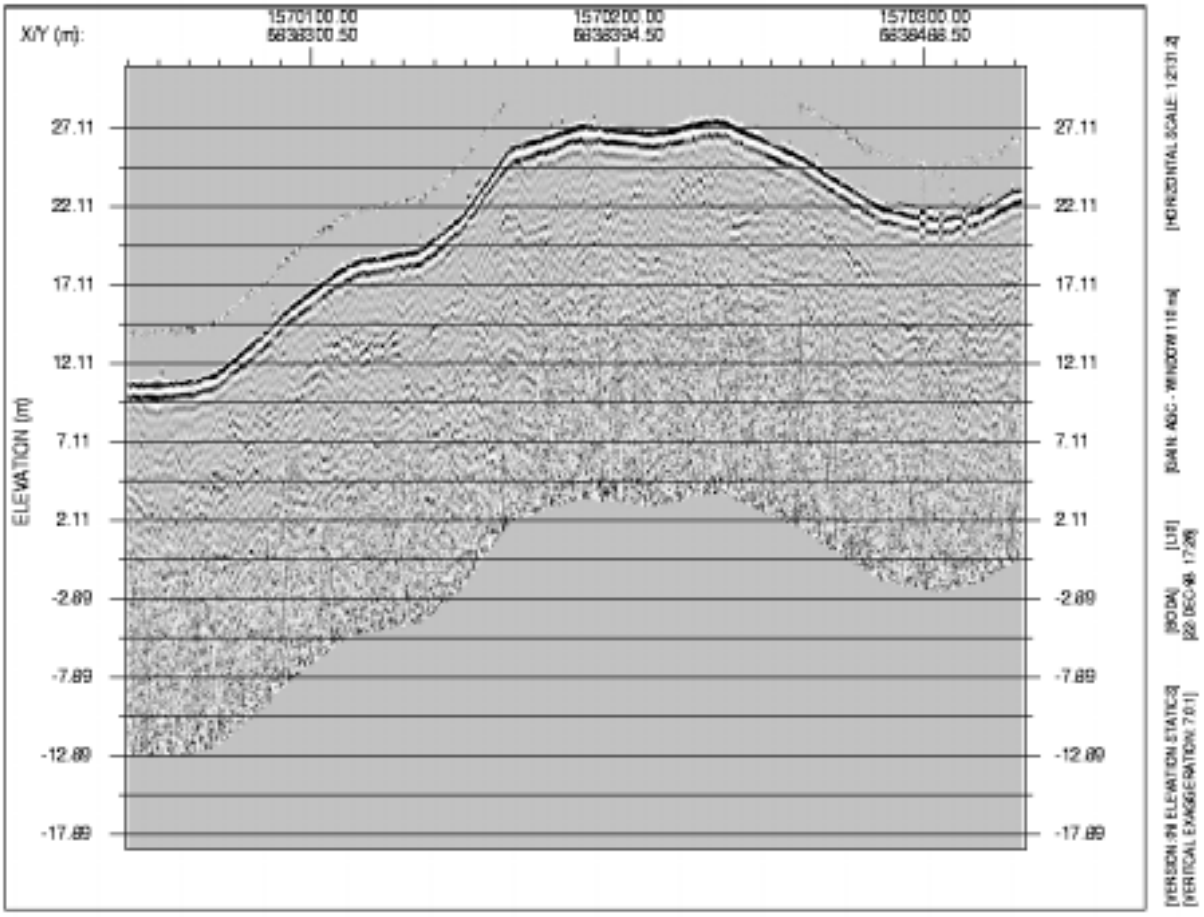

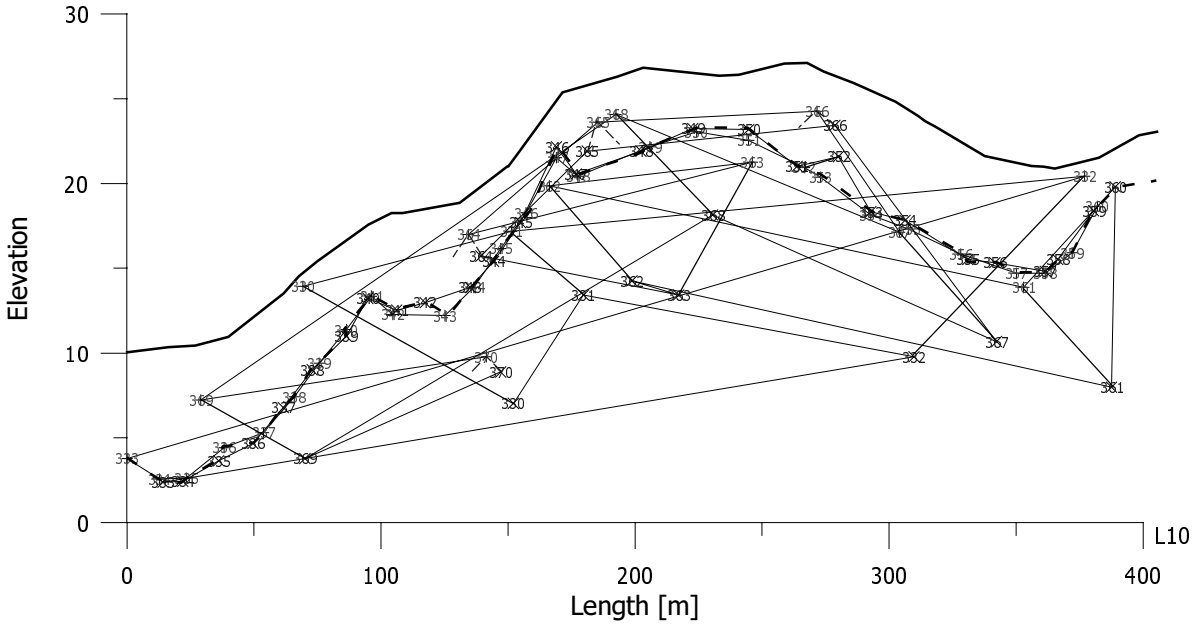

GPR Profile 11

Radar plot missing

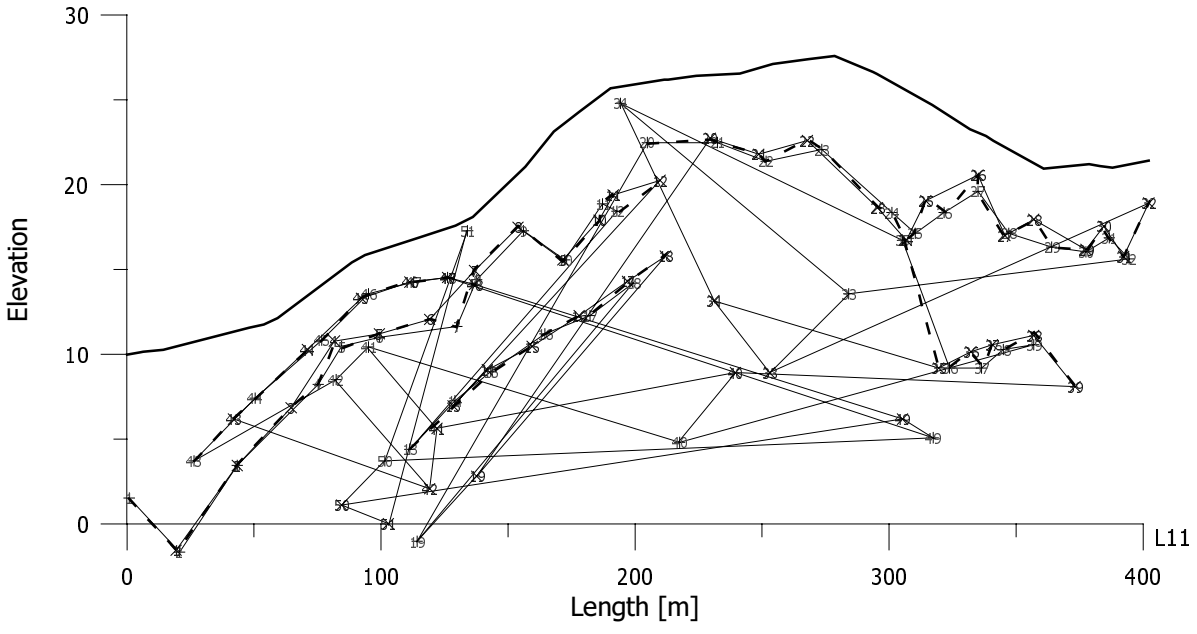

GPR profile 12

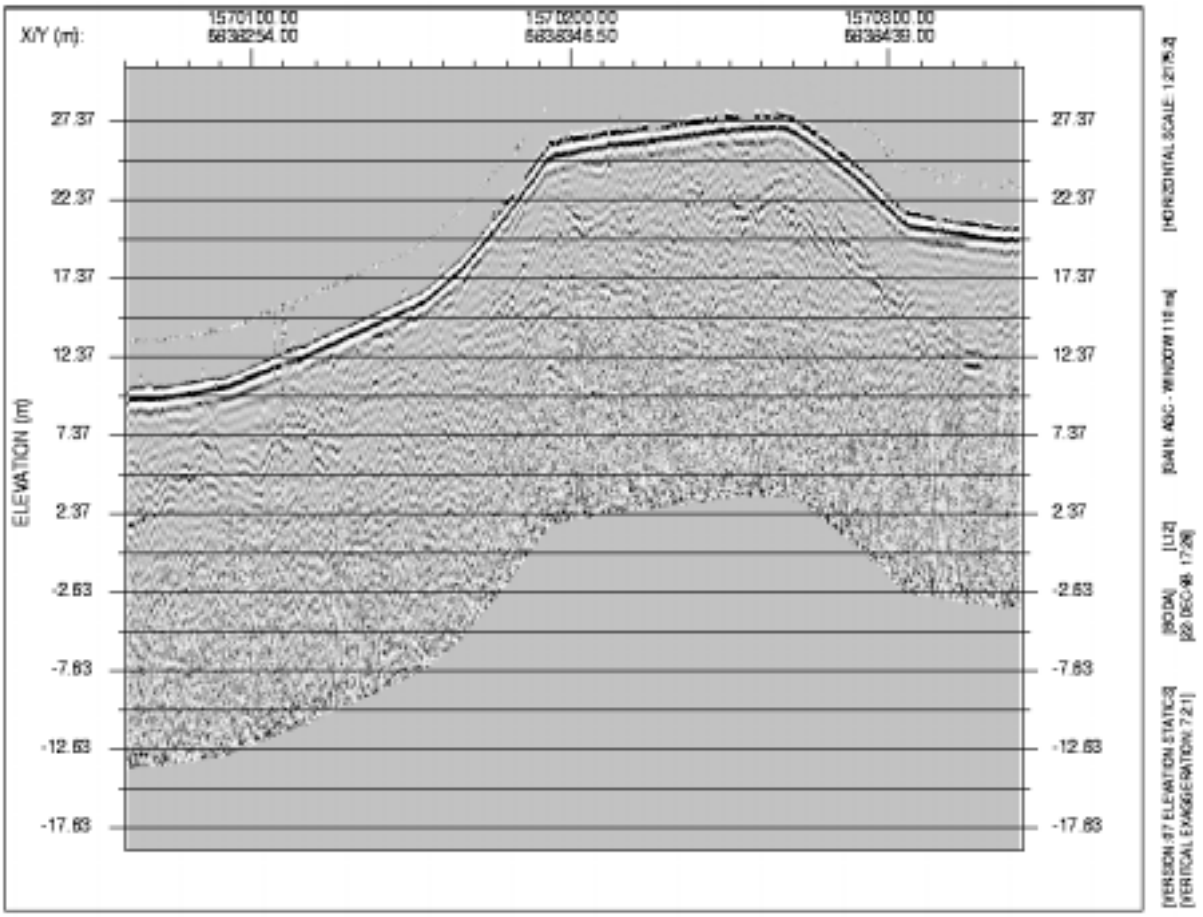

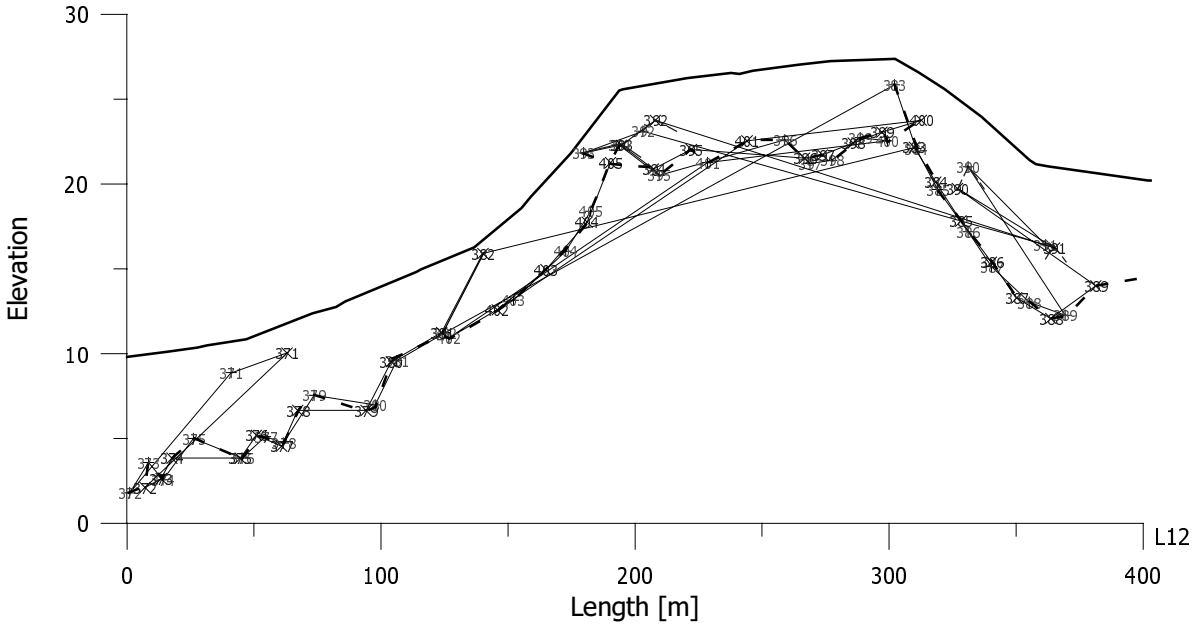

GPR Profile 13

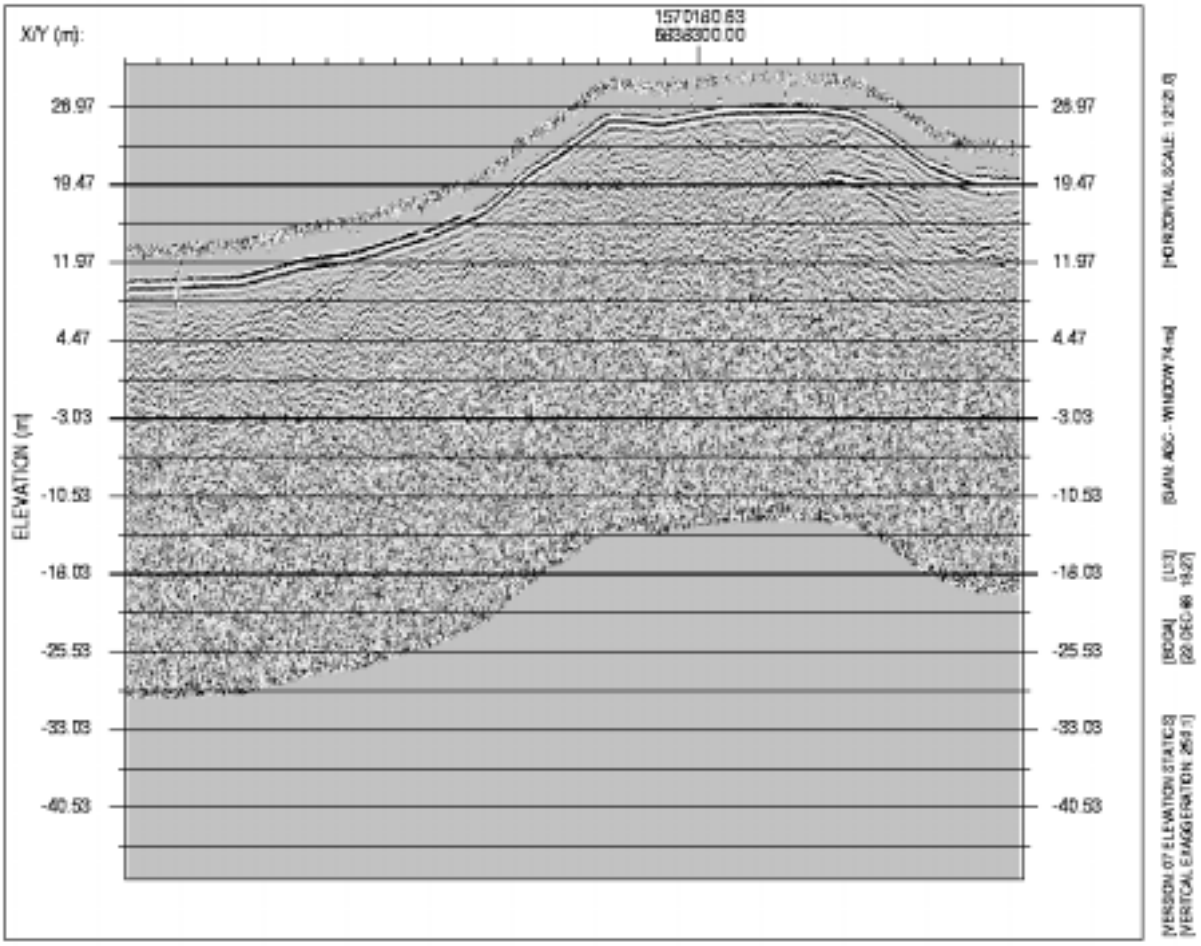

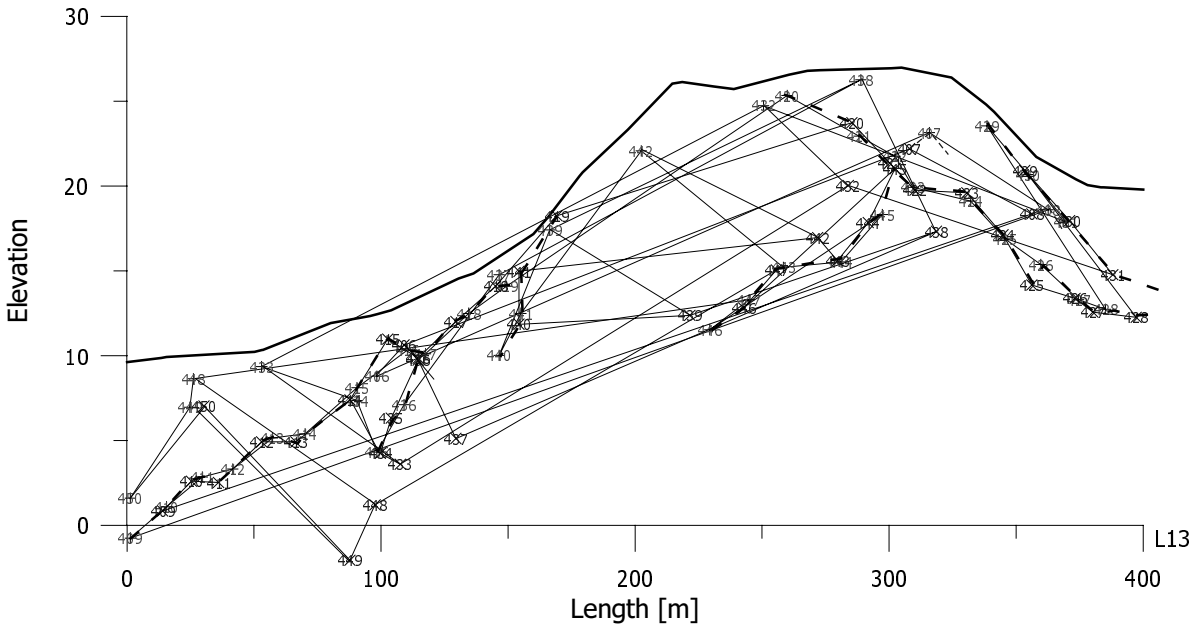

GPR Profile 14

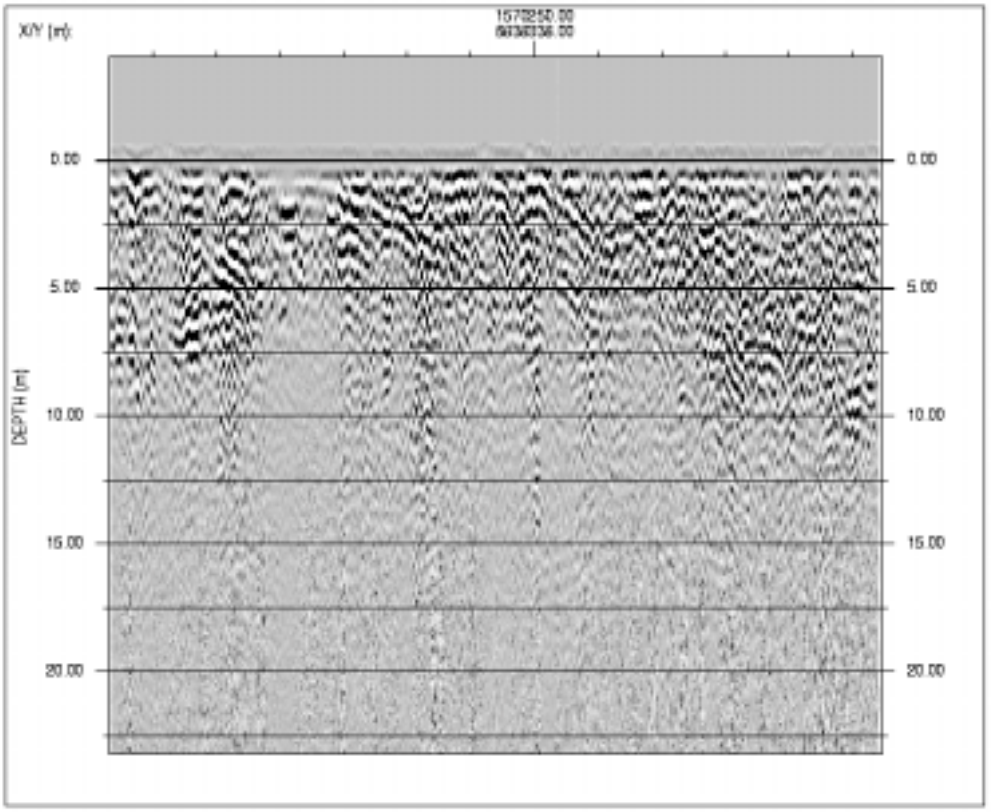

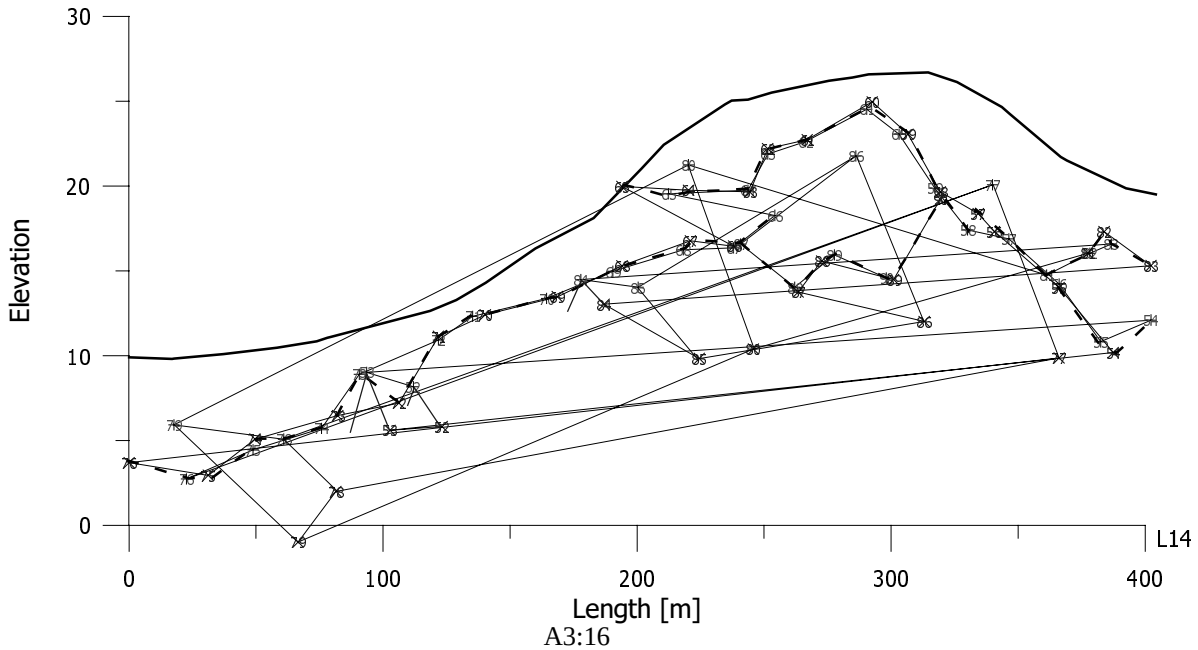

GPR Profile 15

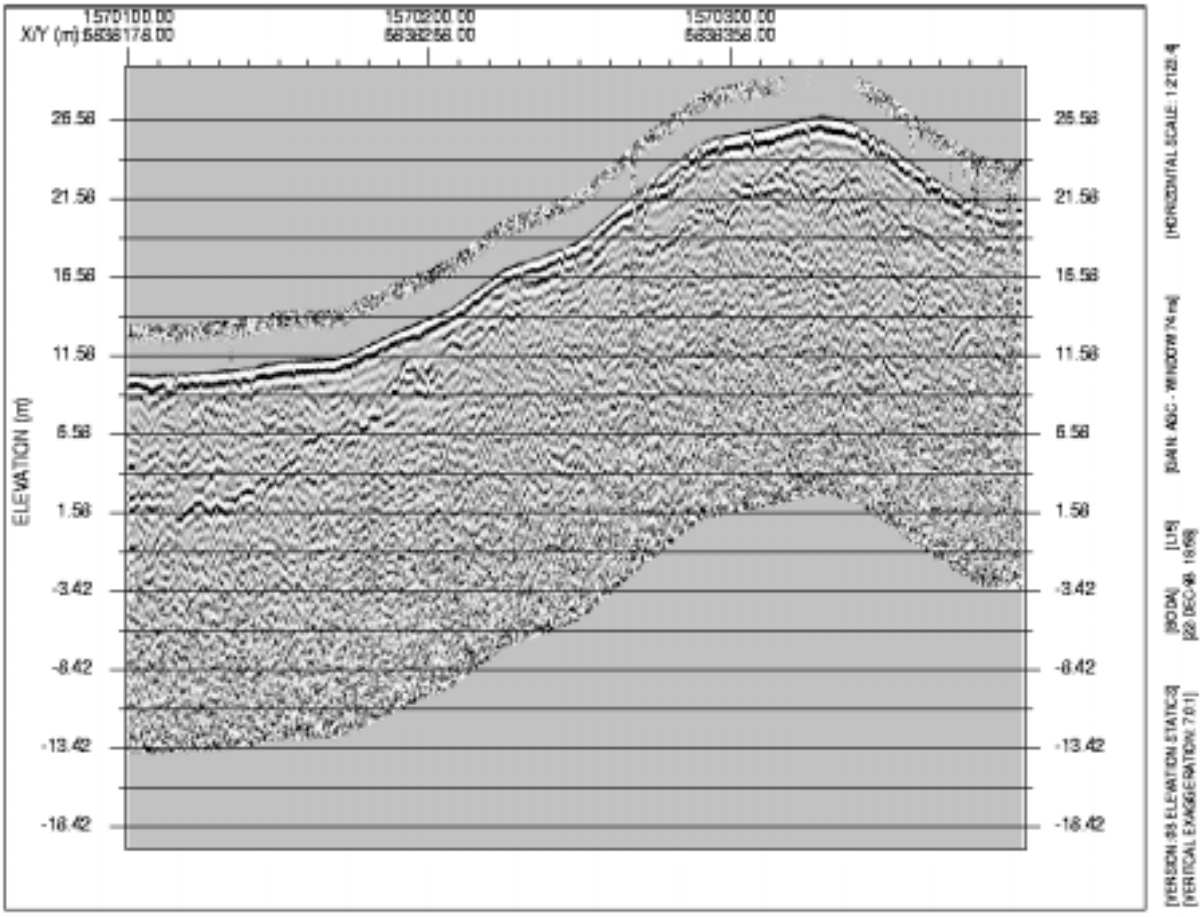

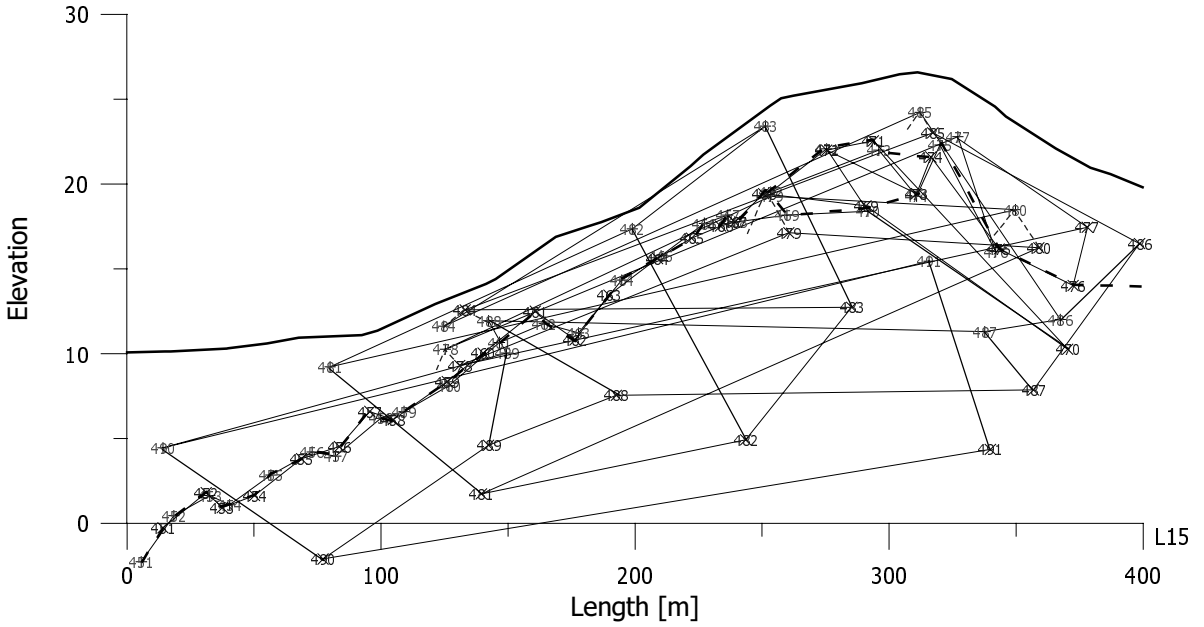

GPR Profile 16

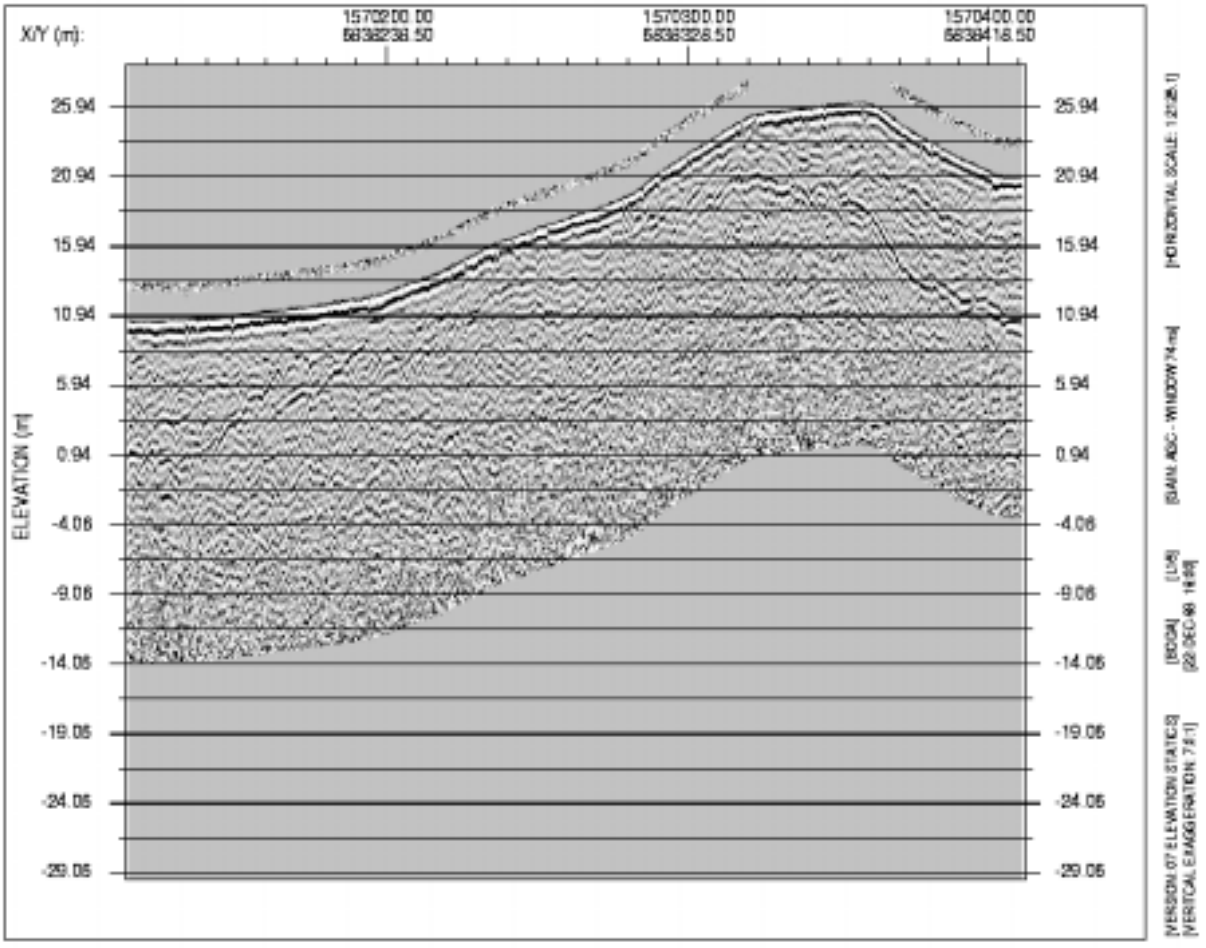

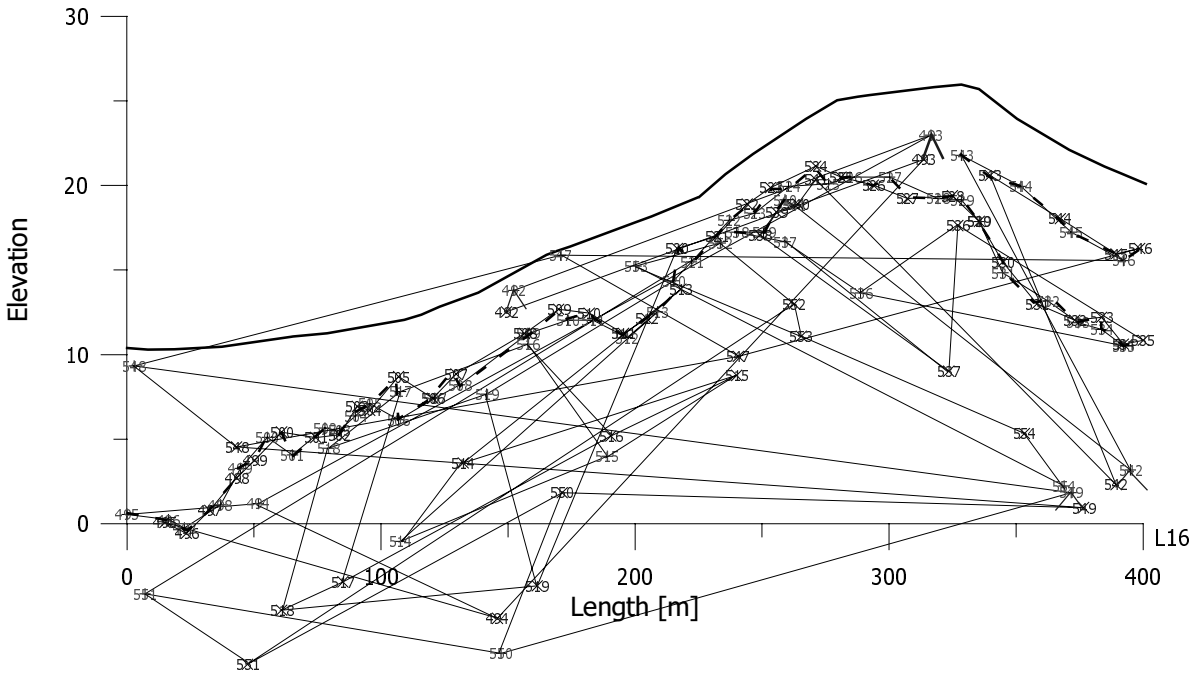

GPR Profile 17

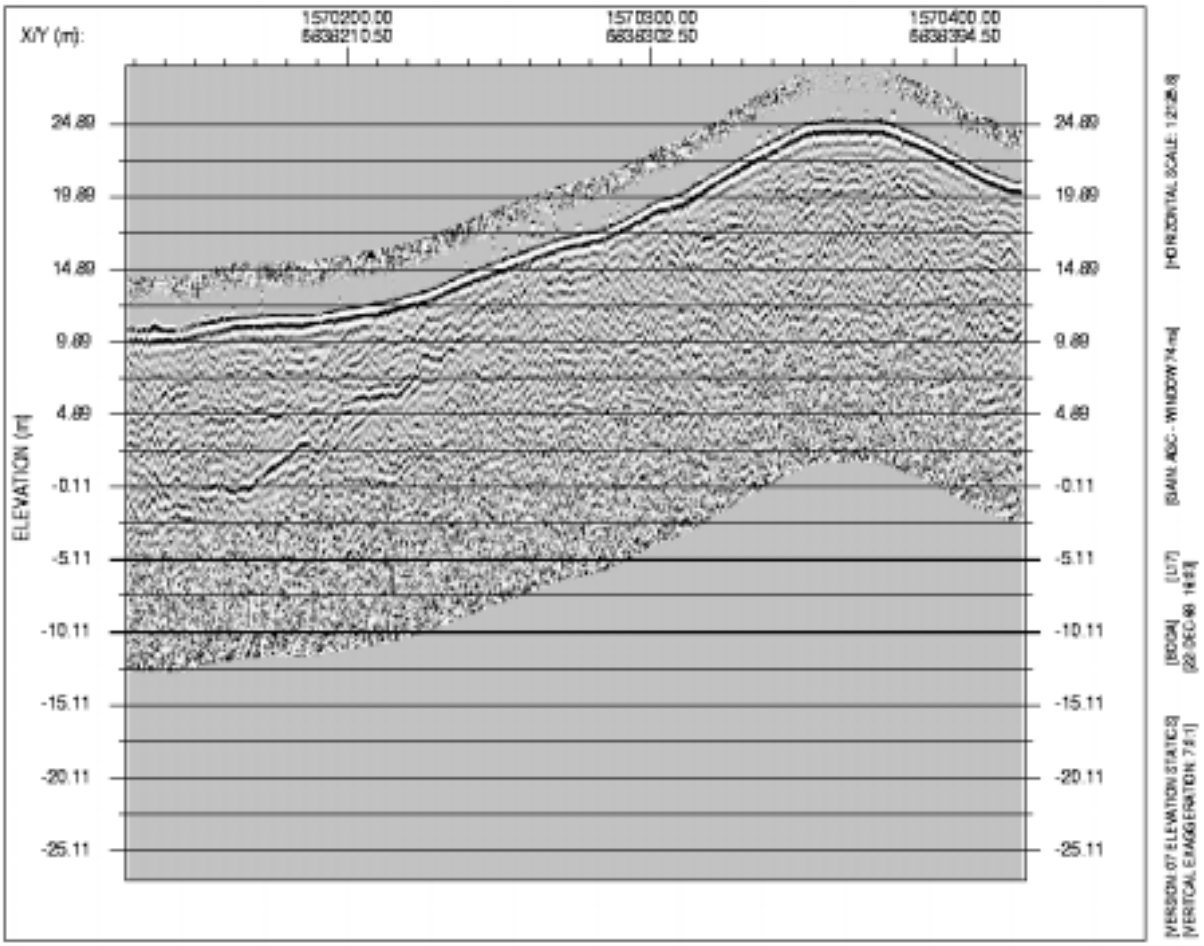

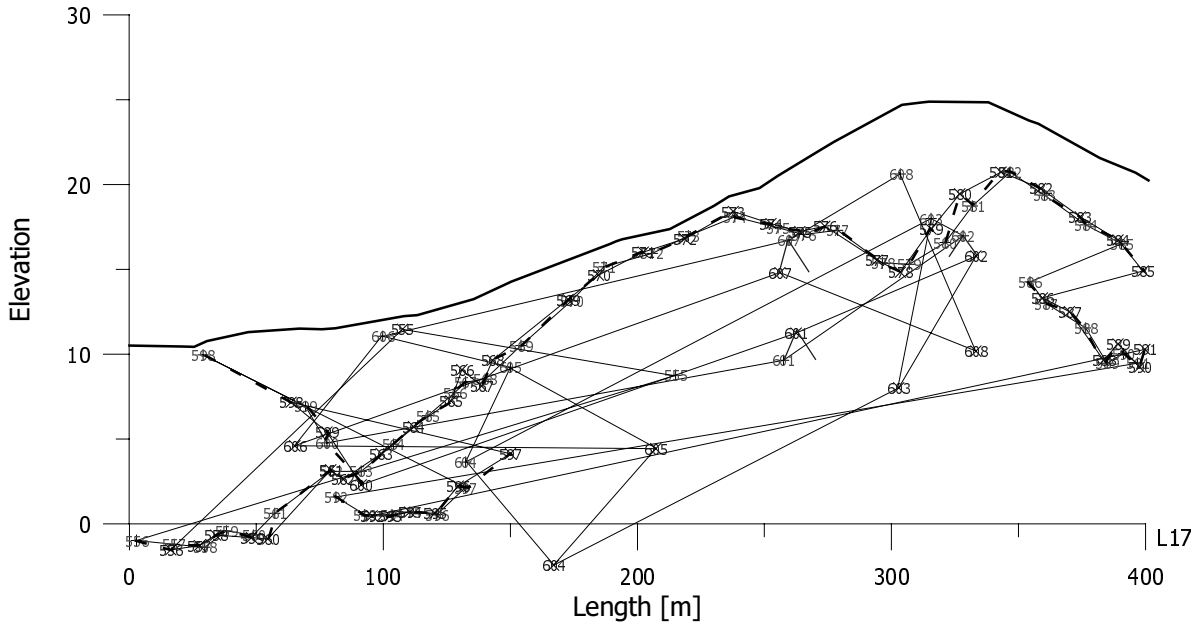

GPR Profile 18

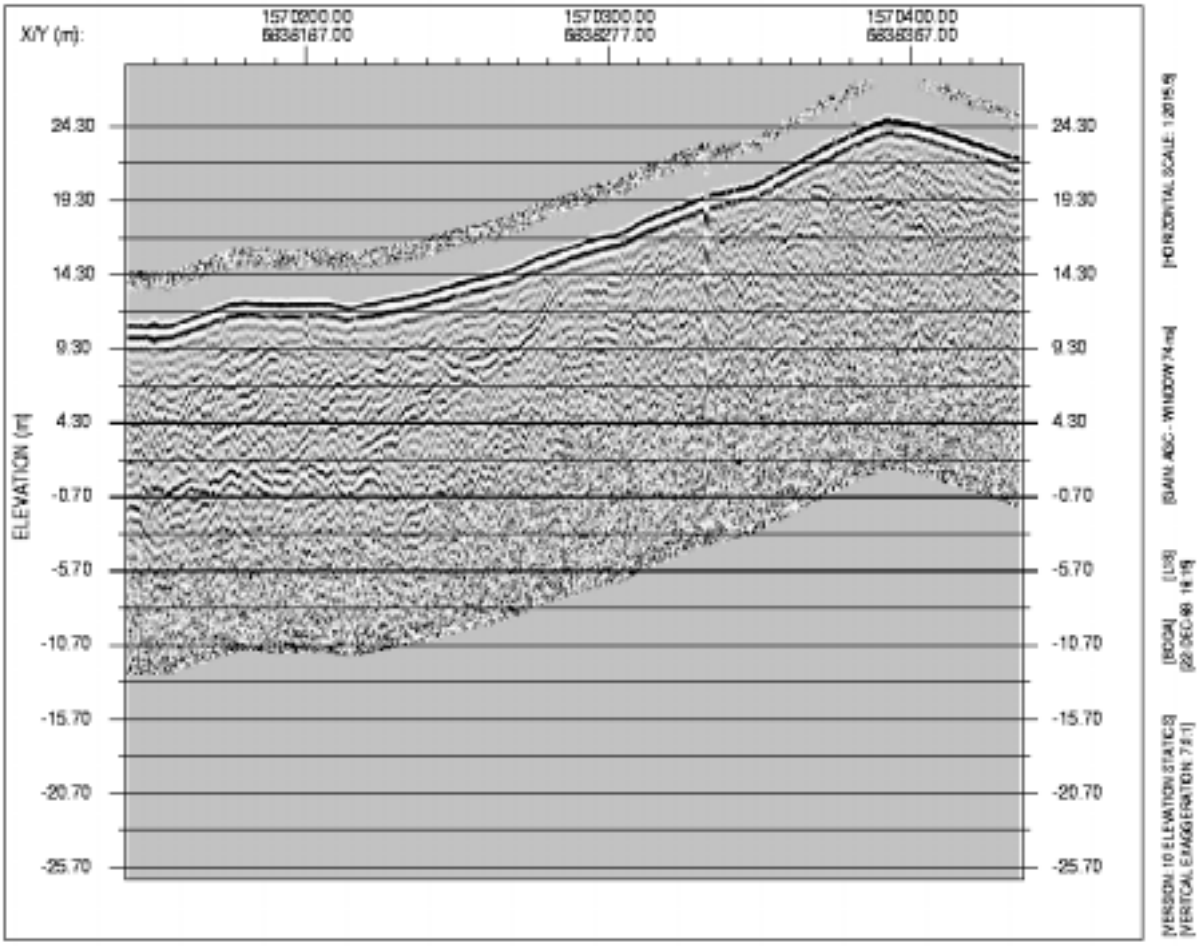

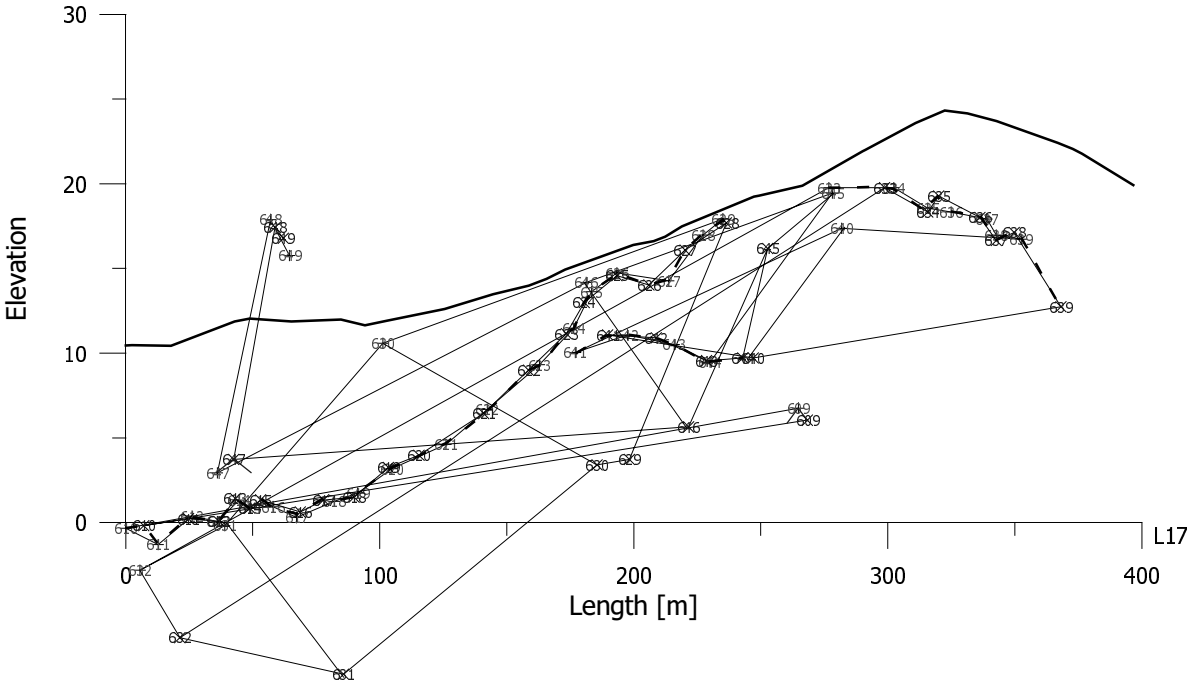

GPR Profile 19

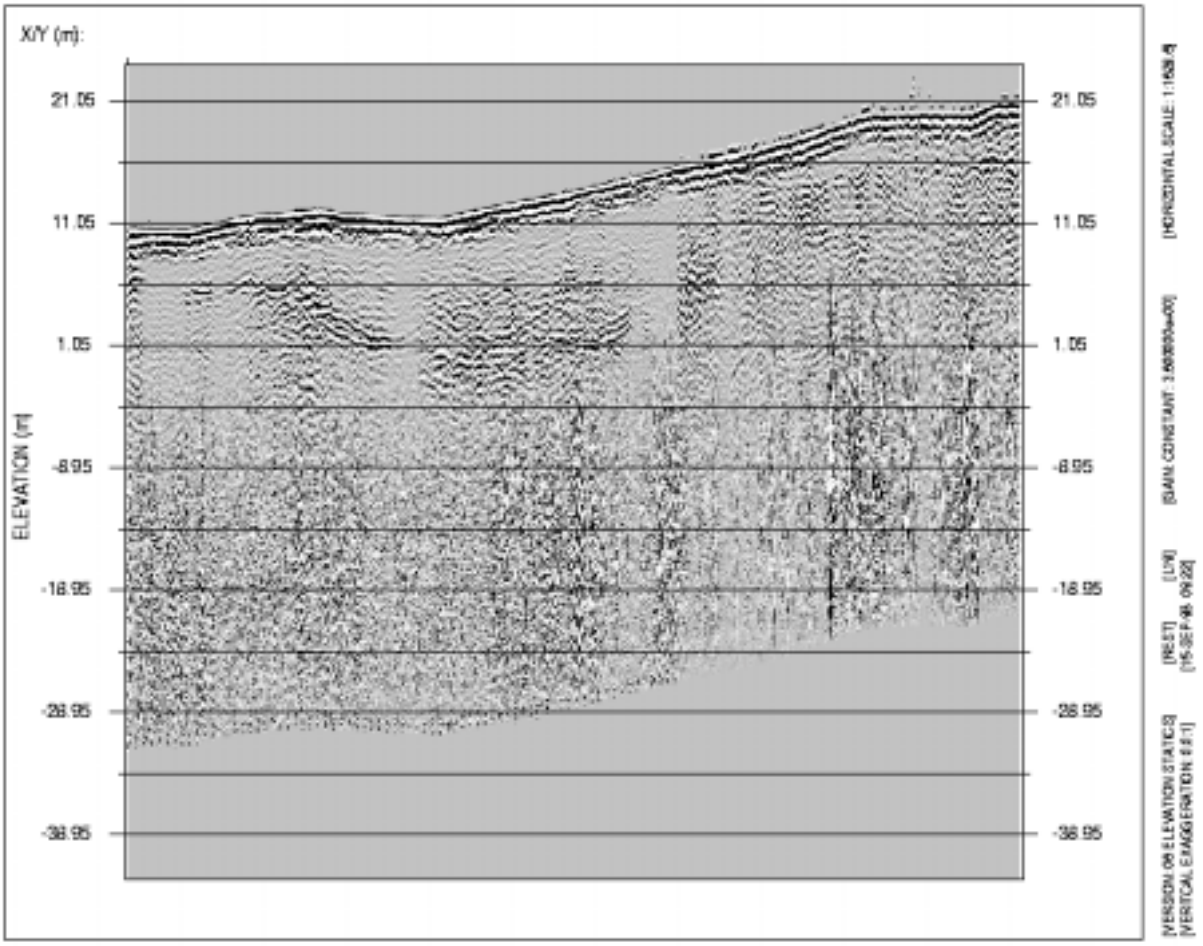

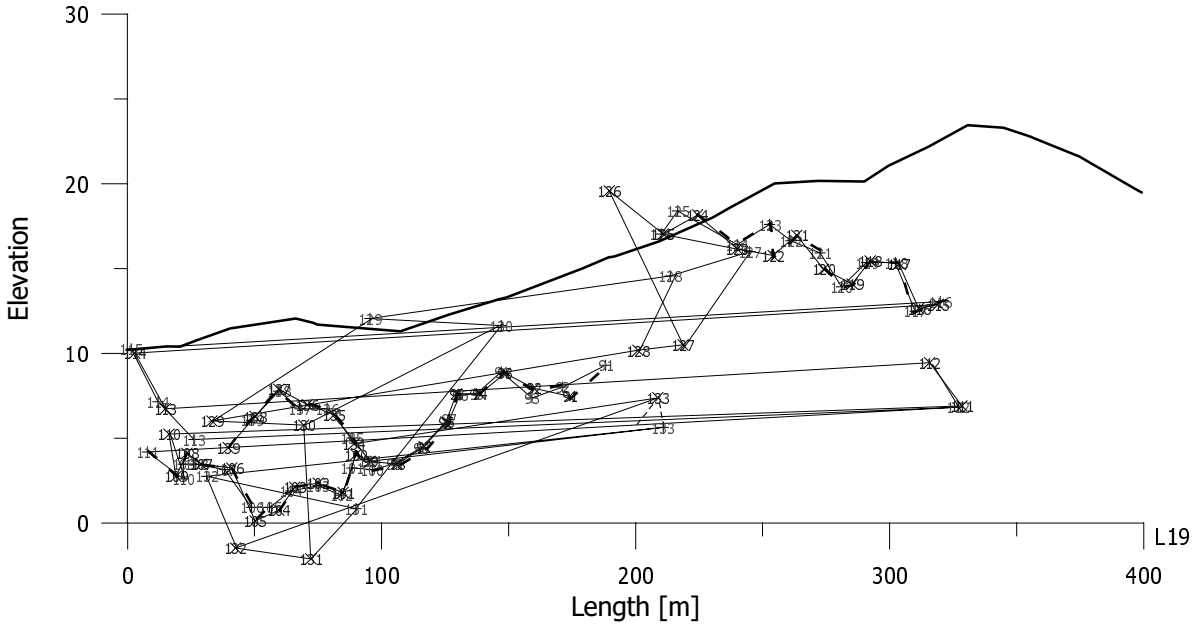

GPR Profile 20

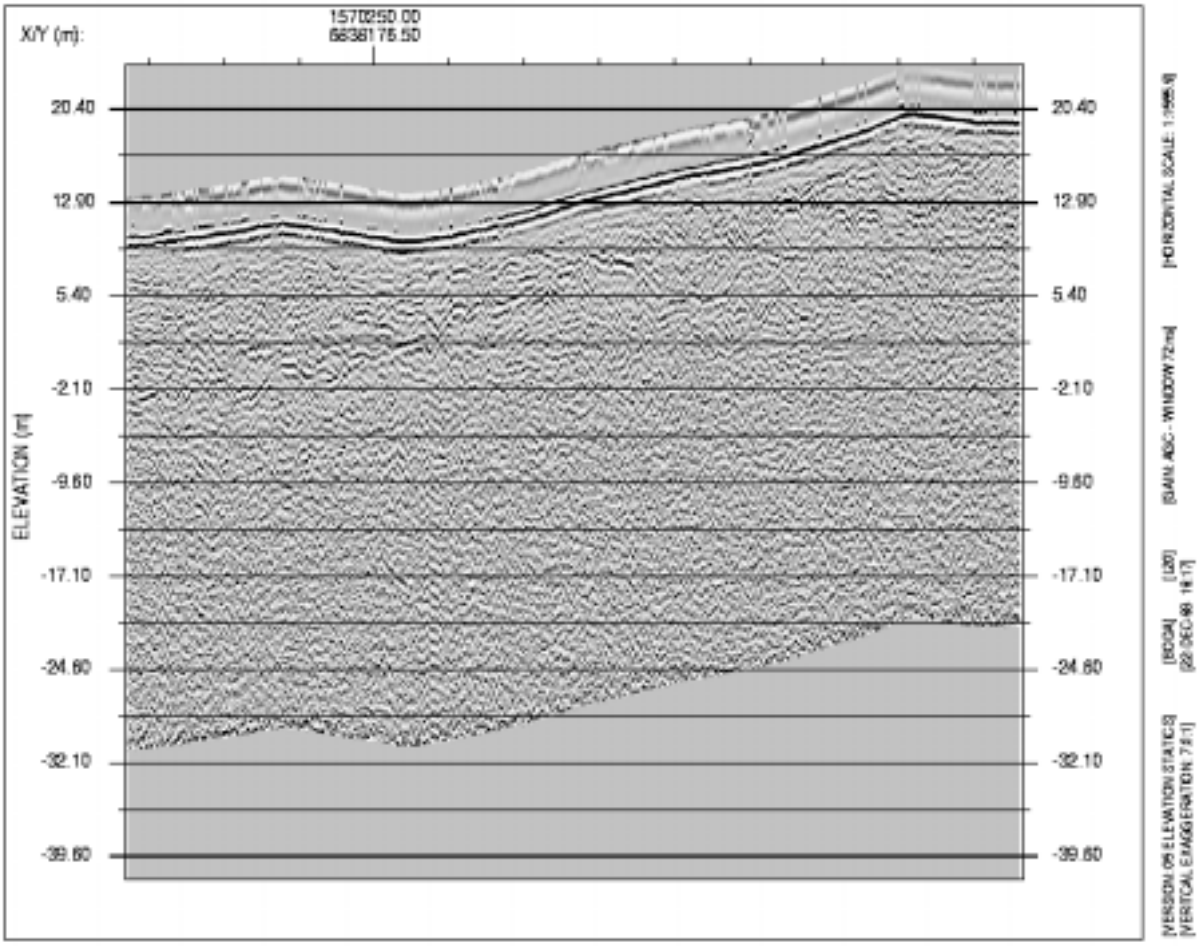

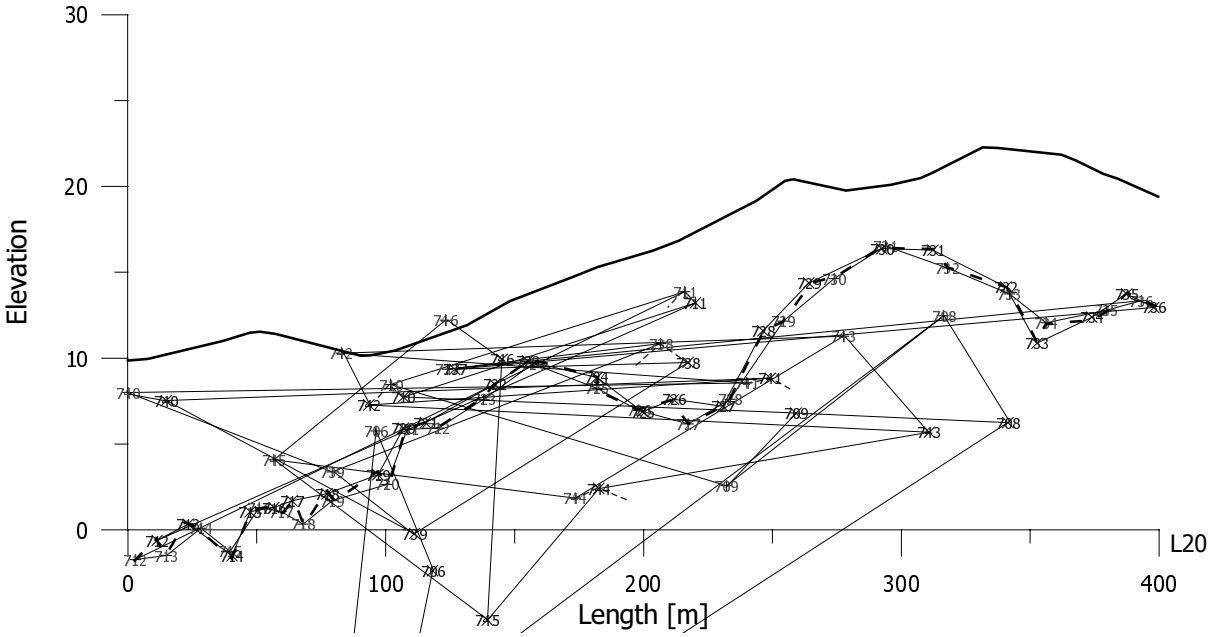

Appendix 4: Short GPR Profiles

Map showing location of short profiles

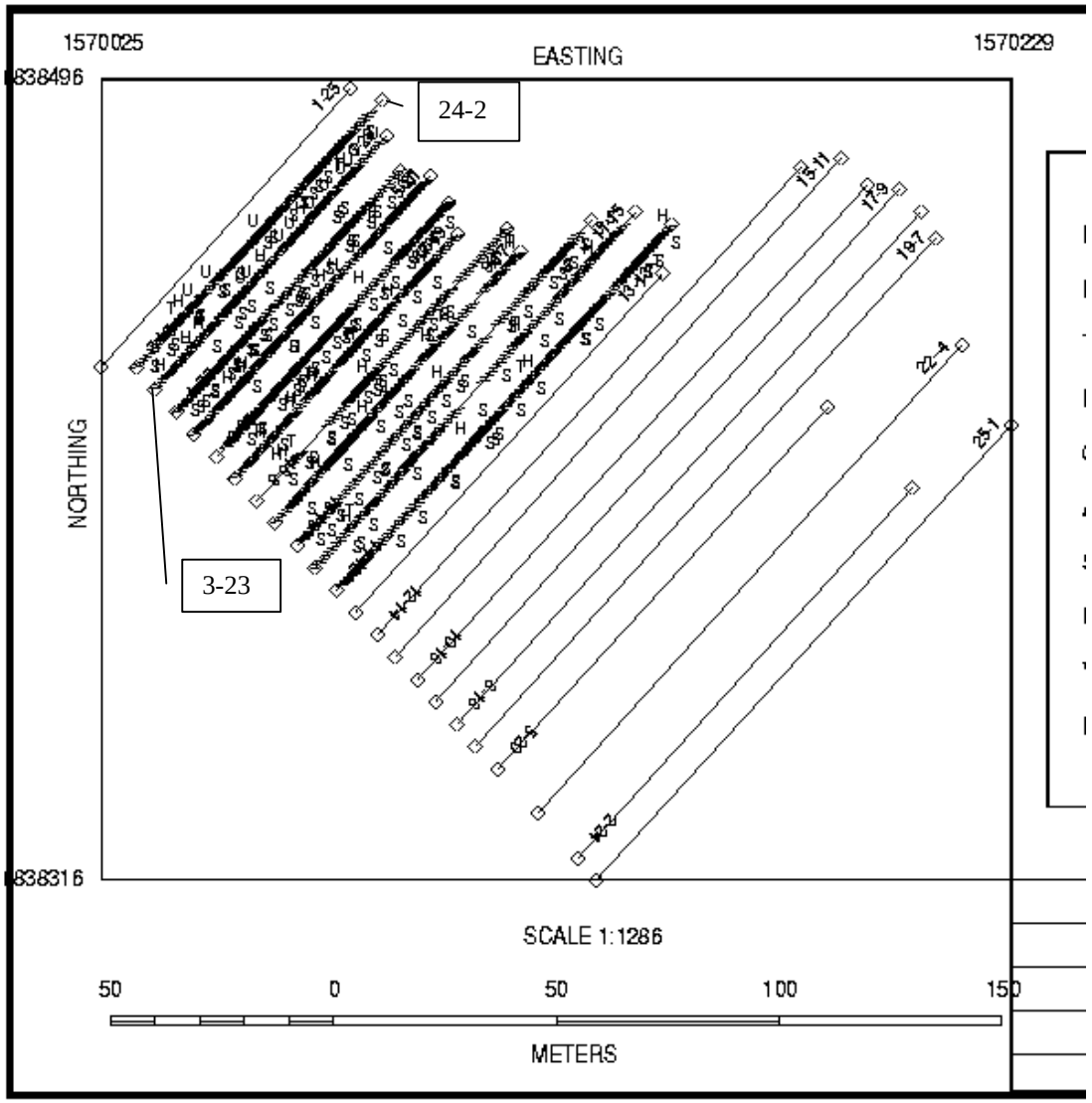

Profile 24-2

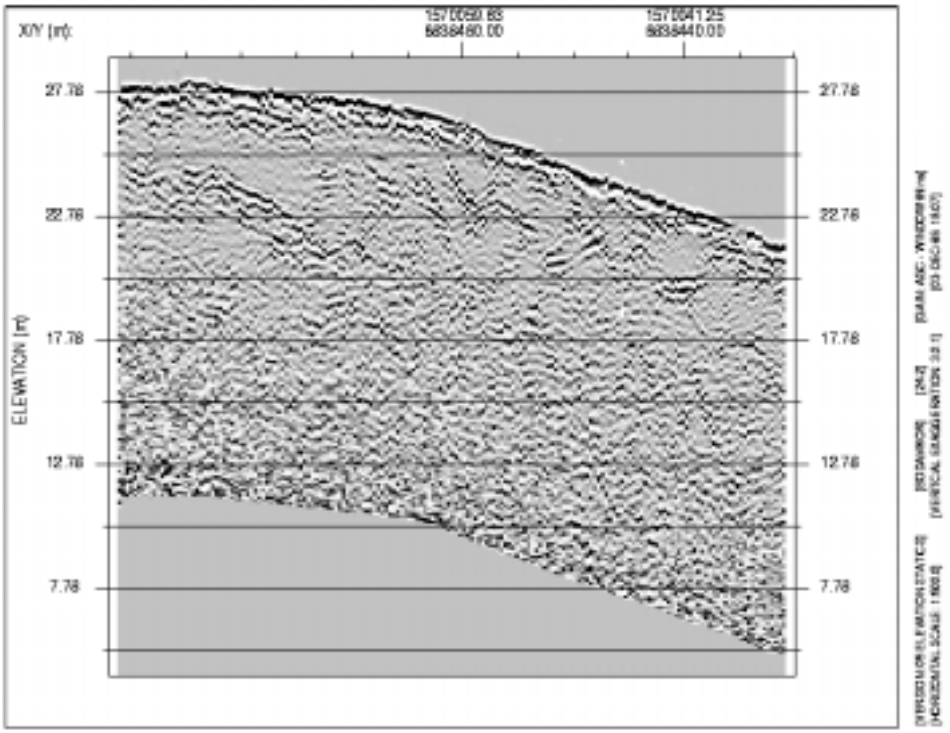
X/Y [m]:
1570068.85
6838460.00
1570041.25
6838440.00
27.78
22.78
17.78
12.78
7.78
ELEVATION [m]

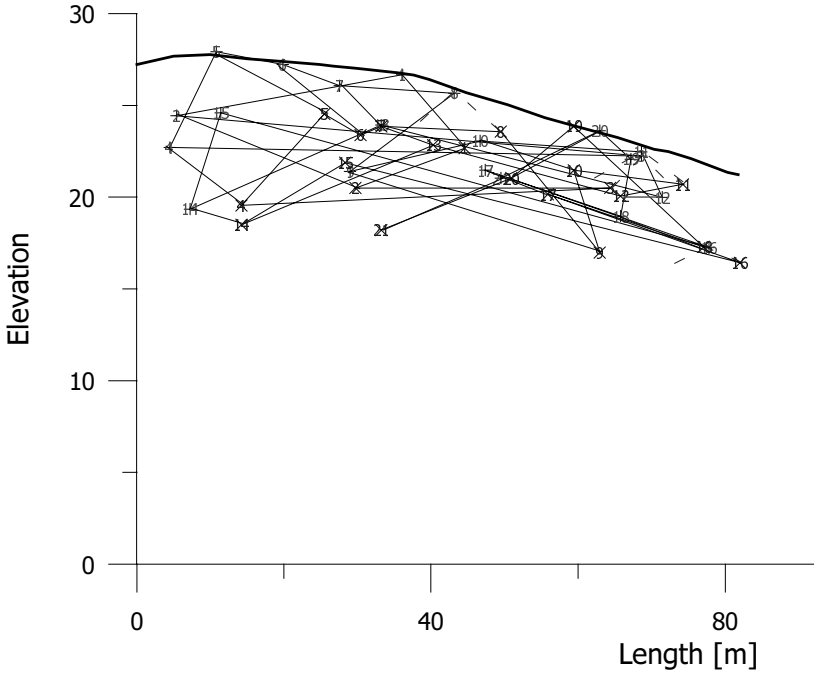
30
20
10
0
Elevation
0
40
80
Length [m]

Profile 3-23

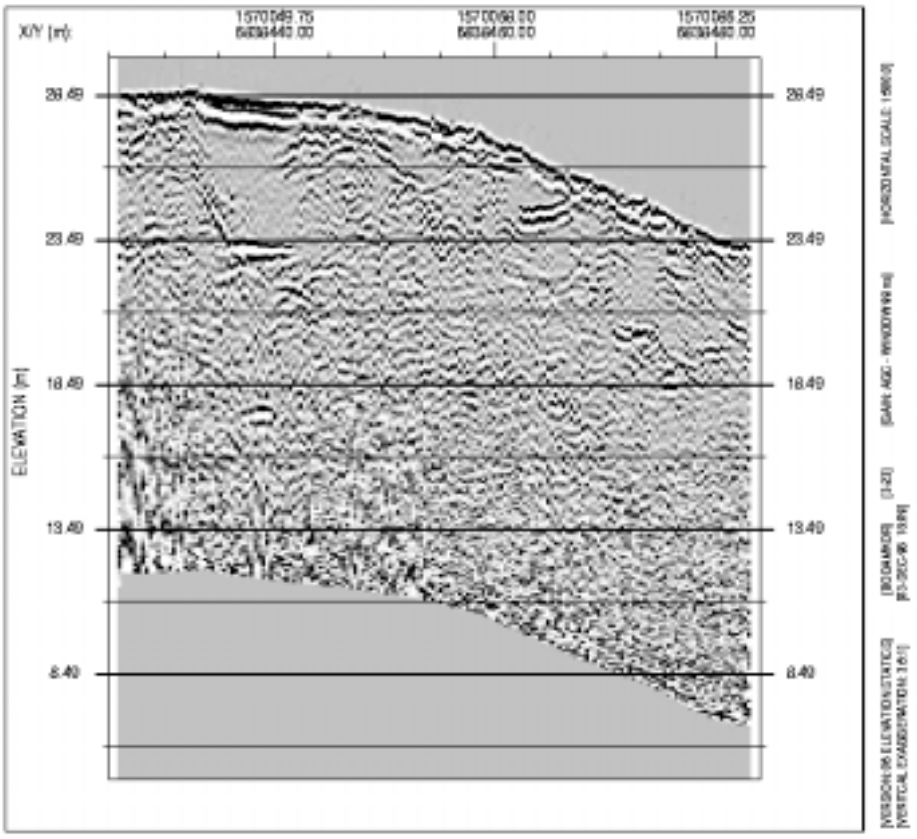
X/Y [m]:
1570049.75
6639440.00
1570068.00
6639460.00
1570086.25
6639480.00
28.49
23.49
18.49
13.49
8.49
ELEVATION [m]

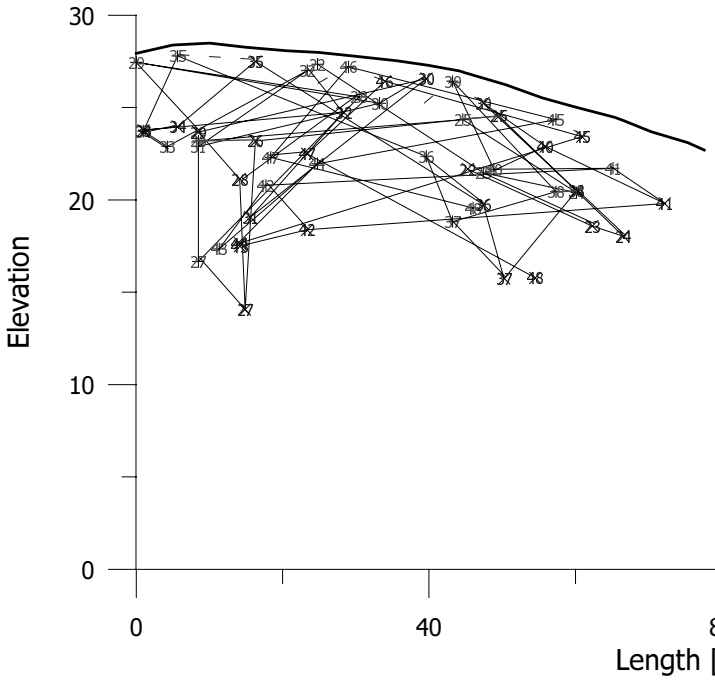
30
20
10
0
Elevation
0
40
80
Length [m]

Profile 22-4

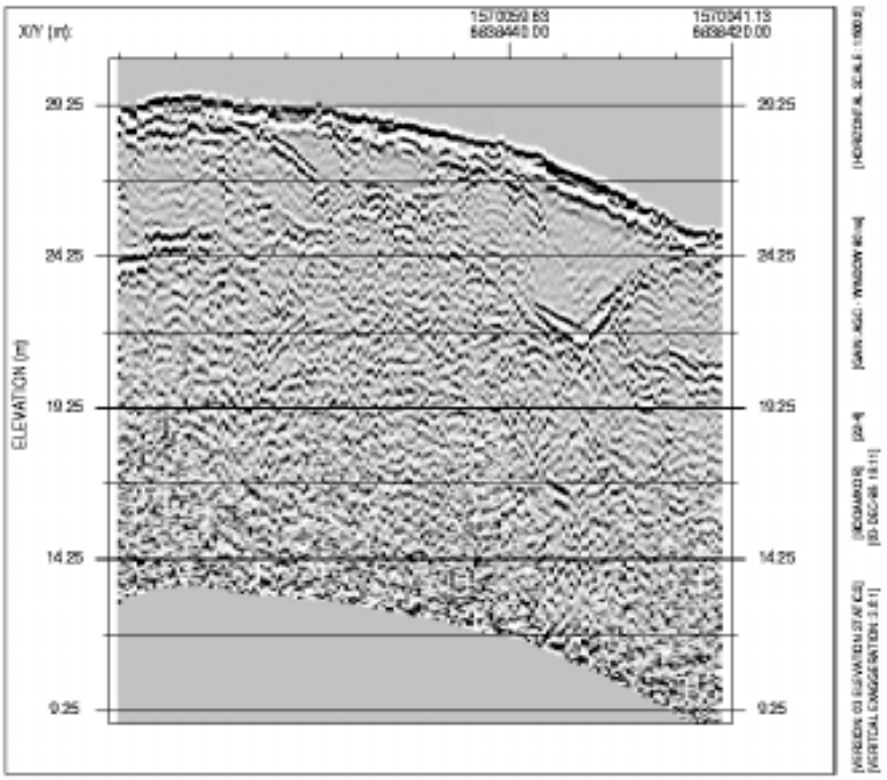
X/Y [m]:
ELEVATION (m)
29.25
24.25
19.25
14.25
9.25

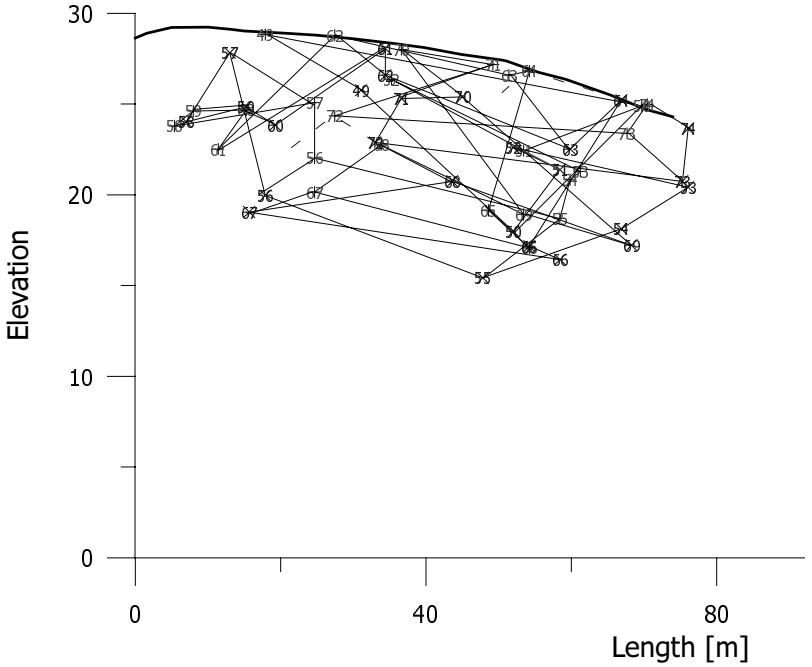
Elevation
Length [m]
0
10
20
30
0
40
80

Profile 5-21

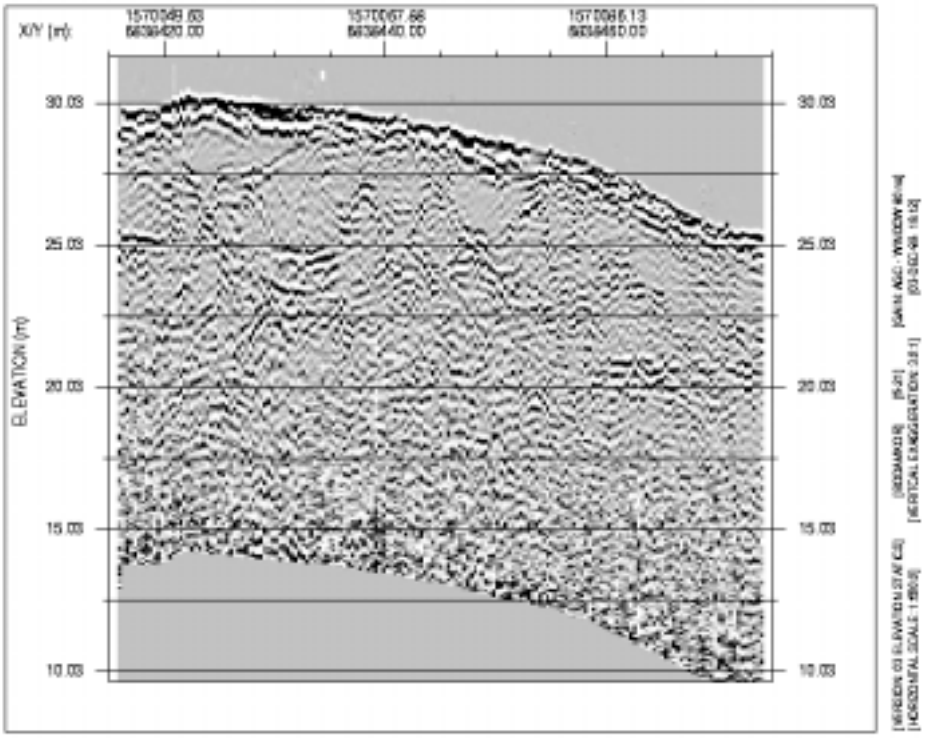
X/Y [m]:
30.00
25.00
20.00
15.00
10.00
ELEVATION [m]

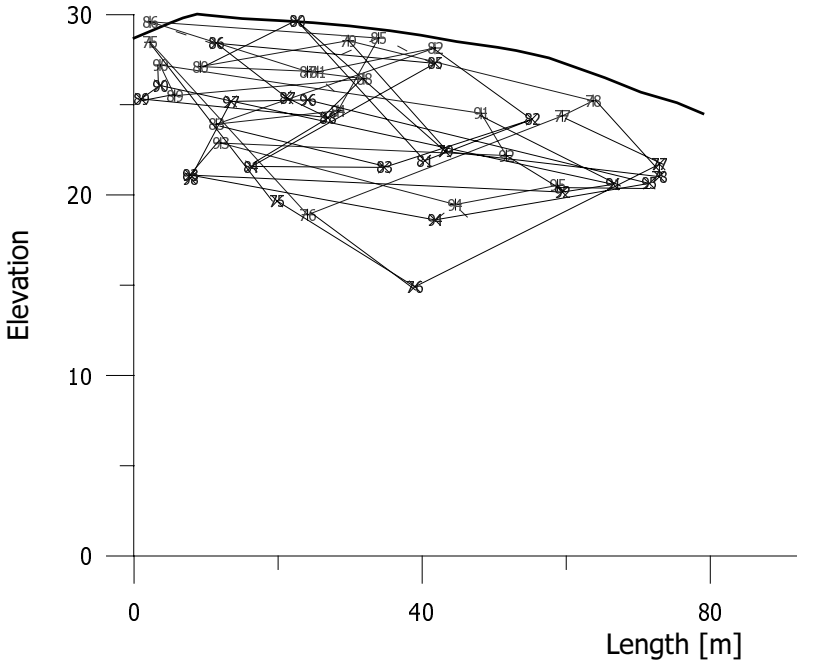
30
20
10
0
Elevation
0
40
80
Length [m]

Profile 20-6

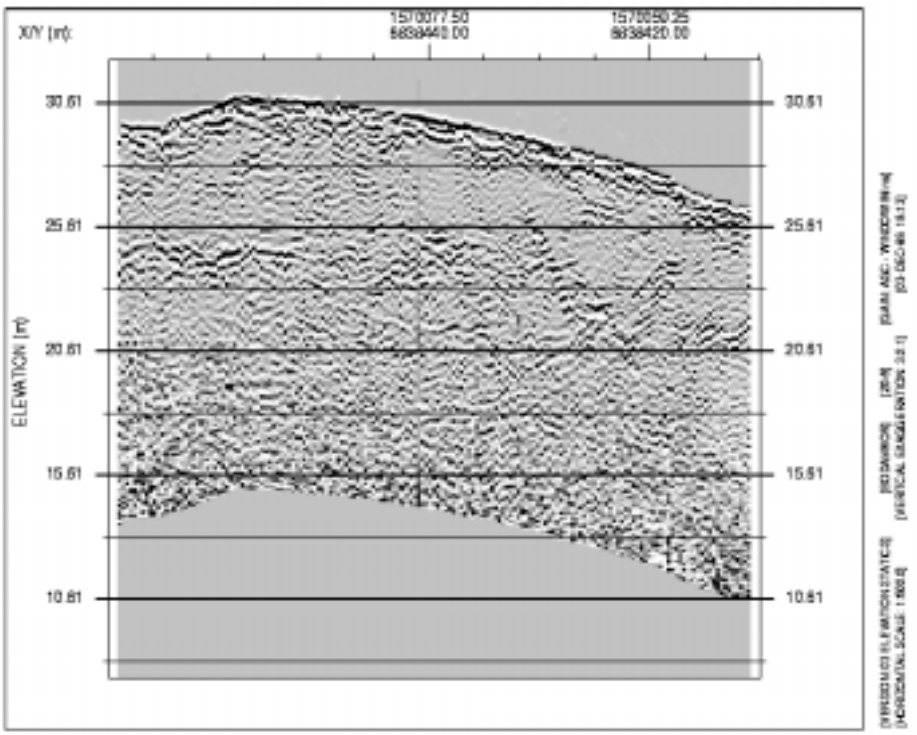
X/Y [m]:
1570077.50
6838440.00
1570550.25
6838420.00
30.61
25.61
20.61
15.61
10.61
ELEVATION [m]

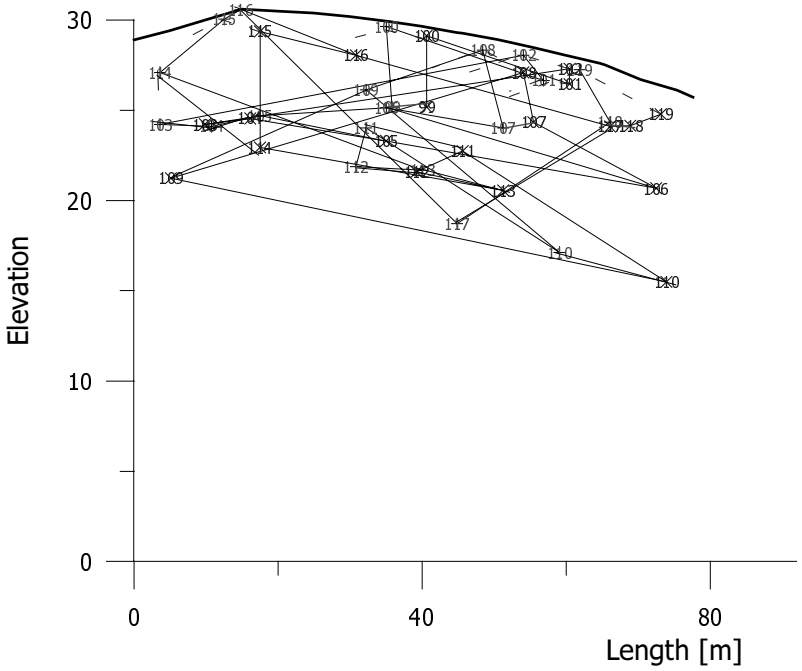
30
20
10
0
Elevation
0
40
80
Length [m]

Profile 7-19

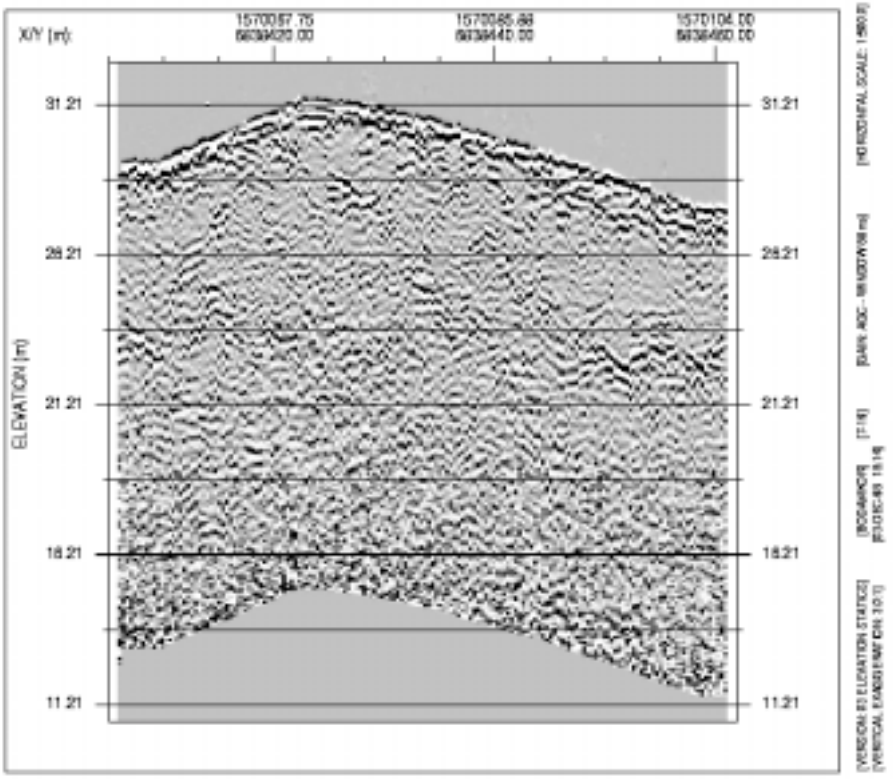
X/Y [m]:
1570057.75
6638420.00
1570085.88
6638440.00
1570104.00
6638460.00
31.21
28.21
21.21
18.21
11.21
ELEVATION [m]

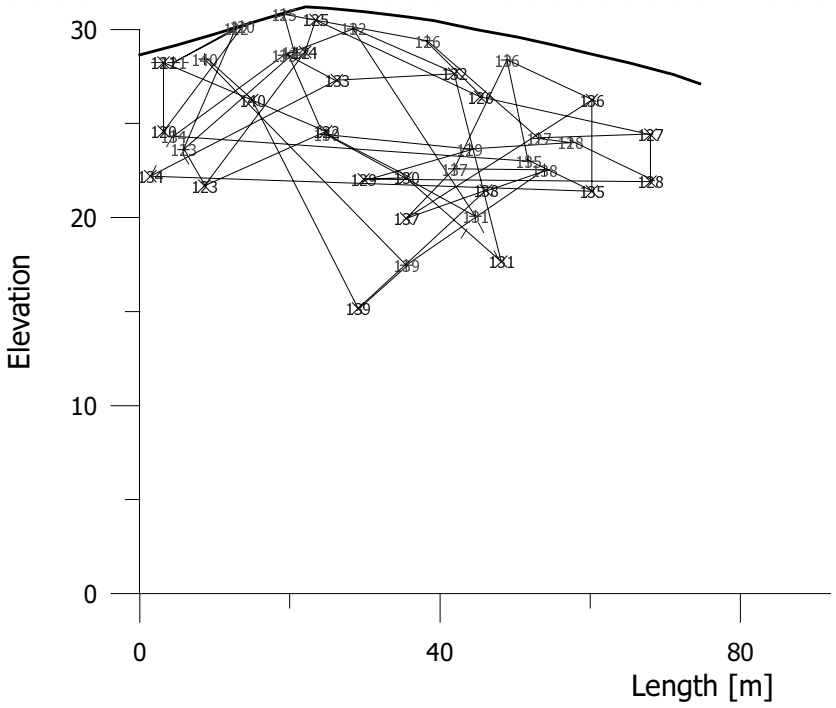
30
20
10
0
Elevation
0
40
80
Length [m]

Profile 18-8

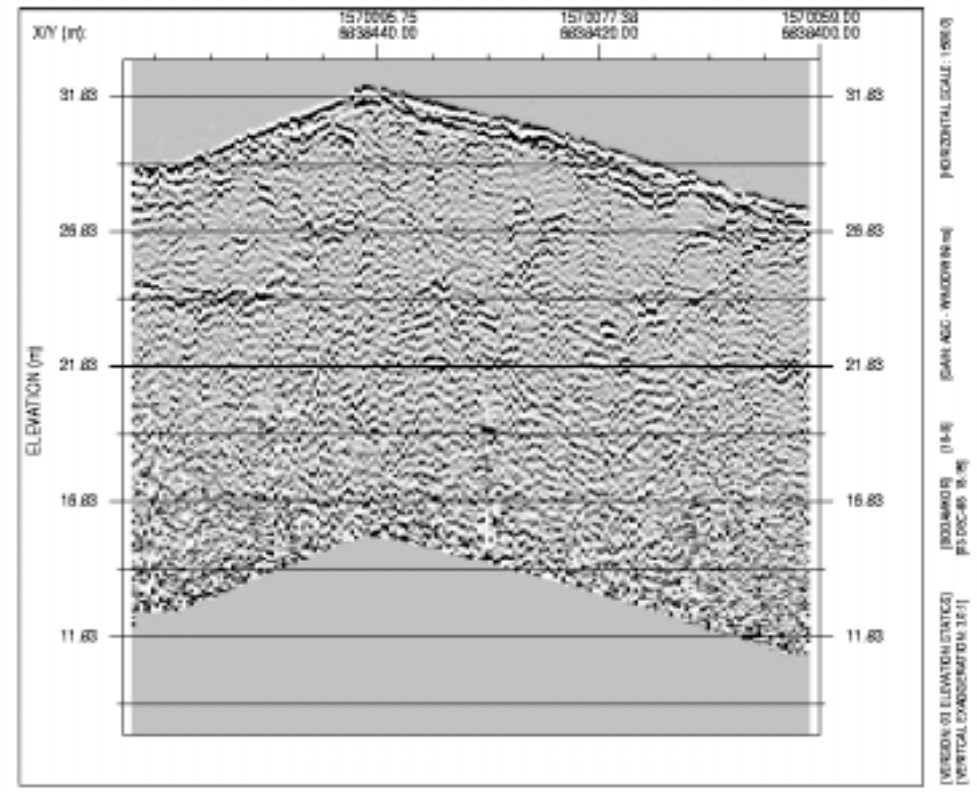
X/Y [m]:
1570095.75
6838440.00
1570077.58
6838420.00
1570060.00
6838400.00
31.83
26.83
21.83
16.83
11.83
ELEVATION [m]

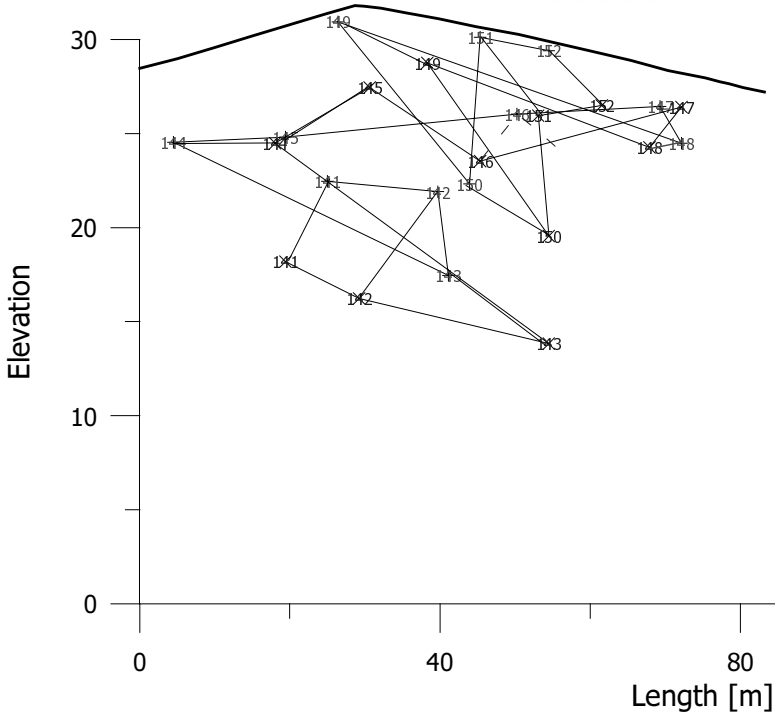
30
20
10
0
Elevation
0
40
80
Length [m]

Profile 9-17

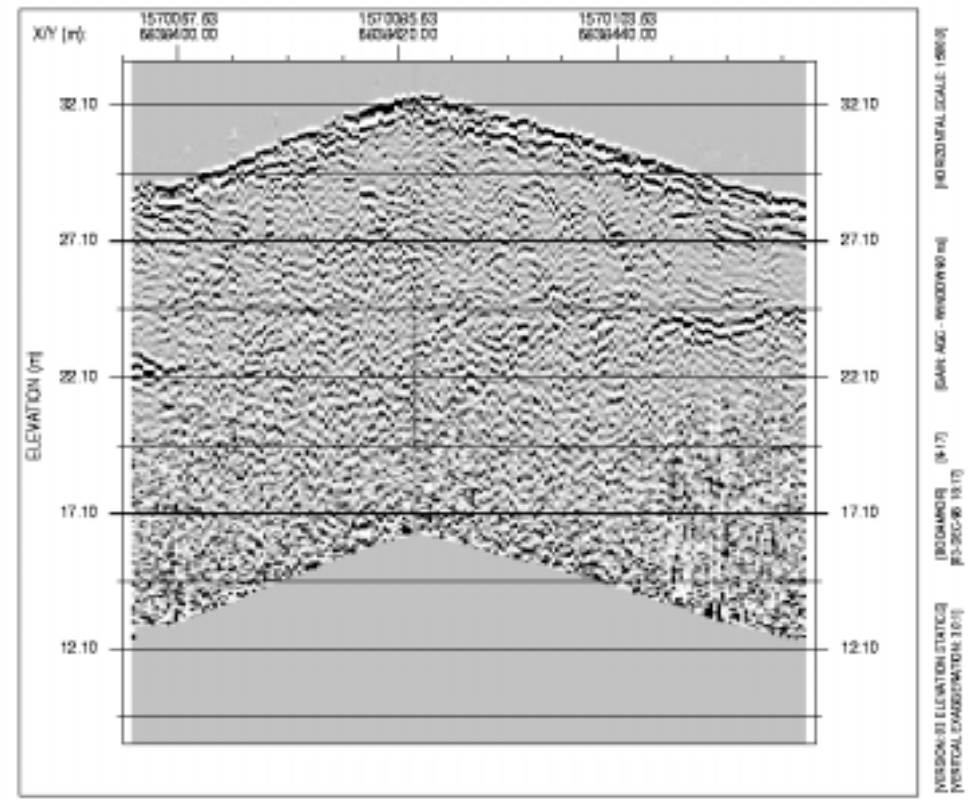
X/Y [m]:
1570057.63
6639400.00
1570085.63
6639420.00
1570103.63
6639440.00
32.10
27.10
22.10
17.10
12.10
ELEVATION [m]

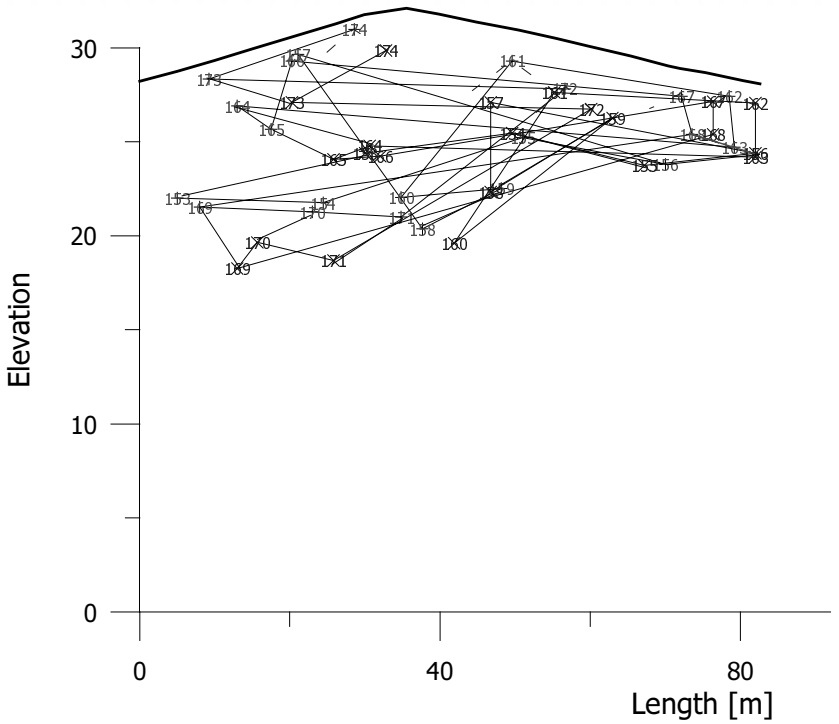
30
20
10
0
Elevation
0
40
80
Length [m]

Profile 16-10

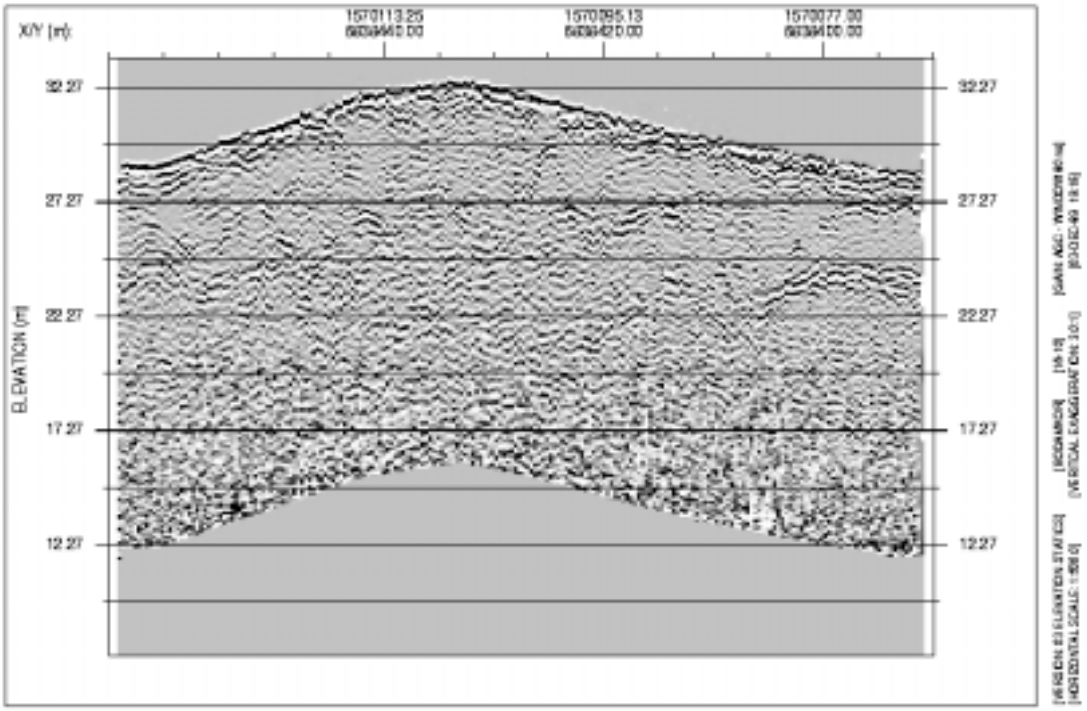

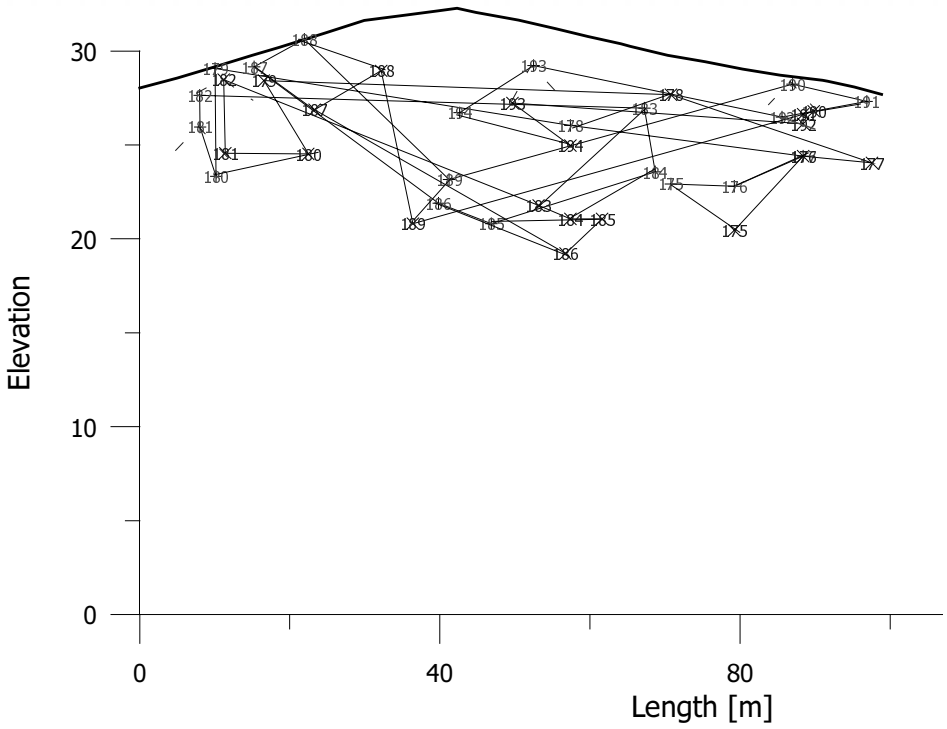

Profile 11-15

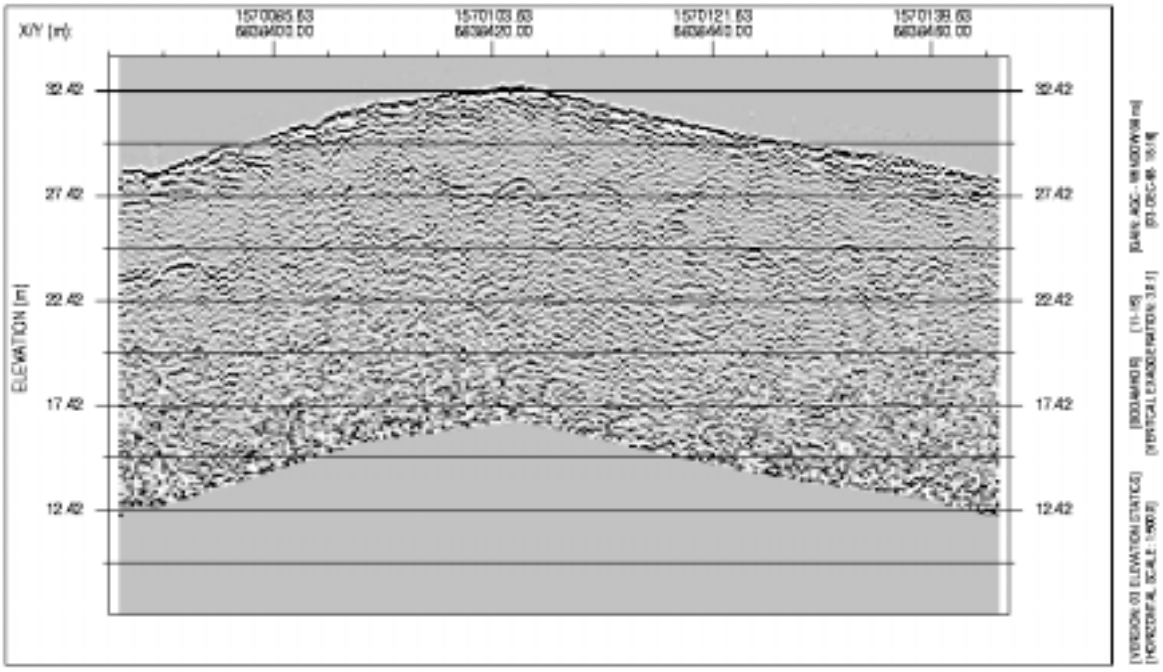

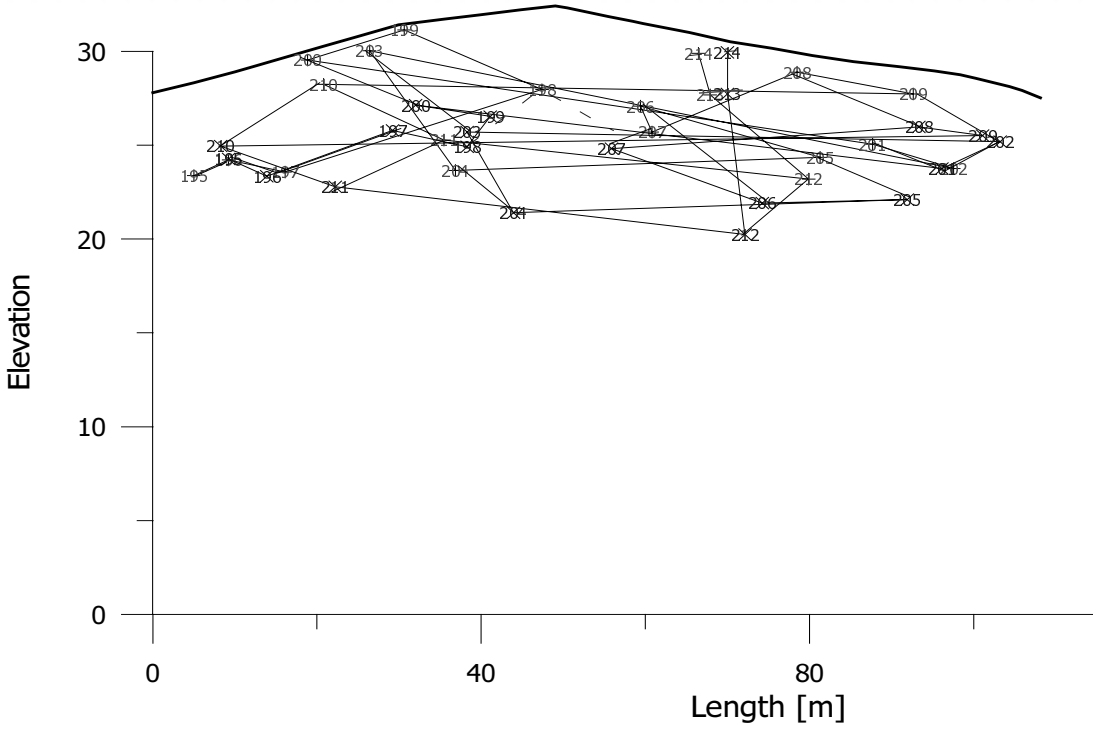

Profile 14-12

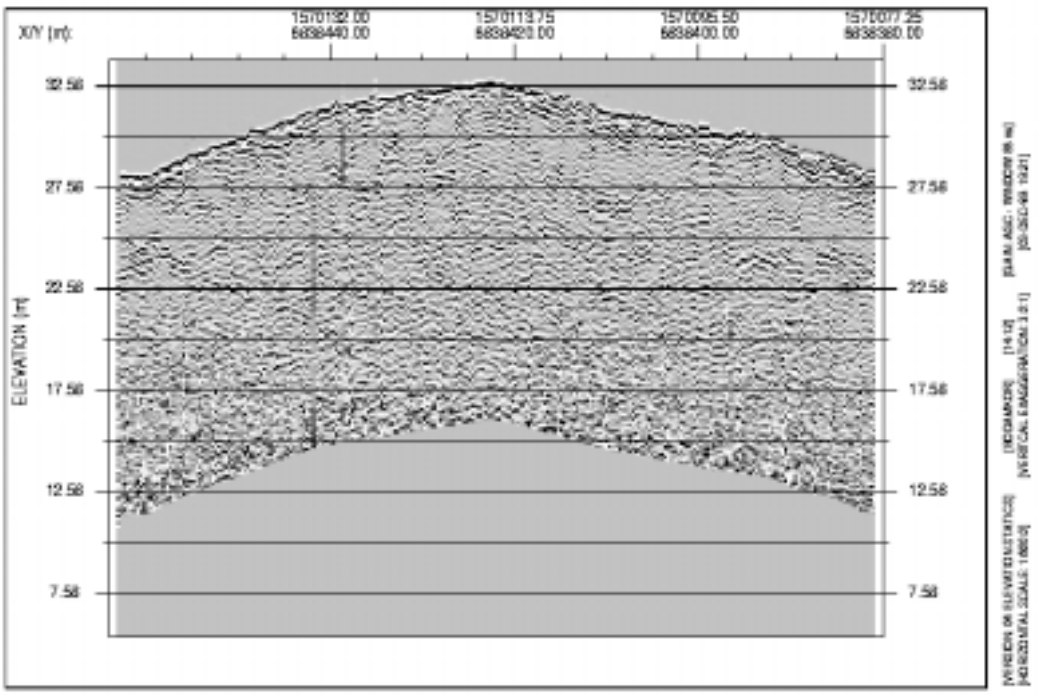

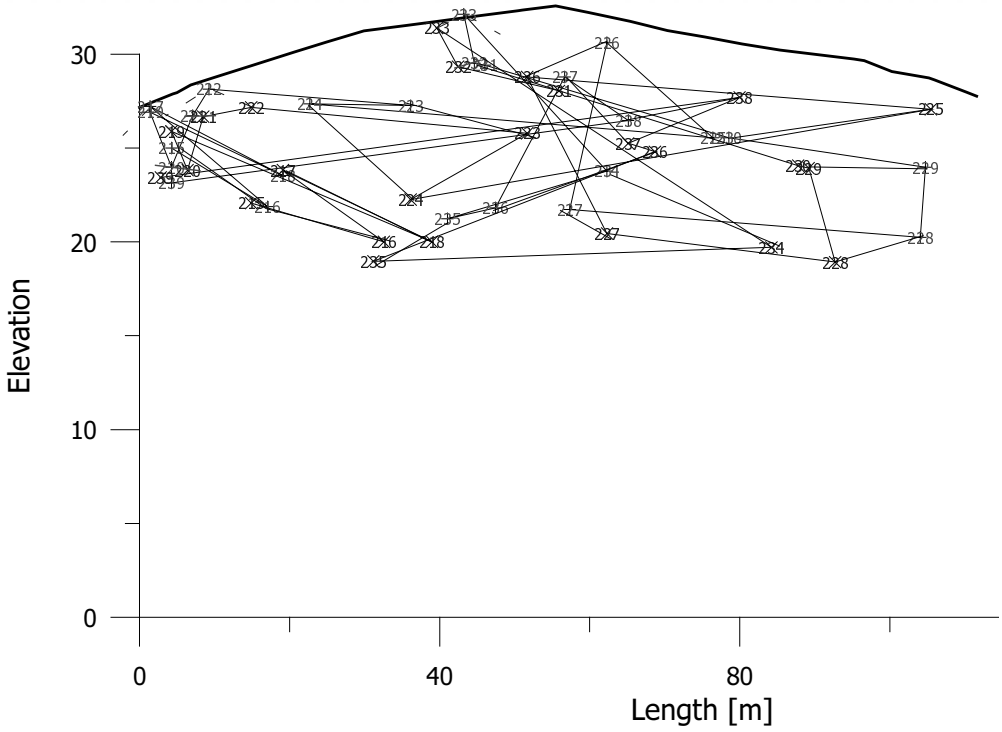

Profile 13-13

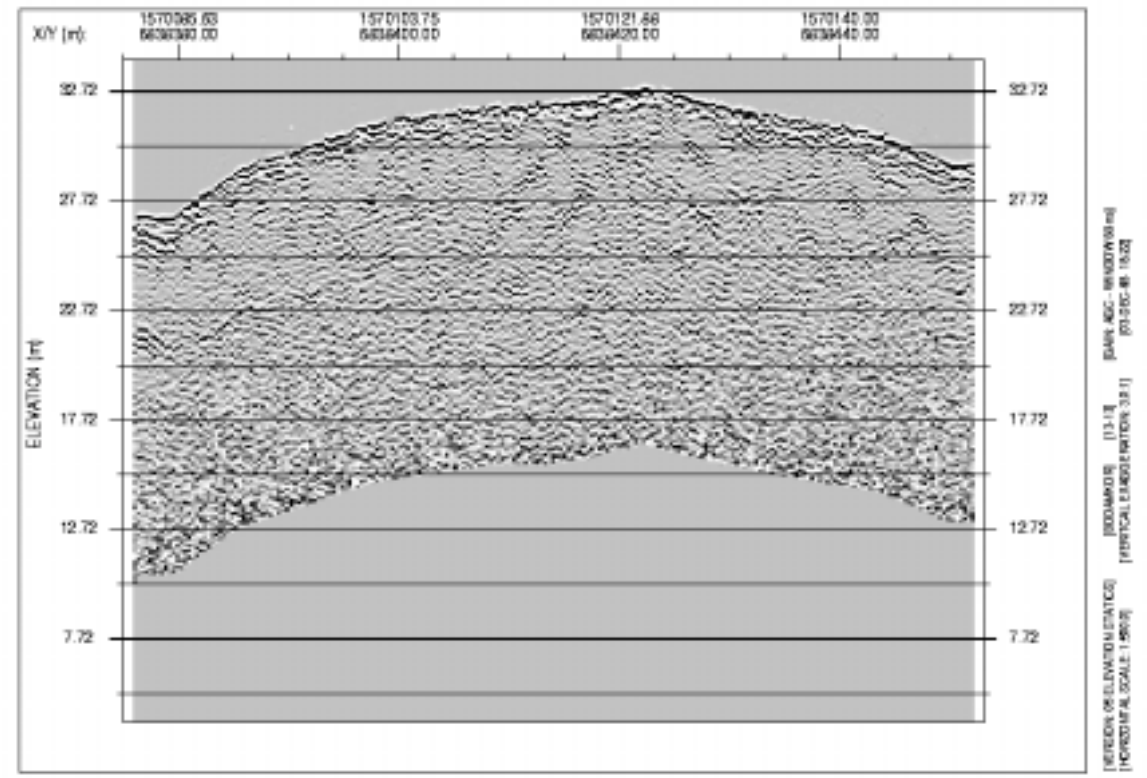

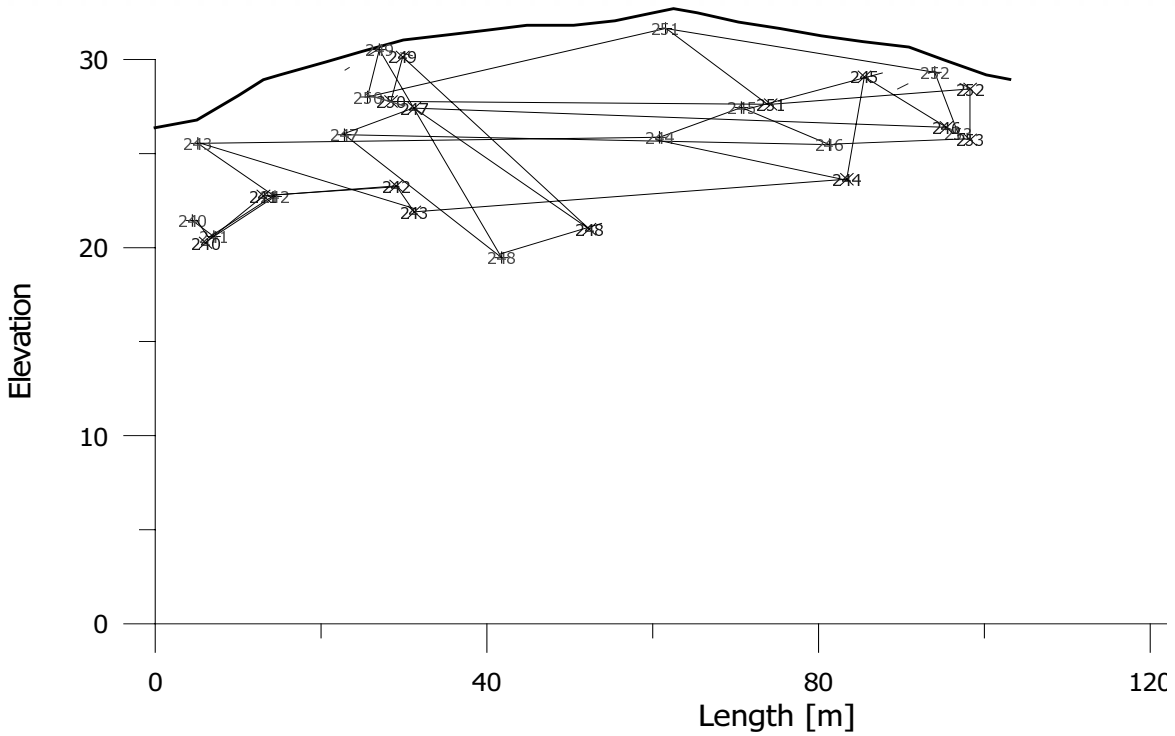

Profile 12-14

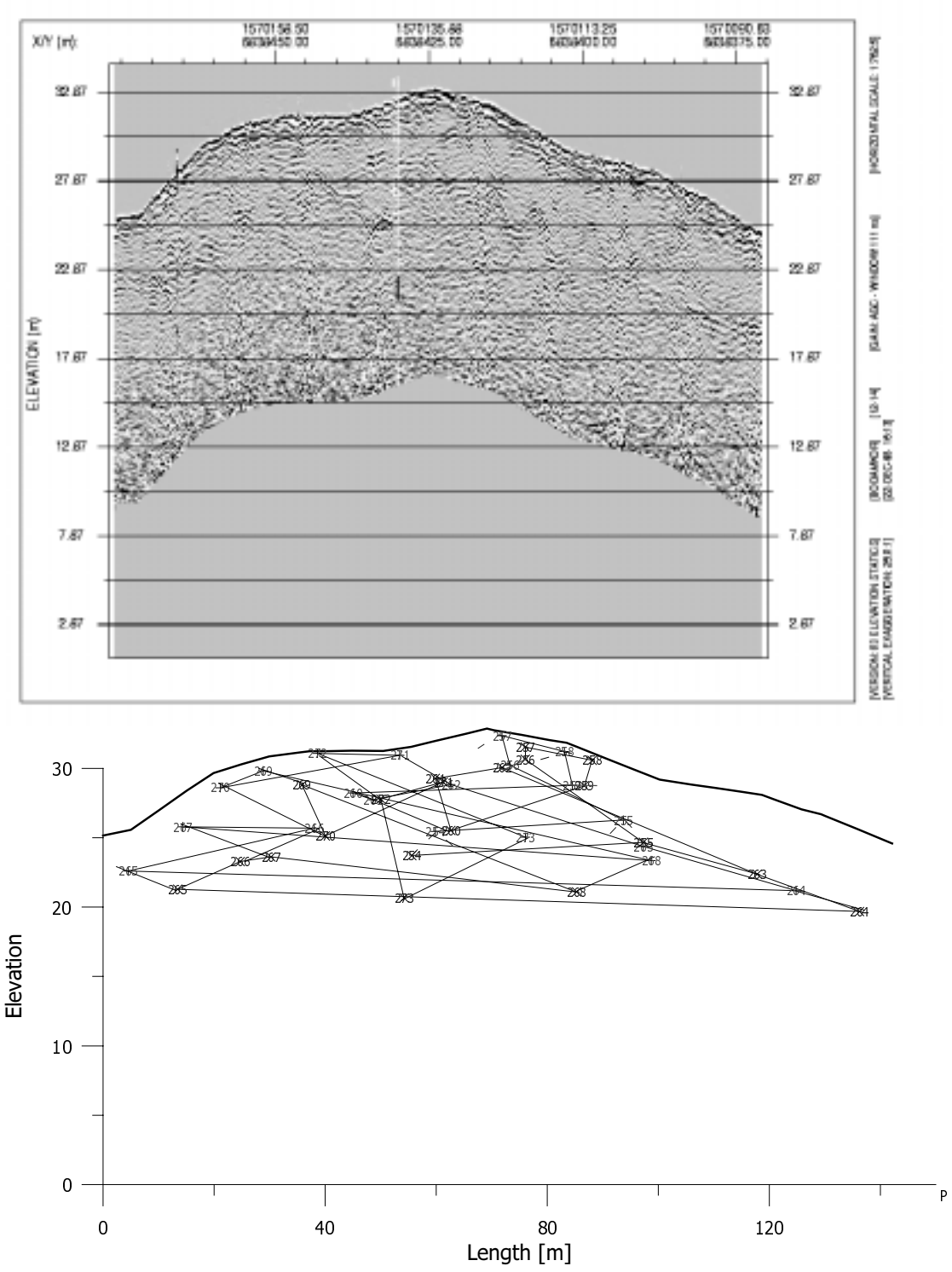

Profile 15-11

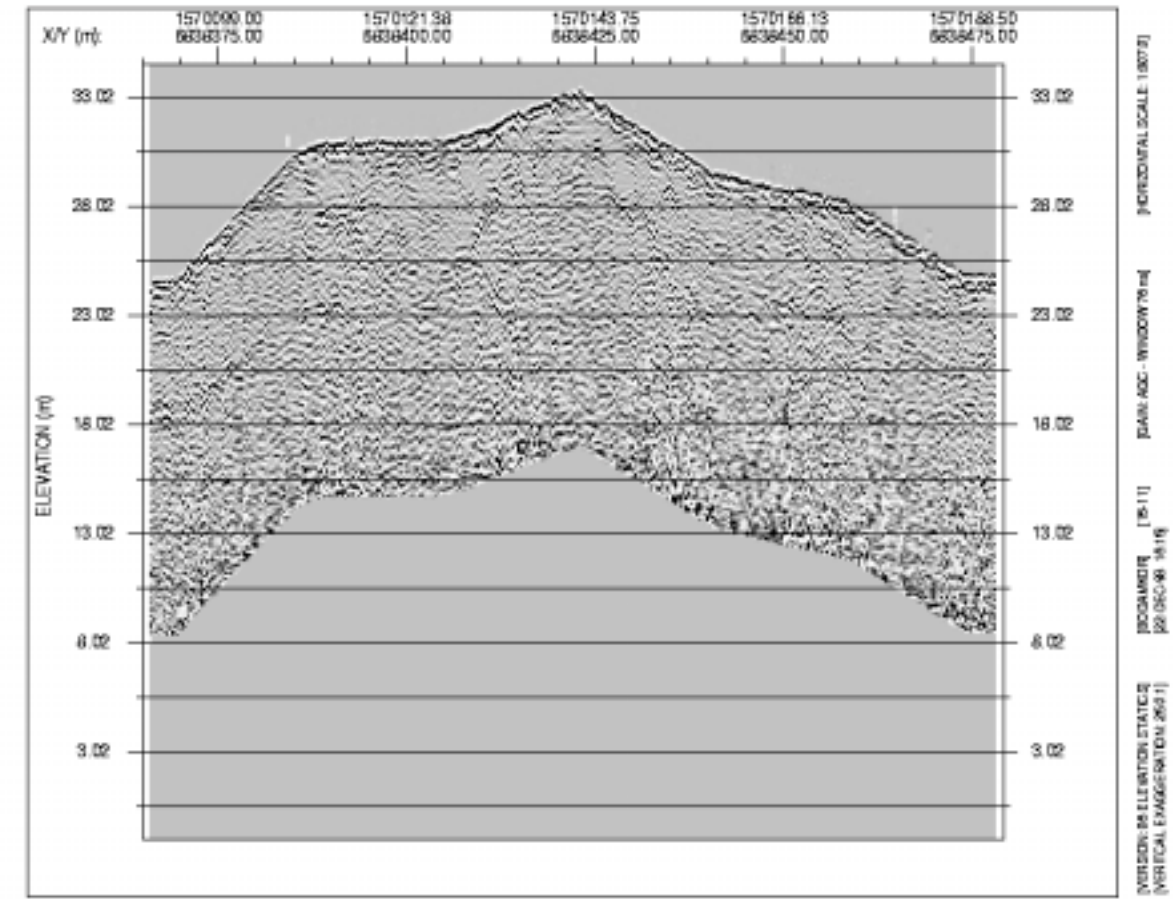

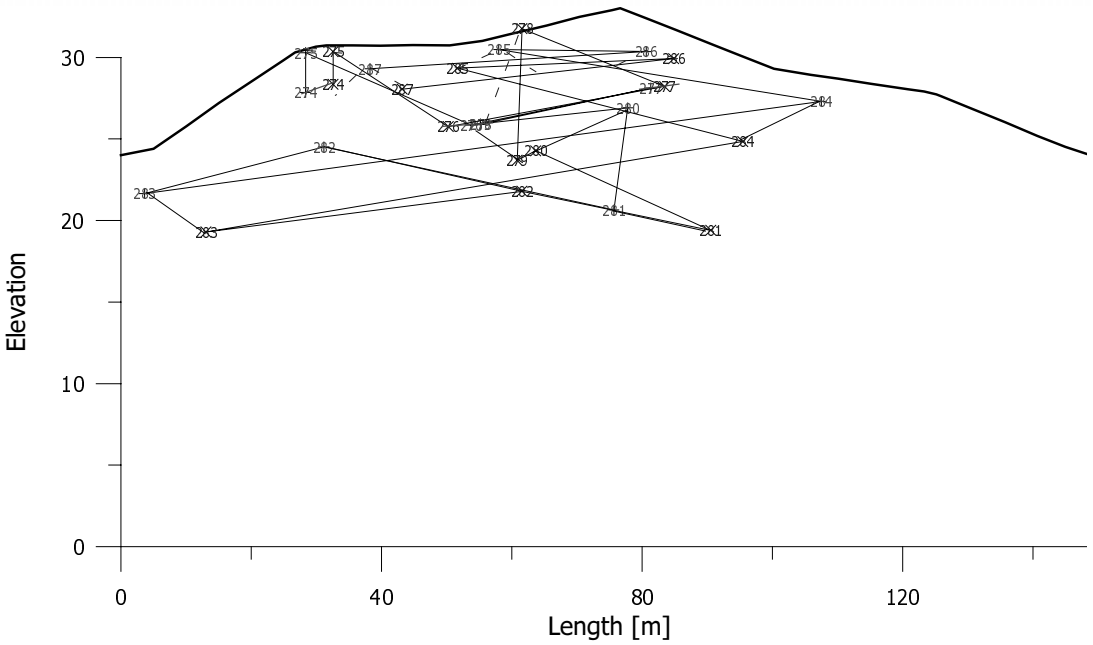

Profile 10-16

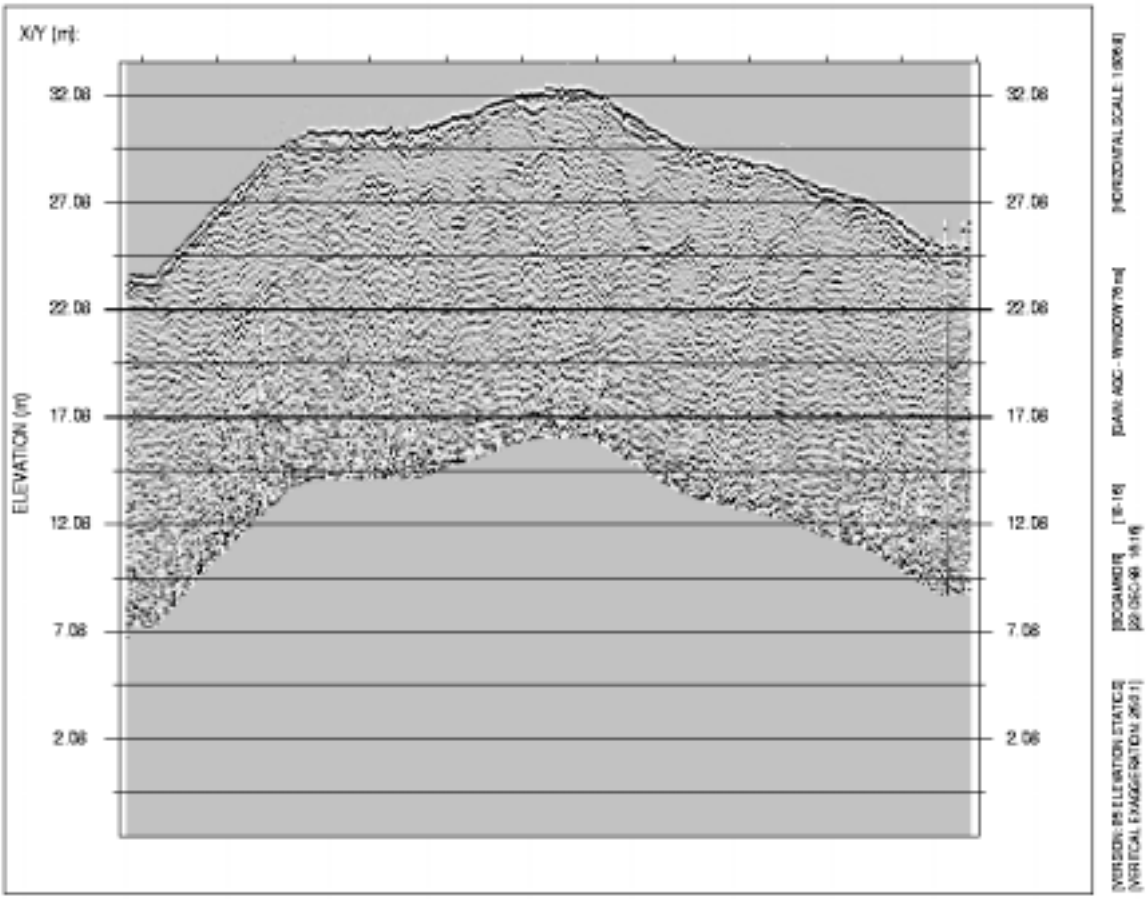

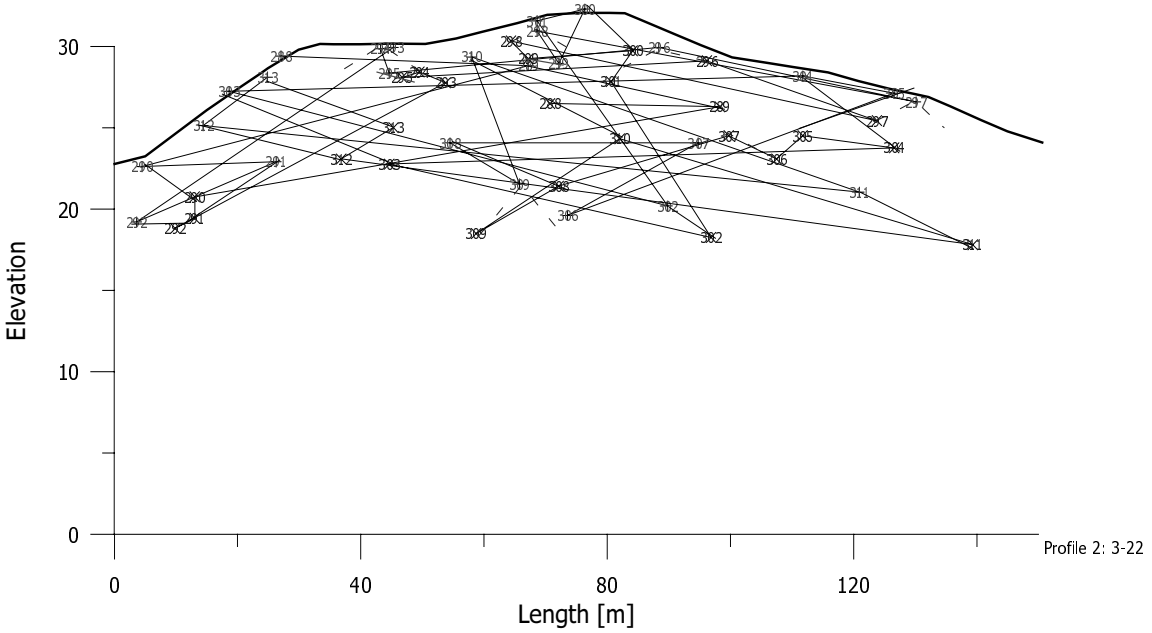

Profile 17-9

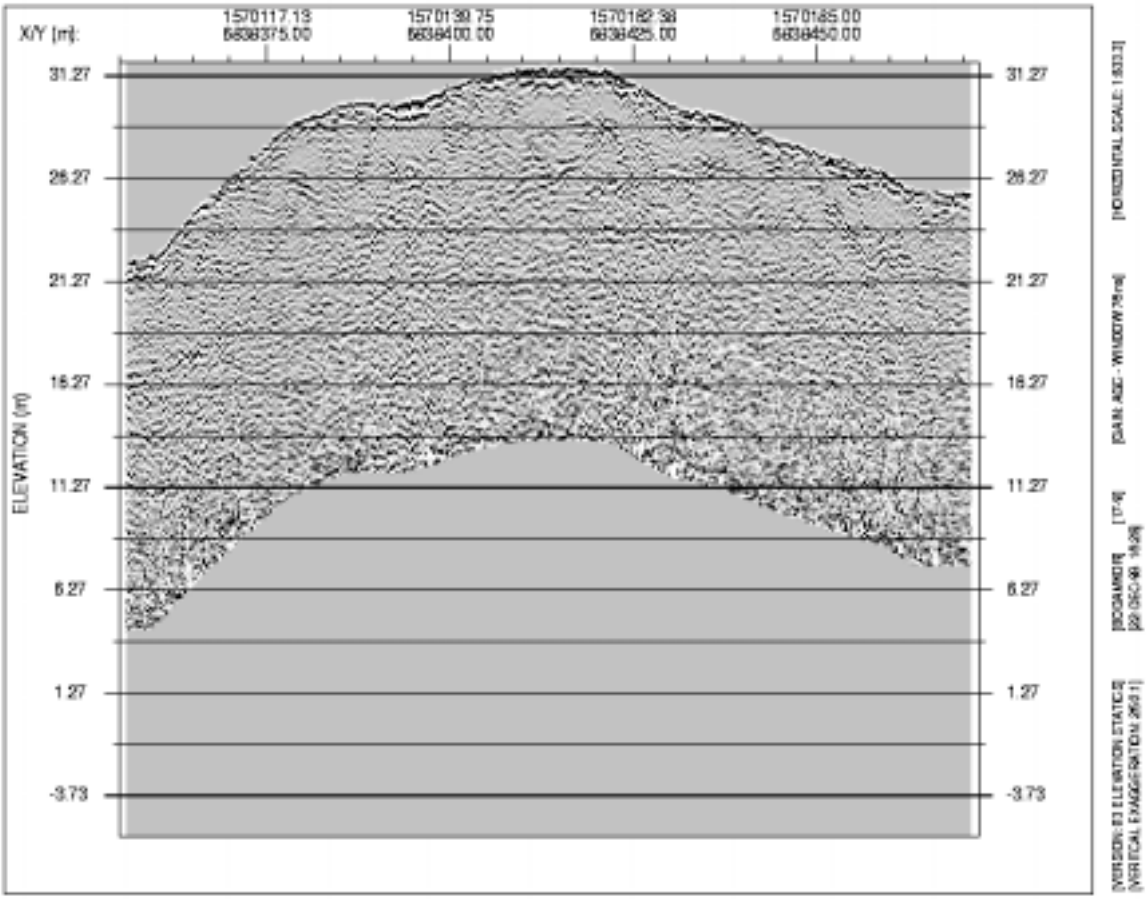
X/Y [m]:
1570117.13
6838375.00
1570139.75
6838400.00
1570162.38
6838425.00
1570185.00
6838450.00
31.27
26.27
21.27
16.27
11.27
6.27
1.27
-3.73
ELEVATION (m)

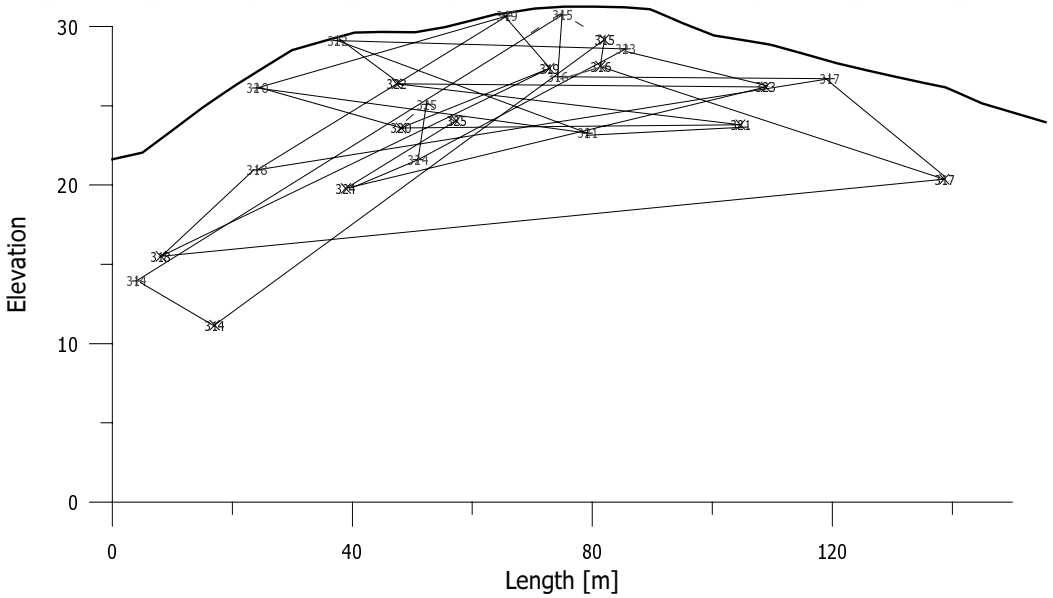
Elevation
Length [m]
0
10
20
30
0
40
80
120

Profile 8-18

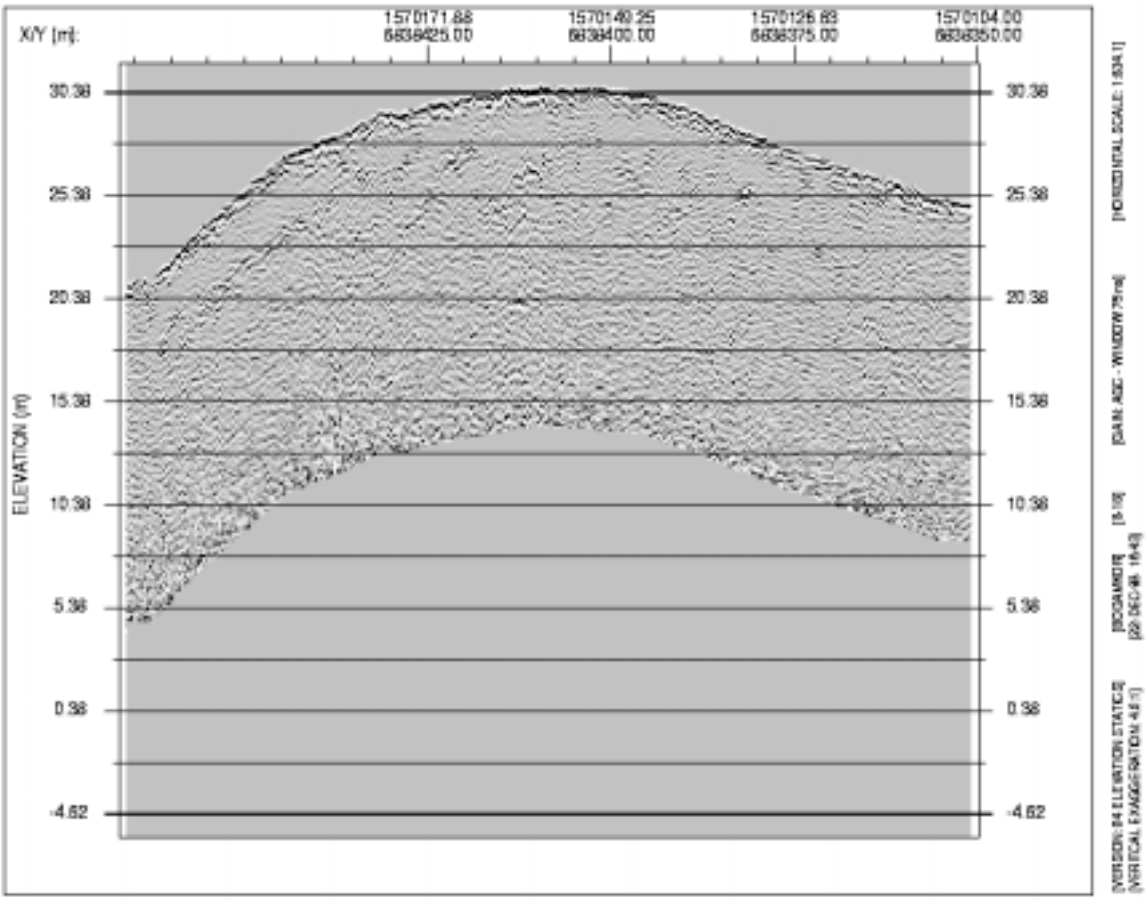
X/Y [m]:
1570171.88
6639425.00
1570140.25
6639400.00
1570126.88
6639375.00
1570104.00
6639350.00
30.38
25.38
20.38
15.38
10.38
5.38
0.38
-4.62
ELEVATION (m)

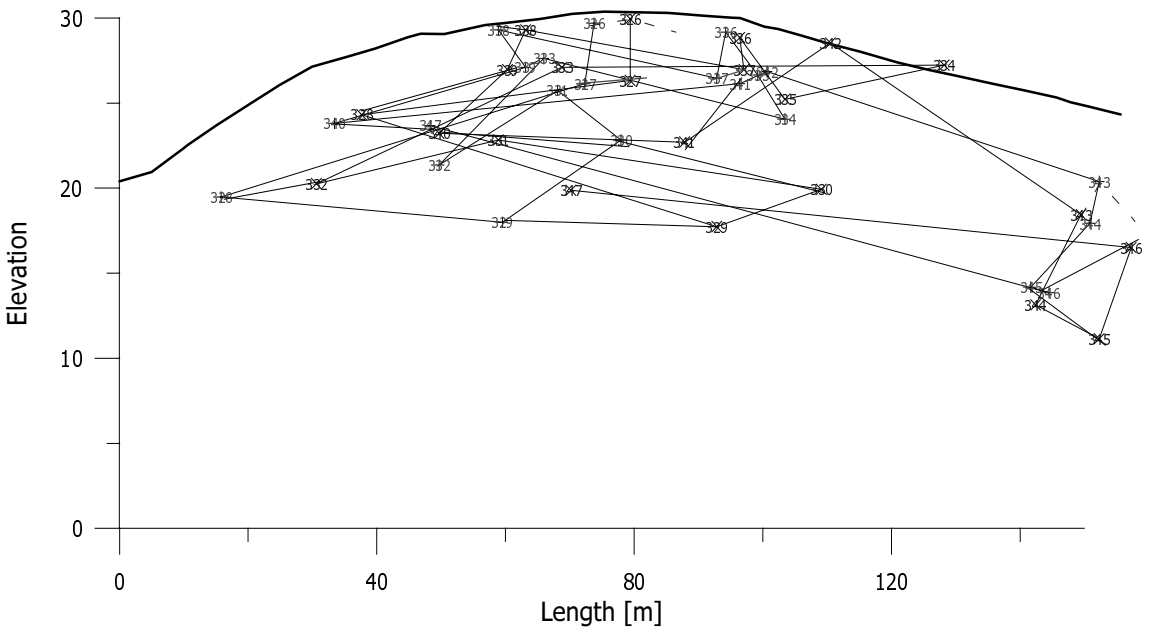
Elevation
Length [m]
0
10
20
30
0
40
80
120

Profile 19-7

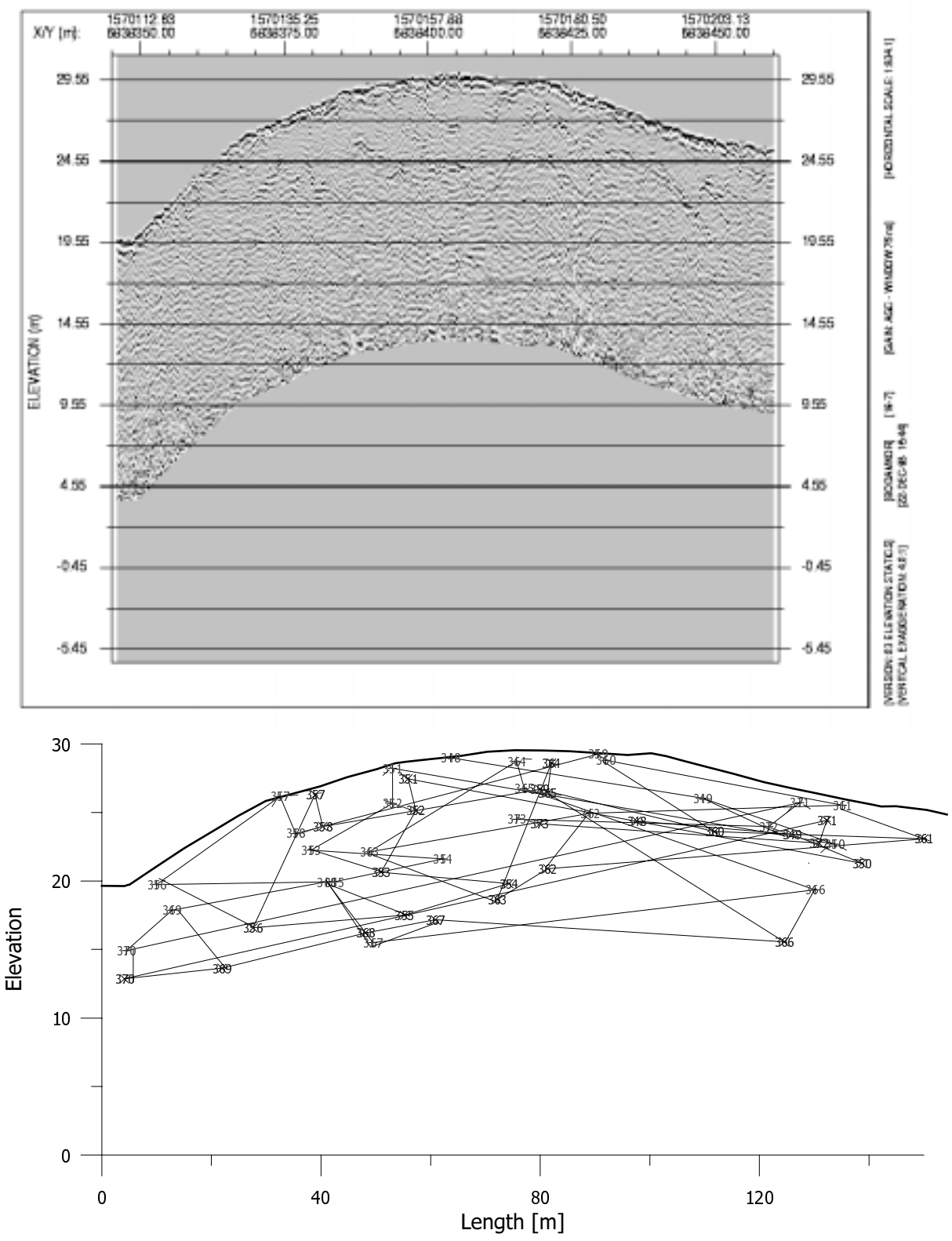
X/Y [m]:
15701112.63
6836350.00
15701135.25
6836375.00
15701157.88
6836400.00
15701180.50
6836425.00
15701203.13
6836450.00
29.55
24.55
19.55
14.55
9.55
4.55
-0.45
-5.45
ELEVATION [m]
Elevation
Length [m]
0
40
80
120
10
20
30

Profile 5-20

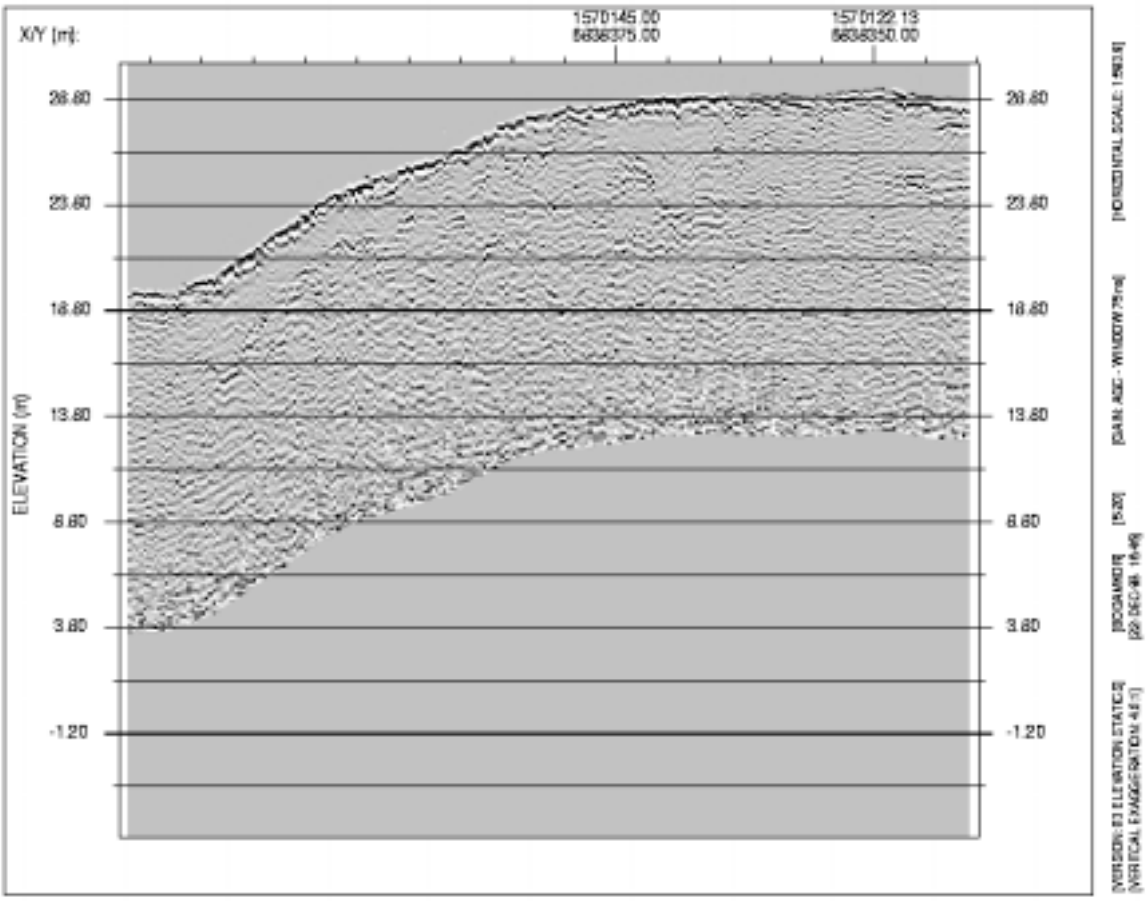
X/Y [m]:
1570145.00
6636375.00
1570122.13
6636350.00
28.80
23.80
18.80
13.80
8.80
3.80
-1.20
ELEVATION (m)

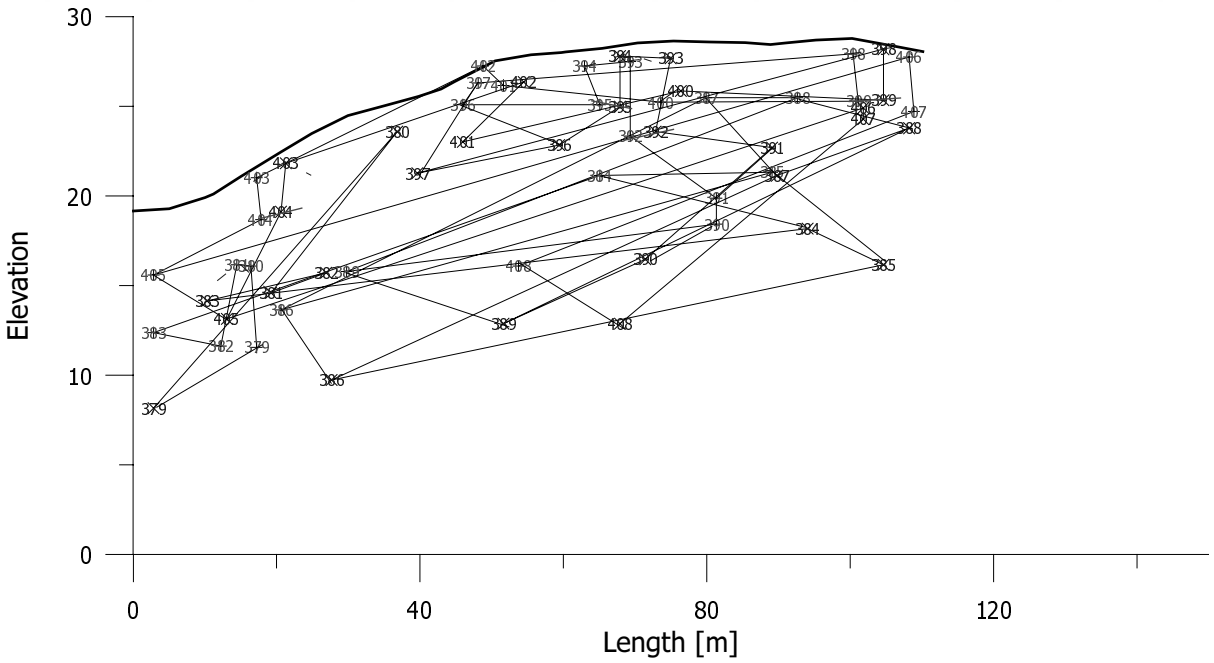
Elevation
Length [m]
0
10
20
30
0
40
80
120

Profile 22-4

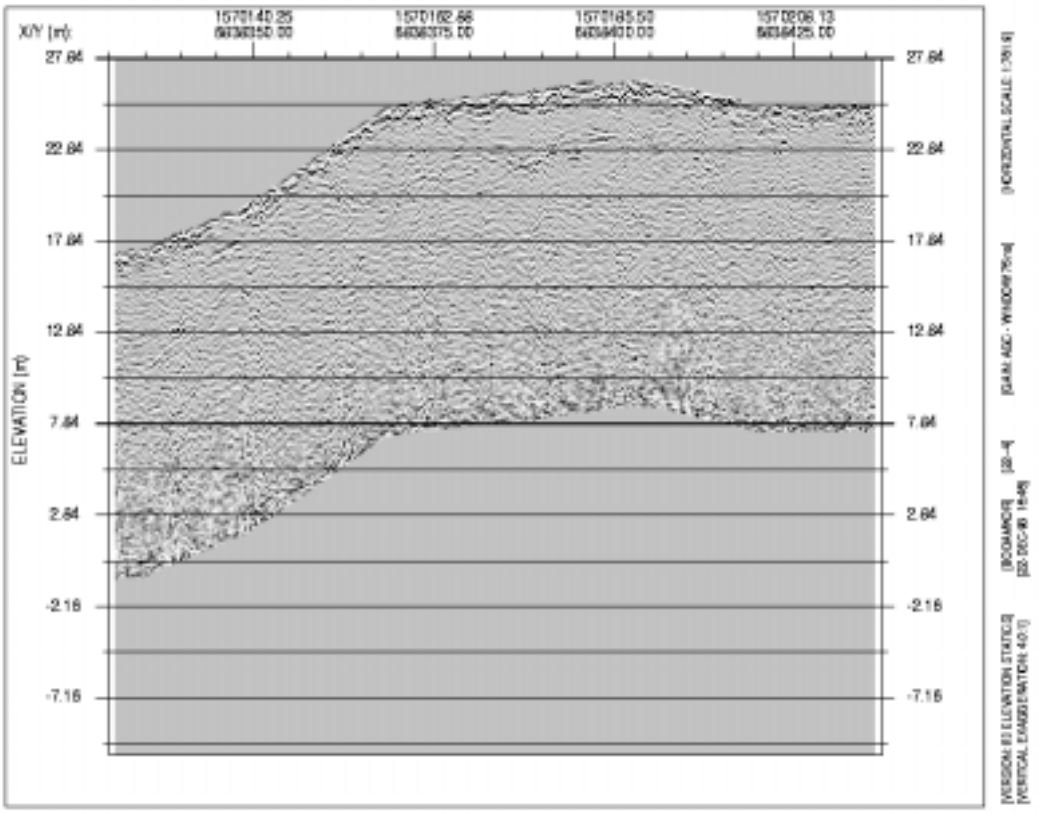
X/Y [m]:
1570140.25
6403850.00
1570162.66
6403875.00
1570185.50
6403900.00
1570208.13
6403925.00
27.84
22.84
17.84
12.84
7.84
2.84
-2.16
-7.16
ELEVATION [m]

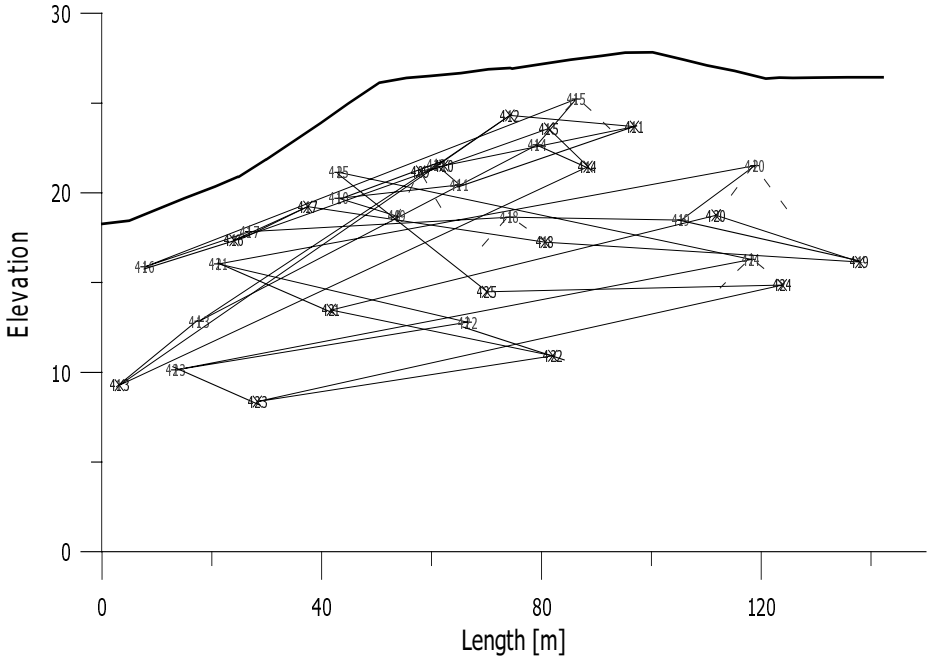
Elevation
Length [m]
0
10
20
30
0
40
80
120

Profile 2-24

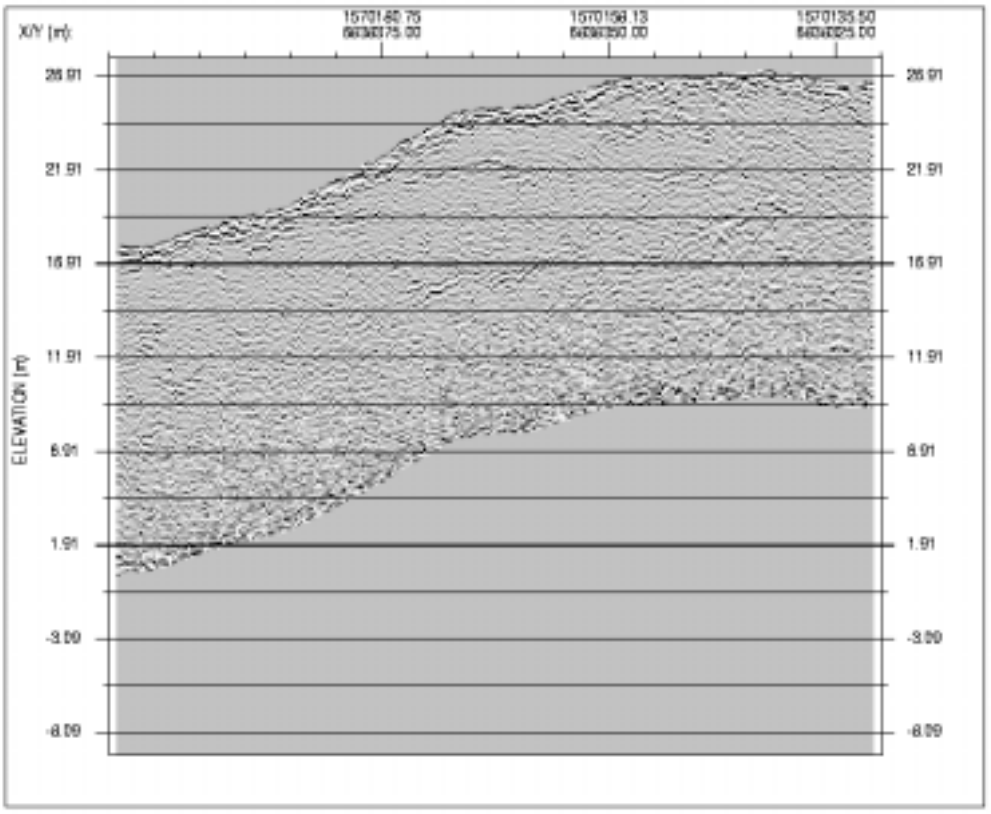
X/Y [m]:
ELEVATION [m]
26.91
21.91
16.91
11.91
6.91
1.91
-3.09
-8.09

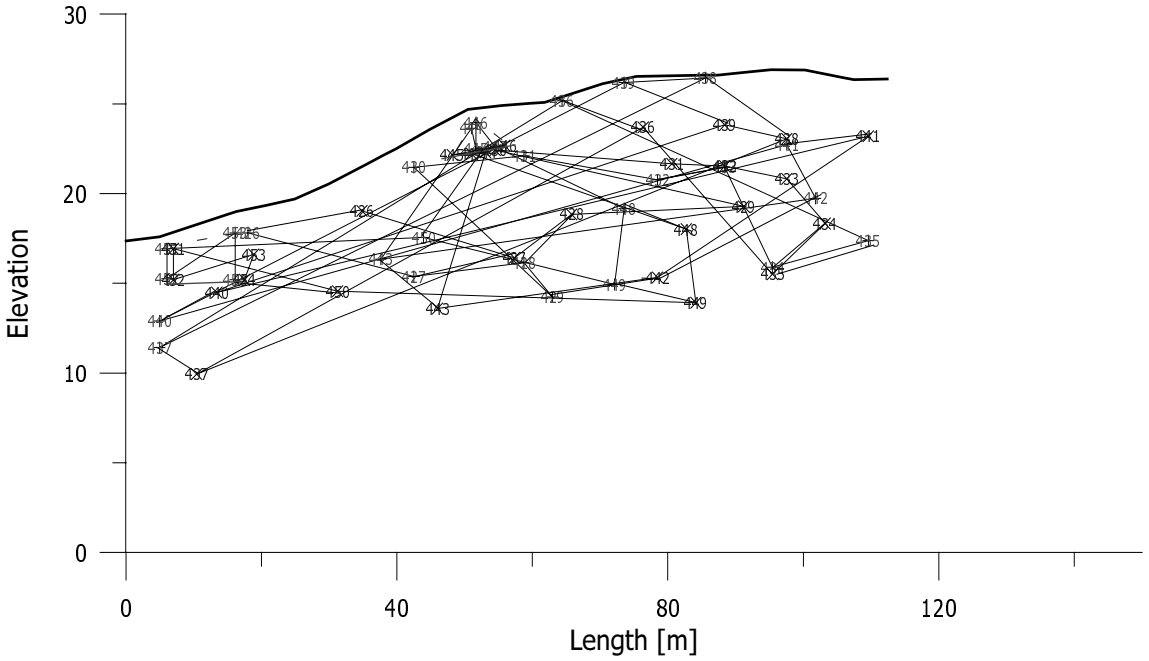
Elevation
Length [m]
0
10
20
30
0
40
80
120

Profile 25-1

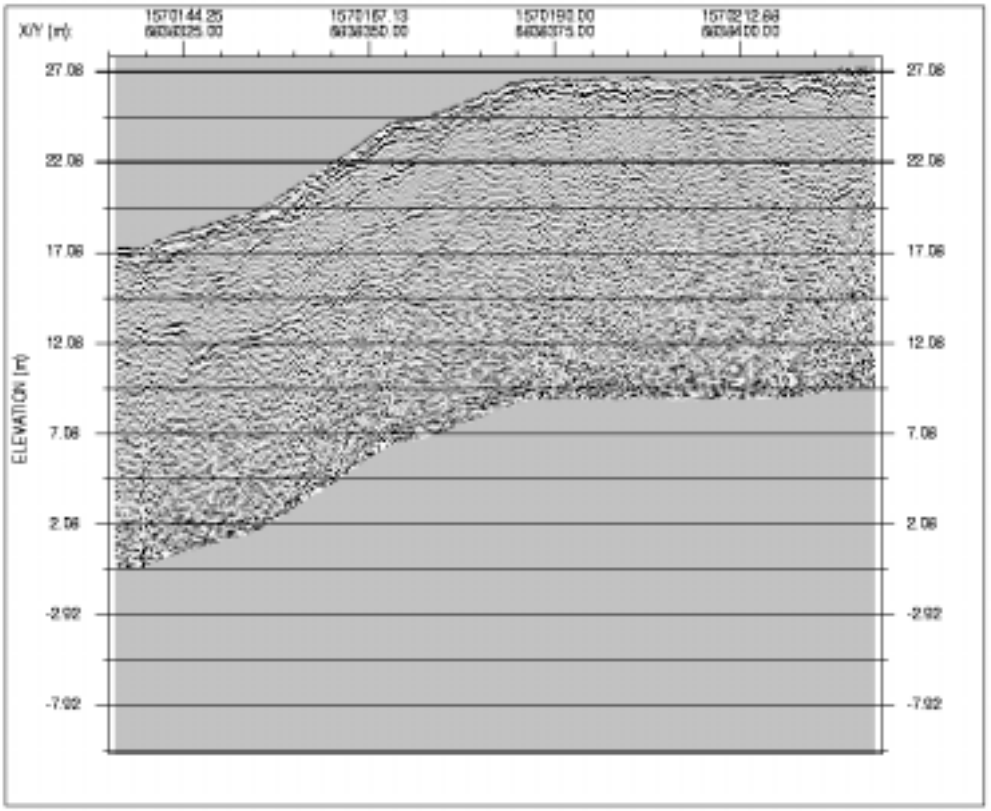
X/Y [m]:
1570144.25
6036025.00
1570167.13
6036350.00
1570190.00
6036675.00
1570212.88
6037000.00
ELEVATION [m]
27.08
22.08
17.08
12.08
7.08
2.08
-2.92
-7.92

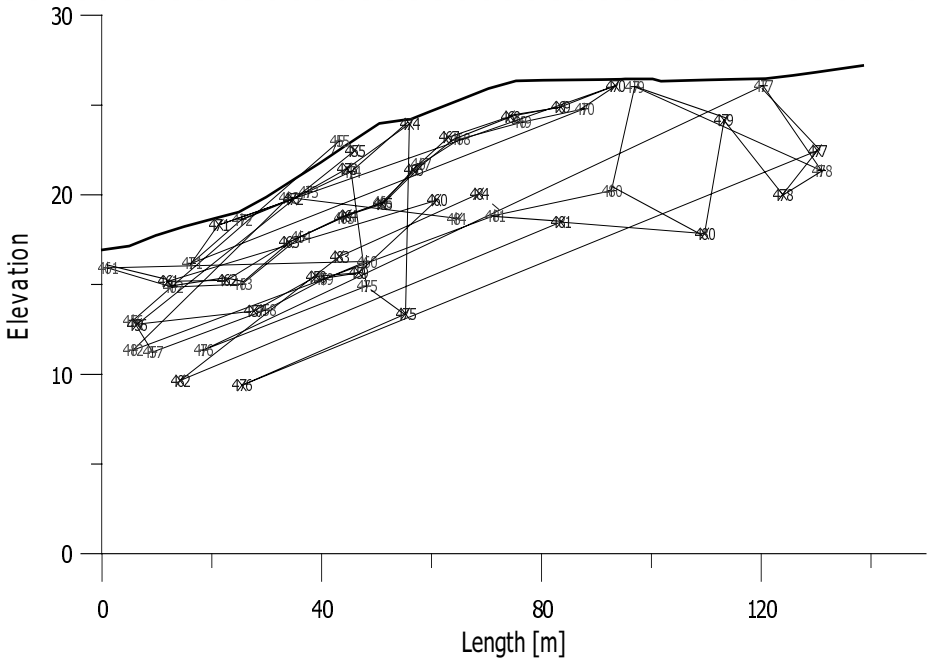
Elevation
Length [m]
0
10
20
30
0
40
80
120